GEOGRID REINFORCEMENT OF GRANULAR LAYERS ON SOFT CLAY - A STUDY AT MODEL AND FULL SCALE

by

Robin Jonathan Fannin

A thesis submitted for the Degree
of Doctor of Philosophy at the
University of Oxford

Magdalen College

Trinity Term, 1986

GEOGRID REINFORCEMENT OF GRANULAR LAYERS ON SOFT CLAY - A STUDY AT MODEL AND FULL SCALE

R.J. Fannin

Magdalen College, Oxford

A thesis submitted for the Degree of Doctor of Philosophy

Trinity Term, 1986

ABSTRACT

The mechanisms by which a geogrid acts to reinforce a granular layer over a soft clay were investigated with reference to trafficking of unpaved roads. The research involved a programme of physical testing at both model and full scale.

Model tests were carried out for monotonic and cyclic loading of a dual footing on to a layer of granular material that was compacted over a consolidated kaolin sample. The tests were made in conditions of plane strain at a quarter scale, and included a scaled geogrid at the base of the granular layer. Measurements of footing load, displacements and photographic observations through a perspex front face to the test box were used to identify the reinforcing actions of the geogrid.

A virtual work procedure was adopted in analysis of the results for both unreinforced and reinforced layers. The procedure accounts for lateral restraint of the subgrade and a membrane action in the reinforced tests, and allows a comparison of the cyclic test results with an equivalent monotonic bearing capacity.

Load tests were also made on footing plates at full scale, involving a similar arrangement of compacted granular layers over a prepared London clay and including a high strength polymer geogrid. Examination of the test results allowed a qualitative assessment of the model performance and the reinforcing mechanisms attributed to the geogrid.

The great tragedy of Science - the slaying
of a beautiful hypothesis by an ugly fact

T.H. Huxley (1825-1895)

ACKNOWLEDGEMENTS

The work reported in this thesis was supported by a postgraduate studentship from the Department of Education for Northern Ireland, and a CAST Award in association with Netlon Ltd.

A research project, and especially one in collaboration with outside institutions, is never the work of an individual and it is with gratitude that I wish to acknowledge the contribution to this study of many friends and colleagues.

Firstly I would like to thank Dr. George Milligan, his advice and sound engineering judgement were an important stimulation to this research, and working with him has been most enjoyable. While extending my thanks to all other members of the research group, I would like to mention Dr. Guy Houlsby and Dr. Richard Jewell for the interest they also have shown in discussion.

The development and commissioning of the laboratory equipment was made with the assistance of Mr. Robert Earl and Mr. Stuart Oldham, and I would like to express my appreciation of their efforts.

In the course of my research I spend a period of time at the Ground Engineering Division of the Transport and Road Research Laboratory that was most rewarding, and I remain indebted to Mr. David Farrar for his invalubale help and enthusiasm.

Finally, and on a more personal note, I would like to thank my mother and family for the support they have given to me throughout my education, and to give a particular mention to Philippa Rowcliffe for her constant encouragement and occasional patience.

JONATHAN FANNIN

CONTENTS

CHAPTER 5 MATERIALS PROPERTIES

CHAPTER 6 MODEL SCALE TEST RESULTS AND ANALYSIS

CHAPTER 7 FULL SCALE TEST RESULTS

Glossary of symbols

B	pore pressure parameter ($\Delta u/\Delta\sigma_r$)
B	footing width
B′	effective footing width
E	work done by external forces
F	footing load
G	shear modulus
G_s	Specific gravity of soil particles
H	thickness of granular layer
K_o	coefficient of earth pressure at rest
LL	liquid limit
N	number of cycles
N_c	bearing capacity factor
M	slope of critical slope line
PI	plasticity index
R_o	overconsolidation ratio for one dimensional compression
R_p	overconsolidation ratio for isotropic compression
W	work done by internal stresses
T	tension per unit width
a	area
c_u	undrained shear strength
c_v	coefficient of consolidation for vertical flow
e	void ratio
$\bar{h}$	average value of measured heave
p′	$= \frac{1}{3}(\sigma'_1 + \sigma'_2 + \sigma'_3)$
q′	$= (\sigma'_1 - \sigma'_3)$

q_b	calculated footing load/unit area (bearing contribution)
q_r	calculated footing load/unit area (lateral restraint contribution)
q_m	calculated footing load/unit area (contribution of membrane action)
q_M	measured footing load unit area
s	tensile stiffness of grid defined by a secant slope or modulus
u	pore pressure
v	specifc volume
w	displacement
α	adhesion factor
β	angle
γ	unit weight
δ	footing penetration
ε	strain
θ	fan angle
λ	slope of normal consolidation line
ν'	Poisson's ratio for effective stresses
σ_r	cell pressure
σ_n	normal stress
τ	shear stress
ϕ'	angle of friction
ψ	angle of dilation, angle
κ	slope of overconsolidation line
mc	moisture content
C-U	consolidated undrained
U-U	unconsolidated undrained
SD	standard deviation

CHAPTER 1

INTRODUCTION

1.1 Reinforcement of unpaved roads

Geotextile is the general term applied to permeable textile materials used in geotechnical engineering. The materials are made from a variety of synthetic polymers in a process involving the combination of plastic fibres by weaving or bonding into a continuous sheet, referred to as a fabric. Closely related to these fabrics is a range of other products such as webbing strips, mats and grids. The research described in this thesis is concerned with one of the latter group, namely geogrids, which are made by uni-axially or bi-axially drawing a perforated polymeric sheet in a technique that produces a mesh structure with uniform apertures.

It has become accepted that inclusion of such a reinforcing material in civil engineering structures such as walls, slopes and embankments may lead directly to cost-related improvements in design. A particular example is the unpaved road, which relies on a load spreading action of a granular layer to prevent local failure of the subgrade soil. Although these structures invariably have a short design life, it is important to avoid progressive breakdown in the granular layer or a resultant destruction of any load spread action, since these failures are both difficult and expensive to repair. Several analytical methods and design approaches describe or attempt to quantify the improved trafficability

of a geotextile or geogrid reinforced unpaved road, and while these methods certainly contribute to an understanding of the reinforcing action, they can be necessarily simplistic and on occasion erroneous in some assumptions. Indeed it could be said that there still lacks a definitive understanding of:

(i) the fundamental reinforcing mechanisms, and importantly the relative contribution of each as system displacements increase, and

(ii) how general assumptions concerning the behaviour of materials relate to their actual performance.

These two issues are examined for a Tensar+ geogrid by investigation at model and full-scale. The experimental approach taken was necessarily a simplification of both the wheel loading from a vehicle and soil conditions in the field, with the model tests performed for plane strain conditions at a quarter scale. Monotonic or cyclic loads were applied to a dual footing in contact with a compacted granular layer over a very soft subgrade; in the reinforced tests a scaled Tensar SS2-type geogrid was included at the base of the granular layer. The full scale tests were carried out in a large test bay and similarly involved monotonic loading of circular and rectangular footings in contact with compacted granular layers over a soft-to-firm London clay; a Tensar SS2 geogrid was included at the base of the granular layer.

While the full-scale tests did not relate directly to the unpaved road problem, they formed a very necessary check on the validity of the

+ Tensar is a registered trademark of Netlon Ltd.

model approach, the nature of the mobilised reinforcing mechanisms and the behaviour of the materials used in the model study. These aspects of the work are discussed at length in the text, however it is important at this stage to mention some fundamental considerations of physical model testing.

1.2 Philosophy of physical modelling in research

Early attention was drawn to the benefits of physical modelling to soil mechanics research by Rocha (1957), who identified the particular value of models in situations where self weight does not dominate. Scaling laws to satisfy stresses, strains and displacements were described, and while it was realised that strict adherence to these conditions of similarity in model and prototype is not feasible, nevertheless it was felt that in many problems the simplifications were quite acceptable.

In a succinct discussion Bassett (1979) clarified the advantages of models in terms of cost, examination of failure conditions and parameter control. Correctly applied, they may identify deformation patterns and mechanisms, and importantly provide data to validate or even direct numerical and closed-form analytical methods. However in extrapolation from model to prototype, the need for careful consideration of modelling laws was emphasised. This aspect was further addressed by Ovesen (1980) in a reminder that dimensional analysis must be applied to establish

similarity requirements, and a justification offered for any departure from the scaling law relationships.

The relationship between appropriate dimensionless parameter groups for this model study has been identified (after Love, 1984) as

$$\frac{q}{c_u} = f\left(\frac{\delta}{B}, \frac{H}{B}, \frac{\gamma_1 B}{c_u}, \frac{s}{c_u B}, \frac{G_2}{c_u}, \frac{G_1}{G_2}, \frac{\gamma_1}{\gamma_2}, \emptyset' \right) \qquad (1.1)$$

where: s - tensile stiffness of grid defined by a secant slope or modulus value (kN/m/%)

G_1 - shear modulus of granular material

G_1 - shear modulus of subgrade

γ_1 - unit weight of granular material

γ_2 - unit weight of subgrade

Since the numerical value of each group in the model and prototype should be the same, and γ_1 and γ_2 will not be scaled in a conventional model test, then the parameters c_u and G must be reduced by the scale factor and s by the square of the scale factor. The nature of these scaling relationships is described by Love in his thesis. For the soft-to-firm subgrades typical of field conditions, two clay undrained strengths in the range 6-12kN/m^2 were examined in this study; the similarity requirements for the geometry and stiffness of the model grid are fully discussed in section 5.2.

CHAPTER 2

LITERATURE REVIEW

2.1 Early work

Initial studies on the benefits of fabric inclusion at the base of a granular layer considered four major functions, drainage; filtration; separation and reinforcement. However, there seemed to be an uncertainty about the relative importance of each function, an uncertainty reflected in the conclusions of several authors at the time.

Jessberger (1977) examined the influence of layer thickness and subgrade strength with simple circular plate bearing tests, observing increases in bearing capacity up to 30% for the inclusion of a geotextile. In contrast, Sorlie (1977) concluded that there was little advantage to be gained from a geotextile. The fabric seemed to avoid complete failure of the system for some conditions, but had little effect on measured bearing capacities, and was assumed to exert a separation function primarily. A similar conclusion was reached by Jarrett et al (1977) for static loading tests on peat. The authors suggested however that at large displacements the fabric could influence the ultimate bearing capacity.

Nieuwenhuis (1977) developed a simple model which unfortunately failed to describe the aggregate-geotextile-soil behaviour, but one that indicated the importance of a soft subgrade to mobilise the fabric

reinforcing effect. Bakker (1977) importantly identified the membrane action in the fabric and assumed a simplified deformed shape which respected constant volume displacement of the subgrade. The author established the importance of rutting on fabric deformations which in turn lead to material strain and mobilised tension. Additionally the significance of a strength modulus for the fabric was indicated. These fundamental ideas were the basis for many subsequent design approaches.

2.2 Laboratory studies

Kinney (1979) reported a series of footing tests conducted in plane strain. Confining pressure on the granular layer beneath the footing increased during loading due to fabric induced shear stresses, and consequently a more effective distribution of load on the subgrade was promoted. The deformed shape of the geotextile developed a membrane support action. Strain energy stored in the fabric reduced plastic strains in the subgrade and acted to limit surface rutting. Slippage was observed to occur between the aggregate and the geotextile, particularly on unloading of the surface. Similar conclusions were reported by Bauer and Preissner (1986) for static loading of small scale footings. A concept of fabric tension was described and further reported by Kinney and Barenberg (1982) wherein strain in the fabric was computed from measured displacements knowing the deformed shape of the geotextile. Tension was then calculated from these strains with a knowledge of the tension/strain relationship for the material.

Kinney reported an improved performance with increased fabric modulus, a finding that had first emerged from the work of Webster and Watkins (1977). Robnett et al (1980), (1982) investigated this influence of fabric modulus on the initial rate of rut formation and number of load repetitions to cause a given rut depth. Increased modulus was closely related to greater rutting resistance.

Gourc et al (1982a),(1982b),(1983) reported a series of plane strain model tests incorporating very weak commercially available fabrics in which a layer of crushed stone overlying a soft clay was loaded with a single footing. Optimum fabric modulus was found to be a function of the anchorage length. The action of the fabric was to increase the resistance to local failure and to generate a membrane effect dependent on anchorage, with slip observed when the ultimate strength of the anchorage was exceeded. In comparison with slow monotonic drives (0.04mm/s), cyclic tests (frequency 1Hz) mobilised a reinforcement effect only after a substantial amount of rutting. There did not appear to be any significant frequency effect on rut development with each cycle of load, Figure 2.1.

In a summary of this model work Gourc and Riondy (1985) proposed an approach which combines the load-displacement results for both monotonic and cyclic tests in what is termed a fatigue criterion. Essentially, for the same rut depth in each test, the ratio p_m/p_s is plotted against N to give a relationship that is independent of rut depth, where

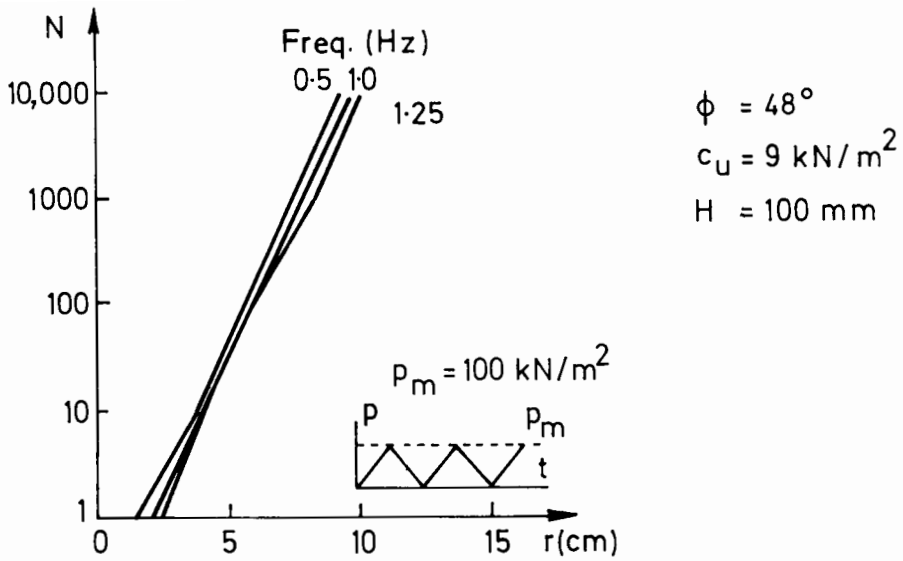

Figure 2.1 Influence of loading frequency on rut development (after Gourc et al., 1982a)

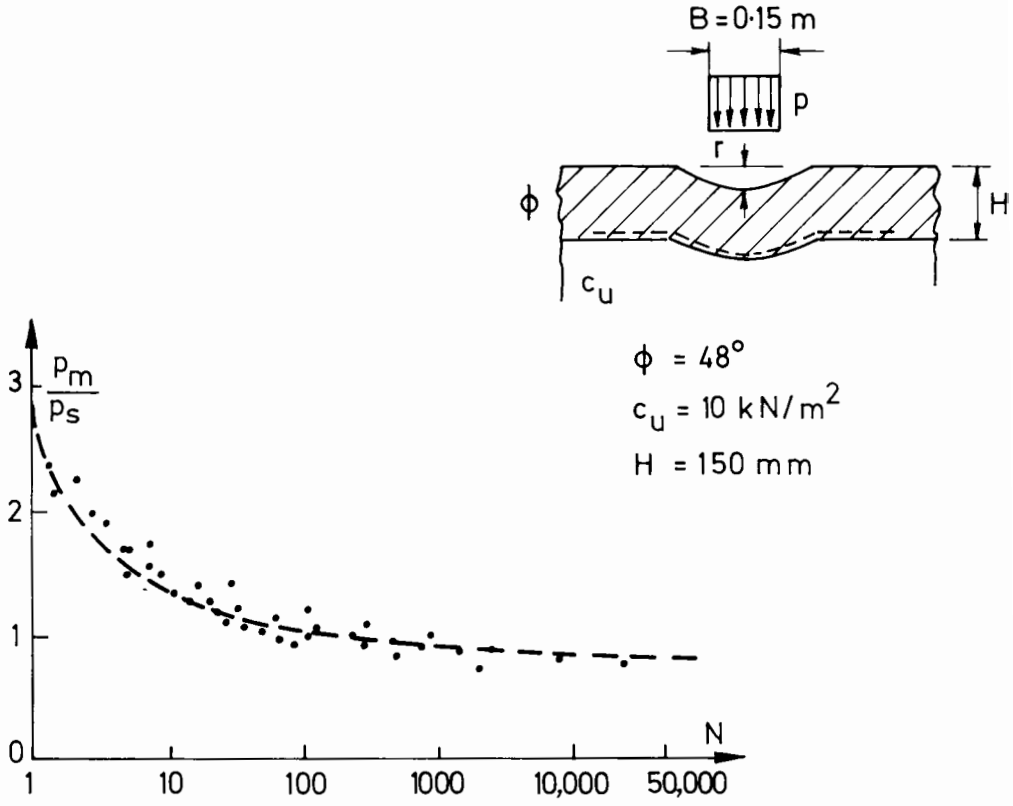

Figure 2.2 Fatigue criterion independent of rut depth (after Delmas et al., 1986)

p_m - constant maximum contact pressure in a cyclic test at rut depth r

p_s - contact pressure in a single drive monotonic test at rut depth r

N - number of load cycles in a cyclic test at rut depth r

The form of this relationship is illustrated in Figure 2.2 for a Bidim 150 fabric, with a mathematical fit to the curve given by

$$\frac{p_m}{p_s} = \frac{a \log N + b}{\log N + c} \qquad (2.1)$$

where a, b and c are experimental constants for the materials. Conceptually the approach is an attempt to relate system performance for cyclic loading (or trafficability) to a plate bearing type test, and as such is very useful. However comparisons of these particular model test results and a limited amount of data from a full scale trial made by Delmas et al (1986) have proved encouraging though rather inconclusive.

Large plane strain tests for a weak peat subgrade and a geogrid reinforcement were described by Jarrett (1984). Little difference in load capacity was apparent for the reinforced and unreinforced system at small footing displacements, however an improvement of over 50% was observed with rut repair. This was attributed to a predominating membrane type reinforcement action of the grid. Significantly, tensile load in the geogrid was measured. Tension was maximum directly under the

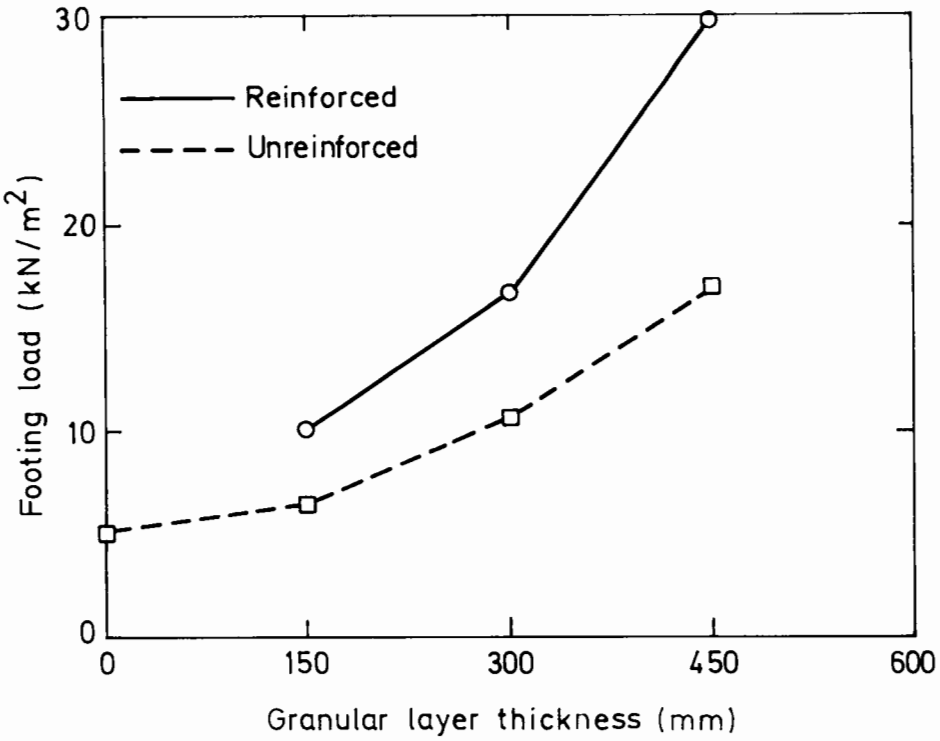

Figure 2.3 Footing loads to cause 200mm displacement (after Jarrett, 1986)

footing. Beyond the point of inflection on the profile curvature, a smaller and limiting value was observed to be associated with anchorage failure and slip movements of the grid. Jarrett (1986) further reported footing load capacity to increase dramatically with an improved anchorage attributed to a thicker granular layer, Figure 2.3.

2.3 Field trials

Webster and Watkins (1977) and Webster and Alford (1978) described a study of various construction techniques for access roads across soft ground. The performance of a geotextile reinforced system was reported for a relatively light (330g/m^2) fabric and a heavier (627g/m^2) material which was stronger and less extensible. While both fabrics led to equal improvements over the unreinforced system at small displacements, the

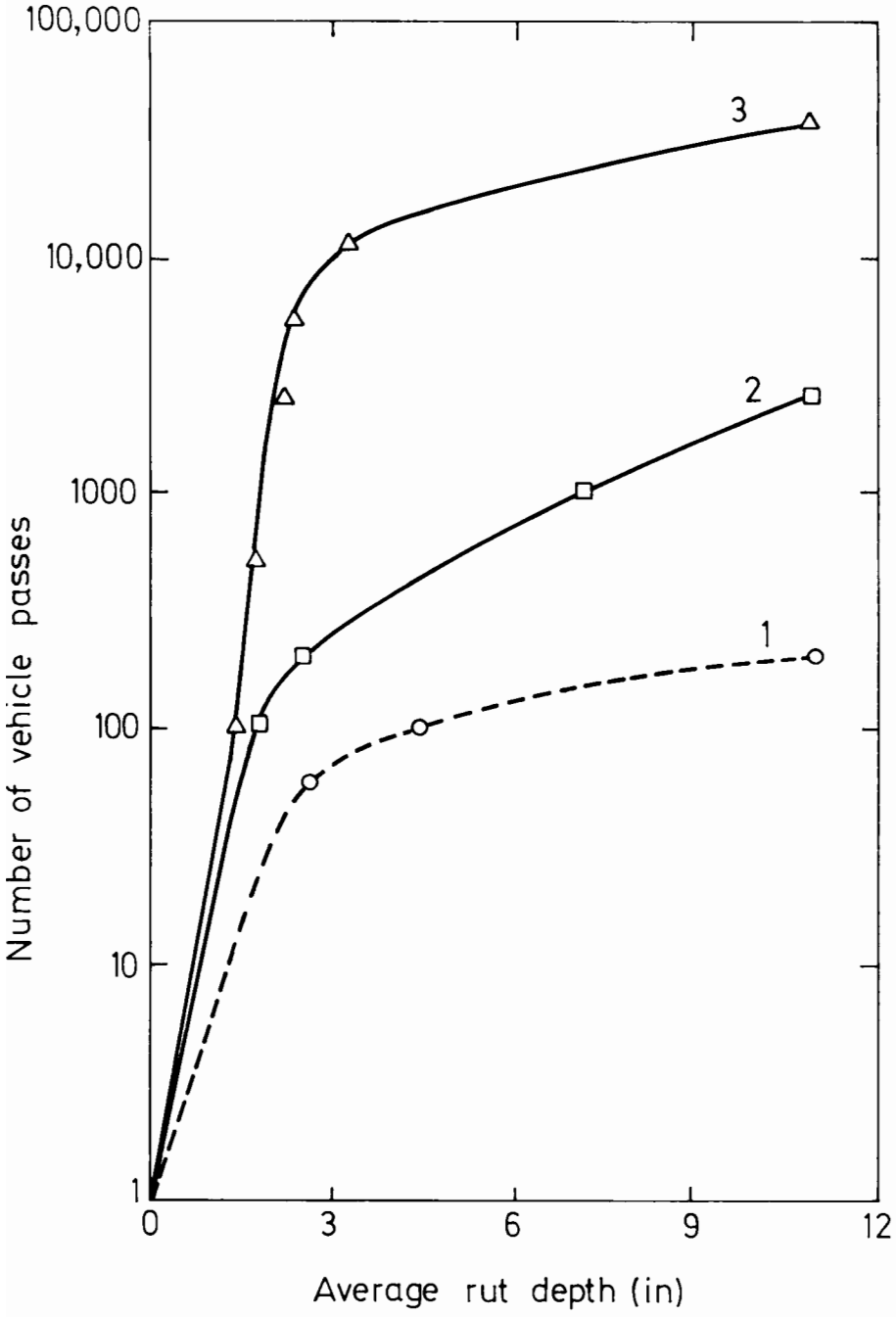

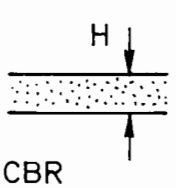

	Fabric	H (mm)	CBR (%)
1	Unreinforced	355	0·9
2	330 g/m^2		1·1 – 1·2
3	627 g/m^2		1·1 – 1·3

Figure 2.4 Development of surface deformation (after Webster and Alford, 1978)

stiffer fabric was observed to give the best result at significant rut depths, Figure 2.4.

Palmeira (1981) described a well instrumented low embankment access road over a very soft soil and indicated the principal function of the geotextile was to prevent excessive and unacceptable local rutting. Ramalho-Ortiago and Palmeira (1982) reported from that study an evaluation of various geotextile installation methods. Complete local failure was avoided with reinforcement; sections with a stiffer reinforcement extending the full width of the embankment or taken close to its edge and then folded inwards gave a similar performance. However, the best result was achieved by anchoring the fabric outside the edges with pegs to restrain it fully, Figure 2.5, with savings of 16-18% in granular layer thickness recorded for reinforced sections, increasing to 23% for the fully anchored system.

A trafficking test for a geotextile placed under only one of the vehicle wheel paths was conducted by Potter and Currer (1981). Although the fabric acted as a material separator, it did not lead to any greater compaction densities. Yet a small improvement in the reinforced section was observed even for the first few vehicle passes, and the rate of surface rutting was greatly reduced thereafter, Figure 2.6. Significantly, gauges embedded in the soil indicated the fabric inhibited development of permanent strain in the subgrade and the base of the granular layer, and that transient horizontal strains in the soil were considerably smaller. Similar conclusions were reported by Ruddock, Potter and McAvoy (1982a), (1982b) for a full scale trial for which a limited degree of vehicle wander was permitted.

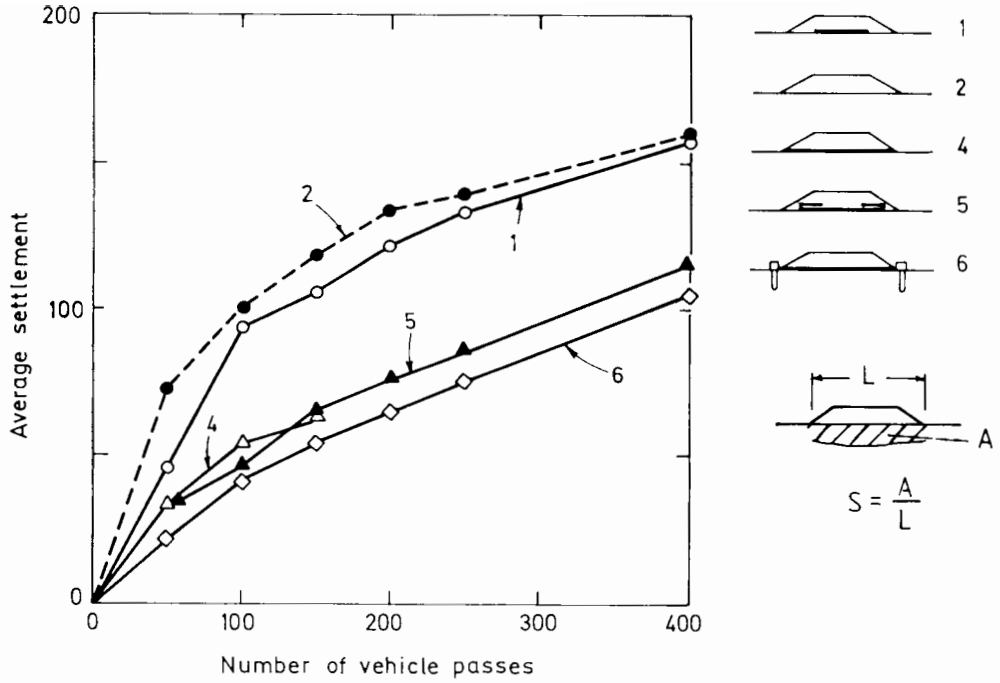

Figure 2.5 Influence of reinforcement type and anchorage (after Palmeira, 1981)

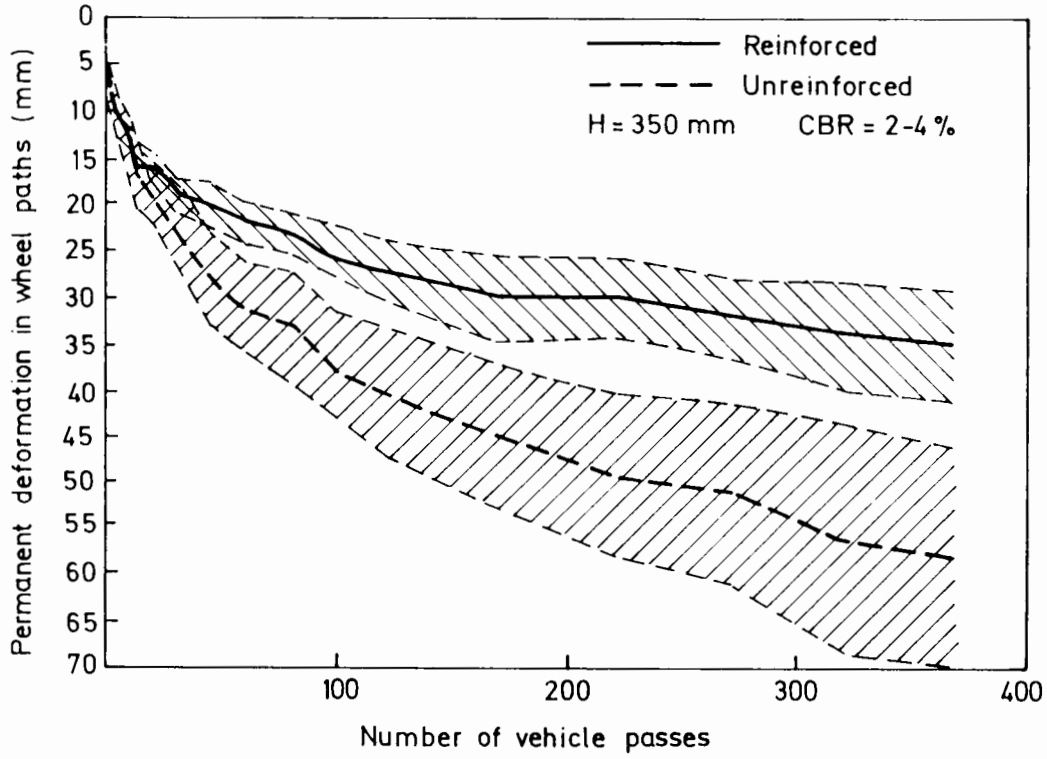

Figure 2.6 Development of mean permanent surface deformation: mean deformation and standard deviation. (after Potter and Currer, 1981)

Chaddock (1985) described a trafficking test for a geogrid placed under only one vehicle wheel path, and a granular layer decreasing from a thickness of 275mm to 150mm. A clear early improvement was observed for the reinforced section, Figure 2.7, an improvement which was reported to be less for increasing layer thickness. Any direct comparison of performance between these two trafficking tests must however allow for the weaker subgrade and thicker granular layer in the study of Potter and Currer (1981).

A comprehensive investigation was completed by Sowers et al (1982) involving a study of selected road failures, plate bearing tests and a field trial. The authors attributed an improved load spreading behaviour in a reinforced system primarily to a separation function of the geotextile, with passing reference to fabric restraint of the aggregate. At large deformations, and with rut repair, a catenary support or membrane action was developed. Plate load tests modelled traffic loading qualitatively, but greater deflections and failure at smaller loads than those of the plate tests were observed for vehicle loading. Rut repair was comparatively more beneficial in the traffic tests. This work formed the basis of an analytical technique discussed below.

2.4 Analytical methods

Sowers et al (1982) described a design procedure based on a membrane effect and plastic failure of the subgrade due to confinement. The membrane effect was related to surface rutting, fabric tension and the deformed geotextile shape by a combination of geometric considerations

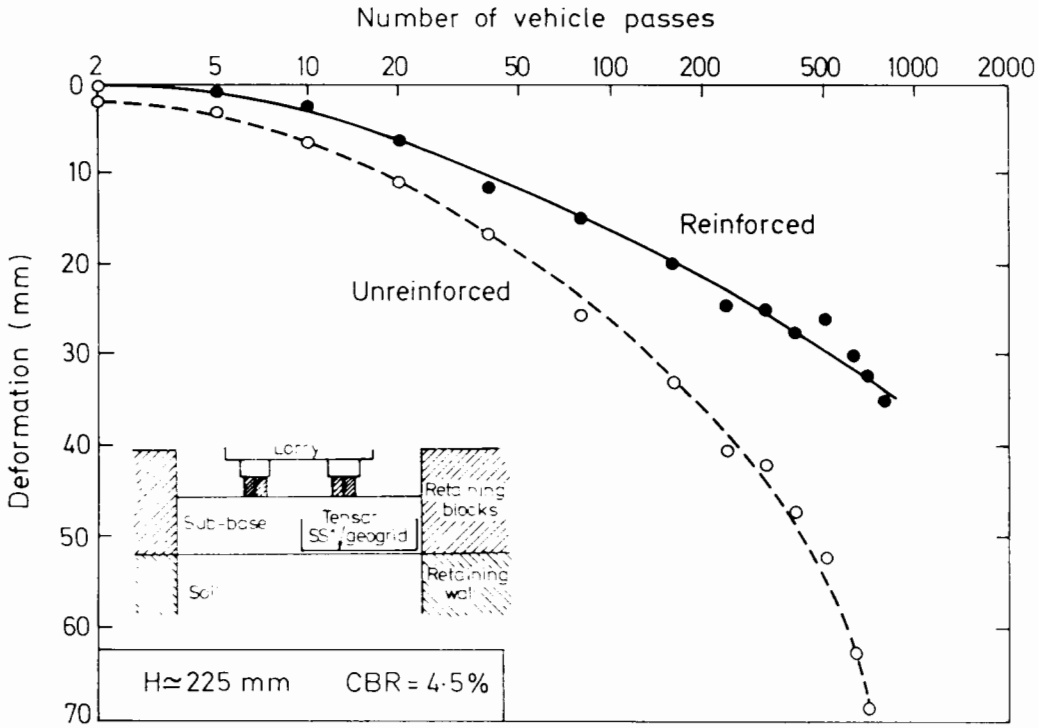

Figure 2.7 Development of surface deformation (after Chaddock, 1985)

and field observations. In contrast to other approaches a non uniform strain distribution was recognised in the fabric and calculated from an empirical formula. The relationship was derived from an assumed parabolic profile and discrete increments of deformation between the points of inflection. A minimum value of tension, taken to be beneath the loaded area was used to calculate an upward component of force. To allow for a surcharging effect outside this region, the force was doubled. An interactive procedure was used to determine a load/rutting characteristic.

An approach based on earlier work by Nieuwenhuis and Bakker which computes the membrane effect by a theoretical consideration of geotextile and subgrade equilibrium was proposed by Sellmeijer et al (1982). The geotextile was described by a membrane type differenial equation and the

subgrade by a bilinear elastoplastic soil model. However the authors did not consider any reinforcing mechanism until plastic deformations prevailed in the subgrade. Fabric strains were calculated for an assumed fixity of anchorage at the edge of the road. To allow for many vehicle passes it was suggested the subgrade undrained strength for design should be considered to be 2/3 of that measured. Greater aggregate savings were achieved with increasingly stiff fabrics, up to a limiting modulus of elasticity 1500kN/m^2, and for subgrade undrained shear strengths up to 60kN/m^2. The calculation routine was applied to two field trials without success, Kenter and Sellmeijer (1983). By incorporating a general empirical formula for an equivalent axle load and number of vehicle passes, the authors back analysed the results of Webster and Watkins (1977) and Webster and Alford (1978). This effectively was a calibration and correction exercise.

Giroud and Noiray (1981) made the first significant contribution directed at formulating a design approach. The geotextile profile was described by a series of parabolae joining at the initial plane of the fabric, Figure 2.8. Uniform strain was assumed throughout the geotextile, and confinement of the subgrade used to justify a calculation of the bearing capacity at the plastic rather than elastic limit. The method was based on an empirical formula relating granular layer thickness to traffic and soil properties for unpaved roads without a geotextile, and a quasi-static analysis to determine the aggregate savings that could be achieved by including a geotextile.

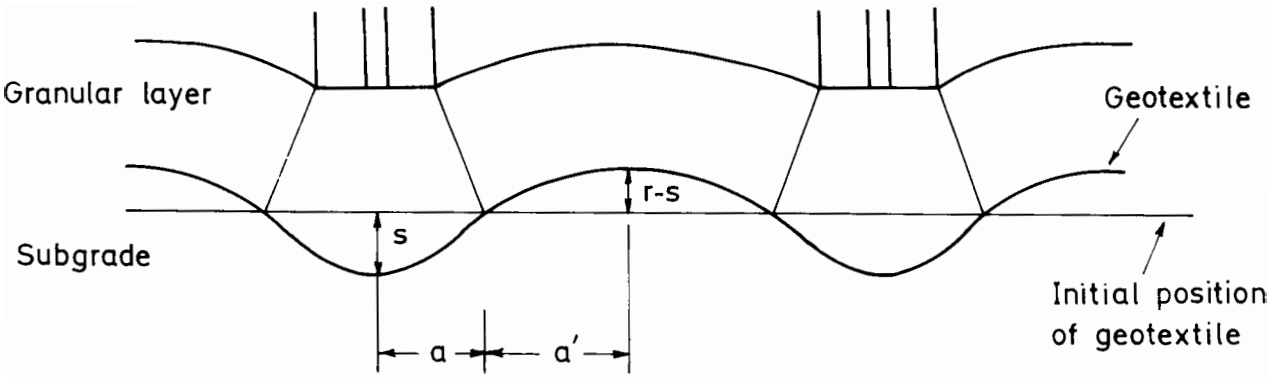

Figure 2.8 Assumed profile of the geotextile (after Giroud and Noiray, 1981)

In order to simplify the analysis of a rather complex and variable system the authors made a number of assumptions. Importantly no account was taken of any failure mechanisms by sliding of aggregate over the geotextile, and general anchorage of fabric was ignored. Consideration was only given to a failure in the subgrade soil or the geotextile itself. The assumption of a uniform strain in the geotextile would appear to be in conflict with the observations of others, Ingold (1982).

Giroud et al (1984) extended this approach to include geogrids. The method accounted for subgrade confinement, a membrane effect and an improved load distribution by the introduction of an increased angle of load spread in the granular layer. However, no attempt was made to consider the fabric tensile forces directly. Instead the normal stress difference between each side of the geogrid resulting from the tensioned membrane effect was considered either to be negligible, or else equivalent to a reduction of 10% in granular layer design thickness when

not so. The authors further suggested membrane effect to be negligible for a rut depth less than 0.15m and/or no channelisation of traffic wheel path. Savings of 30-50% in the granular layer thickness of unpaved roads were predicted, although caution was advised since the approach had yet to be calibrated against test data.

2.5 Research at Oxford

The mechanisms by which a geogrid may improve the performance of a granular layer over a soft clay subgrade have been studied, with particular reference to the unpaved road, by laboratory model tests, Love (1984). Complementary to this work, Burd (1986) has developed a large displacement finite element formulation and used it to perform back analyses of the model tests.

The tests were carried out under plane strain conditions at a quarter scale. Monotonic loading of a rigid footing was applied to a compacted granular layer on a soft clay. Tests were performed at several layer thicknesses and subgrade strengths, for both the unreinforced and reinforced conditions. In a reinforced test a model grid was placed at the base of the granular layer.

The unreinforced system exhibited a typically shallow and very localised failure associated with lateral spreading of the fill. The reinforcing action of the grid, by inhibiting this movement of granular material from beneath the loaded area and thereby resisting lateral strains, gave a much improved performance. A significant membrane action

was identified at large displacements. Characteristically, the displacement mechanism was modified by the inclusion of reinforcement, with deeper and longer failure planes in the clay.

The finite element formulation, when applied to back analysis of these tests, was used to calculate reinforcement tensions and interface stresses with the surrounding soil. Material rotation and mesh displacements were accounted for in an incremental solution procedure. The subgrade behaviour was elastic/perfectly plastic, the reinforcement linear elastic, and the soil/reinforcement interface considered to be perfectly rough.

The results indicated that the granular layer in an unreinforced system transmits outward acting shear as well as normal stresses to the subgrade below. Reinforcement was found to have little effect on the load spread action of the granular layer, but importantly applied inward acting shear stresses to the subgrade which acted to increase the subgrade bearing capacity. Normal stresses on the reinforcement confirmed a membrane effect below the footing and a surcharging effect to the side of it, significant at increased deformations; measurements of reinforcement tension indicated maximum tensile force immediately below the footing, and a point of zero tension moving outwards with increasing footing displacement.

CHAPTER 3

APPARATUS

The laboratory apparatus consisted of a large consolidometer to prepare a standard rectangular kaolin sample, and an electro-hydraulic control assembly to apply strain or stress controlled footing loads during testing. The consolidometer was similar to one used for previous work.

3.1 Consolidometer/test box

3.1.1 Description

The model tests were conducted in plane strain on a kaolin sample consolidated in a long, narrow rectangular consolidometer which was constructed to give an internal length 1600mm and width 300mm, Figure 3.1(a). The length of the box was designed to accommodate projected subgrade deformations based on simple shallow foundation bearing capacity calculations and a consideration of end effects; the width of the box was chosen to minimise wall friction edge effects on the overall sample deformations, while not being unnecessarily large since the required consolidation force increases with sample plan area. The internal height of the box, 761mm was such as to provide sufficient clearance for the initial slurry sample height and top consolidation platen, Figure 3.1(b).

Plate 3.1 Consolidation of a sample

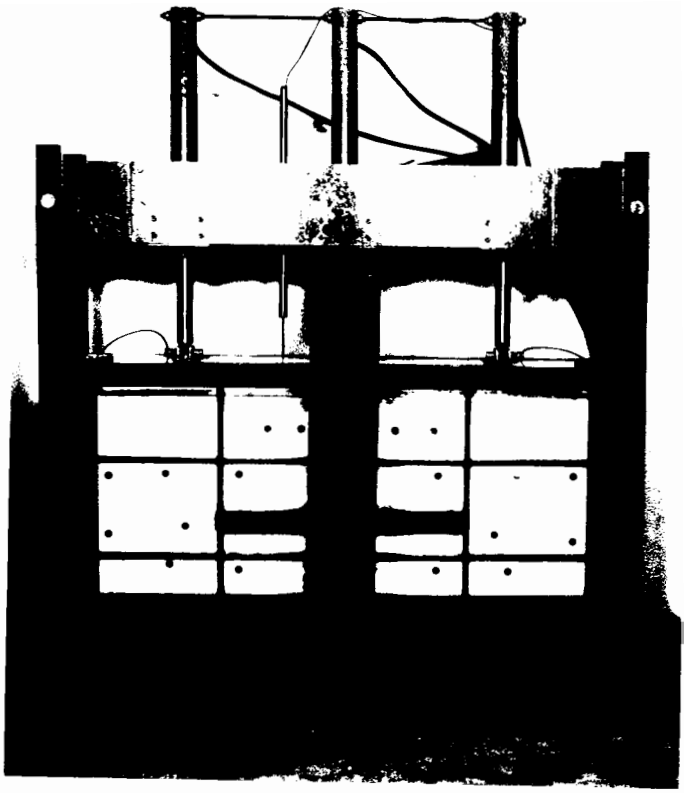

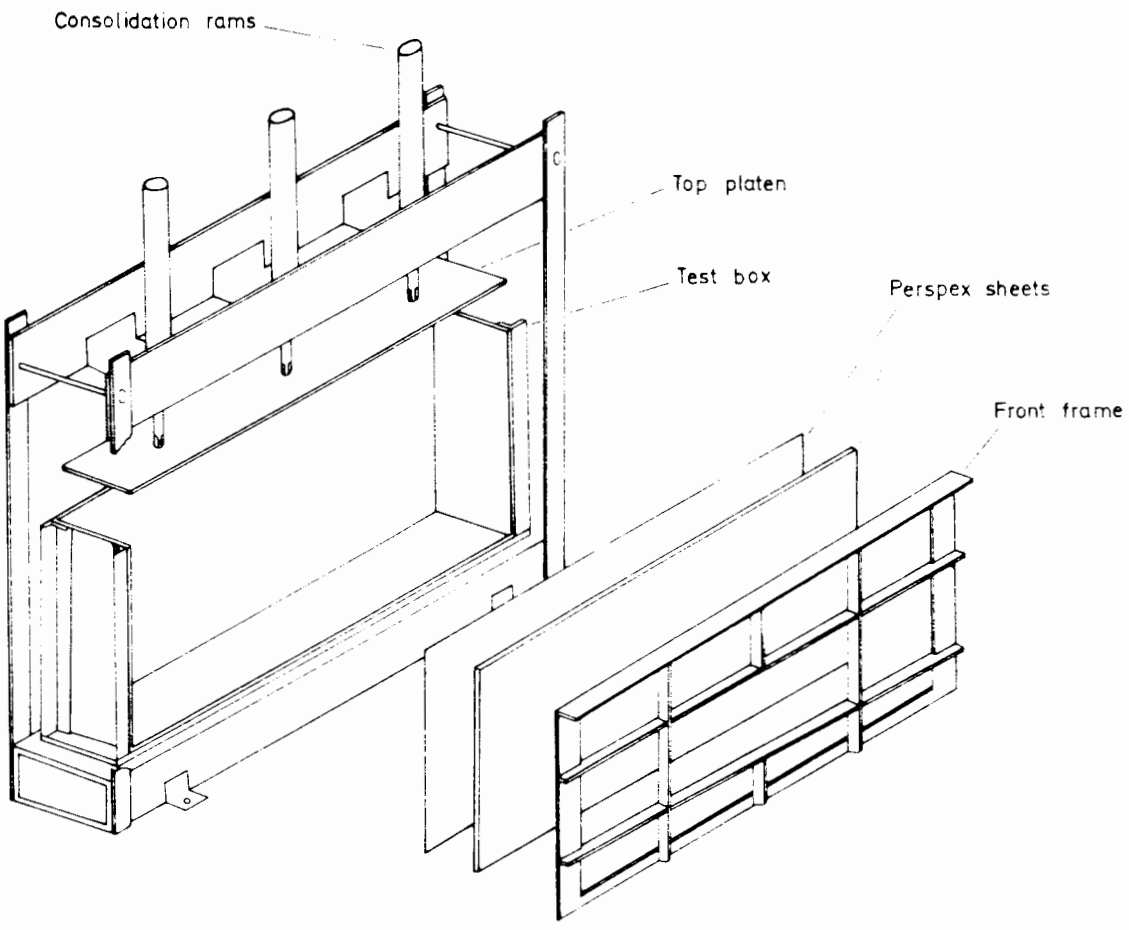

Figure 3.1(a) General view of consolidometer / test box

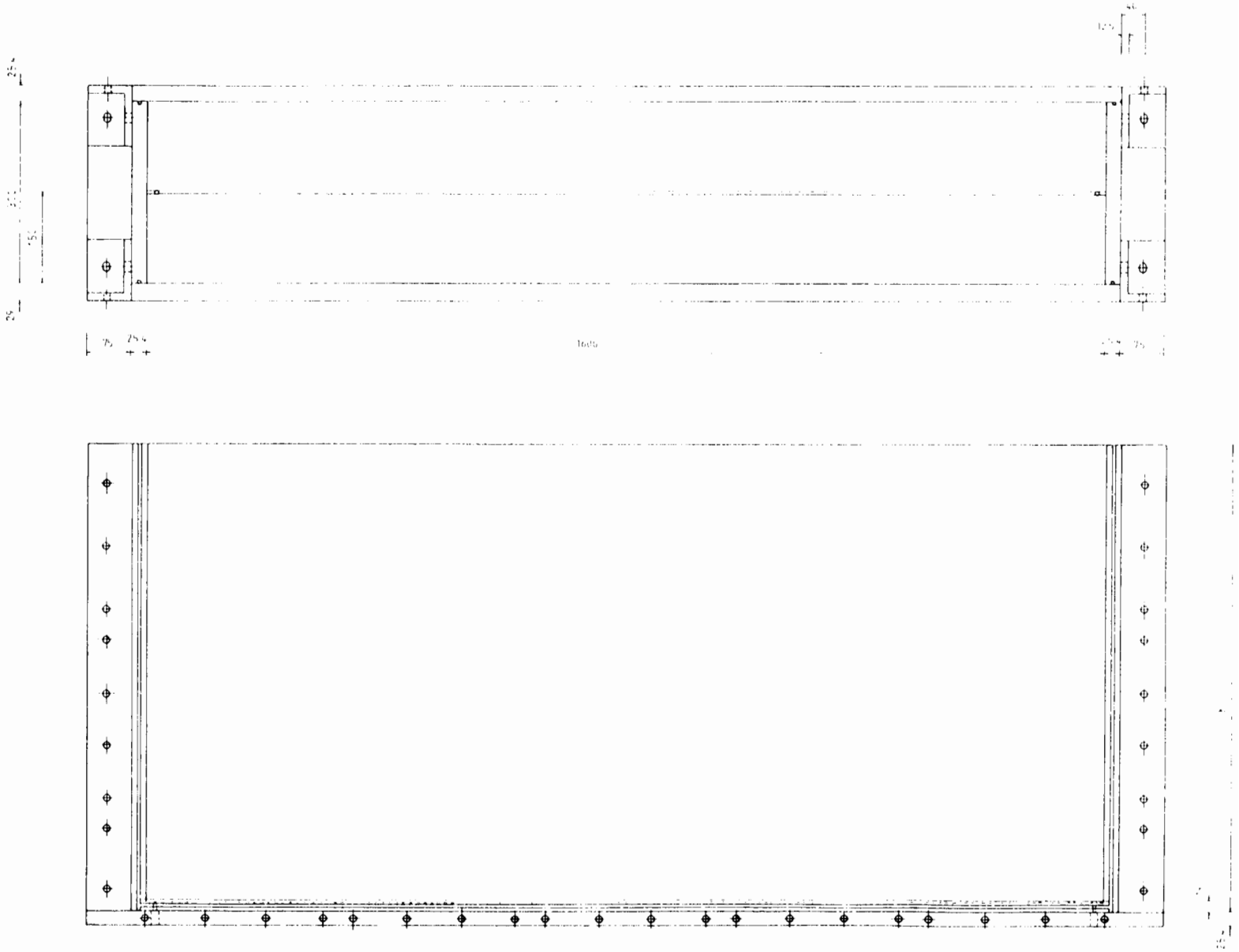

Figure 3.1B Test box plan view and elevation
(dimensions in mm)

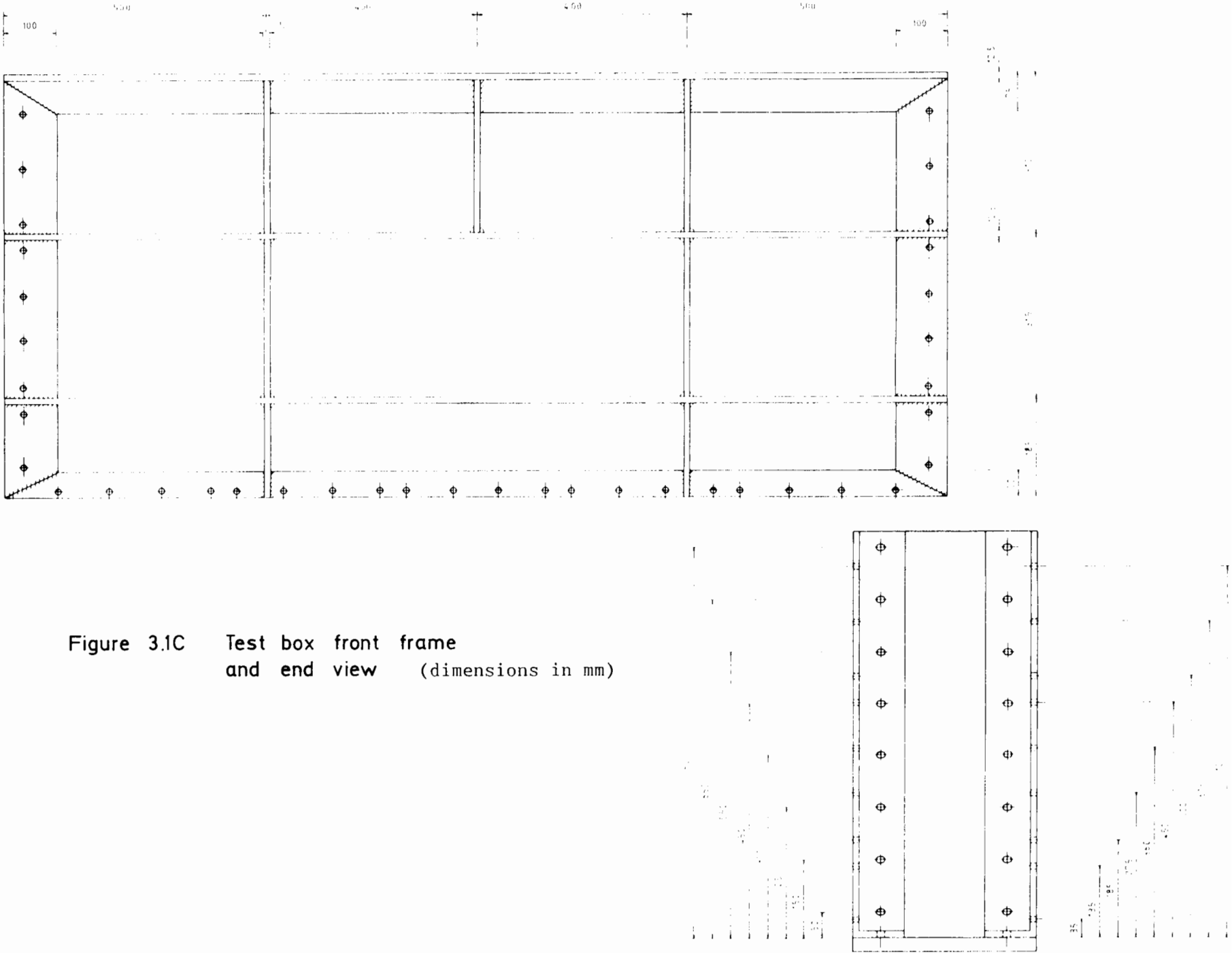

Figure 3.1C Test box front frame and end view (dimensions in mm)

The base and three of the four vertical sides of the box were machined duralumin sheet; the base was 20mm thick and the sides were 25mm thick. They were held bolted in position by a mild steel frame on to a lower supporting duralumin plate 25mm thick. The back face was drilled and tapped to accept five pressure transducer mountings at selected locations. The fourth vertical side, the front face, was of clear perspex and allowed a view of the sample inside the test box. The front face actually comprised two separate sheets of perspex: a 25mm thick external sheet and a 4mm flexible inside sheet. This arrangement facilitated placement of markers in the clay sample as described in section 4.3.1. The front face was similarly fixed in position by a rigid mild steel frame bolted through to the adjoining box sides and base, Figure 3.1(c). The purpose of the rigid frame was to constrain any deflection of the box during testing, and a maximum deflection on the box centre line under load was measured to be only 0.55mm, equivalent to a maximum lateral strain of 0.2%.

The box was designed such that assembly would hold each face against an 'O' ring type rubber hose located in a continuous channel on the front and back of the box. Immediately before assembly a thick film of Loctite silicone rubber sealant was liberally run the full length of the 'O' ring hose to ensure a good final seal.

Provision for bottom drainage was made in the base plate. A 3mm thick porous plastic Vyon sheet cut exactly to plan size was placed in the bottom of the box. Acting as a filter, this allowed water from the sample to pass through it and into a drainage channel 5mm x 5mm cut in

the base plate. Bottom drainage was controlled by taps at either end of the channel.

3.1.2 Application of consolidation load

The test box was supported on a large fabricated rigid hollow base section with provision to be set horizontal. An overhead mounting assembly for the consolidation rams was held in position by four upright slender columns welded to this base section. The assembly was fixed to these columns by two large shear pins. During consolidation, lateral support to the box was provided by reaction pillars placed on either side and fixed together, Plate 3.1.

Sample consolidation was achieved by loading a rigid top platen to the test box through three rams. The pneumatic/hydraulic system used to control the consolidation phase is illustrated in Figure 3.2. Oxygen free nitrogen supplied in cylinders was regulated to provide a known and controlled supply pressure to the independently isolated single acting rams. A Bundenberg graduated gauge measured the ram pressure to $\pm$ 14kN/m^2 (2psi). A relief valve to atmosphere was included on the supply line. During consolidation hydraulic fluid was allowed to flow from the ram outlet to reservoir. To raise the platen at the end of consolidation this flow was reversed; hydraulic fluid was pumped into the lower chamber of the rams and the pneumatic pressure in the top of the rams allowed to exhaust to atmosphere. Complete removal of the overhead mounting assembly to give clear access to the test box during testing or allow maintenance of the rams was achieved with an overhead crane and

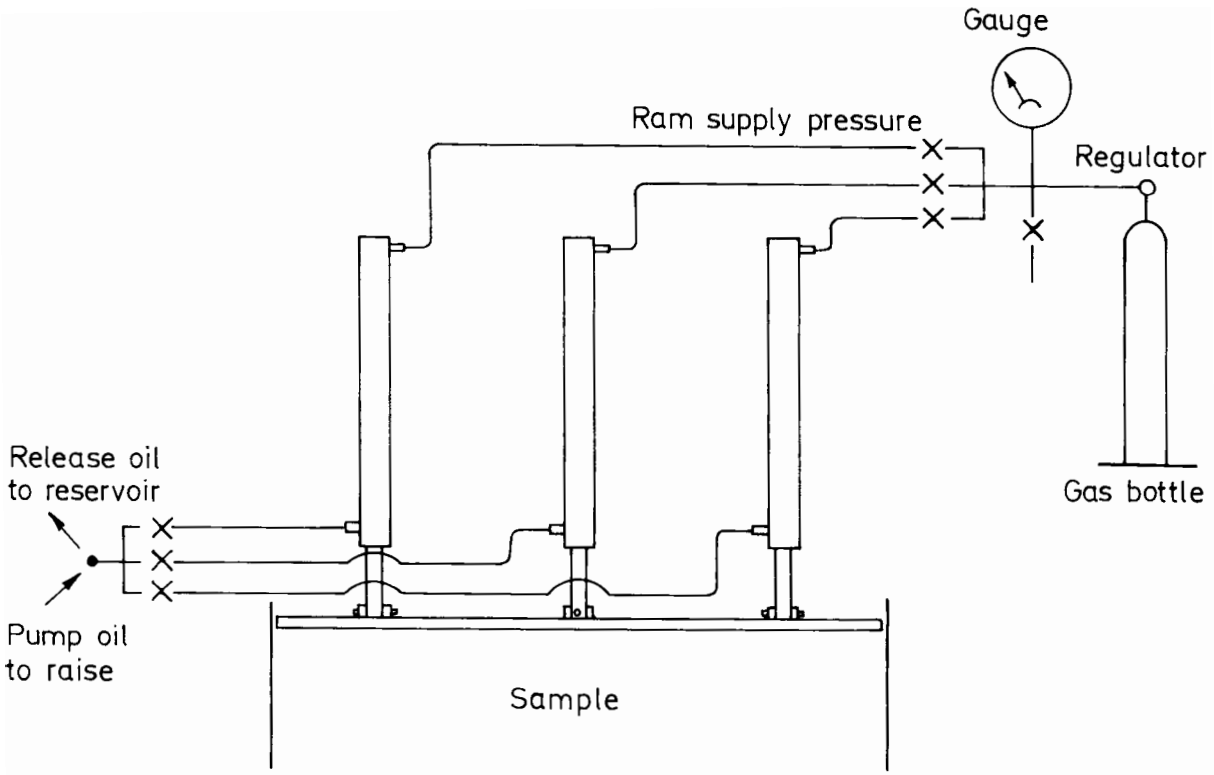

Figure 3.2 Pneumatic/hydraulic ram control

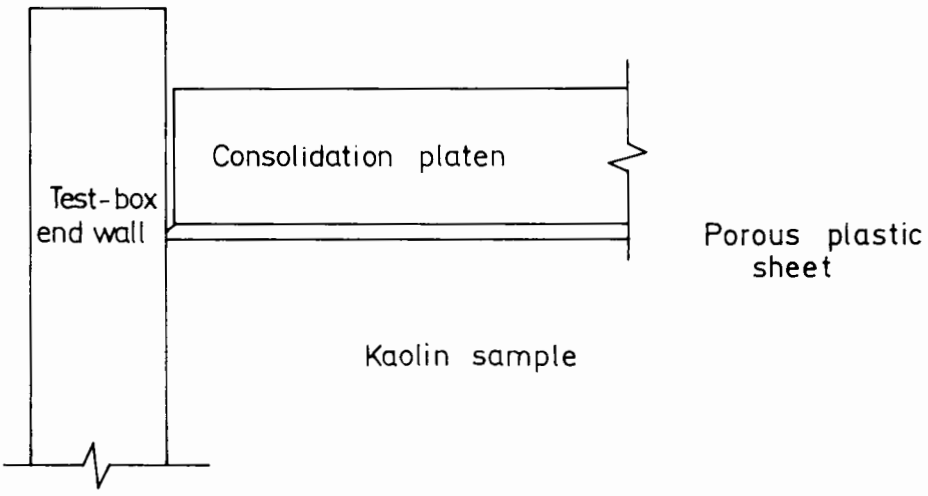

Figure 3.3 Porous plastic seal to the consolidation platen

easy removal of the two shear pins. Generally a good seal was observed in the rams despite a pneumatic/hydraulic interface.

The consolidation platen was made of milled stainless steel 25mm thick. It was 1598mm long and 298mm wide, giving a small clearance of 1mm around the platen when inside the consolidometer test box. A seal between the platen and box walls was achieved with a further porous plastic sheet. Cut oversize to plan dimensions 1602mm by 302mm, it was bevelled slightly as illustrated in Figure 3.3. This configuration gave a good seal to the sample and provided a top drainage layer similar to that at the bottom. Experience indicated a first pressure increment of $20kN/m^2$ could be applied to the slurry sample without difficulty.

3.2 Closed-loop electro-hydraulic servo-controlled loading

3.2.1 Dual footing assembly.

The dual footing was made of Dural HE30TF, and comprised two flat plates 135mm wide at a centre line separation 450mm. Design considerations are reported in Appendix A. Four threaded holes in the footing plates accommodated hardened steel guide rods. The rods ran through ball bushings mounted in bridging bars which bolted across the top of the test box. This rod and bushing arrangement kept the footing in vertical alignment. A load cell was fixed to the footing with a threaded stud. Load was applied to the footing by an Eland double-acting hydraulic servo actuator type HDS 15 which had a 100mm stroke. The

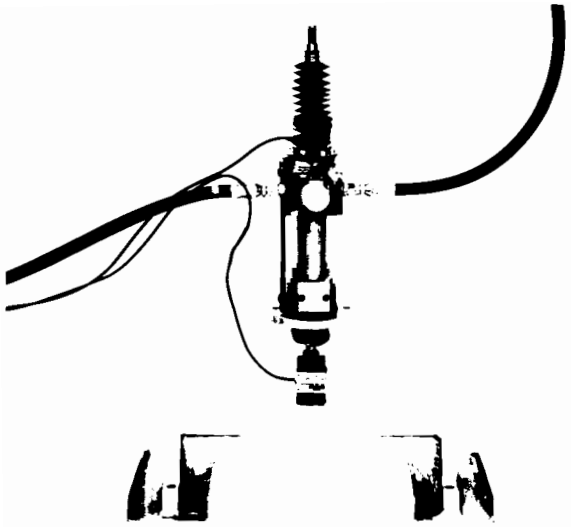

Plate 3.2 Hydraulic actuator

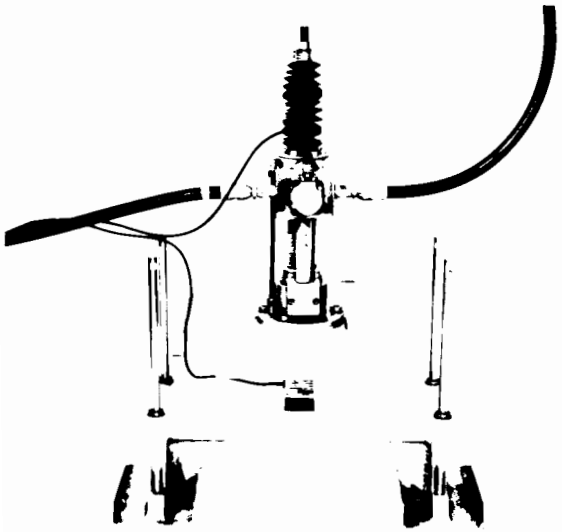

Plate 3.3 Dual footing assembly

actuator rod was threaded up to a shoulder to screw flat against the top of the load cell, Plate 3.2. The actuator was supplied with a mounting flange and was fixed to a mild steel plate. The dual footing assembly, Plate 3.3, was bolted across the top of the test box to support the footing inside the box itself.

3.2.2 Hydraulic supply

Hydraulic pressure to the actuator was controlled by a servo valve mounted directly on the actuator for best performance characteristics. The valve, a Dowty 4653 series miniature servo valve is an electro-hydraulic device designed to convert a low power electrical input into an amplified proportional hydraulic flow output, and was selected because of good performance at low rated flows. Hydraulic supply to the valve was achieved with the system illustrated in Figure 3.4. A fixed displacement

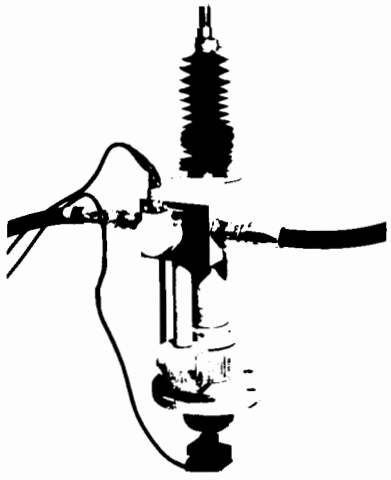

Plate 3.4 Servo-valve mounted directly on actuator

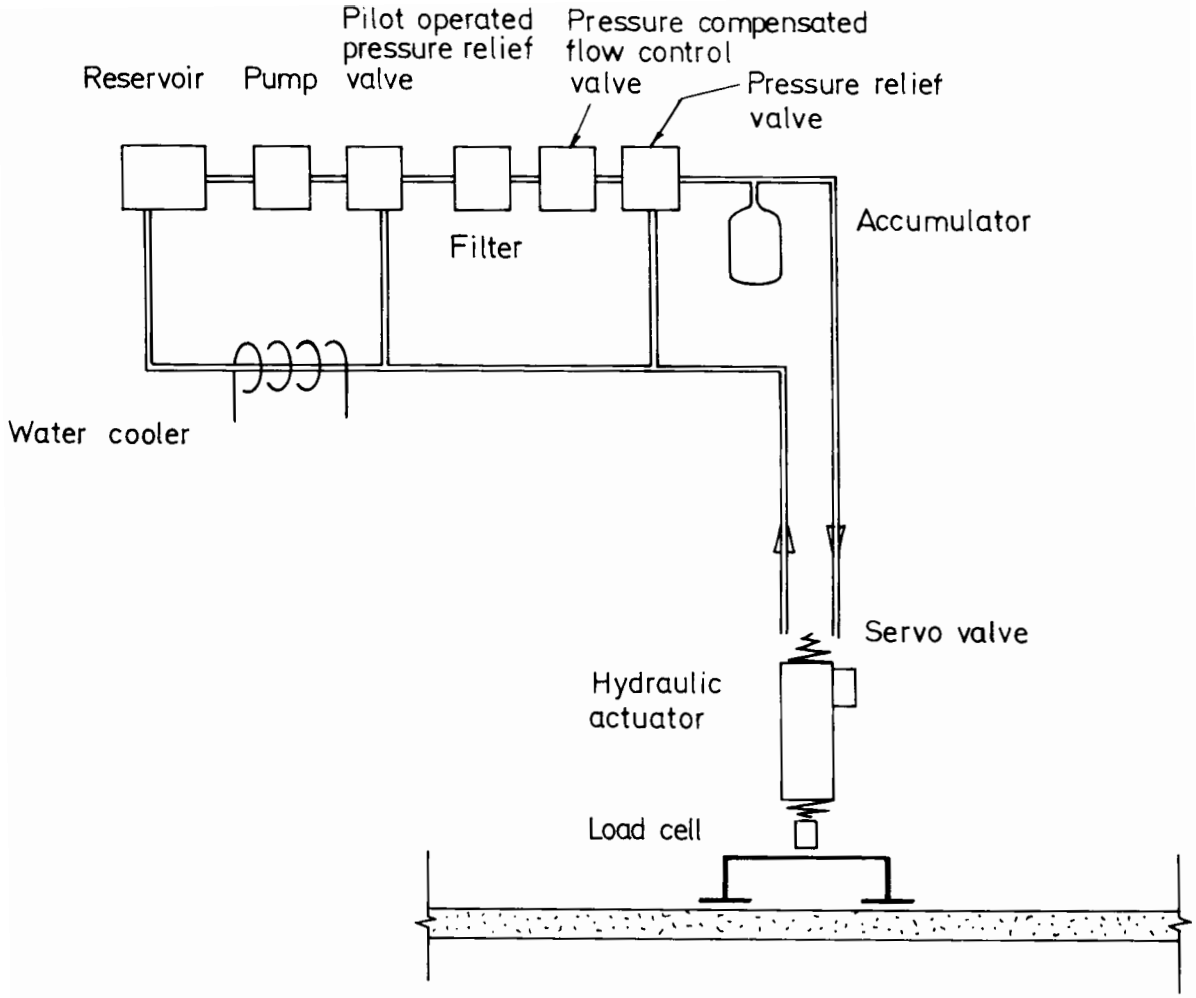

Figure 3.4 Hydraulic supply to the actuator

piston pump with a rated flow 5.7l/min at 1800rpm and 41.5MN/m^2 was supplied from a reservoir mounted above it to provide priming. Control of supply pressure was by a pilot operated pressure relief valve on the pump outlet. Together with a second pressure relief valve, it was used to set the maximum working pressure at 24.2MN/m^2 for static duty and 13.8MN/m^2 for cylic duty. A pressure compensated flow control valve was used to provide a constant flow. Excess flow was returned to the resevoir. An accumulator was included in the system to smooth out fluctuations in the flow of oil, acting primarily as a stilling pool.

The return line to the reservoir passed through a water cooler to dissipate fluid heat before dumping to tank.

All components and hoses were throughly cleaned before assembly, and the system bled after filling with oil to remove any air. A flushing block was mounted in place of the servo valve at this stage, and a 10μ filter placed in the filter block. This was later replaced with a 1μ filter and the process repeated to achieve an acceptable purity that would not cause any damage to the servo valve. Finally the flushing block was removed, the servo valve mounted on the actuator and the system bled again.

3.2.3 Electronic control

Servo valves are invariably used in closed-loop control situations, typically for position, velocity, load or pressure control. The principle was described by Chestnut and Mayer (1961), Figure 3.5.

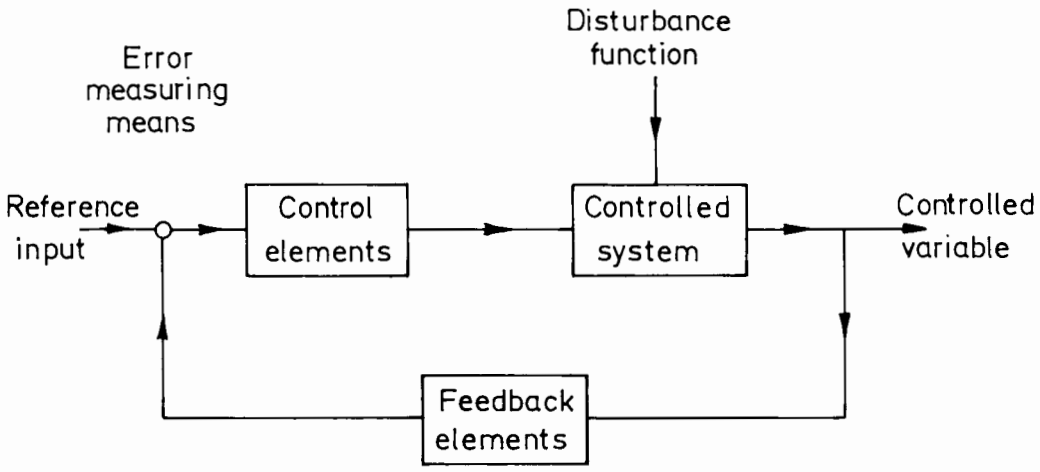

Figure 3.5 Principle of feedback control (after Chestnut and Mayer, 1961)

Significant contributions to the use of such systems in geotechnical engineering have been described by Snaith and Brown (1972), Cullingford et al (1972), Brown et al (1975). For closed loop control, the function to be controlled is continuously measured and used as feedback for comparison with the demand for the function. The difference between measured output signal and demand signal, termed error, is used to correct the system and acts to reduce the error to zero. Hence the servo valve operates on an input signal which is the error signal. Measurement of demand and feedback signals, and generation of a compensating error signal was made by a Dowty series 4791 linear servo drive amplifier.

The type of control is determined by the source of the feedback transducer, and in the test programme either position or load control of the dual footing was maintained depending on the requirements of the test. Typically the demand signal to the servo amplifier is generated to suit the control requirements of the operator, as discussed separately below. Dither is a high frequency, low amplitude electrical signal, and application of dither in the servo amplifier was used to improve the hysteresis and threshold characteristics of the valve according to the manufacturers instructions.

3.2.3.1 Position (strain) controlled loading.

The monotonic driving speed of the footing is based on the relative rate of strain in the reinforcement for the model and prototype conditions. This calculation procedure is fully described in section

5.2.2.2, and indicates a driving speed 2.5mm/s to satisfy the modelling requirements for a single pass to failure of a heavily loaded vehicle.

A schematic diagram of the position control system is given in Figure 3.6. The requirement of the system was to drive the footing at a constant speed and to correct for any variations from the desired value. This caused the demand signal characteristic to be a linearly increasing voltage with time. Consequently, the demand signal was provided by a ramp generator designed and built for the requirements of this project. Linearity ensured a constant rate of change of displacement, while the gradient of the ramp fixed the speed. Provision was made in the unit to vary the ramp gradient setting. Position feedback was from a

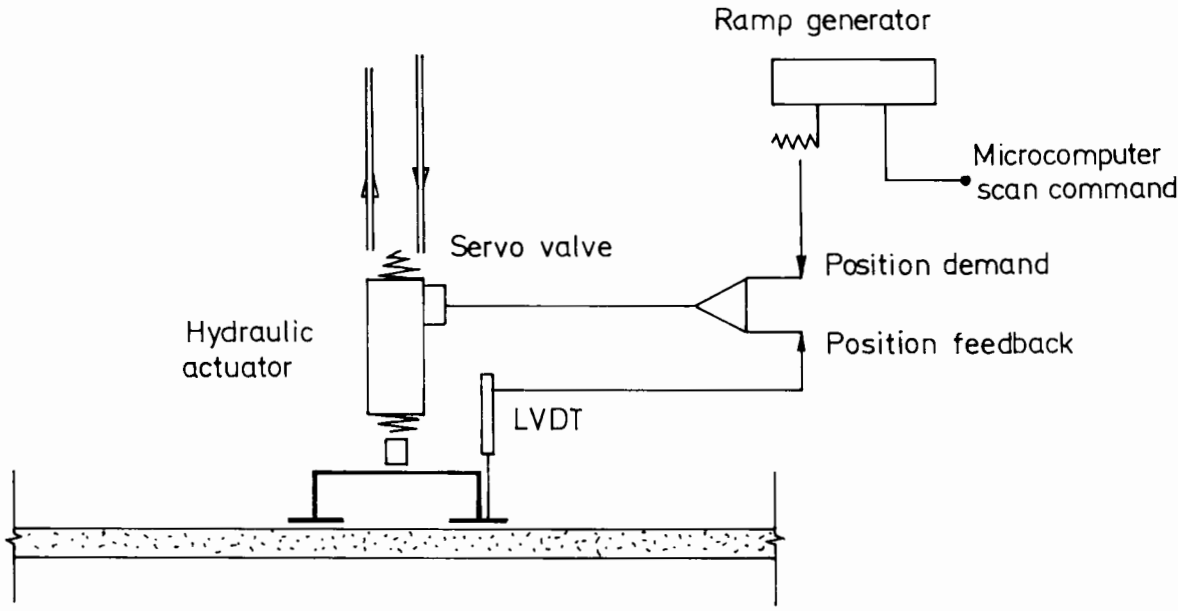

Figure 3.6 Footing position control

displacement transducer in contact with the dual footing. The sytem was calibrated against confined clay samples in a calibration frame to establish the correct setting for a monotonic driving rate of 2.5mm/s.

3.2.3.2 Load (stress) controlled loading

The actual stresses in a road foundation caused by a moving vehicle are complex and only qualitatively understood, involving rotation of the principal stresses as illustrated in Figure 3.7, Thom and Brown (1985).

In practice the variation of vertical stress at a given point beneath a road surface as a wheel load moves over the point is assumed to be similar to the profile indicated in Figure 3.8. To simplify the load application procedure and difficulties of reproducing this shape, it was decided to approximate the actual form of the stress profile to a triangular pulse. In fact, due to inherent damping of an hydraulic system, the control response was unable to follow exactly the sharp reversals of this command signal, and the final load profile was very similar to that observed in the field. Calculation of the maximum contact pressure and loading frequency is given in Appendix A. The derived load profile with time presupposes a continuous line of vehicles each with a standard axle load trafficking the granular layer. It is difficult to estimate a typical pattern of loading for an unpaved road, however this selection could be described as severe given the likelihood of such an extreme configuration.

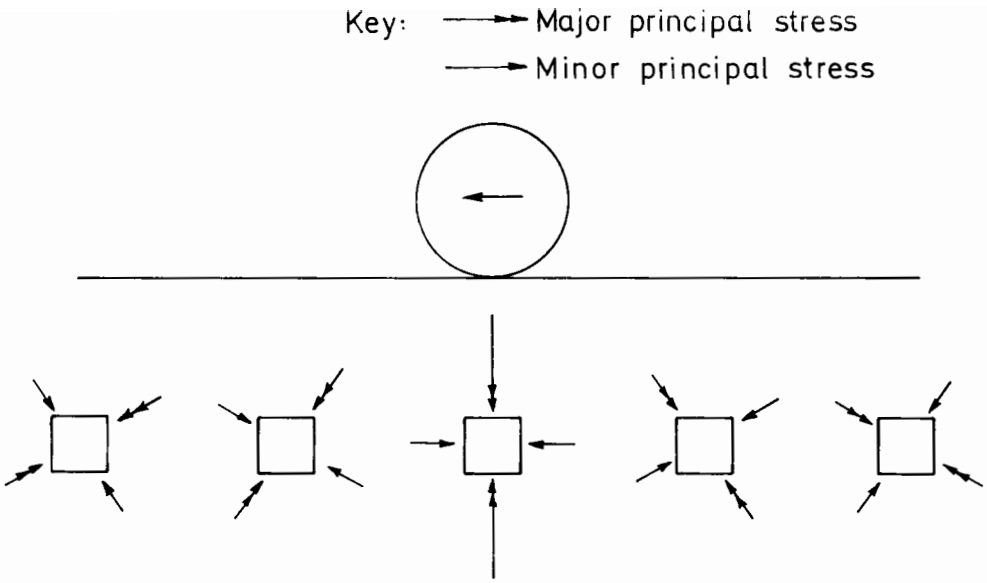

Figure 3.7 Stresses under a moving wheel load
(after Thom and Brown, 1985)

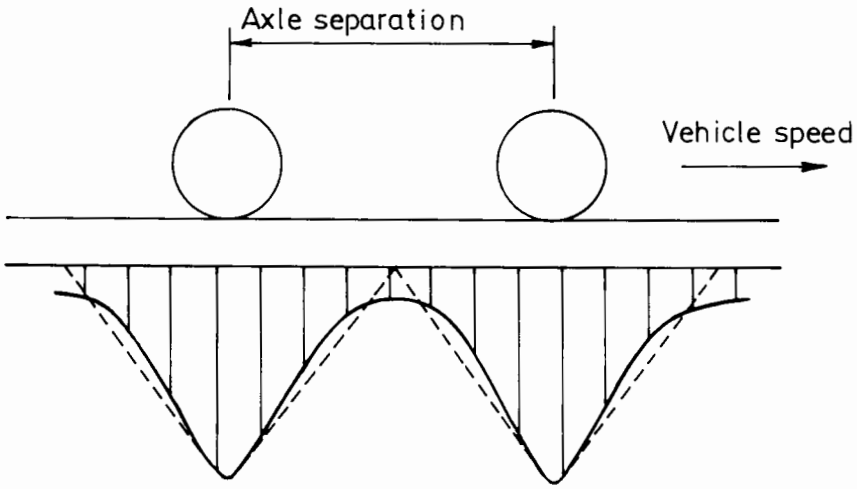

Figure 3.8 Simplified soil stress changes due to a moving wheel load
(after Delmas et al., 1982)

A schematic diagram of the load control system is given in Figure 3.9. The requirements of the system were to load the footing up to a constant maximum value 68kN/m^2 and then unload it at a cycle frequency of 1Hz, according to a triangular waveform. The demand signal was provided by a function generator, a Thandar TG 102. Feedback was from the load transducer located between the actuator and footing. Calibration was again made against confined clay samples. The offset and amplitude control on the function generator, together with the gain potentiometer on the linear servo drive amplifier board, were used to set the observed waveform and amplitude which was measured as a load cell output with time. The synchronous TTL output of the function generator drove a frequency counter to record the number of cycles.

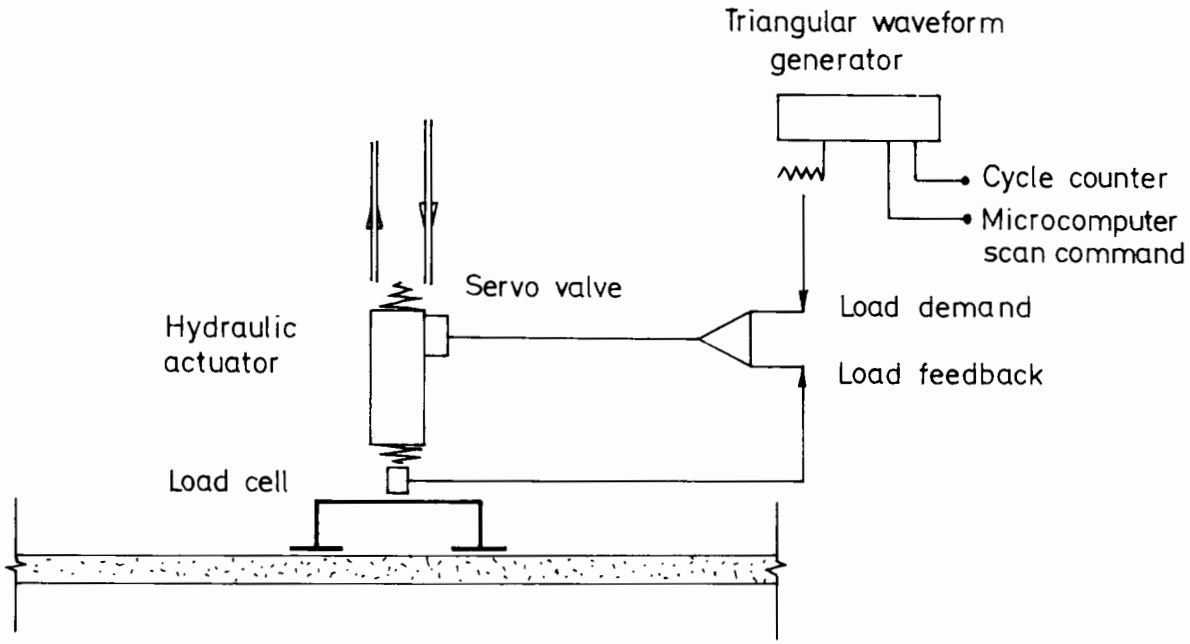

Figure 3.9 Footing load control

3.3 Instrumentation

The instrumentation comprised a number of load, displacement and pressure transducers. Power to the transducers was supplied from a unit which also provided signal conditioning, multi-channel output to a data logger and signal feedback to the footing control system.

3.3.1 Transducers

The load cell, manufactured by Sangamo Transducers, belongs to the D95 series and has a 15kN capacity. A small body deformation under load gives a fast dynamic response. The transducer, powered by a 15V DC supply, is hermetically sealed for total immersion.

Six linear variable displacement transducers (LVDT) were used, all of the AC type. A 500mm stroke AC250, manufactured by Sangamo Transducers, monitored platen descent during consolidation. The instrument was powered by a 10V output from a conditioning card supplied with a 30V DC supply. The output was traced by a J.J. Instruments CR 450 chart recorder to keep a permanent record of platen movement. The other five LVDTs were manufactured by RDP Electronics Ltd; each used a type D-11 conditioning module, powered with 30V DC, to provide the ac supply and convert output voltage to a dc signal. A 200mm stroke type D5/4000C was used to survey the surface of the clay block and granular layer prior to testing; two 100mm stroke type D5/2000 were used to monitor footing position; two 50mm stroke type D5/1000C were placed to measure heave of the granular material.

Pressure transducers, manufactured by Druck Ltd, were mounted in the back wall of the test box. Two PDCR 53 total pressure transducers were used, each powered by a 10V DC signal and with a working range 0-5 bar. Three PDCR 81/S minature pore pressure transducers were used, each was powered by a 5V DC signal and with a working range 0-7 bar. All the pressure transducers had securing flanges and the mounting arrangement, fully described by Love (1984), ensured each transducer was sealed and located with its face flush with the back wall of the test box.

3.3.2 Calibration

It is good practice to ensure a similarity of conditions during transducer calibration and operation, and so all calibrations were made for the transducers supplied by the same power supply unit used in the laboratory. For all calibrations except that of the load cell, signal output was measured and recorded with the voltmeter used in the laboratory tests. Importantly, it was noticed that following warm up of the LVDT's and load cell, the output signal took several hours to stabilise. As a consequence two measures were taken: the transducers were always connected up to the power supply on the evening before testing of a laboratory sample; calibration of these transducers was never made immediately after warm up.

The long stroke AC250 displacement transducer was calibrated against a 0.5mm graduated metal rule with travelling block. All other displacement transducers were calibrated in a mounting against a micrometer.

The pressure transducers were sealed in a machined brass block similar to the mounting port in the test box, and calibration was made for both load and unload pressures. The total pressure transducers were calibrated against a compressed air pressure; the pore pressure transducers were pressurised via an air/water interface. Linearity of the pore pressure transducer response is dependent on proper deairing of the porous filter stone. The transducers were deaired, together with lead connections, in a desiccator chamber to which vacuum was applied using a Genevac type GRS 12 single stage rotary piston vacuum pump capable of pulling 32ft of water. After about 15 minutes the transducers were transferred into a beaker of deaired water in the chamber, and the vacuum on the dessicator released. This routine was cycled many times over a period of a day as suggested by others, Mair (1979), Gue (1984). Examples of some calibrations are included in Appendix B.

3.3.3 Power unit

All transducers were powered from a triple rail power supply. Signal conditioning of the displacement transducers was with commercially supplied conditioning cards or modules; signal conditioning of the pressure and load transducers was achieved by a series of amplifying chips with the gain set by resistors. Offset control for each signal was from a potentiometer on the output voltage. The power supply and signal conditioning were mounted in a single unit. A multi-way switch allowed operator selection of a single channel ouput. A multi-channel cable connector provided signal output to the data logger. Load or

displacement transducer output selection as feedback to the servo amplifier board was made in this unit.

3.4 Data acquisition

The multi-channel cable connector from the power supply and signal conditioning unit fed the transducer outputs to a 7010 Solatron Minate Analog Scanner. This is a 16 channel multiplexer set to communicate with a 7060 Solatron Systems digital voltmeter. The multiplexer scans the transducer outputs and feeds them in turn to the input terminals of the voltmeter, Figure 3.10. The scanner and voltmeter were controlled by a 380Z microcomputer, manufactured by Research Machines Ltd. A program, written in BASIC, was used to record the voltmeter output. There were some important controlling features to the programming.

The internal structure of the 380Z microcomputer is such that the CPu interfaces direcly with two PIO (parallel input/output), and two I/O ports (A and B) on each PIO may be used to interface to peripheral devices. The program set Port A PI01 to operate in input mode and, by continuous interrogation of the contents of the input register of this port, determined the status of the 8 data bits. Data bit zero was seen as a 'zero' if the voltage to the port was less than 0.8V and as a 'one' if the voltage was greater than 2.4V. A voltage change to Port A PI01 could therefore be used as a trigger to the program. A separate program was written for monotonic and cyclic tests. In all tests, the program took an initial scan of transducer readings for the footing in position before driving. Port A PI01 was then monitored for a change in status.

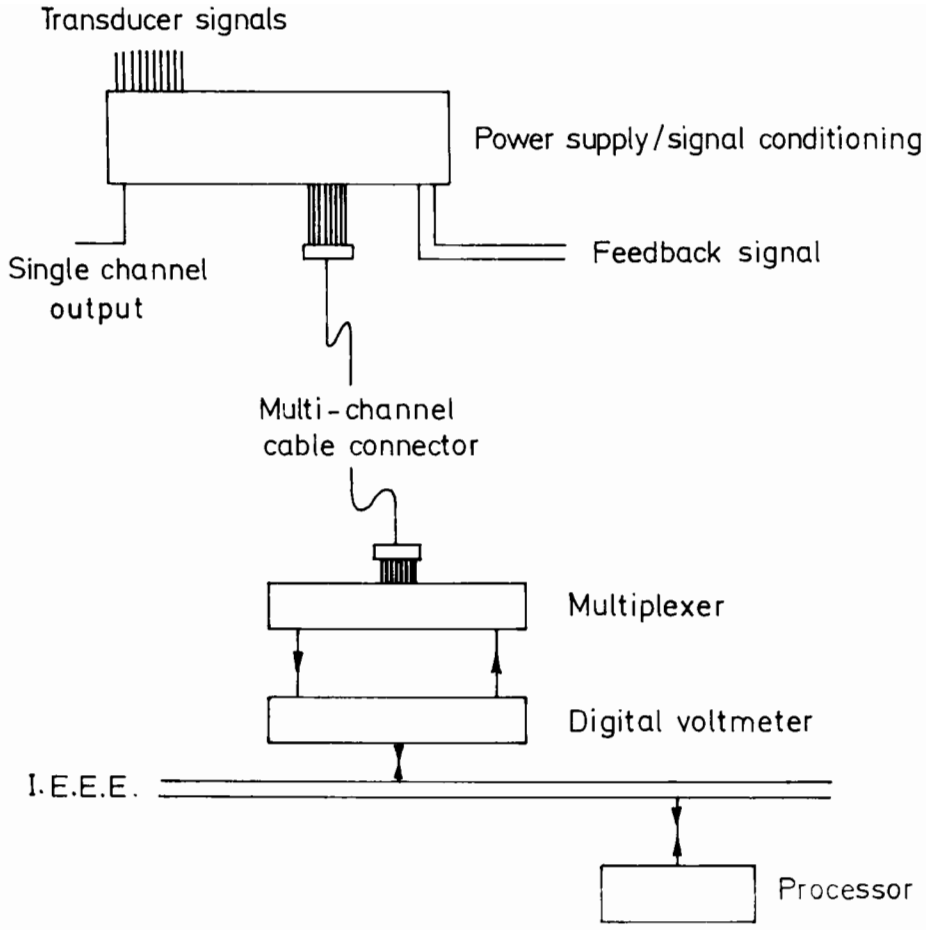

Figure 3.10 Data acquisition system

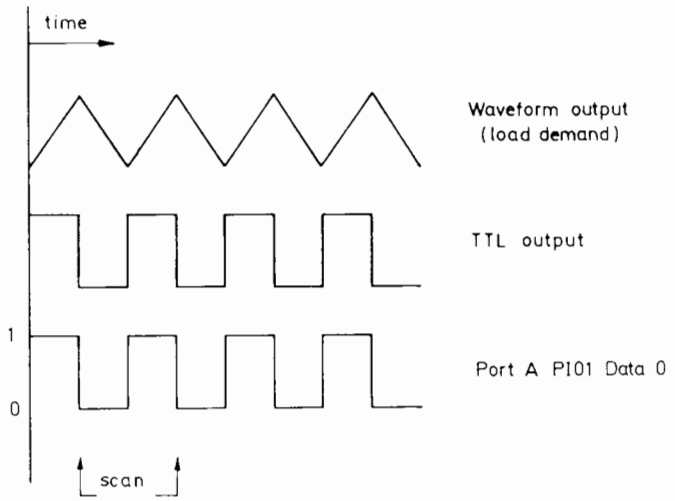

Figure 3.11 Waveform generator output and I/O Port A status with time

A monotonic test was initiated by switching on the ramp generator. A separate output from this same switch caused the voltage on the trigger line to PI01 Port A to be raised, and the program commenced scanning. The transducer channels were scanned in sequence and, for a time of 0.43s for each scan, typically 40-45 series of readings were taken during a drive to 50mm footing displacement. The voltages were read to 'five nines' accuracy. A test of the data acquisition system was made for a constant voltage input from a Time Electronics Ltd 404S DC millivolt source and signal corruption measured to occur at the third decimal place of the voltmeter output in millivolts, which is a very acceptable accuracy for the range of transducer outputs.

A cyclic test was initiated by switching on the function generator. Synchronous TTL output to Port A PI01 was used to trigger the program to scan for a change in status of data bit zero from 'one' to 'zero'. This caused the program to scan at maximum load, Figure 3.11. A scan was made on every peak for the first 20 cycles; every second peak up to 50 cycles; every fifth peak up to 100 cycles; every twenty-fifth cycle thereafter. Interaction with a key on the keyboard enabled a scan to be made at any peak in additon to this routine, and in some tests selected channels were scanned continuously over two cycles of load application at the very end of a test.

3.5 Photographic measurements

A grid of markers was placed in the front face of the clay sample before testing, see section 4.3.2. During testing a sequence of

photographs was then taken to record any movement of these markers using an Olympus OM 10 camera with motor drive and a 100mm lens. The camera was mounted on a tripod and exposure was by remote release. Kodak Ektachrome 400 ASA film was used. The data reduction technique is fully described by Love (1984); a summary is given below.

The slides were mounted in a modified photographic enlarger and individually projected on to a 300mm x 300mm Summagraphics Bitpad digitising board. On this image, a cursor with fine cross-hairs was used to identify by co-ordinates each marker as well as an array of permanent reference targets. These targets were fixed to the outside face of the inner perspex sheet. From accurate physical measurement of the reference targets in the laboratory, the actual position of each marker in the clay was determined with respect to the array using a program written by Houlsby. This mapping routine accounted for photographic distortions across the image. A comparison of two images allowed the difference in each marker position to be calculated. Displacement vectors of marker movement, together with principal strain magnitudes and directions, were then computed.

It is important to comment on possible sources of error arising in the data reduction:

- measurement of the reference target array

- accuracy of cross-hair intersection on the exact marker and target positions on the projected image

- movement of the projected image during digitising

- refractive errors in the perspex face of the test box and the cursor viewfinder

- image length to actual length scaling factor

The technique was applied in this study to identify the extent and nature of subgrade deformations and the results of these measurements are presented and discussed in section 6.2. While the sources of error identified above are such that it is difficult to calculate their magnitude with any confidence, an estimation of the cumulative effect on evaluated strains is proposed in the section.

CHAPTER 4

EXPERIMENTAL PROCEDURE

4.1 Introduction and test programme

Assembly of the test box and consolidation of a saturated clay sample from a slurry is described. Pressure increments were applied according to a routine schedule to produce weak overconsolidated samples to one of two nominal undrained strengths, c_u= 6kN/m^2 or c_u= 9kN/m^2.

Preparation of each sample for testing involved compacting a layer of granular material to a nominal thickness of 75, 100 or 125mm on the surface of the clay. In reinforced tests a single layer of geogrid reinforcement was placed at the interface between the clay and the granular layer. During testing each sample was loaded by a dual footing to a footing penetration of 50mm. Testing consisted of either cyclic loading to a constant maximum contact pressure, or a single monotonic drive at constant speed that was repeated after repair of the generated rut. One test was repeated for nominally identical conditions.

The test programme sequence is given in Table 4.1. A reference code is established to identify each individual test and a summary of the test programme presented in Table 4.2, where each code defines

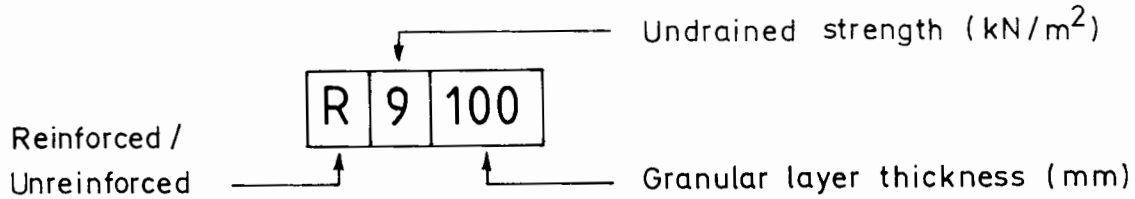

Table 4.1 Test programme sequence

c_u \ H	75mm	100mm	125mm
$6kN/m^2$		h	b,e,m,n,o
$9kN/m^2$	c	f,g,k,l	a,d

Table 4.2 Test programme summary

Sequence	Test code	Comment
a b c d e f g h	R9125 R6125 R9075 U9125 U6125 R9100 U9100 R6100	Cyclic tests
i j	MPS9 MPS6	Material properties samples
k l m n o	R9100M U9100M R6125M U6125M RR6125M	Monotonic tests (repeatibility)

4.2 Sample consolidation

4.2.1 Slurry mixing

Prior to front face assembly of the box, the inside duralumin walls and perspex front face of the test box were thoroughly cleaned. The pressure transducer mountings were also cleaned and all threaded connections checked. The total pressure transducers were then mounted in position. To limit side wall friction on the sample a film of Castrol water pump grease was applied to the four internal sides of the box. This has been observed to be superior to silicon grease, Mair (1979). Care was taken to avoid placing any grease immediately above the mountings for the pore pressure transducers so that the porous ceramic filters did not become clogged during consolidation.

The next stage involved bolting together the front face components. A liberal bead of viscous rubber sealant was run along the front face 'O' ring, and the thin inner perspex sheet placed in position against this seal. The heavy perspex outer face to the box was then lifted to seal against this inner sheet. Finally the mild steel front frame was raised and bolted in place against the perspex. The top platen was always lowered the full length of the ram stroke into the box to check free movement without fouling the walls before the reaction pillars were positioned either side of the box and fixed together with tie rods. Final preparation involved filling the base drainage channel with water and fitting the bottom porous plastic sheet, which had been saturated, in the box.

The clay, a Speswhite Kaolin powder, was reconstituted to a slurry at a moisture content of 120%, which is approximately twice the liquid limit. The slurry was mixed under vacuum in a commercial mixer manufactured by Winkworth and described by Gue (1984). Typically the slurry was mixed for 2 hours under a partial vacuum of 0.8 bar to deair the liquid without causing a boiling action. This value is slightly greater than the 0.5 bar chosen by others, Mair (1979), Francescon (1983), and was made possible by a very good seal to the mixer. The water and kaolin powder were briefly mixed by hand during filling of the mixer to promote a smooth initial slurry, and consequently no kaolin powder was observed to be sucked from the mixer while the vacuum was applied. At the end of the mix, vacuum was released slowly over a five minute period. Slurry was then pumped into the test box using a pneumatic diaphragm pump, manufactured by the Warren Rupp Co., which worked from the laboratory compressed air supply. Four separate mixes were required to prepare a sample.

The three pore pressure transducers were installed during the mixing process when there was sufficient slurry to cover the mounting locations, which had been taped over on the inside wall to prevent leaking. An installation procedure was adopted which maintained saturation of the porous filter stone. The transducers had been subject to the cyclic deairing routine described in section 3.3.2, however a last cycle involving vacuum release for the transducers submerged in deaired glycerene instead of water was specifically included. The intention was not to replace the water in the saturated stone, but to promote a slightly more viscous coat to it during transferral to the test box.

Installation involved removing the tape and locating the transducer. It is conceivable this action could have led to trapping air in front of the transducer, which was avoided by gently drawing slurry in contact with the stone to the surface. With the pore pressure transducers mounted in position, filling of the test box continued to the required height of slurry.

4.2.2 Consolidation schedule

Drainage of the sample was not permitted during the mixing process. The initial volume of slurry was determined in accordance with the one dimensional consolidation line in v:ln p′ space of Speswhite Kaolin, for the mean effective pressure at the end of consolidation. A top seal was made to the sample with a second saturated porous sheet, described in section 3.1.2. Sample drainage was then permitted. The top platen was lowered to contact, and a first consolidation increment applied. Top and bottom drainage was always maintained to the same head of water to avoid establishing an hydraulic flow through the sample. Experience indicated a pressure of $20kN/m^2$ could be easily accepted. Subsequent pressure increments were applied according to an established schedule described by Love (1984) and illustrated in Figure 4.1. During consolidation movement and tilt were measured, and platen descent continuously monitored by a long stroke displacement transducer output to a chart recorder.

Samples were prepared to two nominal undrained strengths $c_u \simeq 6kN/m^2$ and $c_u \simeq 9kN/m^2$. A final consolidation pressure of $110kN/m^2$ or $220kN/m^2$ was applied to the platen respectively. The final increment was held for

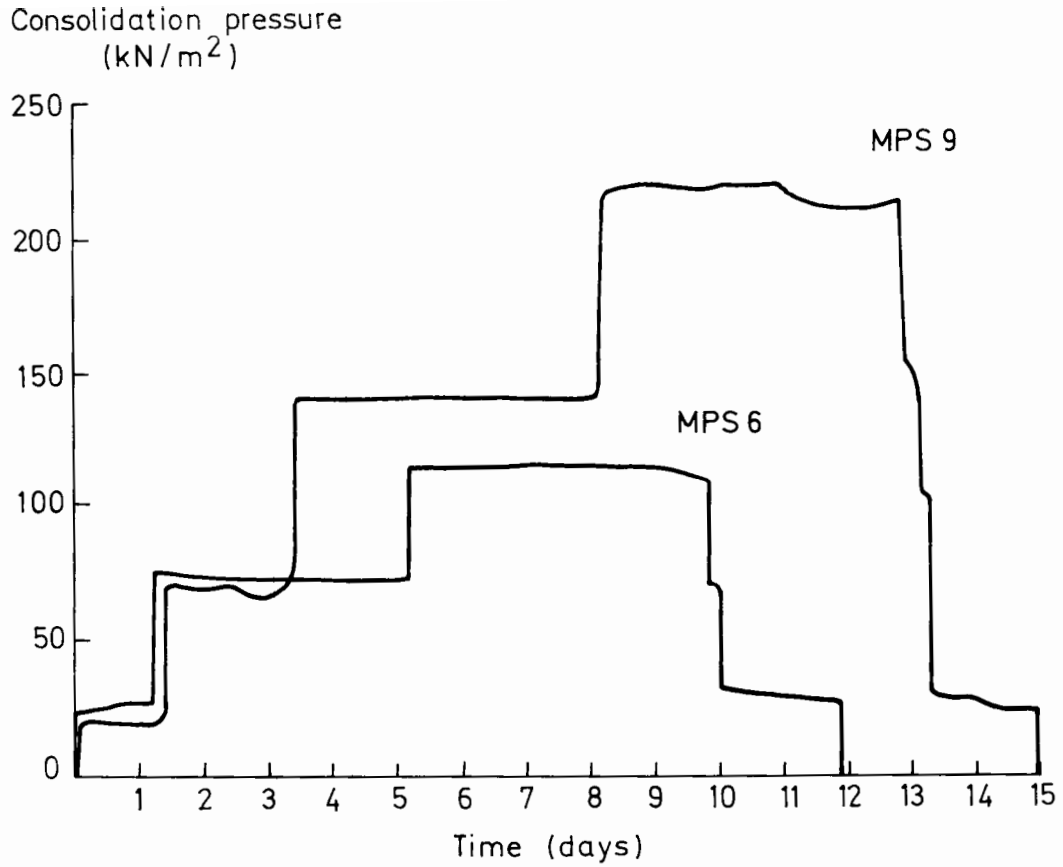

Figure 4.1 Consolidation schedule

five days. At the end of this period the bottom drainage taps were closed and the pressure was released slowly in a number of discrete stages, to avoid inducing cavitation, to a pressure of 30kN/m^2. No unloading stage exceeded 80kN/m^2, and each was separated by a period not less than two hours. The sample was maintained in this overconsolidated state for two days, after which the pressure was released to zero. Sample swelling continued under platen self weight alone for one day, after which the platen was raised and further swelling under water only for 72 hours allowed, until the rate of swelling was sufficiently low that it would not affect testing.

The consolidation schedule described here was strictly adhered to so that all samples were nominally identical, notwithstanding variations of initial slurry volume and consolidation pressure settings. Typically the top platen would tilt slightly out of horizontal during consolidation by ±2mm from the mean; a worst case of ±3.25mm was measured. During swelling, heave of the sample was observed to be generally uniform across the width of the box, which had not been the case for the previous study. Whether this is directly attributable to the use of water pump grease instead of silicon grease for side wall lubrication is difficult to confirm. Swelling under top drainage only promoted a small decrease of moisture content with depth, and therefore an increase in strength with depth, not untypical of that observed in the field. The consolidation and strength properties of the kaolin samples are fully discussed in section 5.1.

4.3 Test preparation

4.3.1 Clay subgrade

Clear access to the sample in the test box was achieved after raising the top platen by complete removal of the ram mounting assembly using an overhead crane. In preparation for testing each sample was surveyed and a series of markers placed in the front face of the clay.

The clay markers comprised a grid of approximately 900 stainless steel 2mm diameter ball bearings which had been previously positioned on a greased paper sheet to a 20mm square spacing. They were transferred to

the clay on the day before testing, according to the procedure described below. Water covering the sample was removed, the front frame to the box was unbolted and removed, and the 25mm thick perspex sheet lifted out. The flexible inner sheet was then eased back from the sample. The markers were placed onto the exposed vertical front face of the clay sample by bringing the paper sheet into contact with the clay and applying a light pressure to seal the markers in it. Following this the paper was peeled off, the front face and frame repositioned and the sample flooded again to a depth about 25mm. Typically a sample was exposed for about fifteen minutes during this operation. For the weak clays the box assembly was tilted back through 15°.

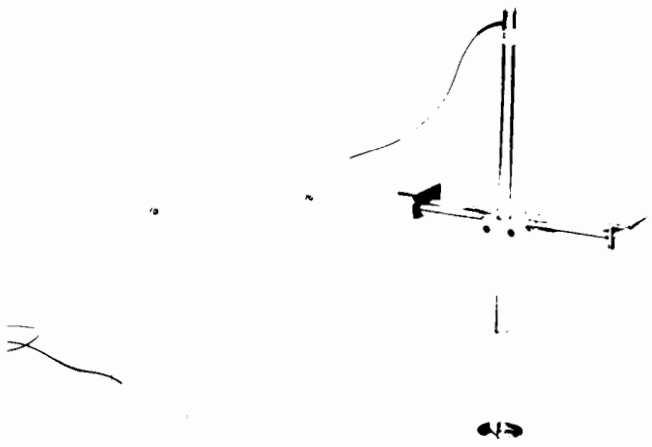

Plate 4.1 Straight-edge and LVDT jockey

On the morning of testing, each sample was surveyed using a displacement transducer mounted in a travelling jockey to establish a contour profile of the surface. Following this, three pre-test measurements of the undrained strength of the clay were made with a Pilcon hand vane at a mid-vane depth of 55mm, Figure 4.3(a), and the sample then trimmed flat to a standard height of 400mm for all tests using a travelling straight-edge, Plate 4.1. The Pilcon vane was first developed to make in situ measurements in undrained clays, Serota and Jangle (1972). The vane spring was calibrated by applying a known torque and recording the corresponding deflection on the dial face, from which a value of undrained shear strength was determined in accordance with BS1377:1975 (see Appendix B). Interpretation of vane readings is discussed in section 5.1.3.4.

4.3.2 Granular layer

A granular layer was compacted over the clay to a finished thickness of 75, 100 or 125mm. The granular material comprised a combination of sands and gravels, and was placed at a moisture content of 10%. A full description of the material and property tests is given in section 5.3.

Compaction was made in a series of 25mm lifts using a 250mm x 150mm board, and a 1kg hammer. Loose material was lightly tamped level. Following this the board was struck five successive blows, and the action repeated for three passes across the surface. The finished layer was surveyed using the same displacement transducer and travelling jockey arrangement.

It was important that the granular layer thickness and material density did not vary greatly between each test, and summary of all tests indicates a highly desirable repeatibility, Table 4.3. Interestingly, and in accordance with the observations of Potter and Currer (1981) for a geotextile, the reinforcement was observed to have no significant effect on the measured compaction densities.

Table 4.3 Granular layer densities

Test conditions	γ_{dry} (kN/m^3)	
	mean	S.D.
Reinforced	18.366	0.202
Unreinforced	18.677	0.262

4.3.3 Grid reinforcement

In the reinforced tests, a layer of geogrid reinforcement was placed directly on to the clay surface before compaction of the granular layer. The geogrid was a quarter scale Tensar SS2 type material, and is fully described in section 5.2. The dimensions of the test piece, 1000mm x 300mm, were such that it represented a section across one manufactured roll width, Figure 4.2.

Markers were attached to every third node along the edge of the grid, Plate 4.2, which was visible through the front perspex face of the

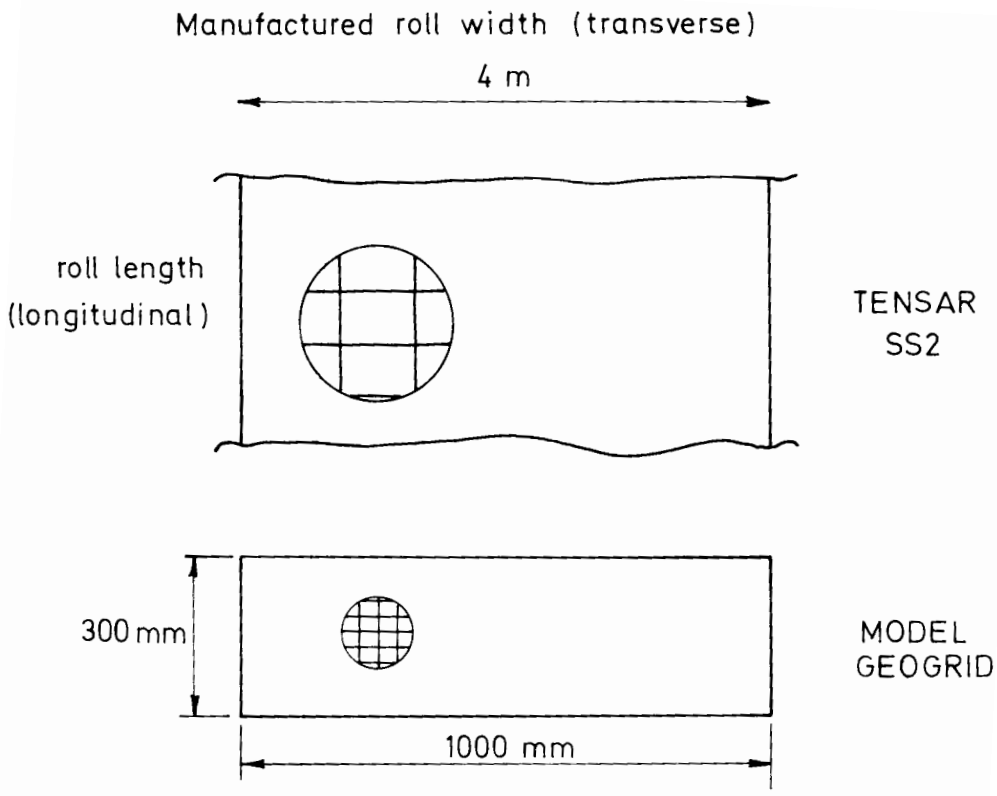

Figure 4.2 Test piece dimensions

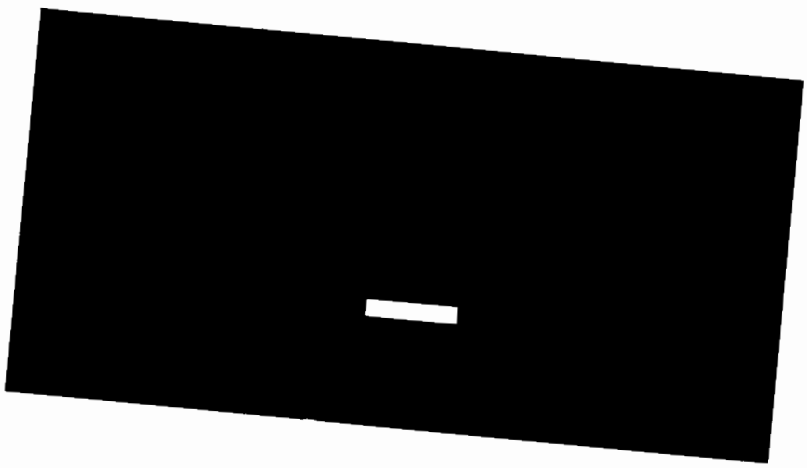

Plate 4.2 Grid test piece

test box. Placement of the grid caused the greased flat face of the markers to rest against the perspex. It was intended that these markers would locate the profile of the grid during the course of the test, however only partial success was obtained. Many of them became obscured by clay, and only those at the ends of the grid remained visible.

4.4 Test procedure

Measurements of footing load and position, together with surface heave of the granular layer and the pressure transducer outputs were made for each test. Before testing, the control and data acquisition systems were checked during a 'trial run' for the footing supported in the calibration frame. Following this the Olympus camera was positioned to take a sequence of photographs through the front face of the test box. During the later tests a video was also made.

Then, with the footing fully retracted, the loading assembly was lifted across the top of the test box and bolted on to it. Four displacement transducers, supported by travelling jockeys, were positioned in the box. Two made direct contact with the dual footing, and two were placed on light metal dishes resting on the granular layer at a distance of 125mm from the footing centres. Following this, the footing was lowered to a start position in contact with the granular layer using a null offset command to the servo amplifier board. A reading of transducer outputs was taken and the scanning program initialised to monitor continuously for the test start.

A cyclic test was initiated by switching on the function generator. Typically between 50 and 200 cycles of load were taken to failure. Failure was considered for a serviceability criterion of a footing penetration greater than 50mm in the model. The test was then stopped and the footing retracted.

A monotonic test was initiated by switching on the ramp generator. A test lasted 20 seconds, which was the time to drive the footing to 50mm penetration. It was then retracted and the loading assembly unbolted and removed. A fixed quantity of additional granular material was placed in the two ruts which had been formed. This was compacted in two separate lifts to nearly the original level. The test was then repeated for a second monotonic drive of the footing as before. The aim was to assess the benefits of rut repair after complete and sudden failure.

4.5 Post test measurements

Immediately after each test a number of moisture content determinations and strength measurements were made according to a fixed routine. The sequence of testing is described below: it allowed a comparison to be made both between individual test samples, and importantly between each test sample and a well defined investigation sample consolidated specifically for testing of material properties.

A moisture content determination was made for several positions along a centre line section in the granular layer, Figure 4.3(b). The

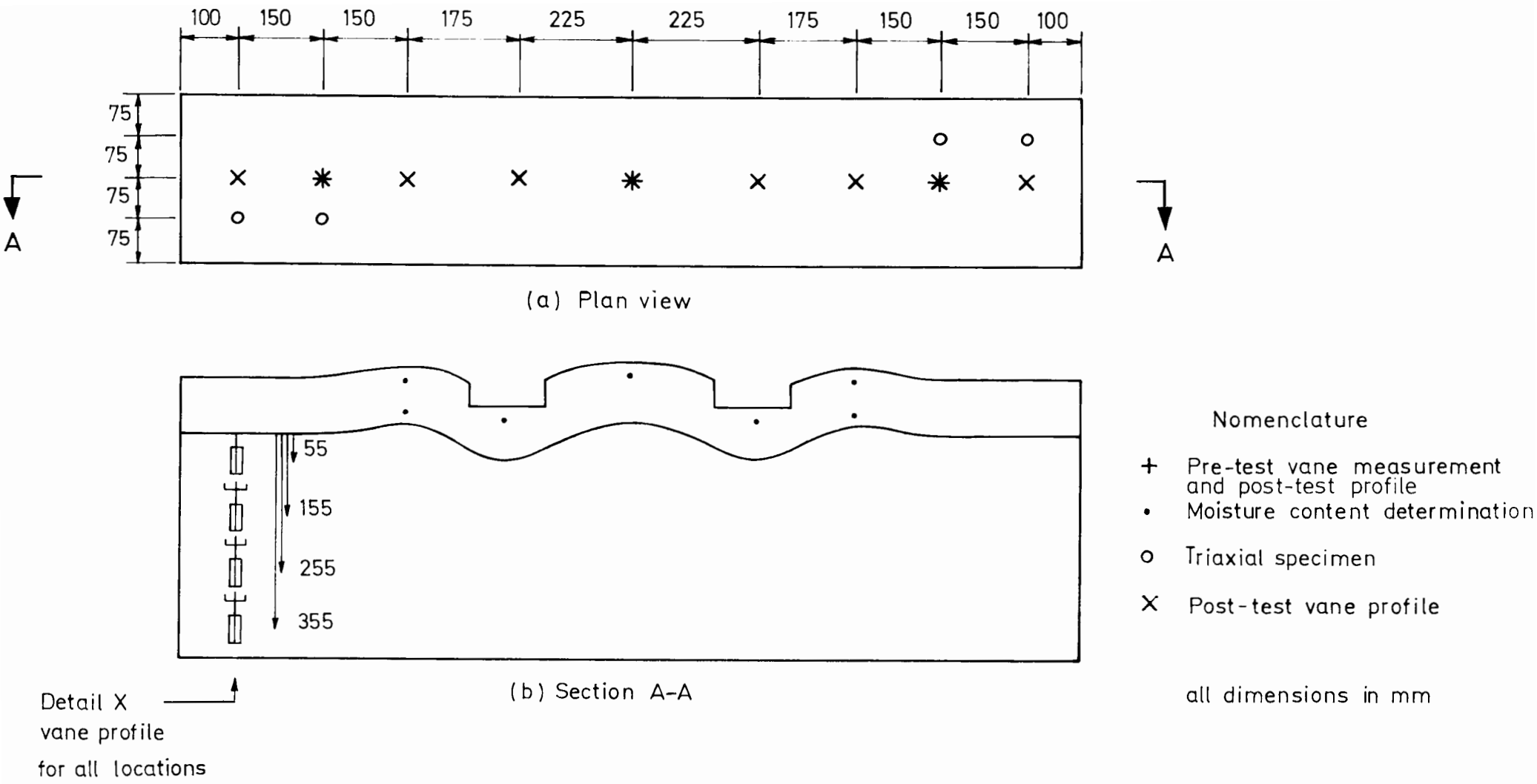

Figure 4.3 Sample measurement locations

granular material was then excavated. In reinforced tests, the position of the geogrid in relation to the deformed clay subgrade was observed. Thin walled U-38 triaxial sample tubes were then inserted at four positions in the test sample to a depth of 120mm. Pilcon vane shear strength tests were made at seven locations, Figure 4.3(a). A profile of four separate readings at depths 55, 155, 255 and 355mm was taken. Finally the triaxial samples were removed and sealed. Unconsolidated undrained tests were made on these samples without measurement of pore water pressures, typically on the day after extraction. A full description of sampling techniques and measurement procedures used is given in section 5.3.1.1 for the investigation samples. For the very severe deformations of the samples subjected to two monotonic drives, the three central vane profiles were not made.

4.6 Repeatability

It is desirable practice to check the repeatability of results for nominally identical test conditions. A repeat was made of a reinforced test, for monotonic loading and with rut repair, on the weaker subgrade with a granular layer thickness 125mm: test code RR6125M.

CHAPTER 5

MATERIALS PROPERTIES

5.1 Clay

5.1.1 Introduction

The clay used in this study was Speswhite Kaolin, supplied as a powder by E.C.C. International Ltd. Index tests and a determination of particle specific gravity were made in accordance with BS1377:1975, and are reported in Table 5.1.

Loading of a granular layer over a soft clay is governed largely by the clay strength. Therefore a detailed knowledge of the subgrade properties is important to an understanding of the model behaviour. For this reason samples MPS6 and MPS9 in the test programme were prepared specifically for testing of material properties, and consolidated

Table 5.1 Review of some Speswhite Kaolin properties

Reference	LL(%)	PI(%)	G_s
Fannin (1986)	62	31	2.61
Atkinson and Evans (1985)	63	34	-
Gue (1984)	65	31	2.60
Francescon (1983)	69	31	2.61
Atkinson et al. (1984)	65	30	2.65

to the two nominal test sample strengths according to the same schedule as for all other samples.

Consolidation behaviour and derived kaolin properties are reported in section 5.1.2. Profiles of undrained shear strength measurements and moisture content determinations with depth for the samples are discussed in section 5.1.3. Triaxial tests and critical state parameters are reported in section 5.1.4.

5.1.2 Consolidation properties

5.1.2.1 Coefficient of consolidation

The high permeability of the clay permits a rapid sample consolidation. Excess pore pressures, lateral total pressures and change in sample height during consolidation are plotted against time for sample MPS6, Figure 5.1. Immediate pore pressure response to loading was measured to be in the range 92-100% of the applied increment, indicating small friction losses in the hydraulic rams to the top platen. Typically no dissipation of pore pressure was measured at these transducer locations close to the centre of the slurry sample during the first increment, and full dissipation occurred only in the final increment. At the end of the final increment on this sample one pore pressure transducer began to exhibit a poor agreement with the others. However in response to sample unloading and throughout swelling it behaved in agreement. Calibration of the transducer after removal indicated a good linear response.

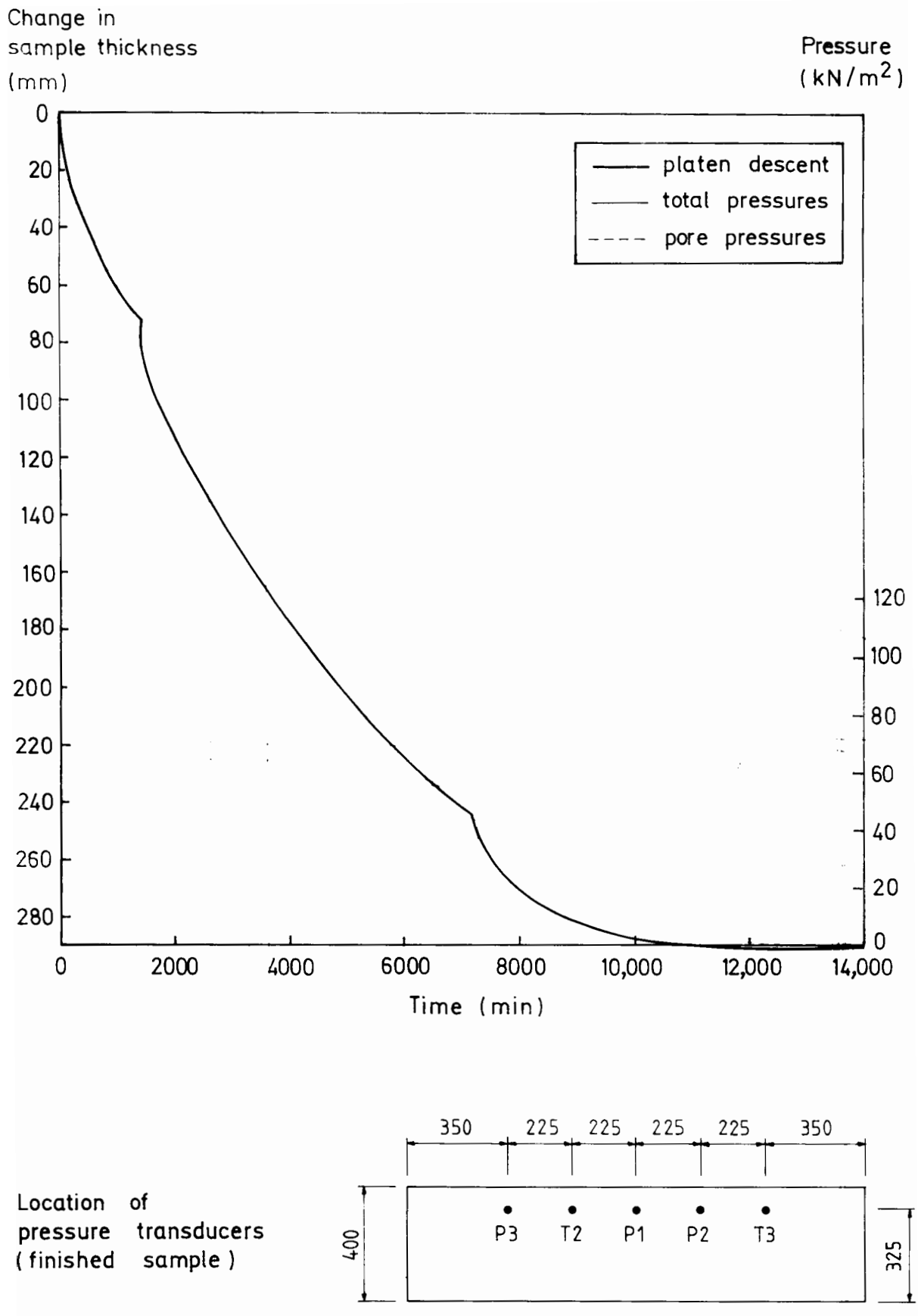

Figure 5.1 Sample MPS6 consolidation

Associated with high permeability is a susceptibility to cavitation at large negative pore pressures. Cavitation is the partial vaporisation of pore water at negative pressures less than -1 atmosphere ($100kN/m^2$), which may cause a reduction in measured sample strength. Mair (1979) reports that cavitation effects in triaxial samples are less significant in large samples and for lower confining stresses less than $400kN/m^2$. In this study pore pressures during the unloading stages were measured to be not less than $-60kN/m^2$.

Values of the coefficient of consolidation c_v were calculated for the last increment of load on samples MPS6 and MPS9. Good agreement is observed for these large test box values and some normal consolidation oedometer test results for a Speswhite Kaolin, after Gue (1984), illustrated in Figure 5.2. Also included are values of c_v calculated for isotropic consolidation under bottom drainage only of triaxial samples from these two material properties samples (see 5.1.4 below). The reported values are for those triaxial samples at confining pressures p'_o in excess of any previous maximum consolidation pressure p'_{max}, and it was assumed that the ratio of sample height to diameter remained unchanged. Interestingly, in a discussion of consolidation Bishop and Henkel (1962) argue that a higher value of c_v will be measured under conditions of no lateral strain, as in the oedometer. However these results would appear to indicate the difference is not significant.

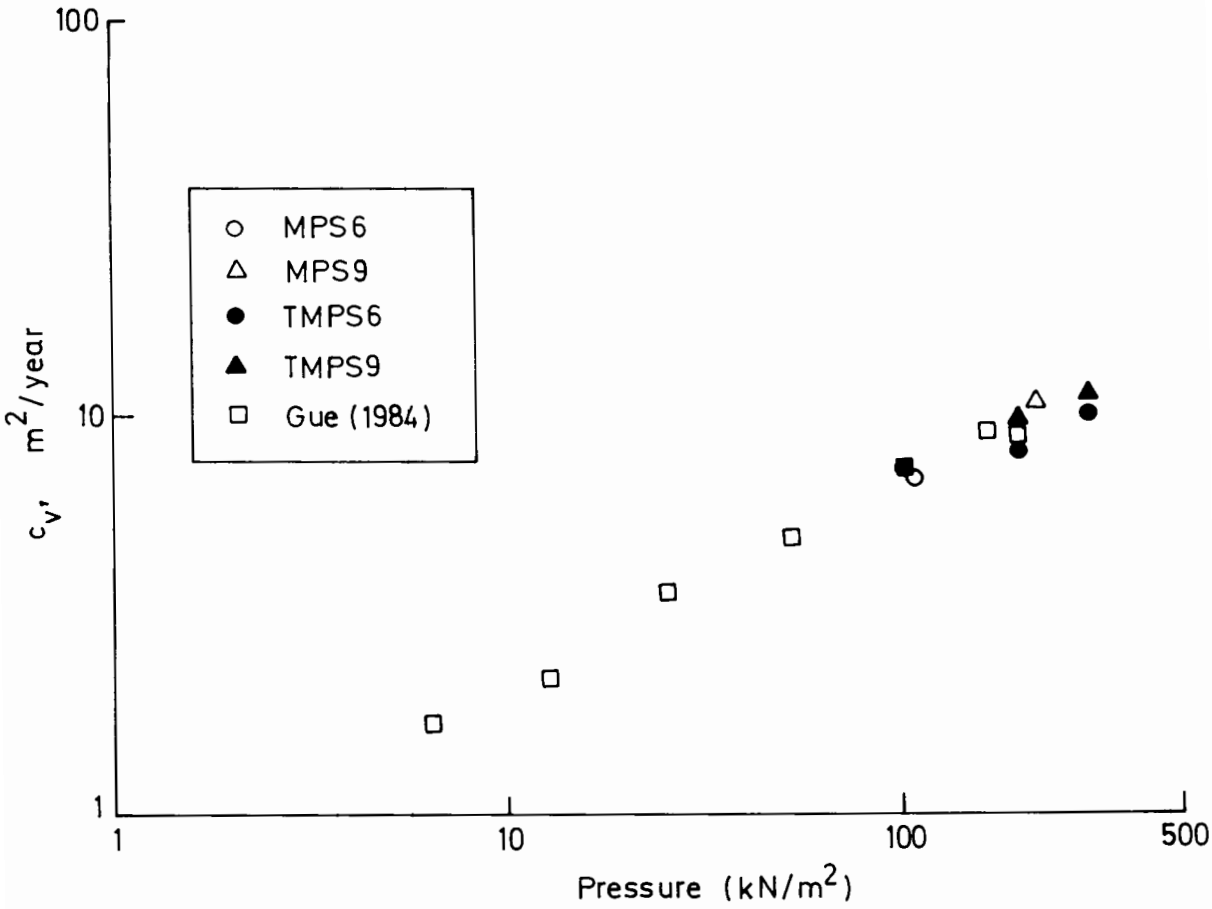

Figure 5.2 Variation in c_v with consolidation pressure

5.1.2.2 Variation of K_o

Experimental values of K_o for one dimensional normal consolidation were calculated from the final consolidation increment on samples MPS6 and MPS9. Some scatter was observed with a range of values 0.59 - 0.69, and a mean K_{nc} = 0.64. An approximate expression for K_o is widely accepted as:

$$K_o \simeq 1 - \sin\emptyset' \qquad (5.1)$$

which would indicate a value of $\emptyset' \simeq 21^o$ for K_o = 0.64

Wroth (1975) derives a relationship between K_o and lightly overconsolidated clays such that, for $1 < OCR < 5$,

$$K_o = OCR.\ K_{nc} - \frac{\nu'}{1 - \nu'}\ (OCR - 1) \qquad (5.2)$$

For heavily overconsolidated clays, where $OCR > 5$,

$$m \left[\frac{3\ (1 - K_{nc})}{1 + 2K_{nc}} - \frac{3\ (1 - K_o)}{1 + 2K_o} \right] = \ln \left[\frac{OCR\ (1 + 2K_{nc})}{1 + 2K_o} \right] \qquad (5.3)$$

and m, the gradient of the rebound line, varies linearly with plasticity.

During swelling, samples were unloaded to a vertical pressure typically of $30kN/m^2$ and held for a period of two days. The variation of K_o with overconsolidation ratio was calculated and is illustrated in Figure 5.3. OCR is defined in terms of σ'_v throughout, and equations 5.2 and 5.3 are plotted for $K_{nc} = 0.64$, $m = 1.90$ and $\nu' = 0.32$. Also included in the figure are data reported from one dimensional consolidation and swelling of a Spestone Kaolin after Nadarajah (1973), for which K_{nc} was also measured to be 0.64, and good agreement is observed.

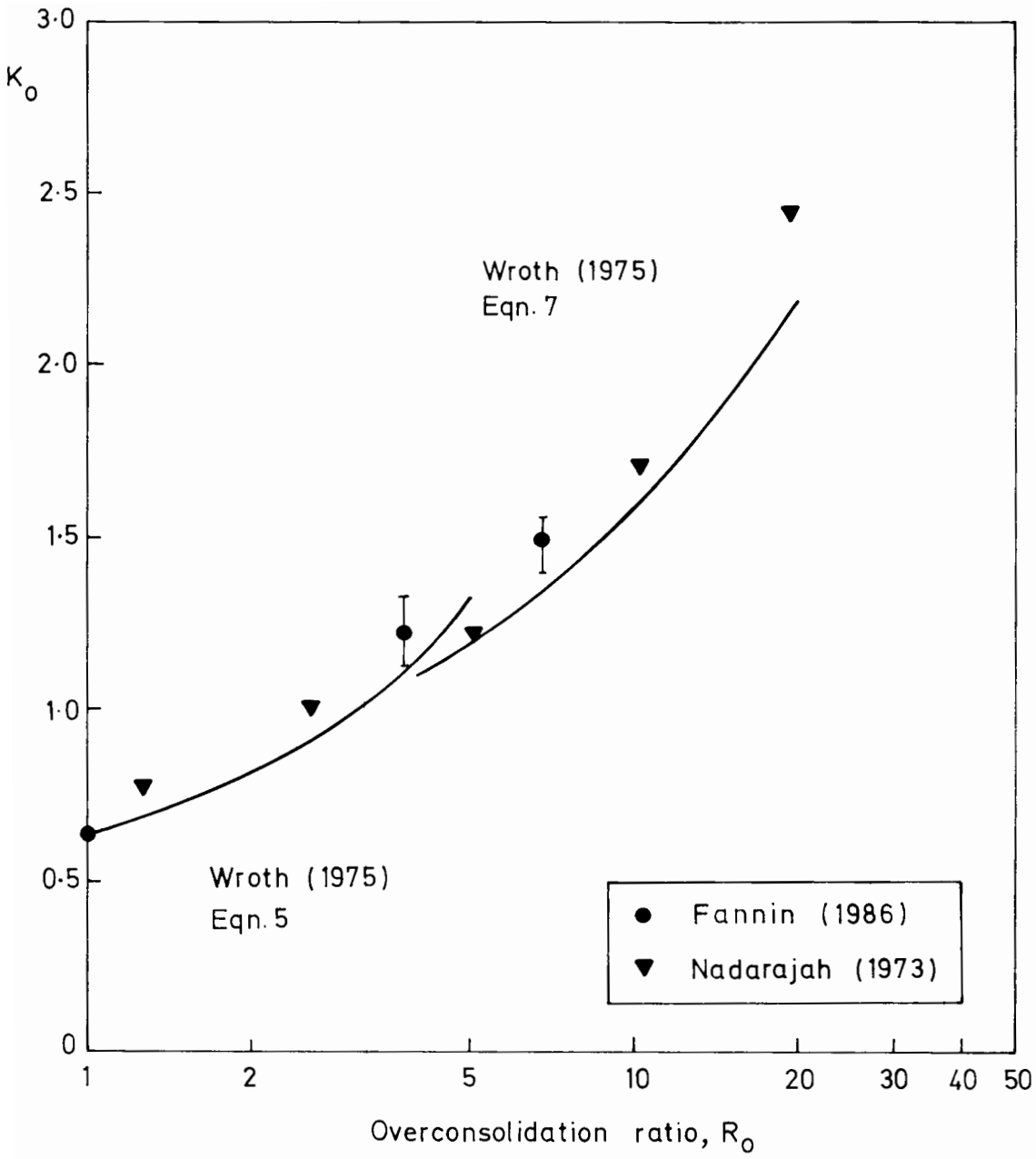

Figure 5.3 Variation in K_o with overconsolidation ratio

5.1.3 Strength properties

5.1.3.1 Sample investigation procedure

The locations and type of measurements made on the material property samples MPS6 and MPS9 are illustrated in Figure 5.4. The sequence of testing is described below.

Lightly oiled, thin-walled triaxial tubes were inserted to a depth of 120mm. These essentially undisturbed samples were extracted after all following measurements had been completed (nearly 3 hours later) and sealed with wax. Unconsolidated undrained tests (without pore pressure measurements) were made for direct comparison with vane strength measurements. Consolidated undrained tests with pore pressure measurement were carried out to establish fundamental clay properties.

A profile of undrained strength with depth was recorded for vane measurements at four depths. The vane was always inserted vertically to a mid-vane depth of 55mm. For the deeper measurements a 32mm diameter hole was augered to depths of 100, 200 and 300mm and an extension to the vane used. Readings were always made at a vane rotation speed of 1 rev/min. The front face to the test box was then removed to expose the sample. Further vane measurements were made on the sample longitudinal centre line with the instrument inserted horizontally. Four such readings were taken at two locations. Moisture content determinations were also made across two transverse sections (a central and a side section).

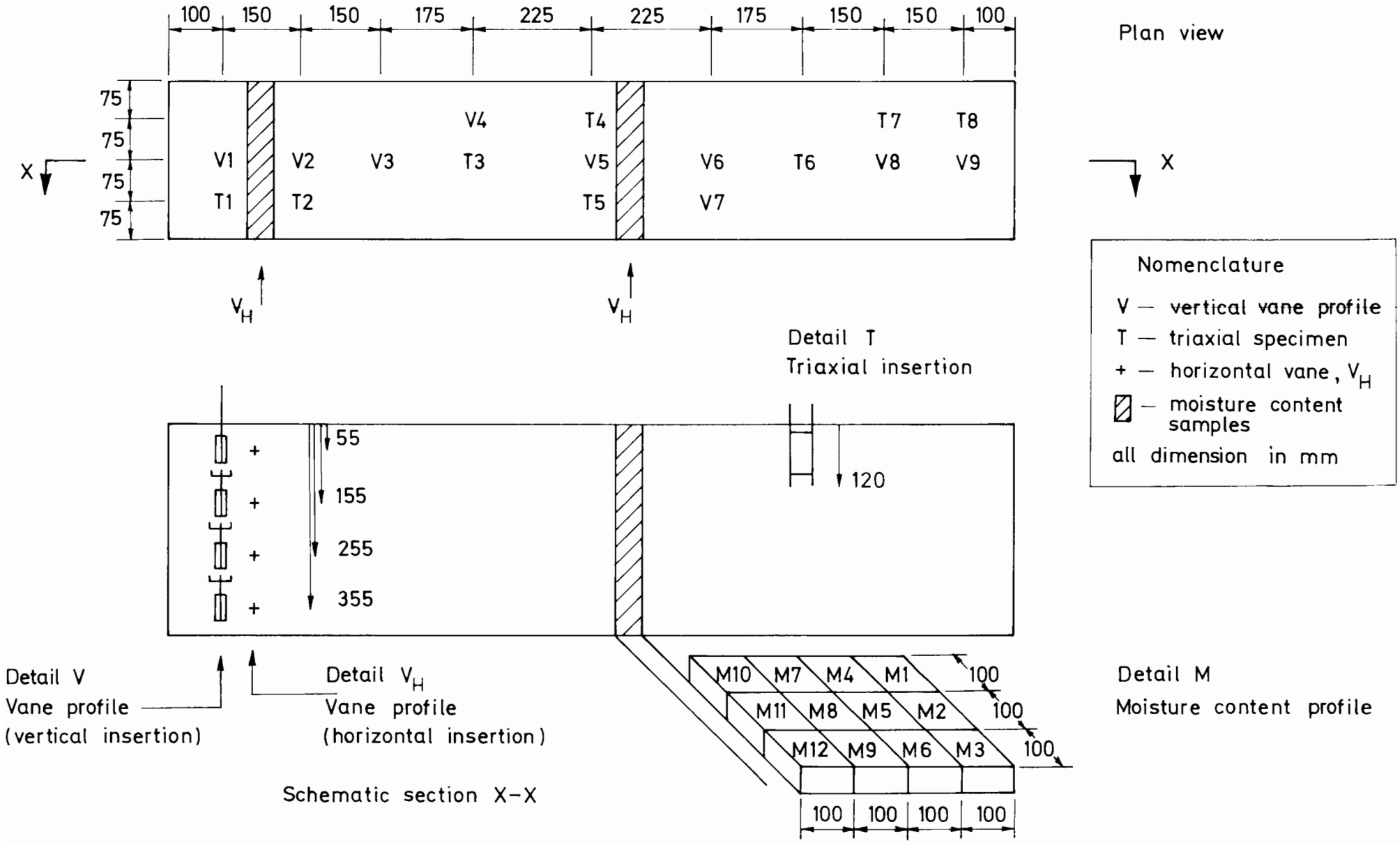

Fig. 5.4 Sample investigation : measurement locations

5.1.3.2 Strength and moisture content profiles.

A strength profile with depth for each of the material property samples is presented in Figure 5.5. The curves are plotted for a mean of the seven vane strength measurements (vertical insertion) along the sample longitudinal centre line. There is a small though not significant variation in strength at any depth, and strength is observed to increase with depth.

A profile of mean moisture content determination is presented in Figure 5.6. A general decrease of moisture content is observed with depth which reasonably corresponds to a period of swelling under top drainage only. There is a small variation in measured values between the side and central sections.

Nageswaran and Houlsby (1982) report that a non-uniformity of strength across a sample can occur if radial drainage is allowed during consolidation, when a stiff crust is promoted close to the boundaries and a relatively softer core develops. In this study drainage for the rectangular samples was vertical only. The variation of strength across the sample taken from vane measurements is given in Table 5.2, and indicates no significant increase in strength near to the side walls of the test box.

A standard 'index' value of undrained strength was assigned to each test sample using the strength profile curves of the material property samples, Figure 5.5. The approach is slightly modified from that first

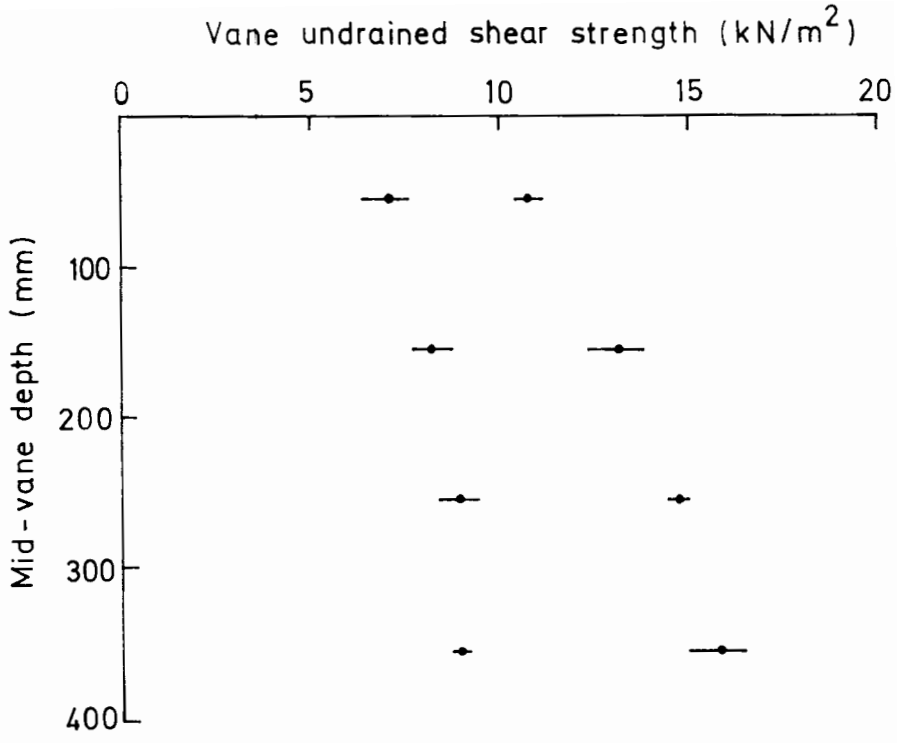

Figure 5.5 Variation in undrained strength with depth

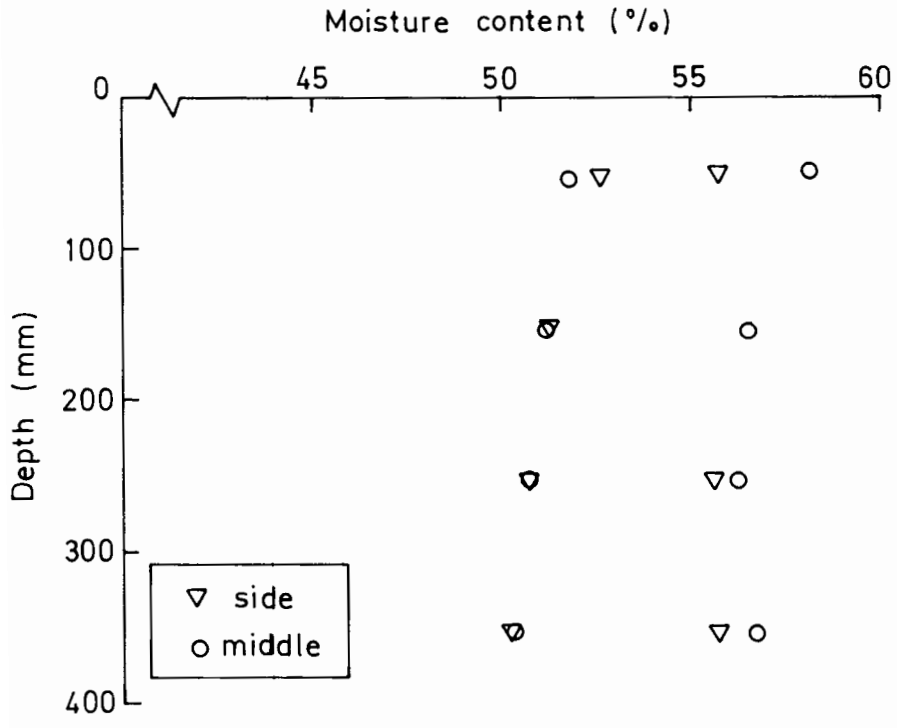

Figure 5.6 Variation in moisture content with depth

Table 5.2 Undrained strength with vane position

Test code	Vane depth (mm)	Vane location V3	V4	V5	V7
MPS6	55	7.3	7.4	7.1	6.7
	155	8.3	7.9	7.6	7.0
	255	8.8	9.0	8.8	8.3
	355	9.2	8.8	8.8	8.7
MPS9	55	10.5	11.1	11.1	10.8
	155	12.3	13.9	13.5	13.4
	255	14.4	15.7	14.8	14.2
	355	14.9	14.1	16.4	14.7

Notes

(1) Unless otherwise stated, all units in kN/m^2
(2) Vane locations from Figure 5.4

described by Love (1984). Three measurements of vane strength were always made on a test sample at a mid-vane depth of 55mm before it was trimmed to a height of 400mm for testing. However the amount of clay removed was not the same for each test sample because of small differences in the initial slurry volume and consolidation pressures. These measured values were therefore corrected for the quantity of trimmed clay. This was achieved by a translation mapping of the strength profile. The increase of strength with depth for any test sample was assumed to be the same as that of the corresponding material property strength curve established in Figure 5.5, which was then translated to match the average of the three values measured at a mid-vane depth of 55mm before the test. Knowing the height of clay removed during trimming, the appropriate strength 55mm below the surface of the trimmed

Table 5.3 Test sample index strengths

Test code	Vane location V2	V5	V8	Index strength
MPS6	6.4	7.1	7.3	6.9
MPS9	10.5	11.1	11.1	10.9
R9125	11.3	11.1	10.7	11.0
R6125	7.0	6.8	6.7	6.9
R9075	12.0	12.0	11.8	11.9
U9125	9.2	9.9	9.4	9.9
U6125	5.9	6.3	6.3	6.2
R9100	10.3	9.1	10.0	9.9
U9100	9.7	9.7	11.5	10.4
R6100	7.0	6.9	7.1	7.1
R9100M	10.5	10.6	11.5	11.2
U9100M	11.0	10.5	10.9	11.0
R6125M	7.1	7.0	7.0	7.1
U6125M	6.1	7.3	7.1	6.9
RR6125M	7.2	7.0	7.4	7.3

Notes

(1) All units in kN/m^2
(2) Vane locations from Figure 5.4

sample could be determined from the profile. In summary, all test samples were therefore described by a strength measurement corrected for the sample height after consolidation, Table 5.3.

5.1.3.3 Comparison of vane and triaxial strength measurements.

It is of interest to compare measurements of undrained strength made with the hand vane to those measured in triaxial compression. Triaxial strengths were determined from 'quick' unconsolidated undrained tests on standard U-38 specimens at a strain rate of $2\%min^{-1}$. Cell pressures used were in the range 100 to $300kN/m^2$. The values presented in Table 5.4 are corrected for changes in sample cross section area and strength of the rubber membrane in accordance with the comments of Bishop and Henkel (1962). A predominantly plastic failure mode was observed, Figure 5.7, particularly in the weaker and less overconsolidated specimens taken from MPS6 and a linear correction for the membrane given by $0.29kN/m^2/\%$ axial strain was applied to the calculated deviator stress, which corresponds to a compression modulus 0.32N/mm for the membrane. A determination of this value is given in Appendix C.

Interpretation of the vane readings was based on BS 1377. Wroth (1984) shows that this standard approach, in assuming a uniform shear stress distribution on the failure surfaces, underestimates the deduced (isotropic) shear strength for a given peak value of torque by a factor of about 9%. For anisotropic conditions the error is slightly less. Since higher strain rates were applied to the failing soil during the vane tests than during the undrained triaxial test, the error is fortunately conservative in that it compensates for greater strengths that would have been measured because of rate effects.

For all test samples except the material property samples, tabulated

Table 5.4 Comparison of vane and triaxial strengths

Test code	Vane location				Triaxial location			
	V1	V2	V8	V9	T1	T2	T7	T8
MPS6	7.6	6.4	7.3	7.1	-	5.9	6.3	7.0
MPS9	10.4	10.5	11.1	10.7	10.8	11.2	10.4	11.4
R9125	11.1	10.5	10.6	11.1	-	-	11.1	11.6
R6125	7.4	6.0	6.5	6.7	5.3	4.8	4.7	5.5
R9075	11.7	10.3	11.0	12.7	14.4	13.9	13.3	12.5
U9125	10.1	8.7	10.5	11.1	10.9	8.3	11.6	12.0
U6125	6.3	5.4	6.2	6.7	6.0	6.1	7.9	5.3
R9100	10.5	10.0	9.5	10.6	11.3	11.0	12.0	13.2
U9100	11.1	9.3	8.5	9.8	11.4	14.4	13.7	11.9
R6100	7.8	6.4	6.9	6.7	8.3	5.8	7.2	9.8
R9100M	10.5	8.2	10.0	11.5	10.4	10.4	11.0	9.3
U9100M	12.2	9.6	10.0	11.7	12.0	9.8	10.2	10.7
R6125M	7.0	6.9	6.4	7.0	5.8	5.2	4.1	-
U6125M	6.4	5.9	6.5	6.6	5.8	4.2	4.0	6.0
RR6125M	8.0	7.4	7.0	7.8	7.8	5.9	5.8	6.8

Notes

(1) All units in kN/m^2
(2) Vane and triaxial locations from Figure 5.4

strengths were measured after the test had been completed. Consequently V2 and V8 strengths were likely to be influenced by some additional disturbance from the pre-test measurements made at these same locations. This would appear to be confirmed by the pattern of vane strengths in the test samples, with V1 and V9 characteristically greater than V2 and V6.

Two consistent trends are apparent from a direct comparison of the vane and triaxial values:

- fairly good agreement is observed between the two groups of measurements

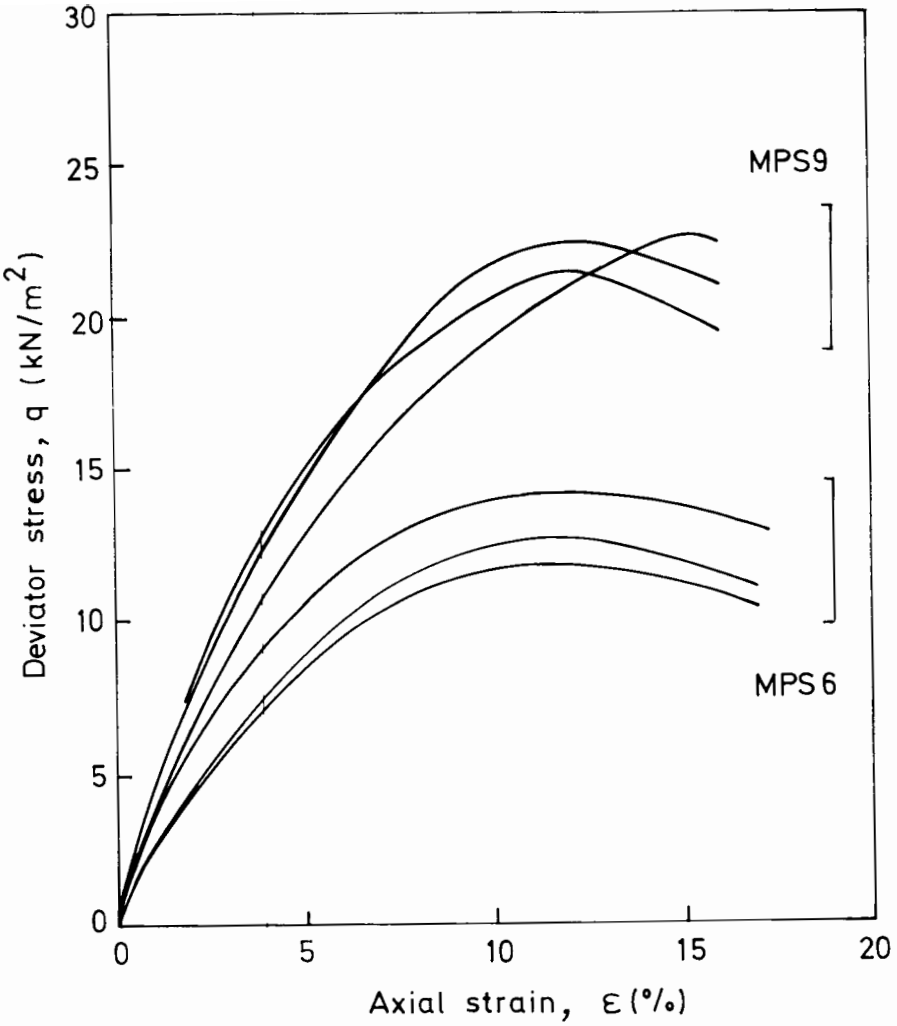

Figure 5.7 Unconsolidated-undrained triaxial test results

- vane strengths show less scatter than triaxial strengths

This repeatibility in the vane measurements is attributed to the simplicity of the test compared to the unavoidable disturbance associated with preparing a triaxial sample, particularly at such weak strengths.

5.1.3.4. Strength anisotropy

Anisotropy in a soil mass may be attributed to a structural anisotropy or a stress induced anisotropy. In the field, a soil will

typically exhibit a change in strength with direction which is a measure of the resistance developed along different planes, and is a consequence of consolidation history as well as stress state. When consolidation occurs under deviatoric stresses, then the plate shaped clay particles tend to align themselves parallel to the plane on which the major principal stress acts, in what could be termed a preferred orientation, Nadarajah (1973). This distinct structural anisotropy promotes a variation of measured strength dependent on the orientation of failure planes. Generally the effects are limited in natural deposits by variations of particle size in the soil matrix and the presence of saline elements.

The variation of undrained shear strength with orientation of the failure surfaces was investigated by comparing measurements of vertical and horizontal vane strength along the sample longitudinal centre-line. The results are presented in Table 5.5. The vane was inserted vertically for measurements V2, V3, V5 and V6, and horizontally for measurements V2.5 and V5.5, Figure 5.4. Typically horizontal vane strength was observed to be 10-20% less than the vertical vane strength which, considering the relative contributions from the surfaces in shear identified by Wroth (1984), suggests that the shear strength on a horizontal plane was somewhat less than 80-90% of the strength on a vertical plane.

Table 5.5 Undrained strength with vane orientation

Test code	Vane depth (mm)	Vane location V2	V2.5	V3	V5	V5.5	V6
MPS6	55	6.4	-	7.3	7.1	7.0	7.0
	155	8.8	7.0	8.3	7.6	6.4	7.9
	255	9.4	7.2	8.8	8.8	7.6	8.3
	355	9.0	7.6	9.2	8.8	7.0	8.8
MPS9	55	10.5	8.2	10.5	11.1	9.1	10.7
	155	13.0	10.0	12.3	13.5	11.3	12.9
	255	14.8	12.5	14.4	14.8	12.9	14.5
	355	16.5	12.0	14.9	16.4	12.6	15.8

Notes

(1) Unless otherwise stated, all units in kN/m^2
(2) Vane locations from Figure 5.4

5.1.4 Critical state parameters.

Critical state theory describes the relationships between the shear strength and void ratio of a soil using a number of soil parameters. In this section, calculated values for some of these parameters are compared with the literature. Results of the consolidated-undrained triaxial tests are then described.

For each test box sample, measurement of the initial voids ratio, change in sample height during consolidation and mean effective pressure at the end of consolidation allows a final point in the consolidation

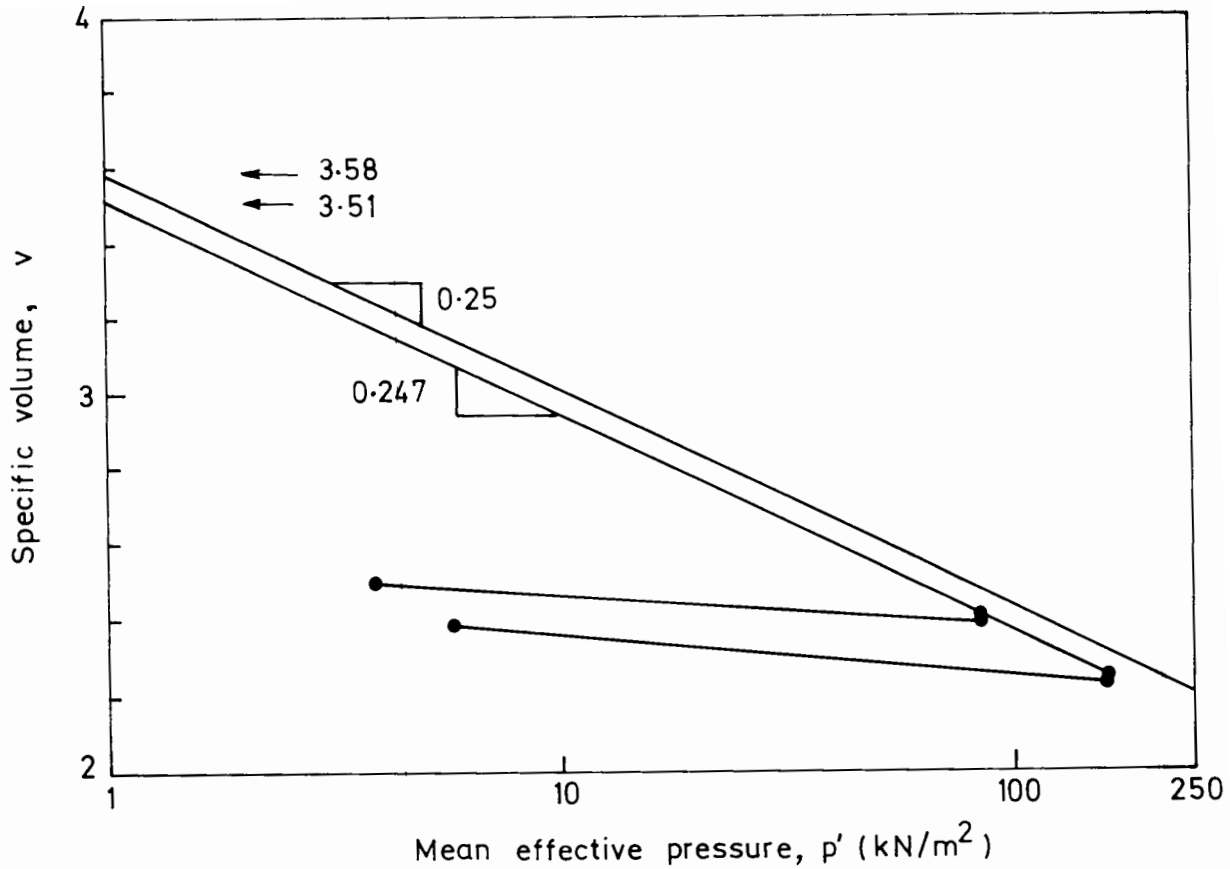

Figure 5.8 Consolidation and swelling behaviour of samples

history to be plotted in v: ln p′ space. An average value for the test samples at each of the two nominal strengths is plotted in Figure 5.8. The observations are consistent with a value λ=0.247 and an intercept $(e_\lambda)_{1\text{-}D}$=2.51.

Mean effective stress in a sample after swelling can be determined from pore pressure equilibrium under confining pressure in C-U triaxial samples before the consolidation stage. Average values 3.9kN/m^2 and 5.8kN/m^2 were measured for MPS6 and MPS9 respectively. Swelling lines were constructed for these values and a gradient κ=0.04 observed in each case.

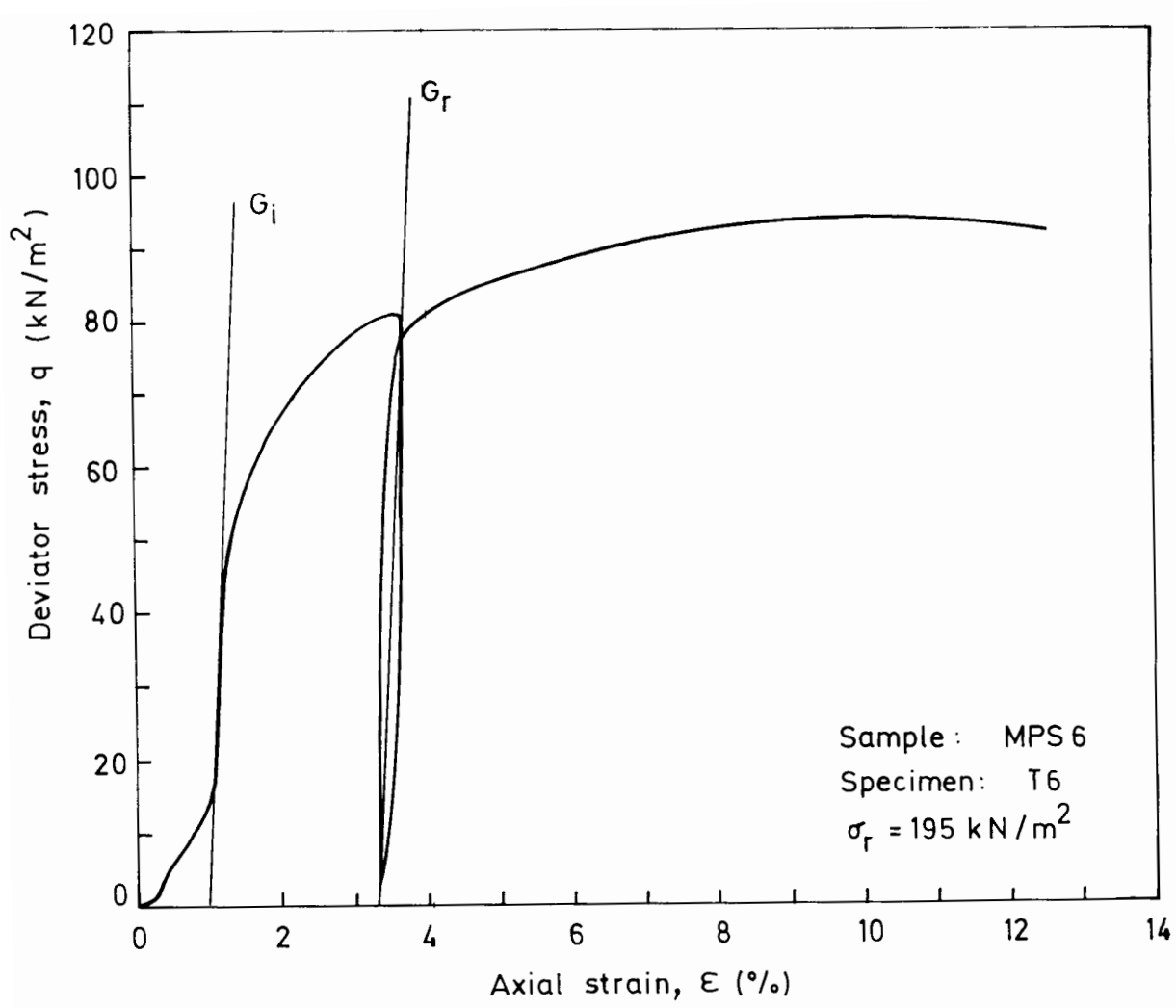

Figure 5.9 Development of deviator stress with axial strain for a C-U triaxial test

The triaxial samples were tested using a Tritest 50 machine manufactured by E.L.E. Load was measured with a proving ring. Change in sample length was measured by an LVDT which, together with a cell and pore pressure transducer, output to a signal display unit. Samples were isotropically consolidated with bottom drainage only to atmospheric pressure at cell pressures approximately 100, 200 and 300kN/m^2. Volume change measurement was made using a burette arrangement. Undrained loading was at a very slow rate of 0.0025mm/min, and most tests included an unload/reload cycle. A typical q : ε plot is illustrated in

Table 5.6 Consolidated-undrained triaxial test results

Test code	Cell press σ_r	c_v	R_p	q_f	p'_f	u_f	e
MPS6	98	6.98	2.7	54	61	57	1.308
	195	8.01	1.2	95	108	119	1.209
	295	9.92	1.0	143	167	176	1.147
MPS9	96	7.66	5.1	62	68	50	-
	198	9.38	2.4	113	123	114	1.184
	298	10.84	1.8	148	172	175	1.116

Notes

(1) σ_r, q_f, p'_f, u_f units in kN/m^2

(2) $R_p = \frac{P'_{max}}{P'_o}$

(3) $P'_{max} = \frac{1}{3} \sigma_{v'_{max}} (1 + 2K_o)$; $p'_o = \sigma'_r$

(4) c_v units in m^2/year

Figure 5.9 for one test, indicating a characteristic seating of the ram on the triaxial specimen and the unload/reload response. In every case failure was defined as a maximum deviator stress, q_f.

A summary of the conditions at failure is presented in Table 5.6. In some tests the pore pressure was observed to be greater than the applied deviator stress, and although it is possible that a very slow leak either in the sample membrane or past the 'O' ring seals to the top

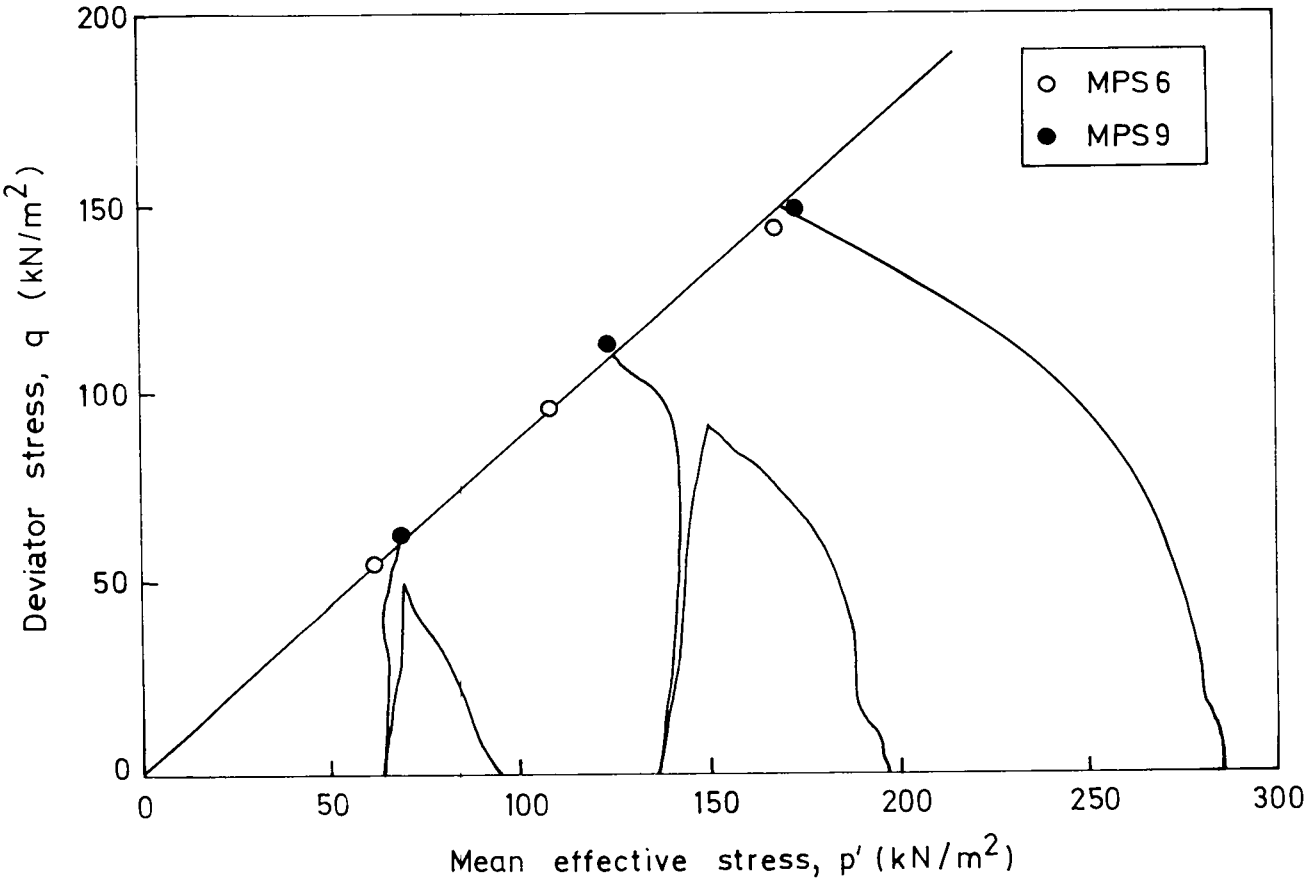

Figure 5.10 Stress paths to failure in effective stress space

cap or pedestal might have caused this, no obvious signs of distress were observed in any of these items and it is difficult to offer a firm explanation. A plot of the failure points for each sample in effective stress space is presented in Figure 5.10. For clarity, only the stress paths to failure of the tests on sample MPS9 are presented. The results are consistent with a critical state line gradient M=0.88. For triaxial compression and failure occurring on the critical state line then

$$M = \frac{6 \sin\emptyset'}{3 - \sin\emptyset'} \qquad (5.4)$$

and a corresponding angle $\emptyset'=22.6^{\circ}$ is obtained.

Table 5.7 Variation in shear modulus with OCR

Test code	Cell press σ_r (kN/m^2)	Initial R_p	Initial G_i (kN/m^2)	Initial $\left(\frac{G_i}{c_u}\right)$	Reload R_p	Reload G_r (kN/m^2)	Reload $\left(\frac{G_r}{c_u}\right)$
MPS6	98	2.7	6.4	237	3.6	12.9	478
	195	1.2	7.8	163	3.3	7.5	158
	295	1.0	11.3	157	3.0	12.5	175
MPS9	96	5.1	5.3	171	7.5	4.4	142
	198	2.4	5.5	96	3.3	6.7	119
	298	1.8	8.3	112	-	-	-

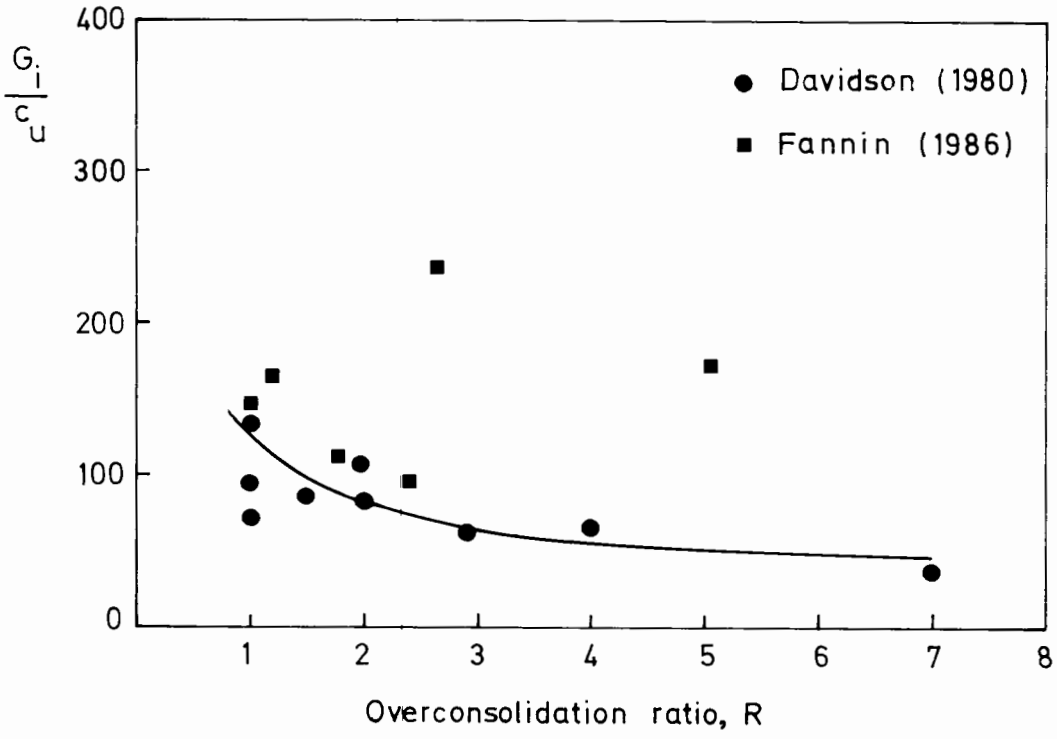

Figure 5.11 Variation in normalised shear modulus with overconsolidation ratio

An initial shear modulus G_i was calculated for a straight line fit to the early part of the curve as shown (usually to G_{33}), and a shear modulus G_r for the unload/reload loop based on a fit to the intersection of the curves, Figure 5.9. The results are given in Table 5.7 and presented in Figure 5.11 together with other data for Speswhite Kaolin taken from Davidson (1980) and calculated for a similar definition. In a comprehensive discussion of the shear modulus of clays Wroth et al.(1984) indicate that the shear modulus would be expected to decrease with increasing OCR, and a best fit to $\left(\frac{G_i}{c_u}\right)$ seems to agree well with such a relationship.

5.2 Reinforcement

5.2.1 Geometry

The model grid was manufactured by Netlon Ltd from a polypropylene material. Several batches of grid were supplied for the test programme, each charactersied by different geometric and strength specifications. Two of these batches, designated grid 'M' and grid 'C', were selected to be suitable for the model requirements, see section 5.2.2.2 below. Grids 'M' were 1400mm x 800mm; grids 'C' were 1500mm x 360mm. In all reinforced tests, a single layer of grid 1000mm x 300mm was prepared from the appropriate batch and included at the base of the granular layer.

Manufacture of a grid material involves stretching a polymer sheet which has been punched to a selected pattern of holes. For any stretched polymer, the final grid geometry and strength are determined by the

Table 5.8 Prototype and model grid dimensions

Grid type	Aperture length	Aperture width	Rib width	Rib thickness	Node thickness
Tensar SS2	40	28	3	1.1-1.2	3.9
	(10)	(7)	(0.75)	(0.3)	(1.0)
Type 'M'	12-14.5	8-9.0	0.4-0.5	0.3	0.8-0.9
Type 'C'	11-14.0	8-8.5	0.4-0.5	0.3-0.4	0.8-0.9

Notes

(1) All units in mm
(2) Ideal scaled equivalent SS2 within parentheses

manufacturing process and are not independent of each other. A comparison of the geometry of the model material and a Tensar SS2 geogrid is presented in Table 5.8, from which it can be seen there is general agreement, although the apertures in the model were found to be slightly larger than the ideal. In summary, the dimensions of the model grid represent a good, though not perfect, geometric scaling of the prototype material.

5.2.2. Strength.

5.2.2.1. Test conditions.

It is generally accepted than the 'in-soil' or confined load-extension behaviour of a fabric may be superior to an unconfined test, and that the use of unconfined strength and moduli can be unduly conservative in some design situations. However it should not be

overlooked that the improvement due to confinement is variable and largely dependent on the fabric type. Non-woven and composite materials exhibit a significant increase in tensile modulus resulting from a prevention of filament reorientation by the surrounding soil, which is not so apparent in woven materials, as shown by McGown et al. (1982). This latter behaviour is likely to be characteristic of geogrid materials, in which the polymer material has been stretched to a preferred orientation during the manufacturing process.

A second consideration in assessing the significance of confinement is the soil type, and importantly the reinforcement application and mode of failure. For the case of low frictional confinement, and where relative movement between soil and fabric is essentially one of shear, Christopher et al. (1986) argue that an unconfined test may be considered acceptable. The unpaved road over a soft clay is a good example of such a system. However an unconfined test would certainly appear less applicable to the pullout conditions in for example, a reinforced slope or wall. Given these considerations and the difficulty of making confined tests which would satisfactorily reproduce a gravel/clay bond, all load-extension tests were made on unconfined grid specimens.

5.2.2.2. Model grid strength.

Polymer based fabrics such as geotextiles and geogrids are viscoelastic, and therefore working performance is dependent on ambient temperature, load magnitude, load duration and loading rate. Strength of

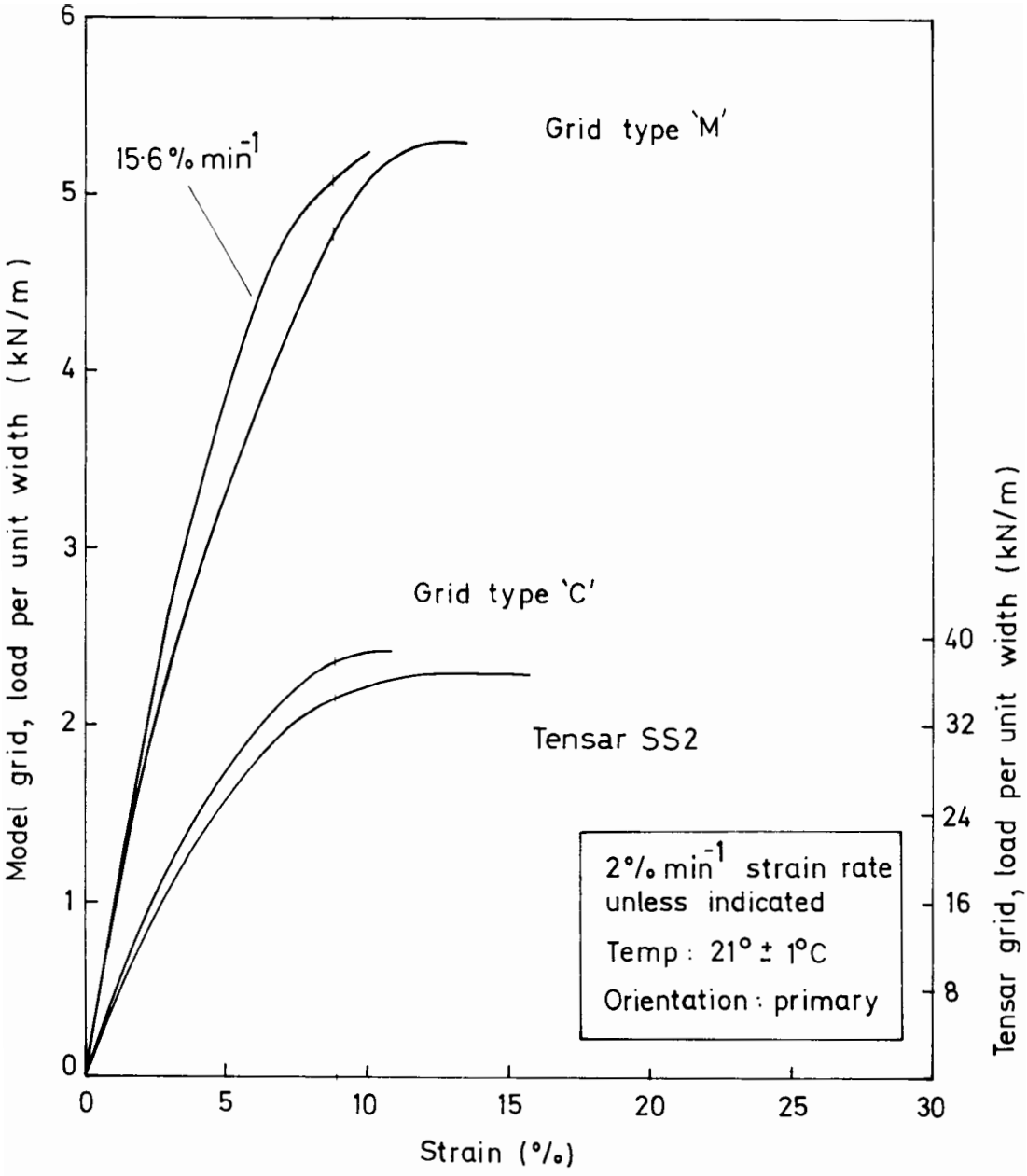

Figure 5.12 Variation in load/unit width with strain during tensile testing of the model grids

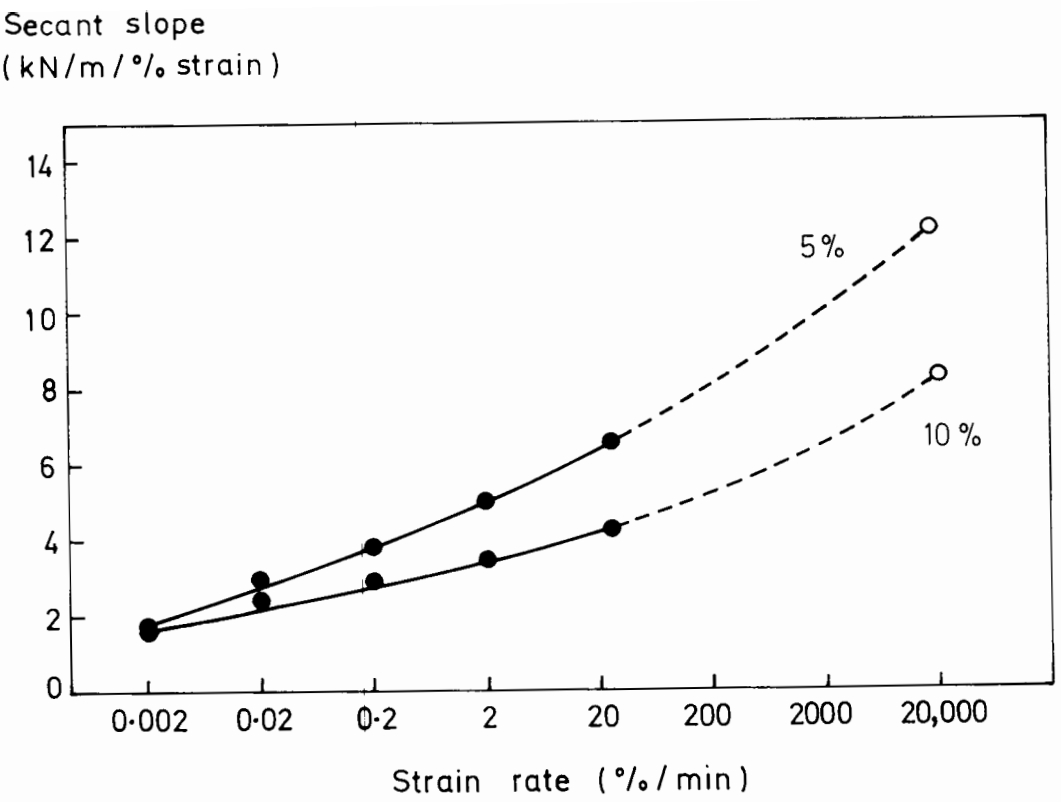

Figure 5.13 Variation in secant slope with strain rate (after McGown, 1982)

a geogrid material is typically measured by an index load/unit width extension curve, determined at 20°C for a constant strain rate of 2%min^{-1} based on the intial sample length. Specimens of the model material were tested in an Instron rig type TM-S. Specimen preparation involved casting the ends of a piece of grid, approximately 110mm wide and with a gauge length 125mm in the transverse (primary) direction, into jaw clamps before testing. A low melting point Ostalloy alloy was used to secure the grid in the clamps. Specimens were 14 ribs wide and 13 ribs long; gauge length was measured from the 2nd to the 12th rib.

Results are presented in Figure 5.12 for the model material and a Tensar SS2 geogrid (after McGown, 1982). Grid type 'C' used in the cyclic tests was very similar to a curve of Tensar SS2 scaled by the appropriate factor 16 to represent an ideal model grid. Grid type 'M'

used in the monotonic tests was observed to be stiffer and stronger, and information from tests made at a strain rate of about 15%min^{-1} is also included for this material. Scaling considerations are discussed below.

The scaling relationship between model and prototype in monotonic tests was reported by Love (1984) and similarly governs this study. From analysis, the average rate of strain in the geogrid during monotonic testing is typically 15%min^{-1} for a driving rate of 2.5mm/s, Burd (1986). The secant slope at 5% and 10% strain for specimens tested at a strain rate of 15.6%min^{-1} was measured to be 0.76kN/m/% and 0.52kN/m/% respectively. Dimensional analysis indicated the corresponding protoype values to be 12.16kN/m/% and 8.32kN/m/%. From extrapolation of test data for Tensar SS2, Figure 5.13, this would suggest equivalent field rates of strain approximately 1.8×10^{4}%min^{-1}. So the rate of strain in model testing is found to be about 1000 times slower than that at full scale. It is important to appreciate that the argument above assumes an extrapolated grid behaviour, and is necessarily a simplification of soil loading beneath a wheel. A time to failure of typically 20 seconds in a monotonic test is therefore equivalent to loading over a period of 1/50th second at full scale, during which a vehicle moving at 15-20kph (4.2 - 5.6m/s) travels nearly 0.1m. In summary, the monotonic tests simulate the rapid failure that would occur during a single pass of a heavily loaded vehicle, and the model grid is a very reasonable, though not perfect scaling of the geometry and tensile stiffness of a Tensar SS2 geogrid.

The scaling relationship between model and prototype grid in the

cyclic tests is more direct. The model tests are a simulation of continuous vehicle passes at standard axle loading, for which rate of strain compatibility is met. Index strengths at 2% strain per minute for model and Tensar SS2 geogrid are seen to be in good agreement, Figure 5.12.

5.3 Granular Material

5.3.1 Description

The granular material used in the model study was a combination of equal quantities by weight of three sands and three gravels supplied by A.L. Curtis (ONX) Ltd., Plate 5.1. Sieve analyses were made, for which particle size distribution curves are presented in Figure 5.14. In accordance with the model requirements the grading profile is a scaled equivalent of a Type 1 granular material, as described in the D.Tp. Specification for Road and Bridge Works (1976), and the curve lies within the designated particle size envelope when translated by the scale factor of 4. The shape of the curve indicated that it was a well graded soil.

A dry density/moisture content relationship was derived according to BS1377:1975 using the 2.5kg rammer method (Test 12). The results, presented in Figure 5.15, exhibit a certain amount of scatter. However there is a clear indication of an optimum moisture content of approximately 10%, and compaction of the granular material in the model tests was made at this value. A specific gravity determination for the particles gave a value of G_s=2.65.

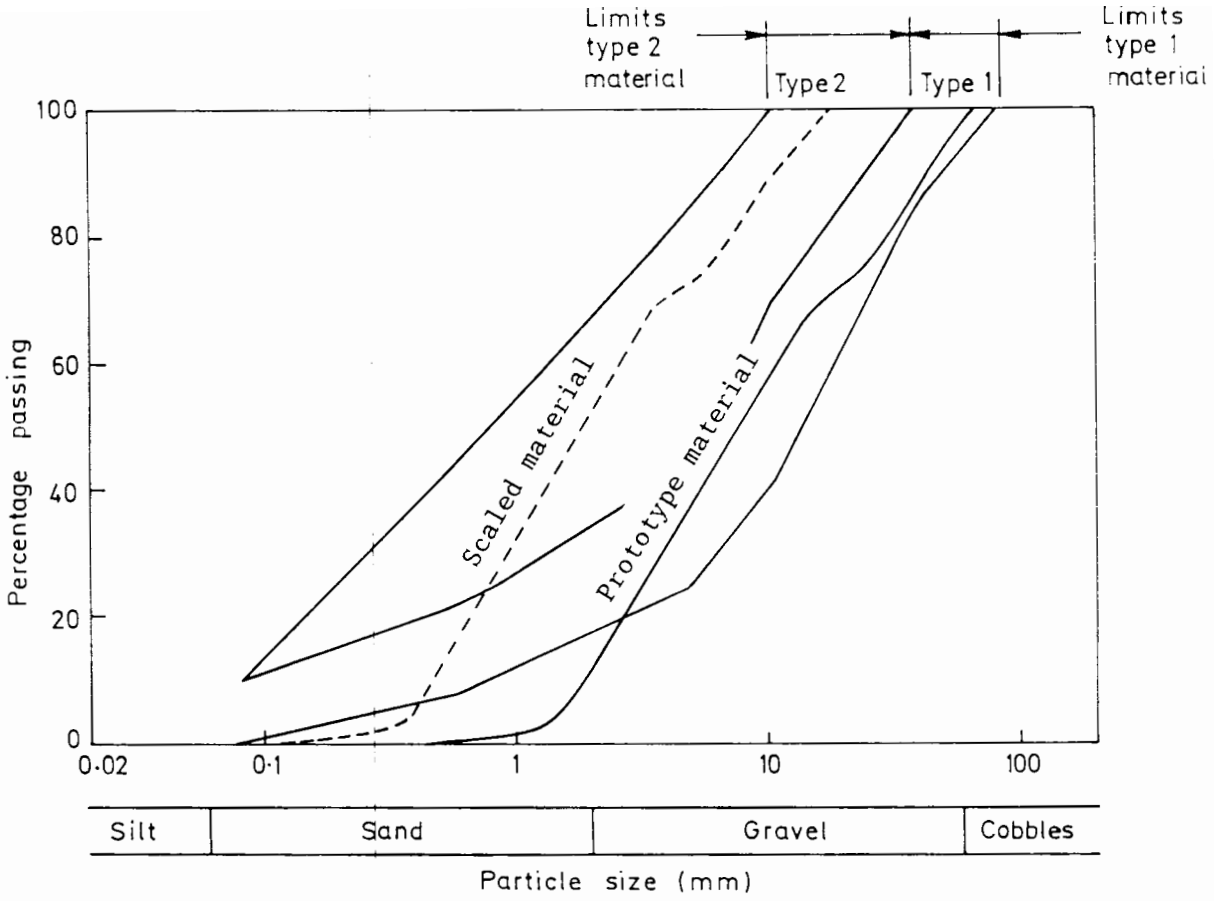

Figure 5.14 Grading analysis of the granular material

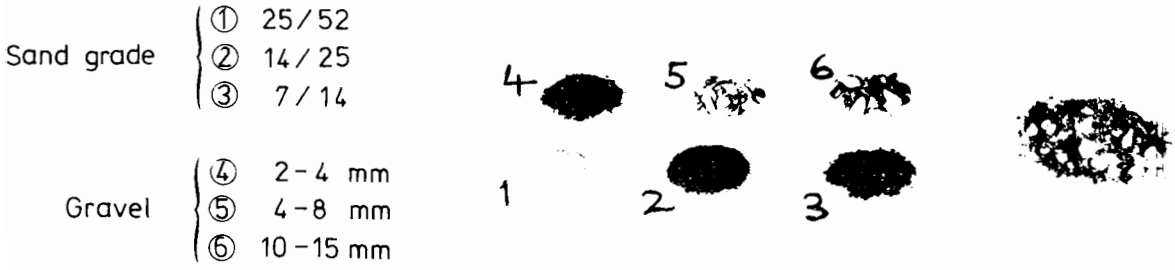

Plate 5.1 Granular material used in the model tests

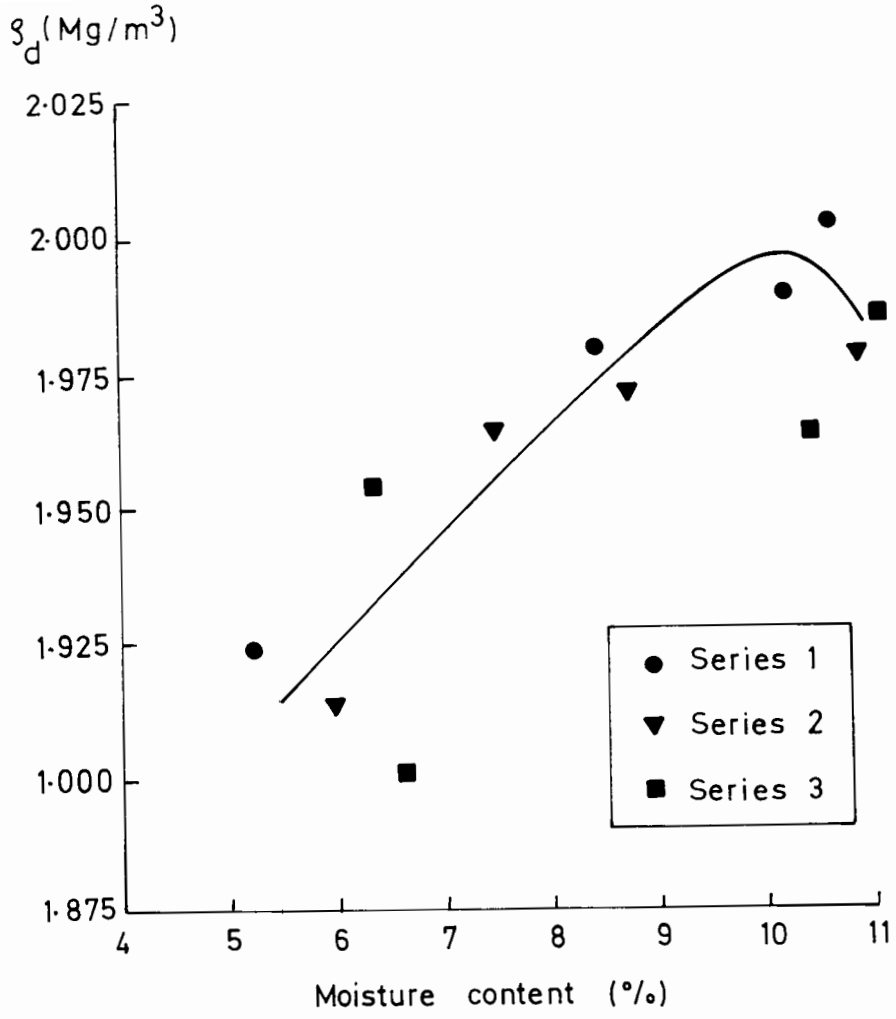

Figure 5.15 Variation in dry density with moisture content

5.3.2 Shearbox tests

Direct shear tests were made on the granular material using a moderately large shearbox apparatus. The internal box dimensions were 153mm x 254.5mm, with a lower box height 75mm and an upper box height 127mm. A rigid top platen to the box was unclamped and free to move as the sample changed volume during shearing. Normal stress was applied to the sample using a yoke mount and hanger. A multispeed gear box provided

a range of shearing rates, and applied shearing force was calculated from the measured deflection of a reaction bar. Dial gauges were used to monitor horizontal displacement of the lower box, and the mean change in sample height.

The sample was placed and compacted in six nearly equal layers in the shearbox according to the same method as used in the model tests. Loose material was levelled by eye, and then a board 250mm x 150mm placed in contact with the surface and struck with a 1kg hammer. Each layer recieved a total of 15 blows. A dry sample mass was chosen to give a nominal finished sample height 150mm for a dry density similar to that achieved in the model tests, section 4.3.2.

Normal stress was applied to the sample before releasing the upper and lower sections of the box. Tests were made at normal stresses of 10,20 and 30kN/m^2 and for a nominal shearing rate of 0.4mm/min, measured to be 0.389mm/min. This rate was selected to allow the variation of force and displacement to be well defined throughout a test. The test at 30kN/m^2 was repeated, and the test at 10kN/m^2 repeated for the sample wetted to nearly 10%. Typically tests were continued until small changes in shear force were observed with further horizontal displacement, although some were terminated before this point was reached in a test because tilt of the upper box was becoming excessive.

All samples gave a similar response during shearing, characterised by a peak shear strength and an overall volume increase; peak shear strength was associated with a maximum rate of dilation. At large

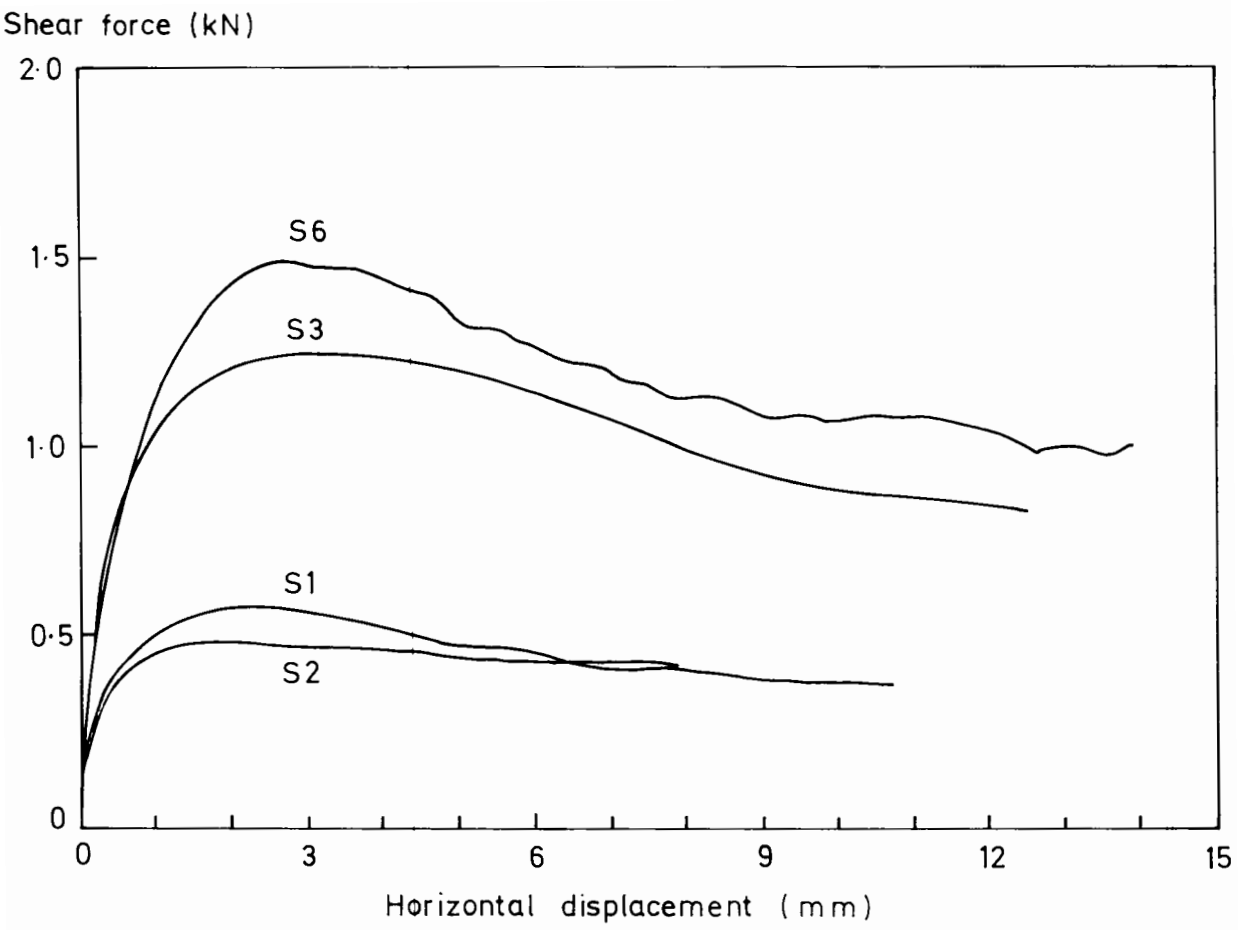

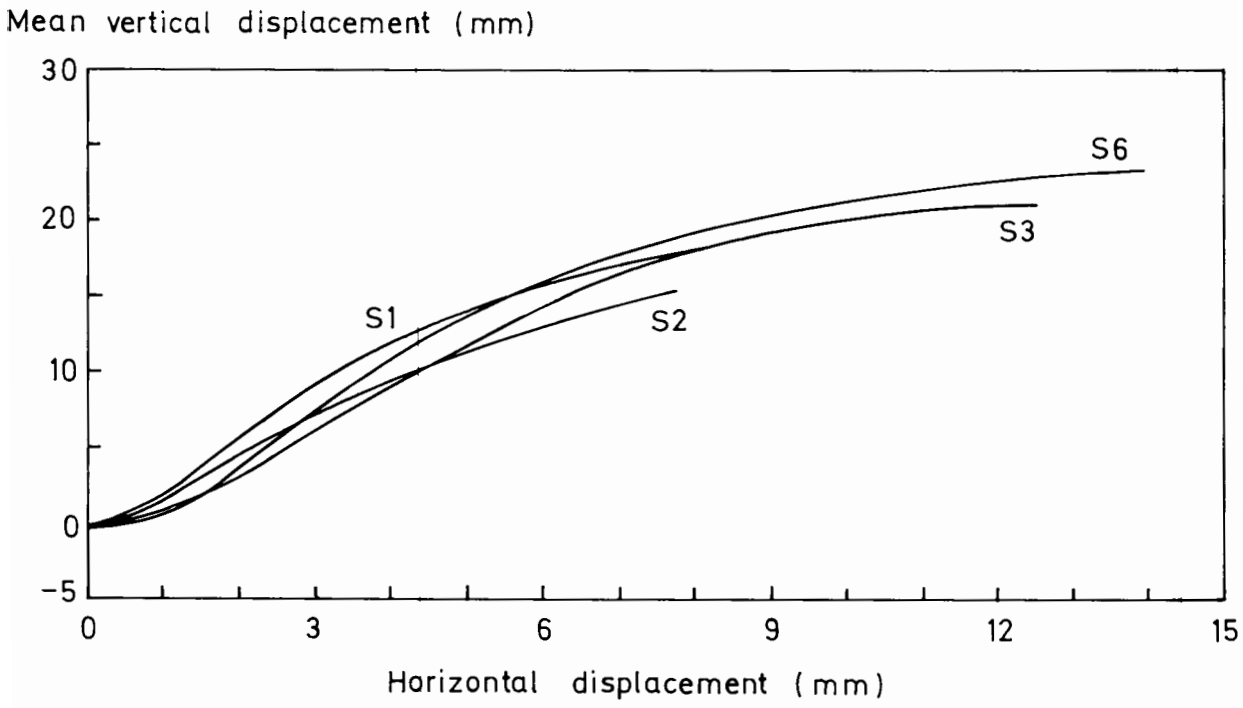

Figure 5.16 General behaviour during shearbox testing

Table 5.9 Shearbox test results

Test	Description	Peak σ_n	Peak τ	Large disp σ_n	Large disp τ	Dilation angle	Dry density, ρ_d
S1	dry	10.1	15.0	10.4	10.1	20.2	1.904
S2	mc = 7.8%	10.2	12.2	10.3	11.1	15.1	1.799
S3	dry	20.2	32.4	21.0	22.5	16.4	1.912
S4	dry	30.3	37.6	-	-	18.6	1.911
S5	dry	30.3	32.8	31.6	25.0	17.1	1.908
S6	dry	30.3	38.5	31.7	27.2	20.3	1.883

Notes

(1) σ and τ units kN/m^2

(2) ρ_d units kg/m^3

displacements the rate of dilation tended to zero as the mobilised shear force tended to a constant value. General behaviour in the shearbox test is illustrated in Figure 5.16. Some experimental scatter is observed which is not unreasonable given the nature of the sample preparation. Test S2 which was prepared and compacted to a slightly less dense state than dry test S1, mobilised a smaller peak shear stress and a lower angle of dilation; yet after peak the two curves were in close agreement and it would appear that wetting the sample did not significantly influence behaviour.

All tests are summarised in Table 5.9 and in Figure 5.17. Initial dry density was determined for a sample thickness measured after normal load had been applied. The total normal load was calculated from the

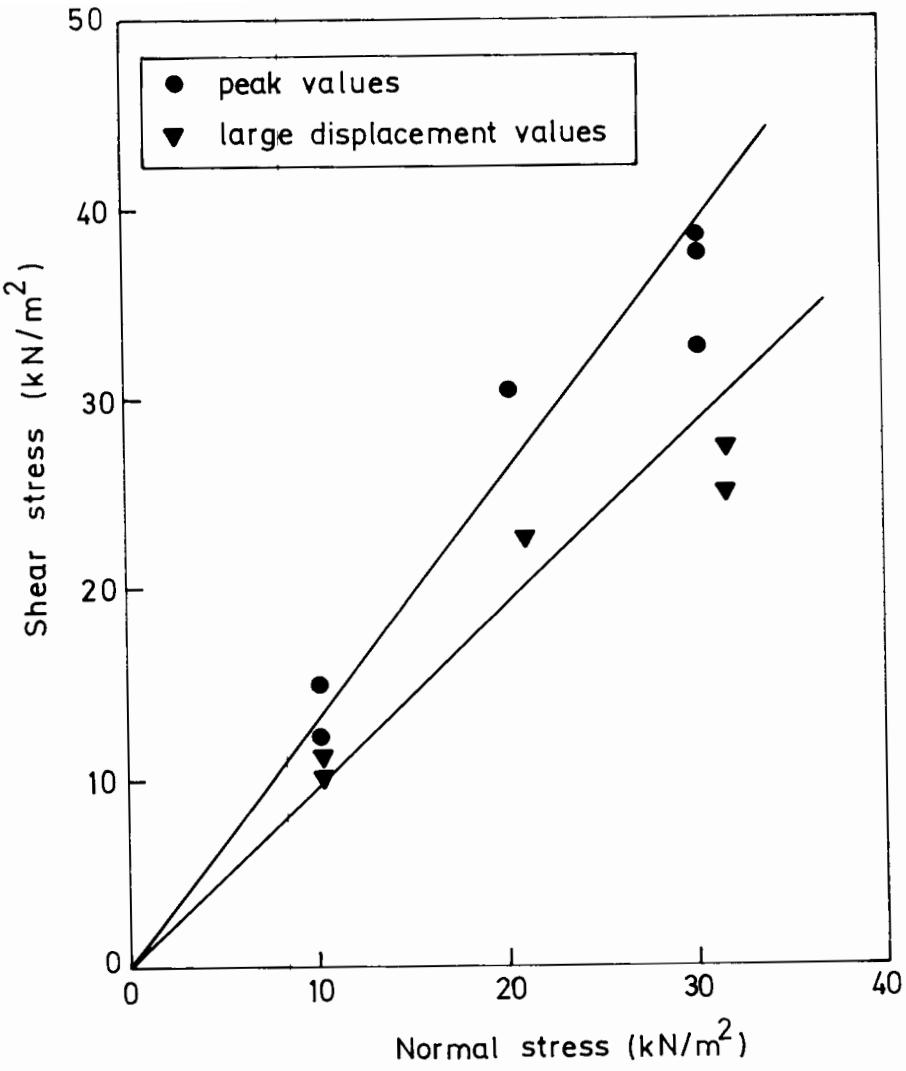

Figure 5.17 Summary of shearbox test results

applied dead weights, together with the mass of the yoke assembly, top platen and the material in the top half of the box. Normal and shear stresses were calculated for a sample plan area corrected for shear displacement of the box halves. Generally the results indicate a mean value $\emptyset'_{peak}$ of 52.1° and a mean value $\emptyset'$ of 42.4° at large displacements as shown. However there is a strong suggestion of a non-linearity in the results, so that a best fit envelope is a curved and not a straight line.

CHAPTER 6

MODEL SCALE TEST RESULTS AND ANALYSIS

6.1 Results

Measurements and observations made during the monotonic and cyclic tests are presented in this first section to the chapter. Discussion is limited to the influence of the reinforcement and a qualitative assessment of the reinforcement mechanisms only.

6.1.1 Footing load-penetration

Footing load-penetration curves for the monotonic tests are presented in Figure 6.1 for both initial loading of the dual footing (designated by M1), and reloading after rut repair (designated by M2). The shapes of the curves are broadly similar, all with a distinct early yield point at a footing penetration $\frac{\delta}{B} \simeq 0.1$ beyond which the rate of increase of footing load with penetration is noticeably reduced. The reinforced tests were observed to have a greater bearing capacity than the unreinforced tests, and typically exhibit a stronger behaviour at large displacements approaching a serviceability failure criterion. Reloading of the system after repair of the granular layer produced a moderate improvement in the reinforced tests, and none at all in the unreinforced tests.

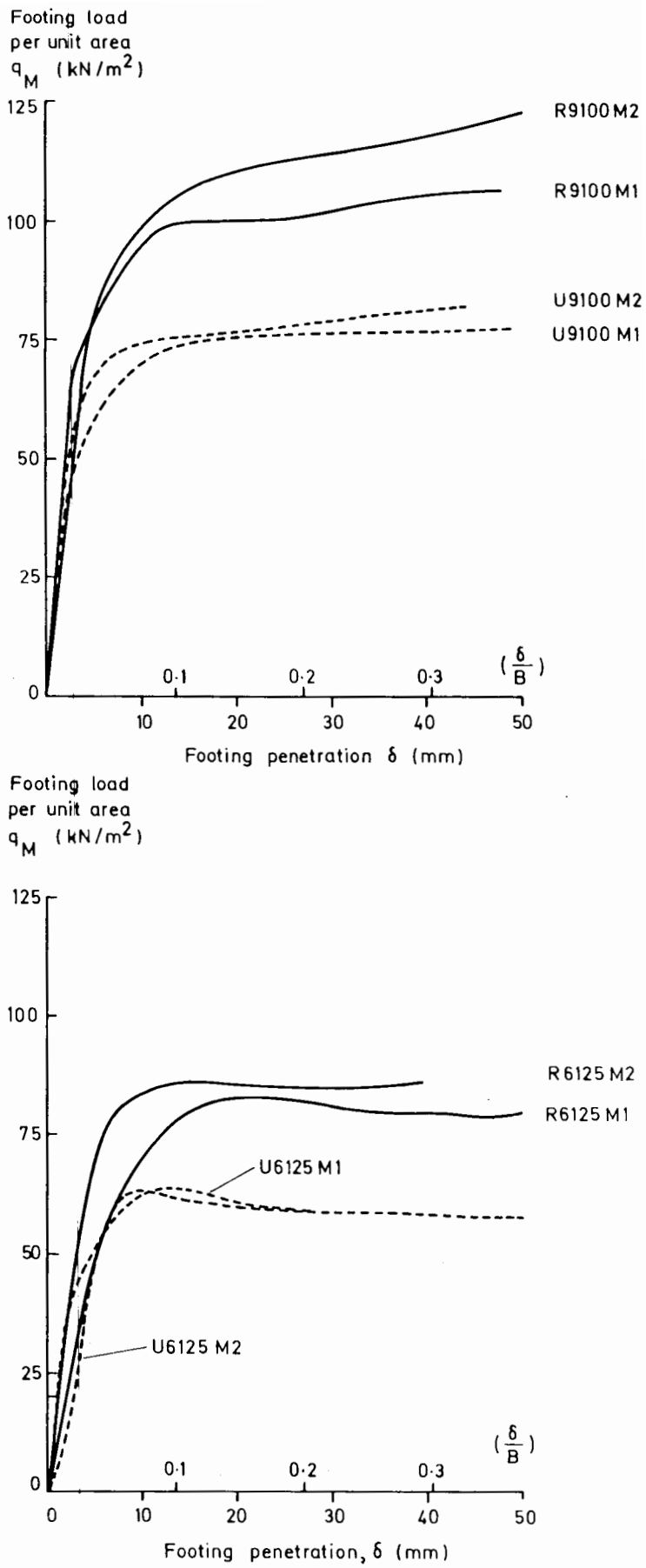

Figure 6.1 Development of footing load with penetration

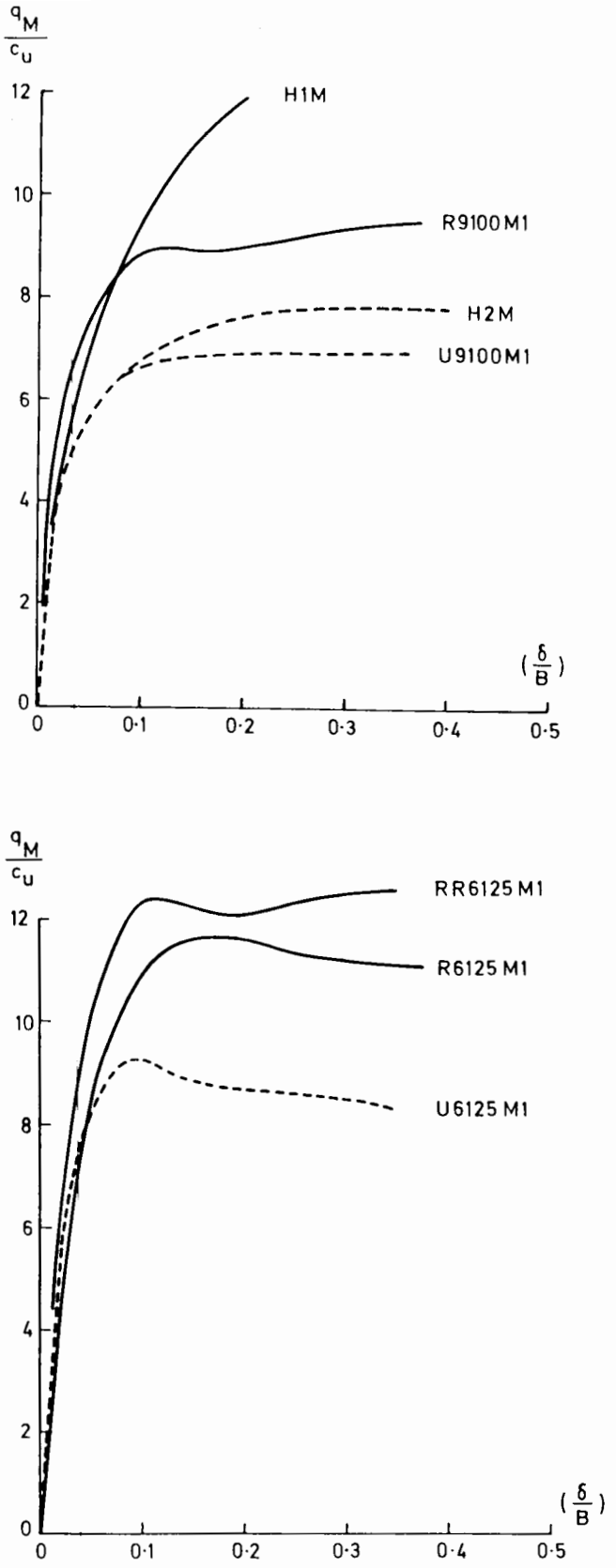

Figure 6.2 Development of footing load (normalised by c_u) with penetration (normalised by B)

A full comparison of the effect of reinforcing the granular layer is given in dimensionless plots of the initial loading curves, Figure 6.2. Included in the figure is a curve for the repeated test RR6125M. Clearly the footing load to cause early yield is significantly increased by the presence of reinforcement. Thereafter and at large displacements there is a continued moderate improvement in capacity over the unreinforced system. Curves for two equivalent single footing tests H1M and H2M, taken from Love (1984), are also included in the figure. Again, comparing the shapes of the curves, it is interesting to observe a very good agreement throughout the unreinforced tests and in the initial behaviour of the reinforced tests. However the continued improvement measured in the reinforced single footing tests, which is not so marked in the dual footing tests, is an important difference between the two studies. It is caused by the very long anchorage length in the single footing tests that was not available in the dual footing tests, and consequently a capacity to generate a larger tensile force per unit width and a resulting greater membrane action with the single footing. Lateral slip movement at the ends of the grid associated with an anchorage failure occurring in the later stages of each test tends to confirm these observations.

6.1.2 Granular material heave

Heave at the surface of the granular layer during testing was observed to be largely symmetric. However since each test was a real engineering event, measurements taken at the same location either side of the footing proved to be similar but of course not always equal,

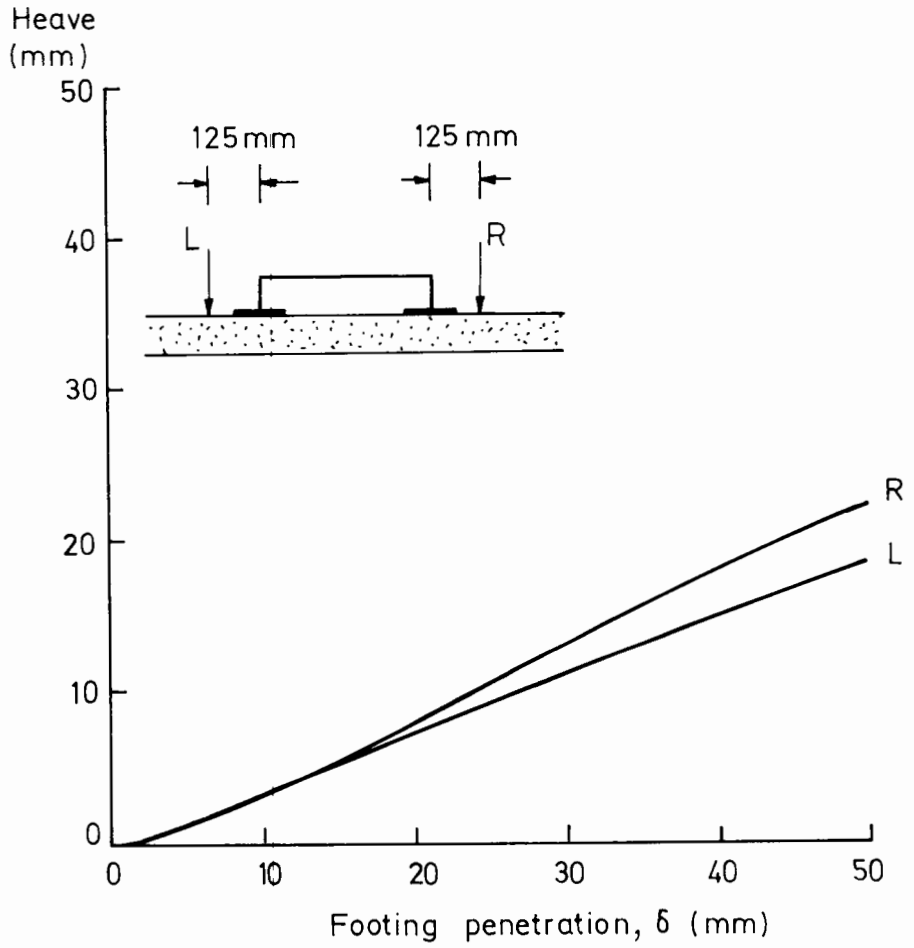

Figure 6.3 Development of heave with footing penetration during test R9100M

Figure 6.3. While the measurements were made on the centreline of the box to allow comparisons between tests, characteristically the amount of heave varied across the width of the test box, being greatest in the middle and slightly less at the boundary walls. The effect, which was also noted by Love (1984), must be a consequence of friction on the test sample at these boundaries.

A summary of the trend in results for both the monotonic and cyclic load tests is illustrated in Figure 6.4, with heave $\bar{h}$ calculated as an average of the two measured values. Common to every test was a small

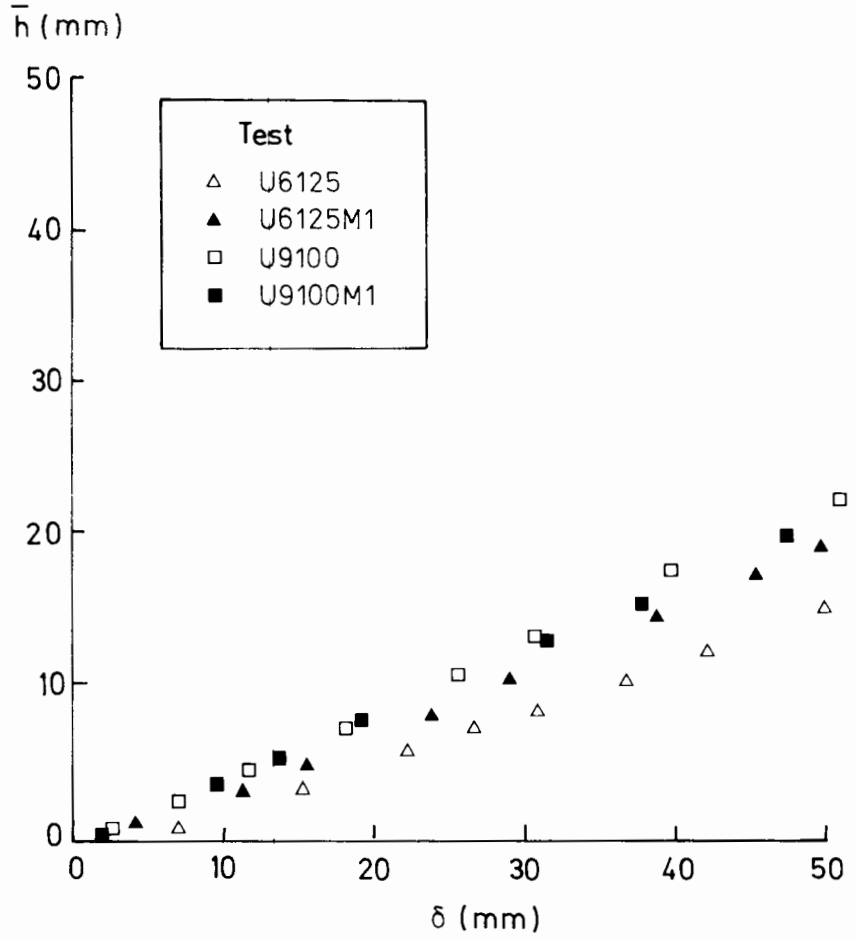

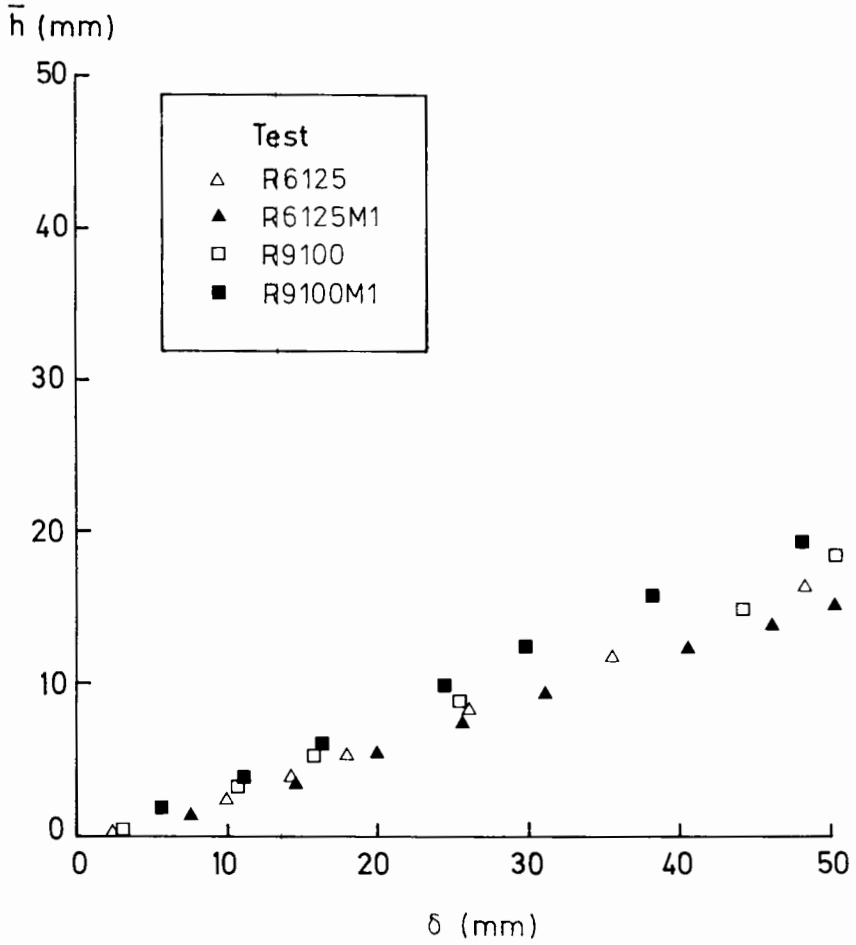

Figure 6.4 Development of mean heave with footing penetration

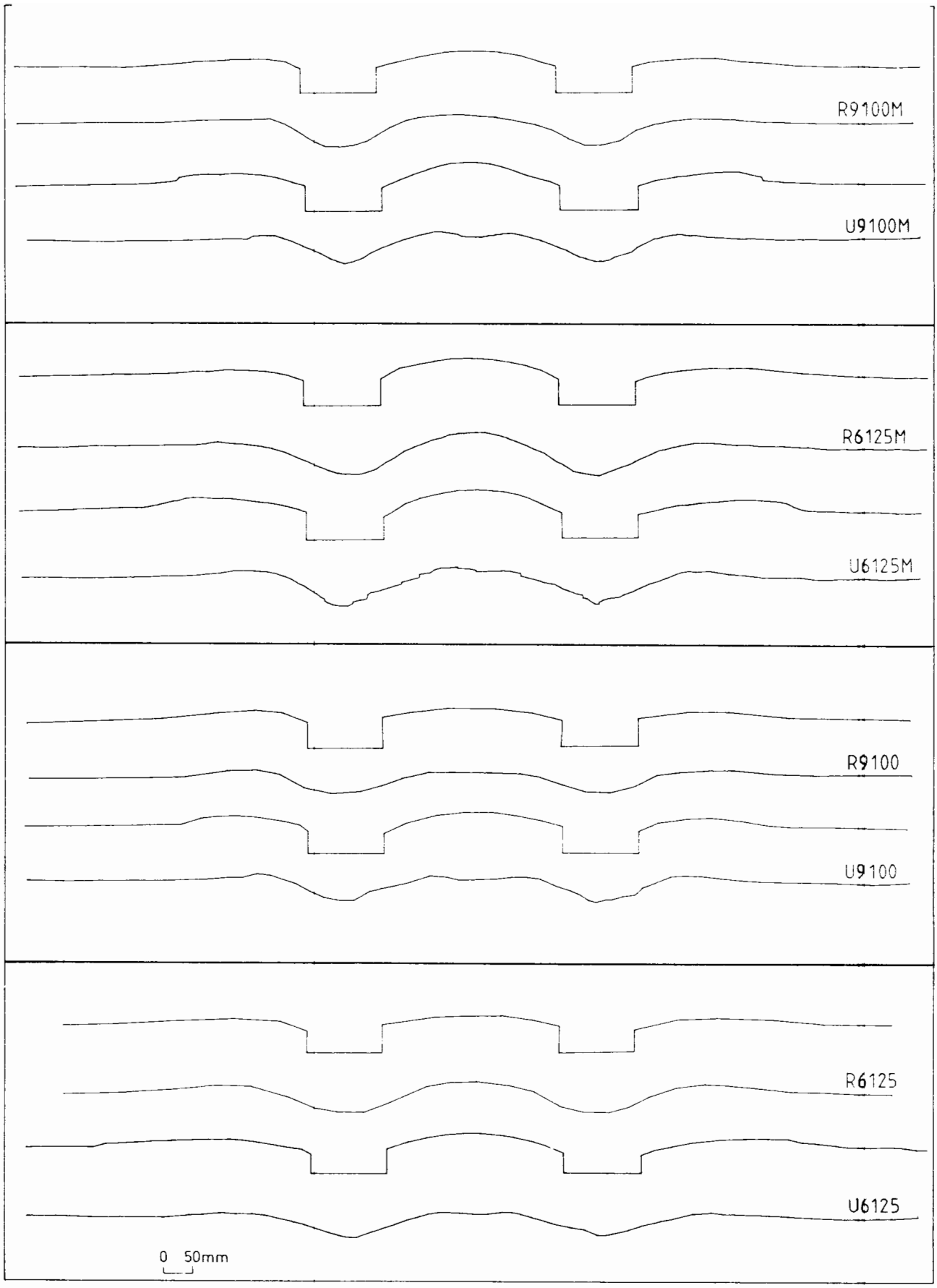

Figure 6.5 Summary of granular layer profiles

initial footing penetration without heave, which is not unreasonbable; thereafter heave $\bar{h}$ was found to increase linearly with footing penetration, with no significant difference in behaviour between the monotonic and cyclic tests. Typically for any given footing penetration, maximum heave $\bar{h}$ was measured to be less in the reinforced tests. Yet the reduction was moderate indeed, and more important than the difference in heave was the complete surface profile of the granular layer. A summary of such profiles is illustrated in Figure 6.5. In an unreinforced test surface deformations were very distinct, with a pronounced rupture zone and associated heave either side of the footing. Undoubtedly dilation in the sand and gravel contributed to this overall result. Reinforcement however acted to cause material displacements to occur less locally around the footings, so that in the reinforced tests the surface profile was noticeably smoother and the integrity of the granular layer better maintained.

6.1.3 Subgrade pore and total pressures

Pressure transducers mounted in the back face of the test box were not only used to monitor consolidation, but also to record lateral total and pore water pressure responses to footing load.

Results for the monotonic tests are presented in Figure 6.6, and indicate a clear pattern of behaviour. Pore pressure transducer P3 and total pressure transducer T3 both exhibit a small, almost zero response throughout each test: while it is not surprising to record negative pore pressures during shearing of a heavily overconsolidated clay, the

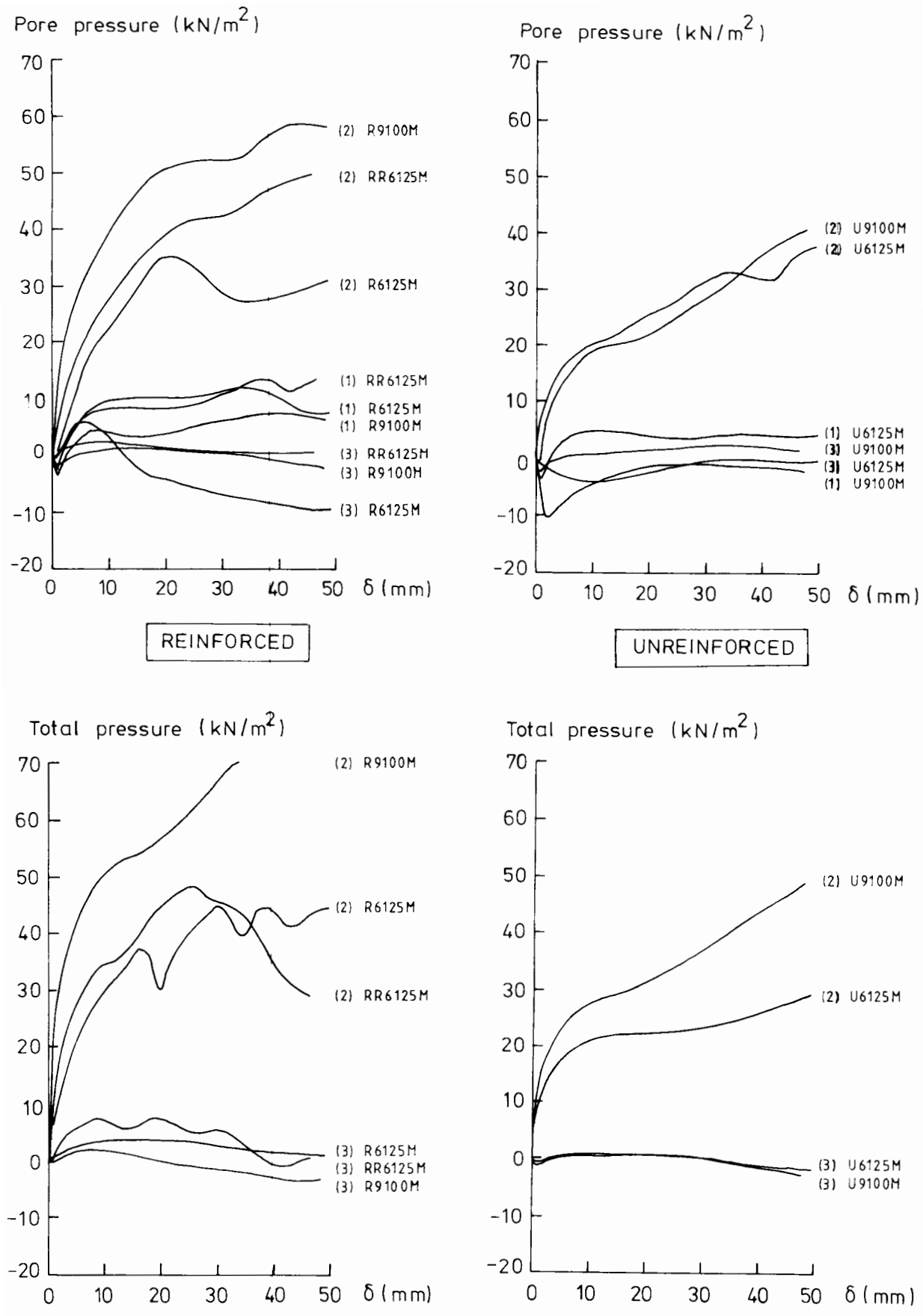

Figure 6.6 Response of pressure transducers: monotonic tests

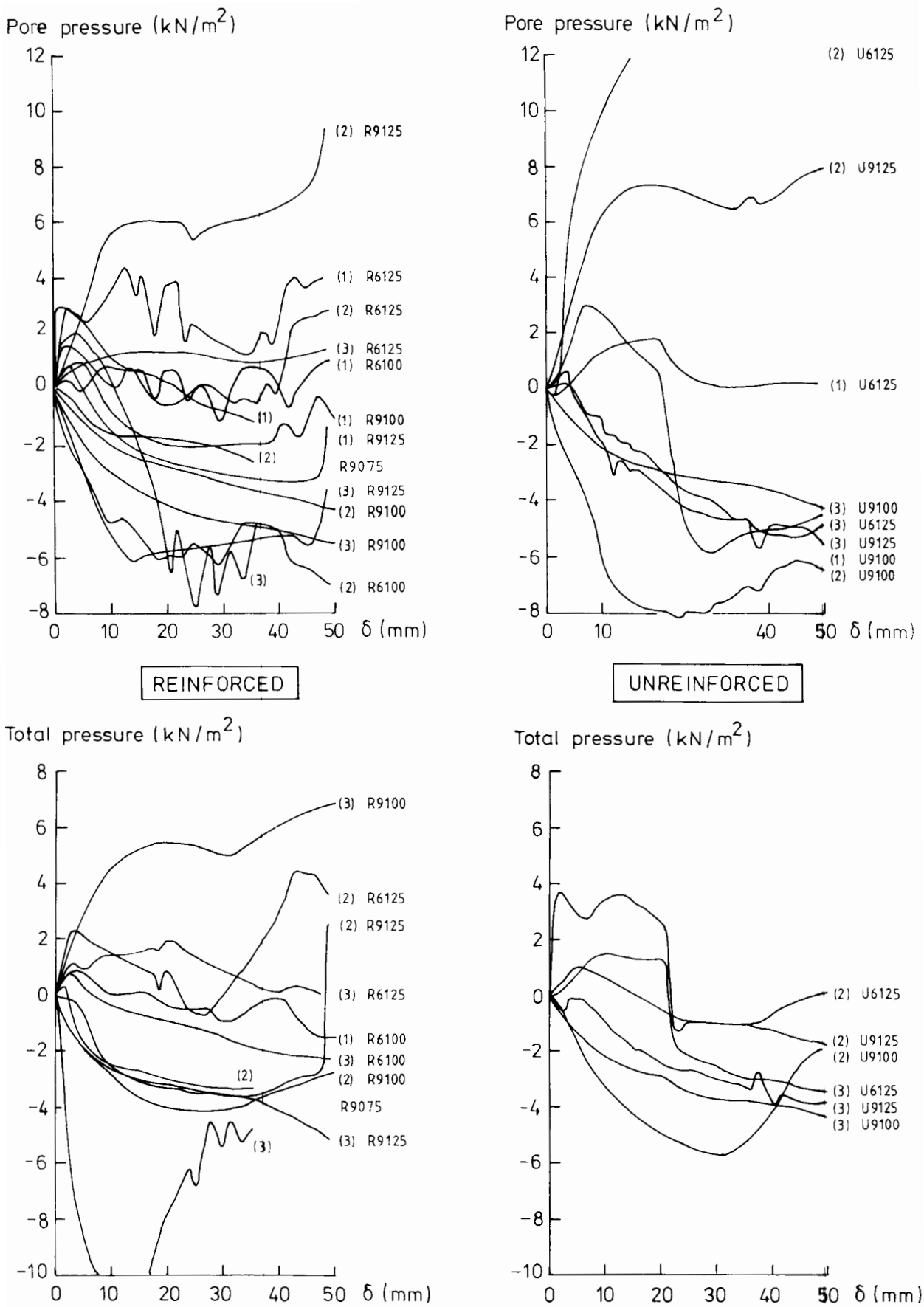

Figure 6.7 Response of pressure transducers: cyclic tests

occasional measurement of small negative total pressures does suggest the possibility of a degree of flexure in the back face of the test box. Interestingly, pore pressure transducer P1 output is also generally small, and virtually identical to P3 in the unreinforced tests, although slightly more positive in the reinforced tests. This behaviour tends to confirm a very localised failure of the unreinforced system.

In all tests the responses of pore pressure transducer P2 and total pressure transducer T2 located on the centre line of each footing were observed to be large and positive. The curves are in general agreement with the load-penetration results, wherein the greater bearing pressures measured for the reinforced systems are characterised by a more positive output of the transducers in these tests.

Unfortunately it is difficult to draw any such specific conclusions from the results for the cyclic tests, presented in Figure 6.7. A probable explanation for the lack of common pattern in the responses is that, since the pressure transducer outputs were recorded during a period 200-400ms after peak load, the system was in fact rapidly unloading at that time.

6.1.4 Footing penetration - number of load applications

The typical measured relationship of footing load per unit area with time in a cyclic test is illustrated in Figure 6.8. While the profiles are similar, the applied maximum load was not identical in every test. This was a consequence of small variations in the control setting to the

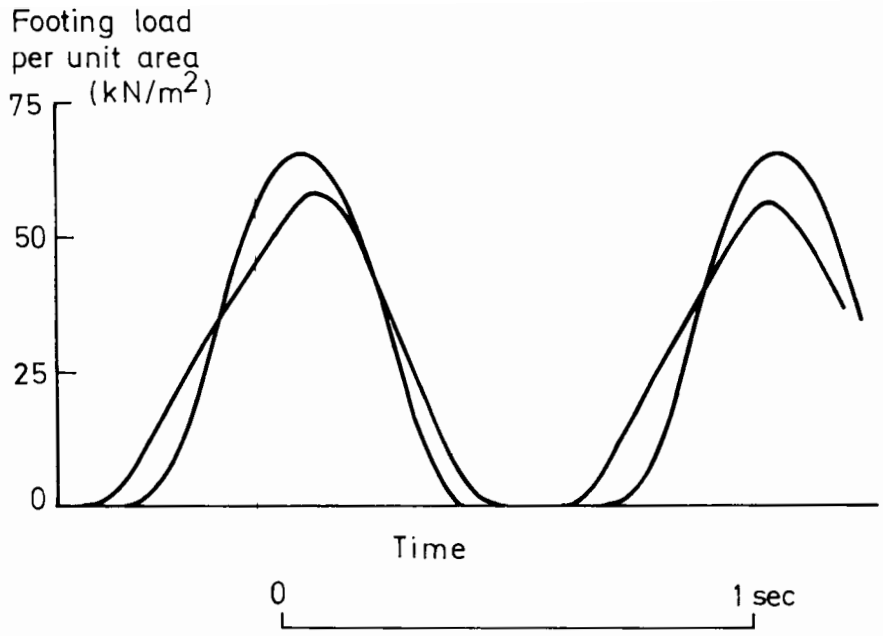

Figure 6.8 Typical variation of footing load/unit area with time

hydraulic actuator made during the first few cycles of load to establish the nominal test loading and in response to the overall system stiffness. In analysis each test is therefore characterised by the mean value of the maximum contact pressure that was applied throughout a test.

The cyclic test results are presented as a maximum footing penetration against number of load applications, Figure 6.9. The progress of each test follows a similar profile with the exception of that for U6125, which was a result of the nominal maximum contact pressure of 68kN/m^2 exceeding the ultimate bearing capacity of this test arrangement. Difficulties were experienced with the control of load to

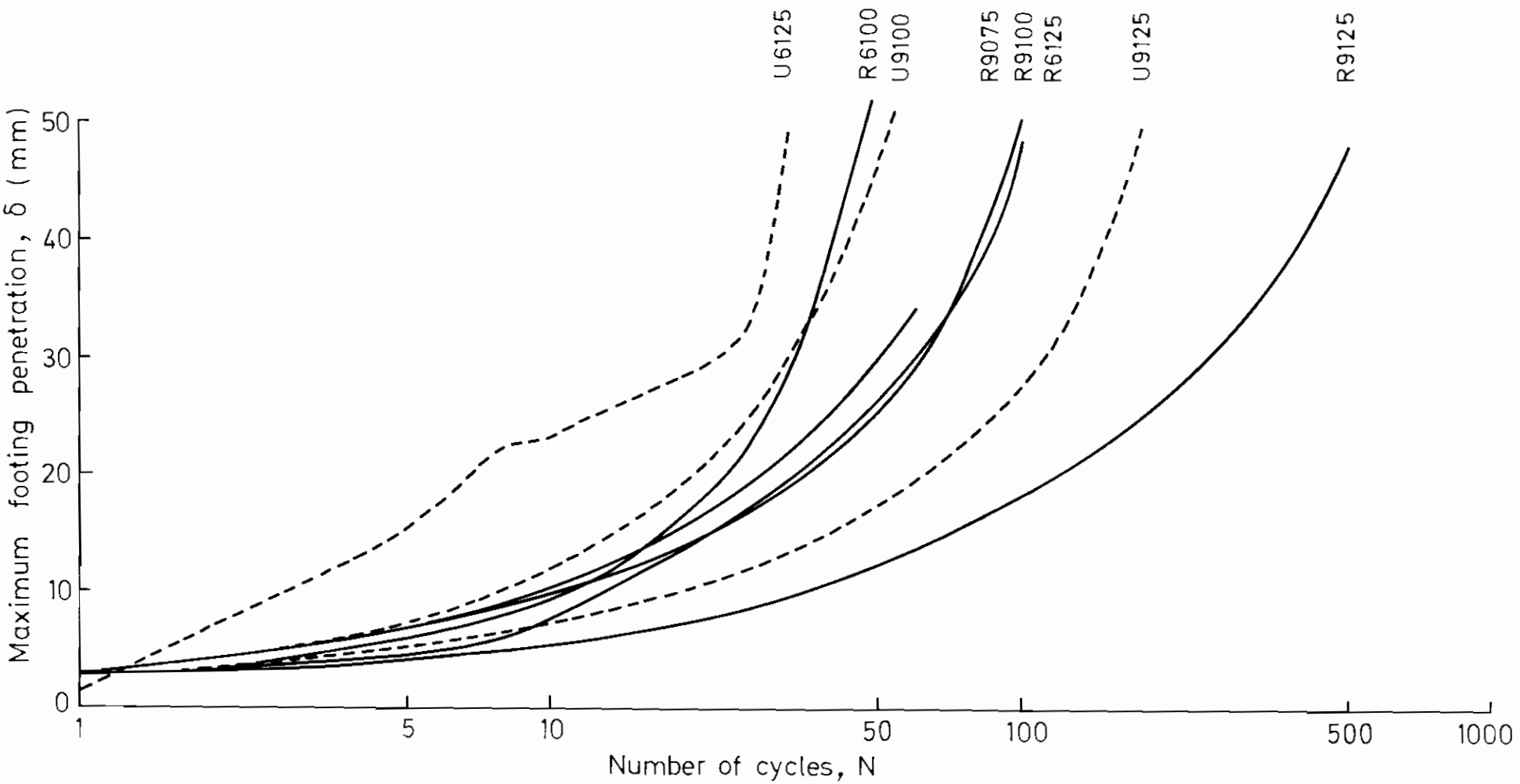

Figure 6.9 Cyclic test results

the footing in these conditions, and a rapid initial failure was followed by an underloading of the footing at one stage and a reduced rate of footing penetration. However in general, a common footing penetration on the first load application was followed by a clear early improvement in the reinforced systems, so that at small displacements and for N between 10 and 20, the reinforced tests were beginning to exhibit a significantly better capacity than the unreinforced tests. Indeed a reinforced test was typically observed to take about twice as many load applications to a footing penetration of δ=25mm, increasing to a ratio of 2.5 at δ=50mm.

Displacements for end-of-test conditions in two similar tests, one of which was reinforced, illustrate very well some general observations made throughout the test programme, Plates 6.1 and 6.2. In an unreinforced system granular material at the clay interface was noticeably displaced from under the edges of the footings as the test proceeded, causing the load spreading action of the granular layer to be eroded. However granular material under the footings in the reinforced system was effectively restrained by the grid, which acted to preserve the integrity of the granular layer and maintain its load spreading ability.

6.1.5 Clay marker movements

From an examination of a series of photographs of each test, the position of markers in the clay and a profile of the granular layer during a test was recorded using the digitising facility described in section 3.5. Processing of the data allows the marker movements to be

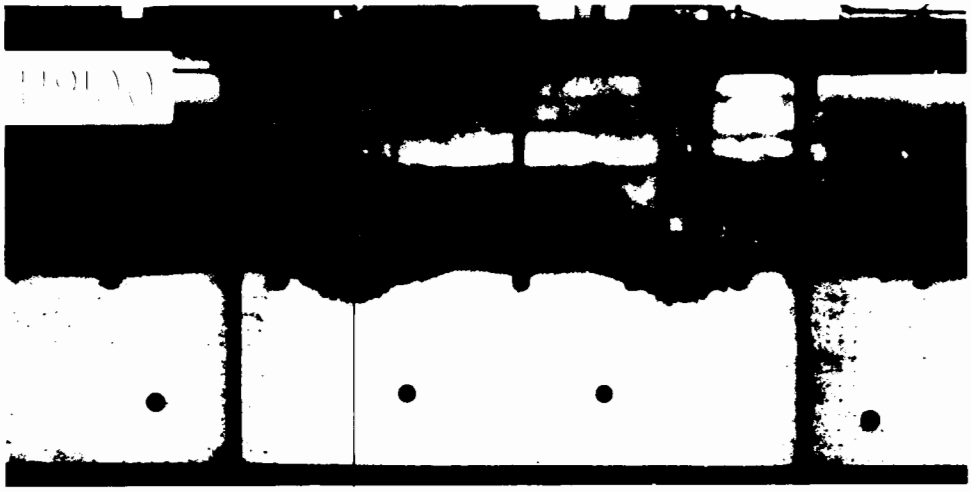

Plate 6.1 Displacements during test U9100

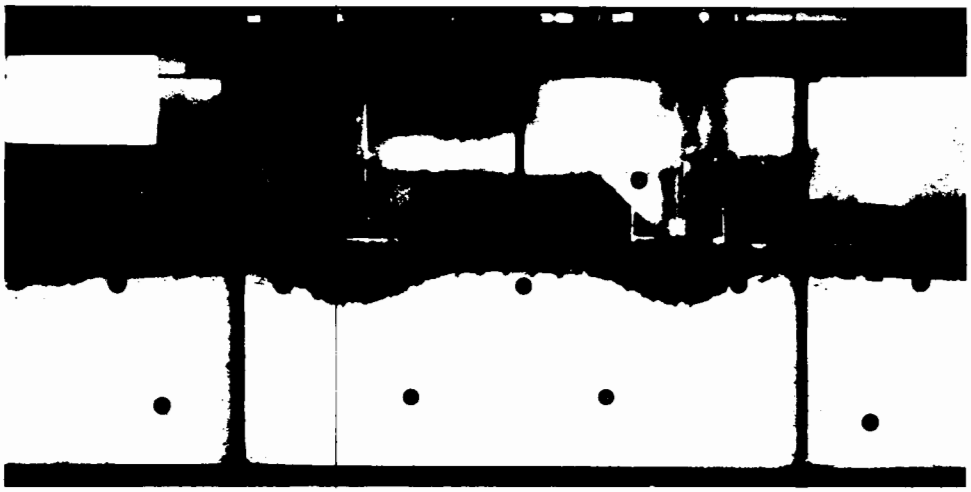

Plate 6.2 Displacements during test R9100

plotted as displacement and strain vectors which may be used to describe the nature of the failure deformations in the subgrade. These results are described separately below.

6.1.5.1 Subgrade displacements

In all cases subgrade displacements were seen to be symmetric about a centre line to the dual footing and asymmetric about a centre line to each footing plate, with greater movements occurring outside rather than between the footings, Figures 6.10 and 6.11.

Comparing these displacements vector plots for either the unreinforced or the reinforced systems, there is a clear similarity in the pattern of equivalent monotonic and cyclic tests. Characteristically, displacements in an unreinforced system were shallow and relatively localised. Indeed little interaction was observed between the separate deforming zones beneath each footing plate, which tends to confirm the previous observation that in an unreinforced test the dual footing acts as two single footings. However the presence of grid reinforcement, in preserving the integrity of the granular layer and improving the overall bearing capacity, seemed to mobilise significantly deeper movements in the clay. Consequently in the later stages of a test displacements in a reinforced system were both noticeably greater in magnitude and more extensive.

The development of subgrade displacements during a load test is illustrated in Figure 6.12 for test R6100. Essentially the magnitude of

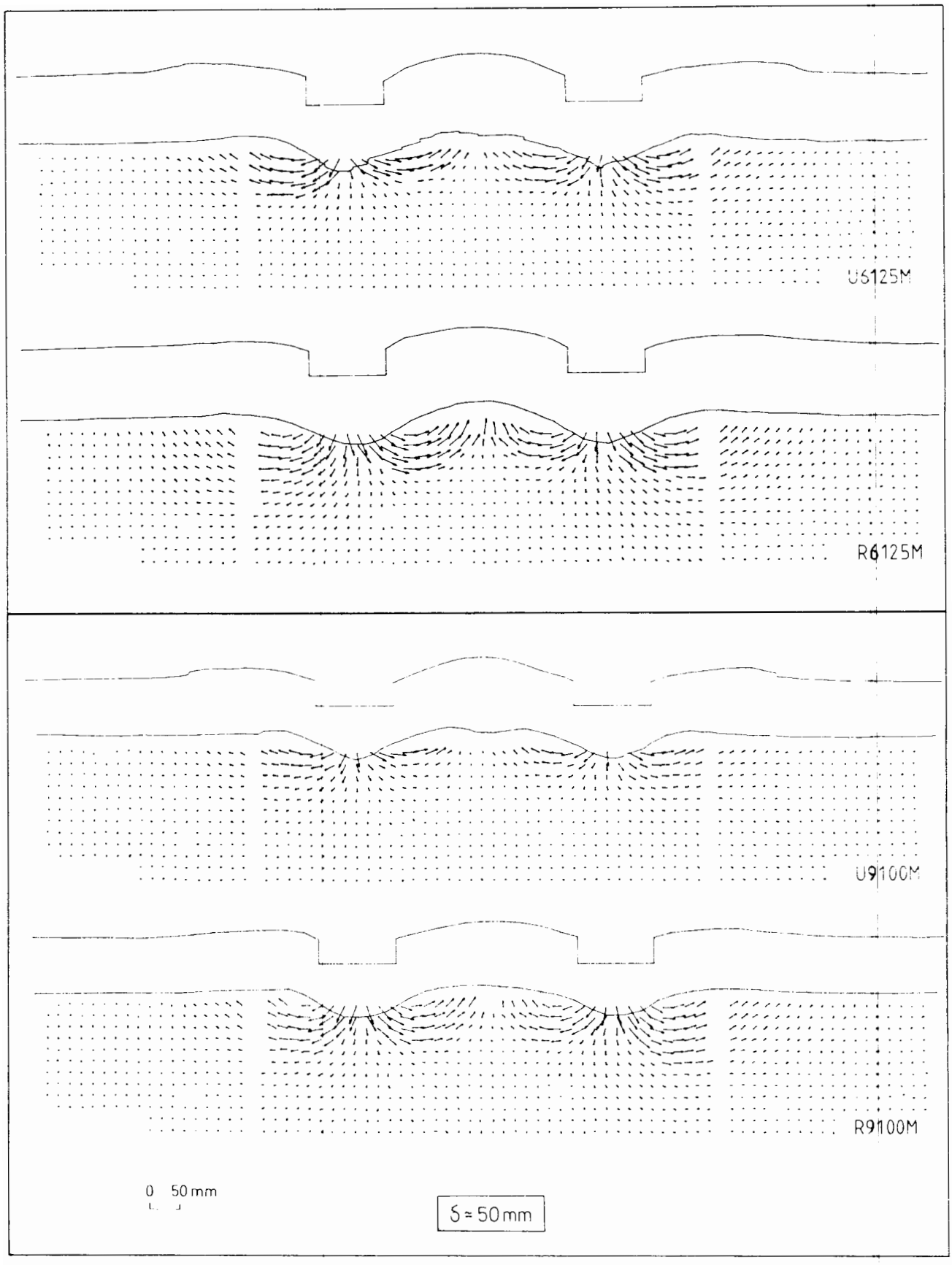

Figure 6.10 Subgrade displacement vectors for some monotonic tests

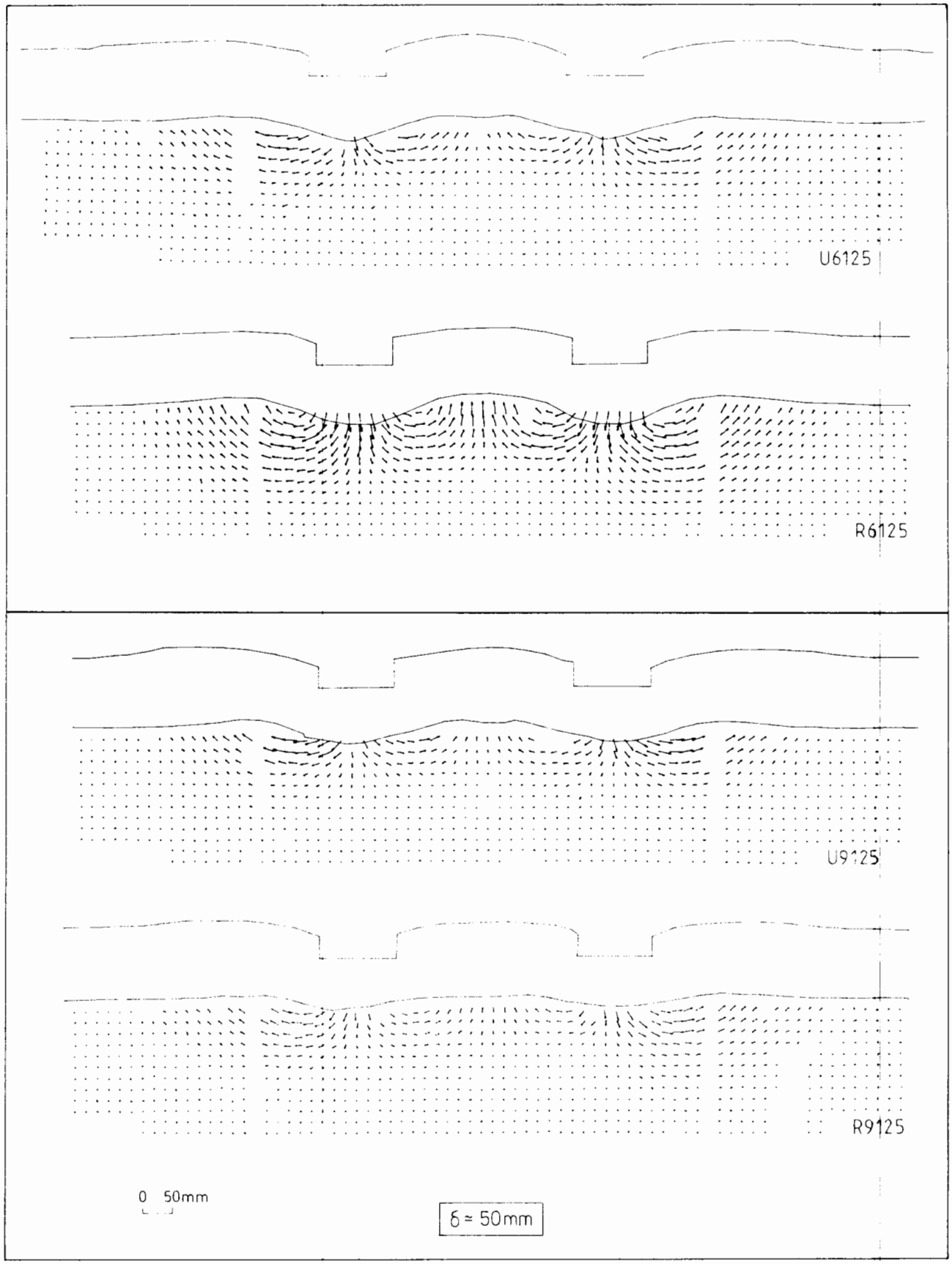

Figure 6.11 Subgrade displacement vectors for some cyclic tests

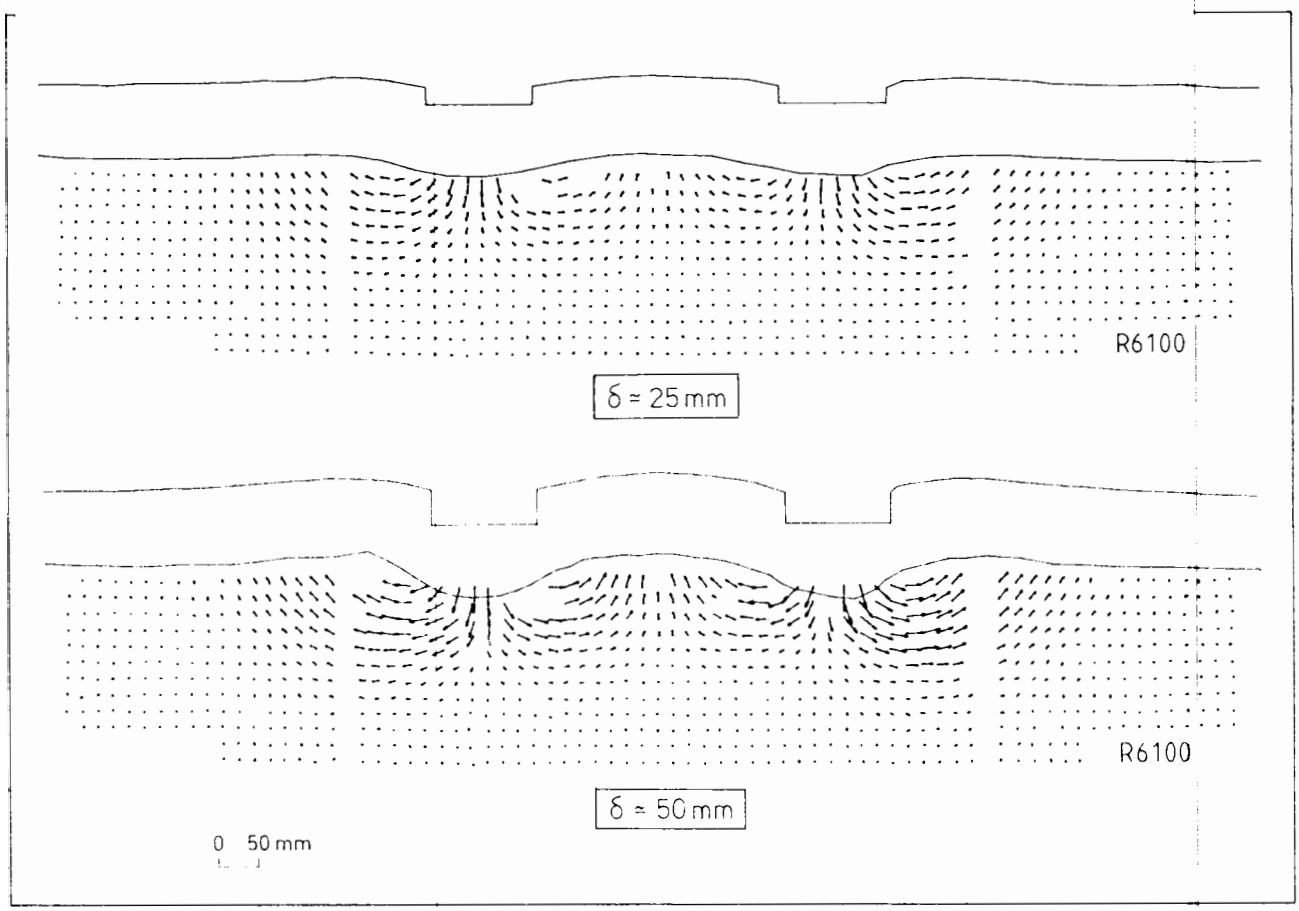

Figure 6.12 Development of subgrade displacements during test R6100

displacements increase with continued footing penetration, while the relative size and shape of the deforming zones remained largely unchanged.

6.1.5.2 Subgrade strains

Principal strain calculations were made to complement the displacement vector plots, and a typical strain pattern is illustrated in Figure 6.13 for two tests. The absence of some strain vectors in a plot was a result of any obscured markers causing the strain calculation for all adjoining elements to be lost, with the effect particularly noticeable close to the vertical members of the front face frame.

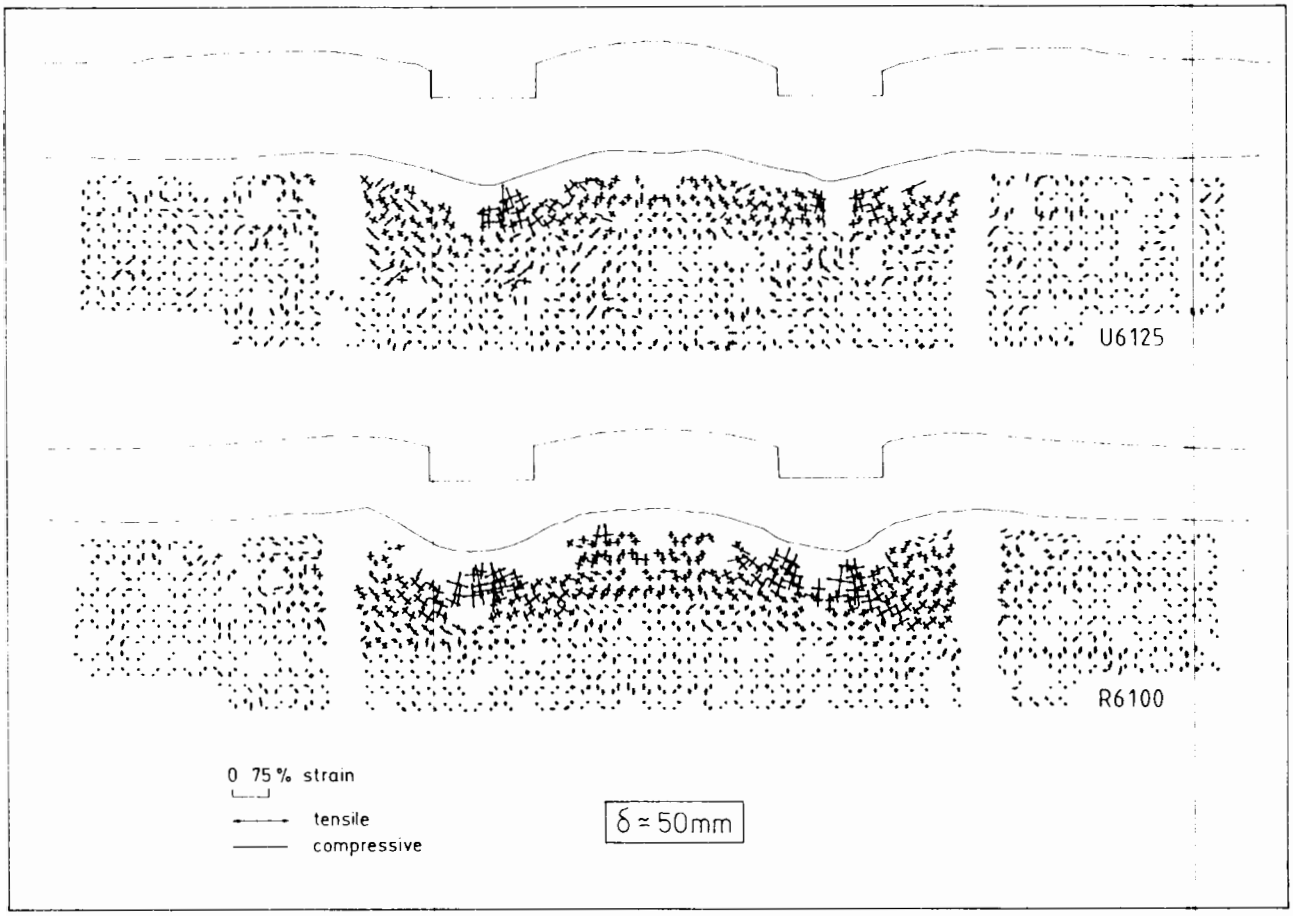

Figure 6.13 Principal strain plots for two tests

Notwithstanding this, the strain vectors broadly agree with the subgrade displacement observations. There are two specific points of interest. Firstly, there was very little strain associated with displacements that occurred in the zones of heave outside each of the footings, which suggests the clay was tending to move as a block. Secondly the characteristic of equal tensile and compressive strains is in agreement with an undrained behaviour in the clay.

The variation of horizontal strain along the uppermost row of subgrade marker elements is illustrated in Figures 6.14 and 6.15 for a footing penetration $\delta \approx 25$mm. In the analysis of these strains in the

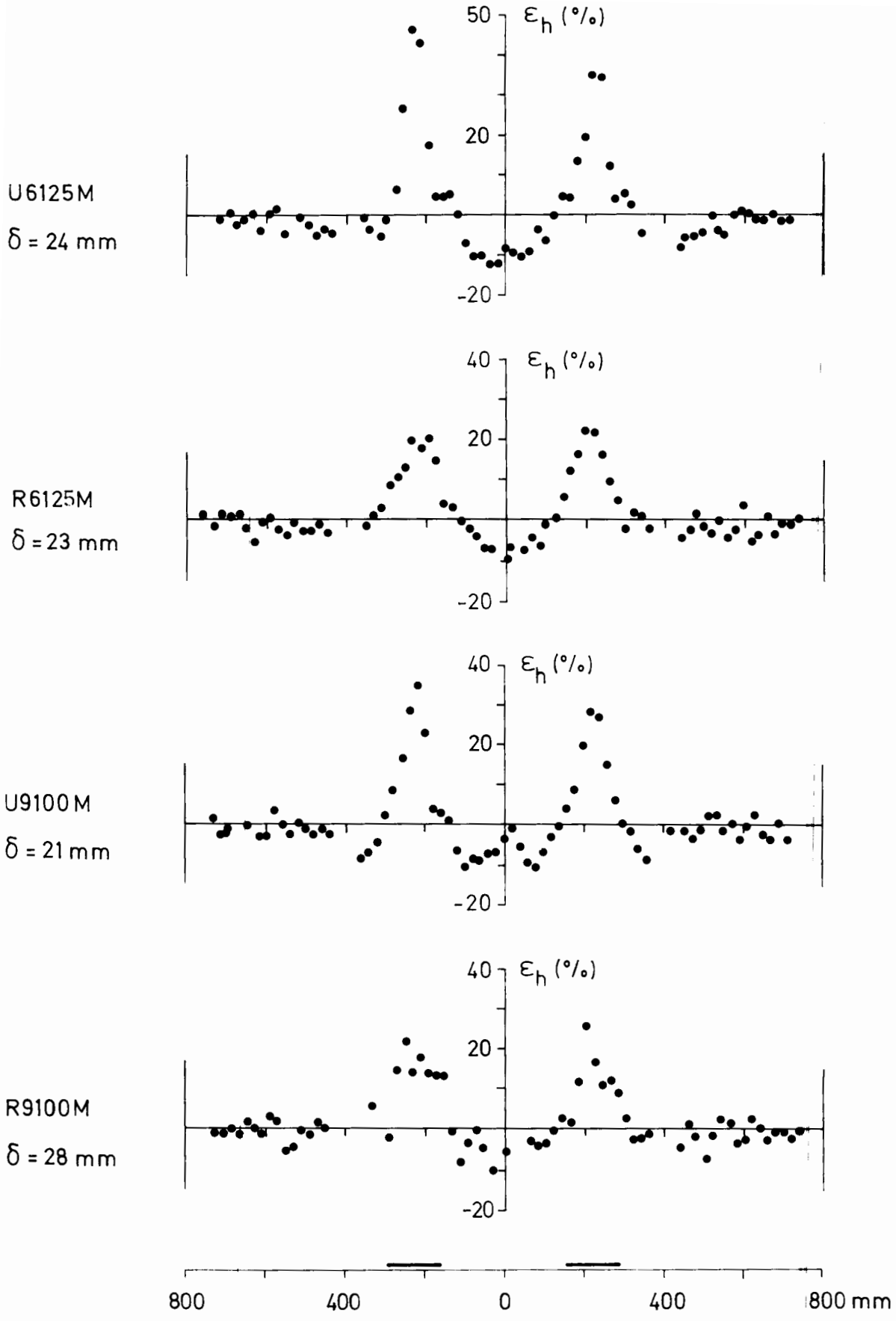

Figure 6.14 Variation in horizontal strain near the surface of the clay: monotonic tests

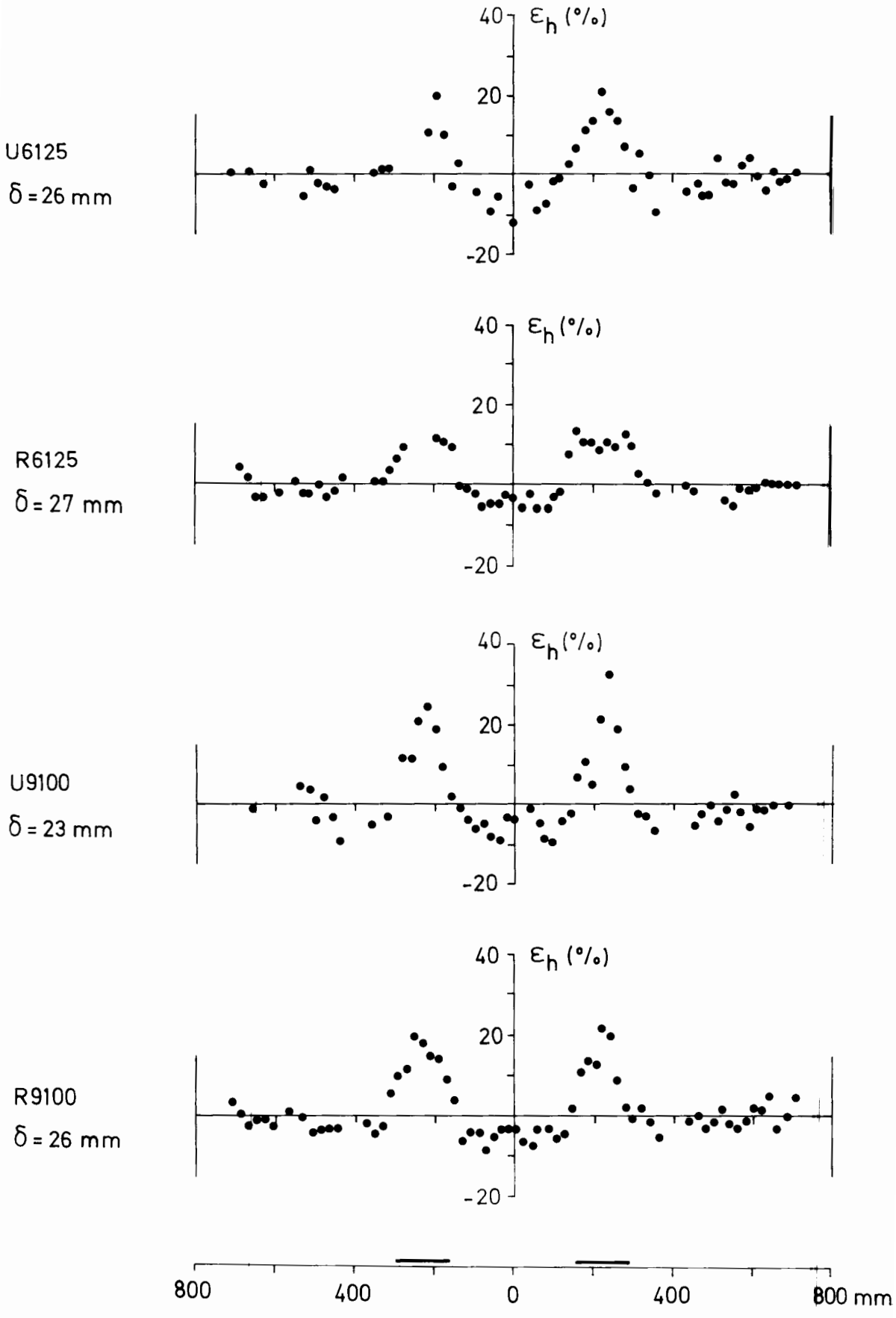

Figure 6.15 Variation in horizontal strain near the surface of the clay: cyclic tests

clay immediately below the granular layer, tensile strain is considered positive and compressive strain negative. While it is difficult to make a precise calculation of the error in the values of strain, scatter recorded for elements away from the loaded area indicates it is of the order ± 4%.

Generally a pattern of tension beneath the footings and compression between them was observed, however a distinct feature in all tests was that the magnitude of horizontal tensile strains in the clay immediately beneath the footing was significantly less in the reinforced tests. Clearly in accepting outward acting shear forces from the granular material and so going into tension, reinforcement was causing lateral strains transmitted to the subgrade to be reduced. It would therefore appear that the early improvement in performance of the reinforced system over the unreinforced system, during loading to these moderate displacements, is primarily a result of lateral strain inhibition rather than any development of a membrane-type effect.

6.2 Analysis

The test results are described by an analysis based on upper bound solutions to the observed failure mechanisms. In addition to the classical bearing contribution to footing load capacity, consideration is also given in the reinforced tests to lateral restraint of the subgrade and a membrane component.

6.2.1 Plastic collapse therorems

In structural mechanics, upper and lower bound theorems of plastic collapse have been proved for perfectly plastic materials to set limits to the collapse load of a structure. Proofs are derived from the principle of virtual work and may be stated, (Atkinson, 1981)

"If there is a set of external loads and a mechanism of plastic collapse such that the increment of work done by the external loads in an increment of displacement equals the work done by the internal stresses, collapse must occur and the external loads are an upper bound to the true collapse loads."

UPPER BOUND THEOREM

"If there is a set of external loads which are in equilibrium with a state of stress which nowhere exceeds the failure criterion for the material, collapse cannot occur and the external loads are a lower bound to the true collapse loads."

LOWER BOUND THEOREM

Extending the use of these bound theorems to undrained loading of a saturated soil continuum in plane strain, Atkinson argues that the appropriate failure criterion in such soils is the ultimate strength given by

$$\tau = c_u \qquad (6.1)$$

To establish an upper bound solution a compatible mechanism of plastic collapse must be identified. This is made by assuming a series of slip planes which, as illustrated for a footing in Figure 6.16, may be straight lines or circular arcs. Compatibility between individual rigid

blocks moving in different directions is maintained by an arrangement of radial slip planes termed a slip fan. For an increment of plastic collapse, the work done by the external loads δE is equated to the work done by the internal stresses δW where

$$\delta W = c_u L \delta w \quad \text{(for a slip plane)} \tag{6.2}$$

$$\delta W = \Sigma\, c_u R(\delta w \delta\theta) + \Sigma\, c_u (R\delta\theta)\delta w \quad \text{(for a slip fan)} \tag{6.3}$$

and δw is an increment of displacement. In fact the particular failure mechanism of Figure 6.16 may be shown to give a value for the footing bearing pressure at failure of $(\pi+2)c_u$ which is an exact solution, and therefore represents a lowest value to the upper bound.

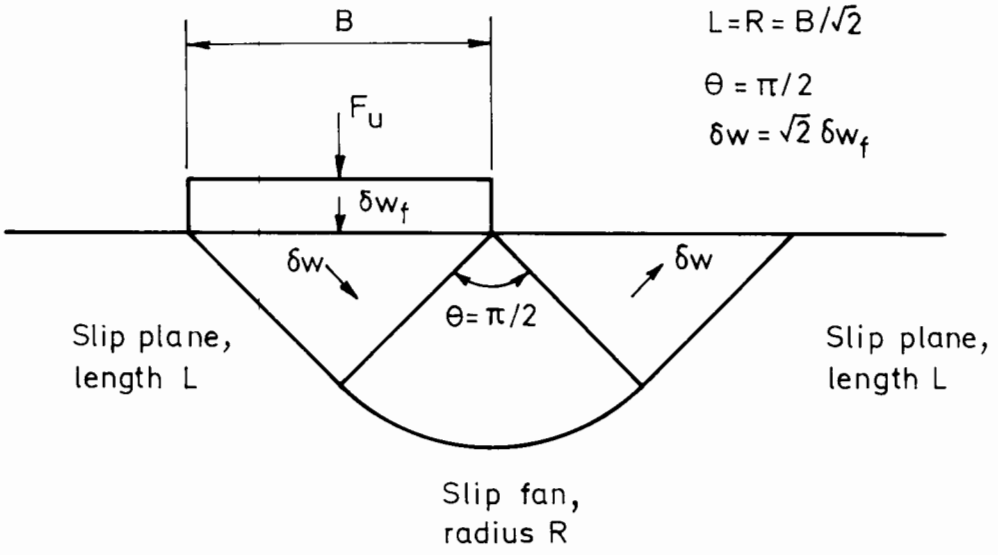

Figure 6.16 Mechanism of plastic collapse in undrained loading (after Atkinson, 1981)

For no surcharge, a smooth footing and self-weight forces summing to zero

$$\delta E = F_u \delta w_f \tag{6.4}$$

From the geometry of the collapse mechanism,

$$\delta W_{planes} = c_u \frac{B}{\sqrt{2}} \sqrt{2}\delta w_f + c_u \frac{B}{\sqrt{2}} \sqrt{2}\delta w_f \tag{6.5}$$

$$\delta W_{fan} = c_u \frac{B}{\sqrt{2}}(\sqrt{2}\delta w_f \frac{\pi}{2}) + c_u (\frac{B}{\sqrt{2}} \frac{\pi}{2}) \sqrt{2}\delta w_f \tag{6.6}$$

and equating

$$\delta E = \Sigma \delta W \tag{6.7}$$

$$F_u \delta \omega_f = 2c_u B \delta w_f + \pi c_u B \delta \omega_f$$

$$F_u = (\pi+2) c_u B \tag{6.8}$$

6.2.2 Observed collapse mechanisms

The previous example solution was for direct contact between a loaded footing and a saturated soil mass. The laboratory test arrangement of a compacted layer overlying the subgrade may be similarly described, Figure 6.17, taking into account a load spreading action of the granular material and an effective footing width B′. Conceptually this establishes two points, between which the clay is displaced

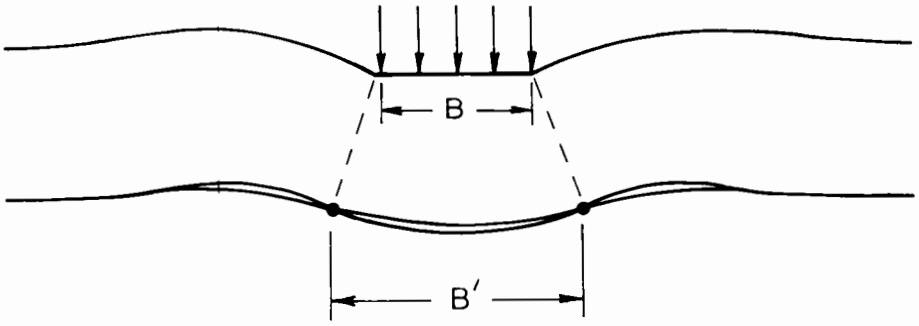

Figure 6.17 Effective footing width B′

downwards and outside which the clay is displaced upwards, termed 'stationary points', Love (1984). At any stage in a test B′ could be measured from a superposition of two profiles of the granular layer taken from successive photographs, so establishing the points of intersection on the profiles. Generally the results indicated that during an unreinforced test B′ tended to decrease as material was displaced from under the footing, while in a reinforced test there was a greater tendency for grid restraint to oppose this lateral flow of material and consequently limit the decrease in the value of B′, particularly at larger footing penetrations.

Examining once again the displacement vector plots for the subgrade deformations, it is possible now to identify failure planes and slip fans in terms of B′ which describe the mechanism of collapse that was previously identified. The appropriate mechanism is illustrated for the unreinforced tests in Figure 6.18 and for the reinforced tests in Figure 6.19. The particular arrangement of slip planes within the mechanisms was established from a consideration of a minimum upper bound solution,

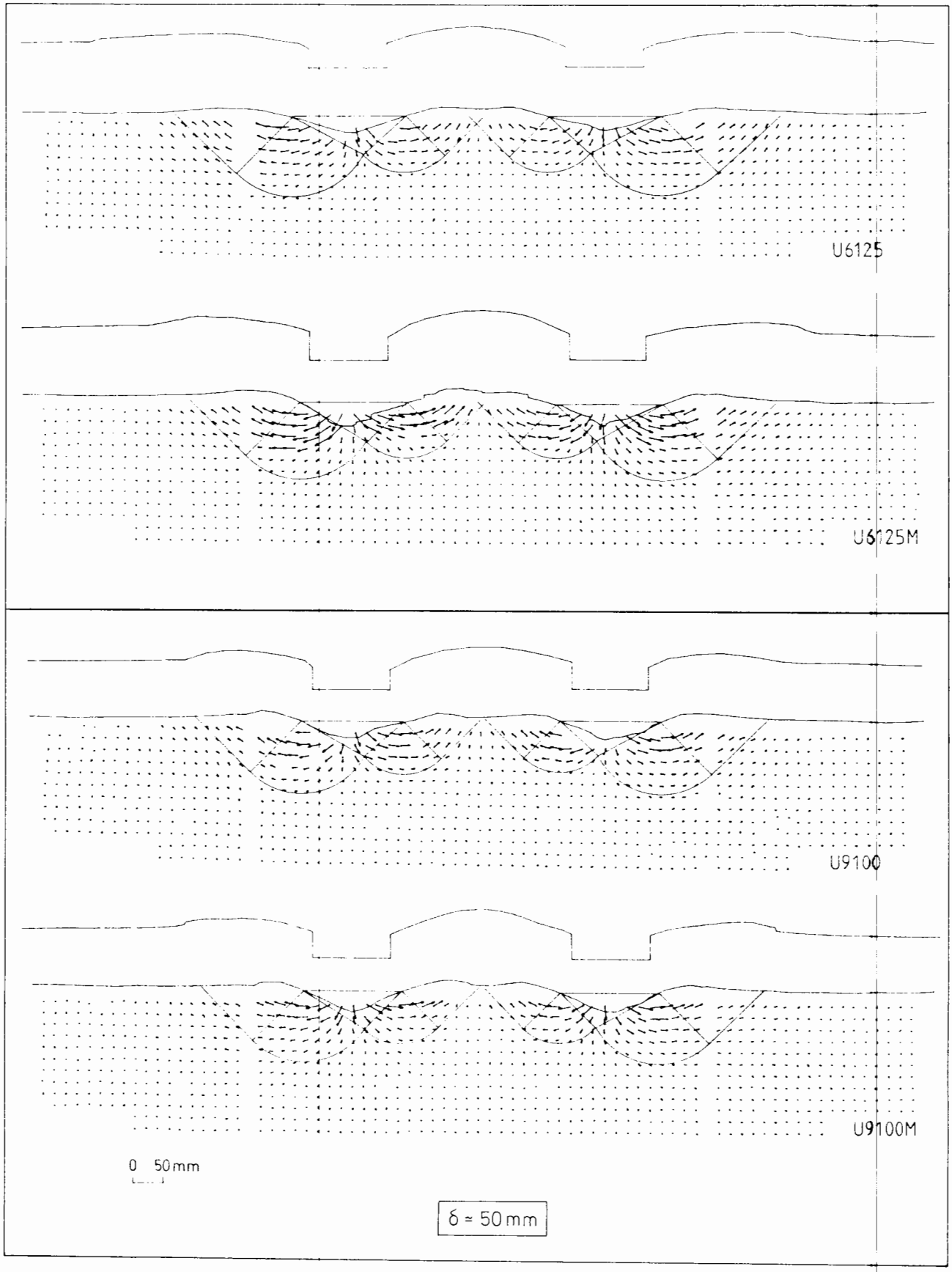

Figure 6.18 Collapse mechanism in the unreinforced tests

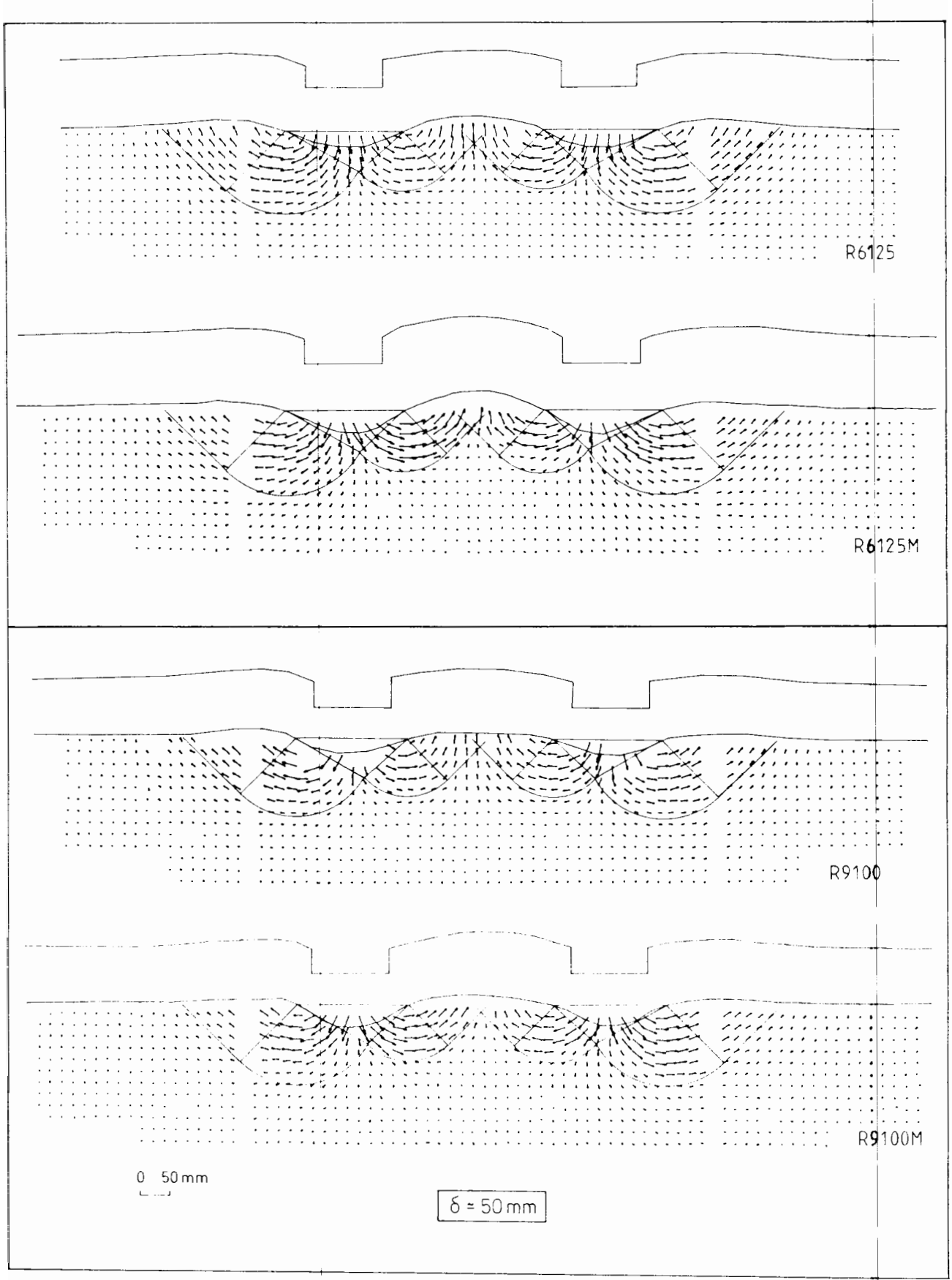

Figure 6.19 Collapse mechanism in the reinforced tests

for which calculations are presented in section 6.2.3 below.

Encouragingly the general shape of the failure patterns in the subgrade closely resembles that of the classical bearing capacity approaches, and a good fit is observed for both the monotonic and cyclic tests. In many of the tests there were indications of a small, though developing interference between the footings. This effect in adjacent foundations has been studied by Stuart (1962), who comments that while interference between footings may influence settlement characteristics, for the case of saturated clays the interpenetration of deforming zones will not lead to a change in bearing capacity.

6.2.3 Upper bound stability calculations

Analysis of the test results has established a general pattern of the failure or collapse mechanism in the reinforced and unreinforced tests. The mechanism is described by a series of rigid blocks and variable slip fans as shown in Figure 6.20. In accordance with the expectations of plasticity theory, intersection of the rigid blocks with the free surface must occur at 45^{o}. The angles of θ_1 and θ_2 are therefore established, and the magnitude of displacement vector for each rigid block may be determined from a displacement diagram or hodograph. Equating the external and internal work done, a solution for the bearing contribution to footing may be obtained as shown below.

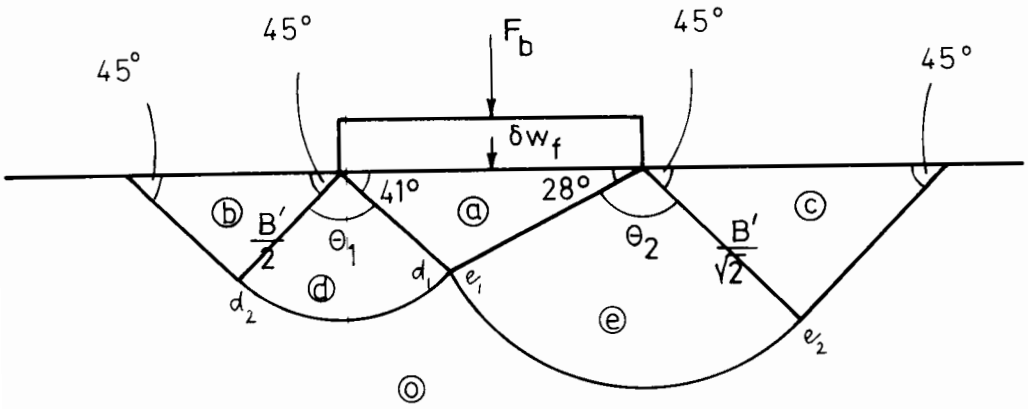

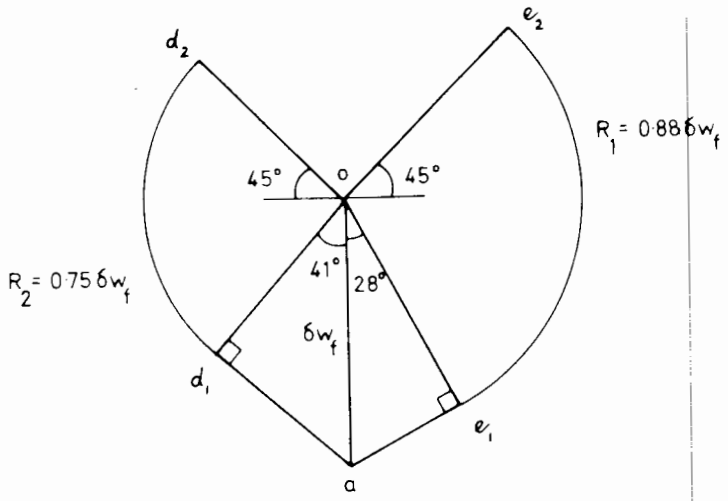

Figure 6.20 Schematic mechanism of plastic collapse in a reinforced and unreinforced test, with displacement diagram

From the geometry of the mechanism,

$$\theta_1 = 94^{o} \tag{6.9}$$

$$\theta_2 = 107^{o} \tag{6.10}$$

From the displacement diagram,

$$R_1 = 0.88\delta w_f \tag{6.11}$$

$$R_2 = 0.75\delta w_f \tag{6.12}$$

Equating the external and internal work done,

$$F_b\delta w_f = c_u \frac{B'}{\sqrt{2}} \delta w_f \sin 28° + 2c_u \frac{B'}{\sqrt{2}} \theta_2 \delta w_f \cos 28° + c_u \frac{B'}{\sqrt{2}} \delta w_f \cos 28°$$

$$+ c_u \frac{B'}{2} \delta w_f \sin 41° + 2c_u \frac{B'}{2} \theta_1 \delta w_f \cos 41° + c_u \frac{B'}{2} \delta w_f \cos 41° \tag{6.13}$$

and by substitution for θ_1 and θ_2 where

$$\theta_1 = \pi(\frac{94}{180}) \quad \text{and} \quad \theta_2 = \pi(\frac{107}{180}) \tag{6.14}$$

then,

$$F_b\delta w_f = 5.22\ c_u B' \delta w_f \tag{6.15}$$

and arranging as a bearing term,

$$q'_b = \frac{F_b}{B'} = 5.22c_u \qquad (6.16)$$

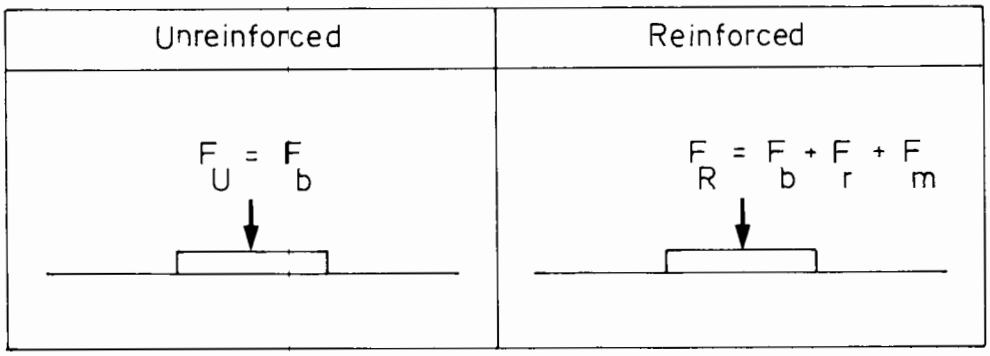

Figure 6.21 Schematic consideration of the separate contributions to footing load

In analysis of the results, this bearing contribution to footing load F_b is of course common to both the reinforced and unreinforced tests. In addition, consideration is given in the following sections to a lateral restraint contribution F_r and a membrane contribution F_m that were observed to operate in the reinforced tests only, as shown in Figure 6.21.

Now,

$$q'_b = 5.22c_u > (\pi+2)c_u \qquad (6.17)$$

where $(\pi+2)c_u$ is the classical and well accepted bearing factor. A likely explanation for this larger observed value is the undoubted interaction that occurred, not in the subgrade, but in the granular layer between the two footings. In this region the heaving clay blocks were tending to drive two opposing wedges of granular material into each other, and since the $(\pi+2)$ factor is applicable to conditions of direct surface loading only, it is not unreasonable to expect a somewhat greater capacity to be mobilised in the tests.

6.2.4 Lateral restraint of the subgrade

During testing the grid maintained an interlocking action with the granular material directly under the footing by an interpenetration of the particles into the grid apertures. Outside this region compaction of granular material during the preparation for testing had also caused the grid to interlock with the base of the granular layer. However as a test proceeded upward heave movements of the deforming subgrade caused this interlock to be lost, with the grid being drawn increasingly into the clay. Lateral restraint of the subgrade may therefore be described separately as

- a sliding action of clay along the base of the granular layer and grid at moderate displacements
- a movement or flow of clay through the grid apertures at large displacements

This first mechanism of shearing in which the grid is interlocked with the granular material has been shown by Burd (1986) to mobilise a shear stress nearly $0.9c_u$ along the interface. From Figure 6.22, the restraint mechanism can therefore be described using the principle of virtual work by

$$\begin{aligned} F_r \delta w_f &= \delta W_b + \delta W_c \\ &= 0.9c_u 0.625B' \, 0.75\delta w_f \cos 45^\circ + 0.9c_u 0.875B' \, 0.88\delta w_f \cos 45^\circ \\ &= 0.8c_u B' \delta w_f \end{aligned} \tag{6.18}$$

and arranging as a subgrade restraint term, then

$$q'_r = \frac{F_r}{B'} = 0.8c_u \tag{6.19}$$

However at large footing penetrations the second mechanism referred to above governed lateral restraint to the subgrade, an effect which may be charactersied separately as a bearing and sliding action on the grid members. The particular collapse mechanism observed in tests, with outward acting displacement vectors at 45°, may be conservatively described as bearing by the inclined component of displacement on to the longitudinal rib members of the grid and sliding along the lower surface only of the grid, Figure 6.23. Now, a general expression for pull-out force for a grid in a cohesive material is given by Ingold (1983) of the form,

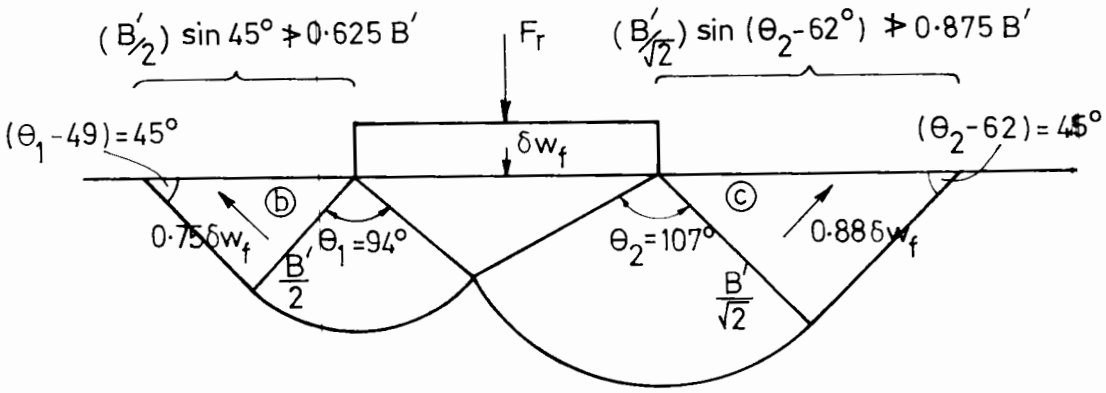

Figure 6.22 Lateral restraint of the subgrade: virtual work approach

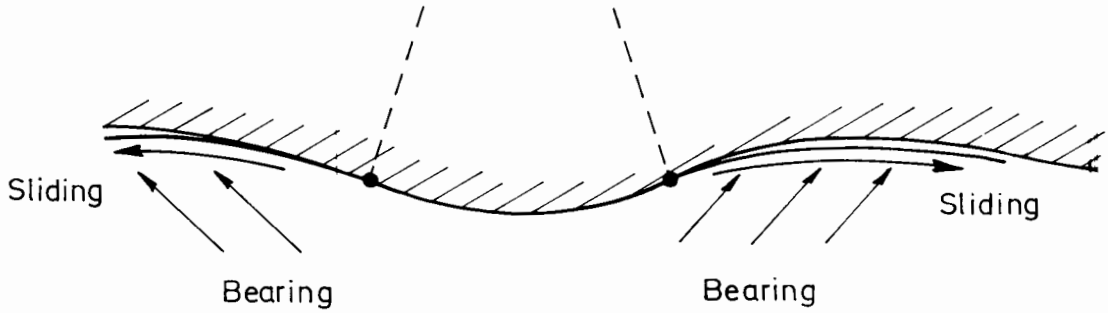

Figure 6.23 Lateral restraint of the subgrade at large displacements: simplified physical mechanism

$$T = N_c \, c_u \, \Sigma a_b + \alpha \, c_u \, \Sigma a_s \qquad (6.20)$$

where, Σa_b is the total area in bearing

Σa_s is the total area in sliding

and N_c and α are a load factor and an adhesion factor respectively. Given a proper selection of these parameters, such a relationship may be used to describe the lateral restraint exercised by the grid. Consider the grid movement and flow of soil round the members simply as a rod in a soil mass. An exact solution for undrained loading of laterally loaded piles in a cohesive soil is described by Randolph and Houlsby (1984) for plane strain conditions, and the results expressed as a load factor varying almost linearly with roughness between $\pi + 6$ for the perfectly smooth case (α=0) and $4\sqrt{2} + 2\pi$ for the perfectly rough case (α=1). Some pull-out tests were made to check the validity of this approach and are reported in section 6.2.4.1 below. A value of α=0.7 and therefore a corresponding load factor of 11.34 were selected from analysis of these test results; calculated grid areas in sliding and bearing are shown in Figure 6.24 and given in Table 6.1.

Equation 6.20 can now be arranged as an expression of force per unit area where,

$$\text{T/unit area} = 11.34 \, c_u \left(\frac{a_b}{a} \right) + 0.7 \, c_u \left(\frac{a_s}{a} \right)$$

$$= \underset{\text{(bearing)}}{0.25 \, c_u} + \underset{\text{(sliding)}}{0.04 \, c_u} \qquad (6.21)$$

and a is the aperture area.

Table 6.1 Characteristic grid parameters

a_b	lateral bearing area	2.4 mm^2/aperture
a_s	base sliding area	5.9 mm^2/aperture
a	aperture area	110.5 mm^2

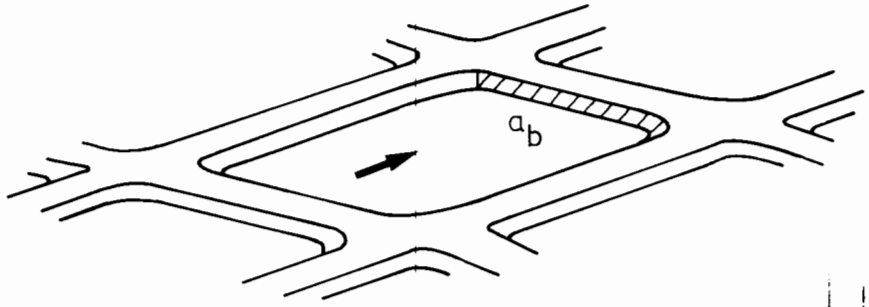

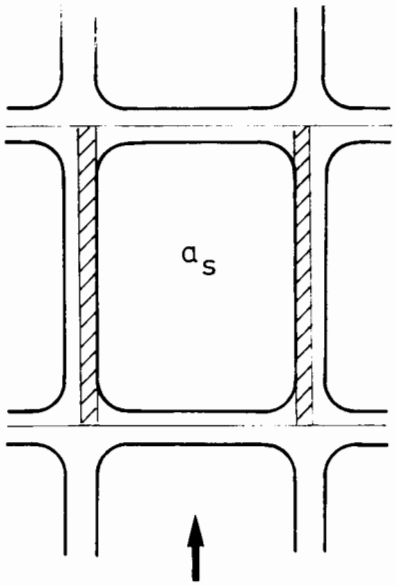

Figure 6.24 Areas of grid in bearing and sliding

This equation was used to calculate a subgrade restraint component to the collapse load of the reinforced system based on the same virtual work principle as before Figure 6.22, where

$$F_r \delta w_f = \delta W_b + \delta W_c$$

$$= \left[0.25 c_u 0.75 \delta w_f \frac{B'}{2 \sin (139^\circ - \theta_1)} + 0.04 c_u 0.75 \delta w_f \frac{B'}{2 \sin (139^\circ - \theta_1)}\right]$$

$$+ \left[0.25 c_u 0.88 \delta w_f \frac{B'}{\sqrt{2} \sin (\theta_2 - 62^\circ)} + 0.04 c_u 0.88 \delta w_f \frac{B'}{\sqrt{2} \sin (\theta_2 - 62^\circ)}\right] \quad (6.22)$$

where $\frac{B'}{\sqrt{2} \sin (\theta_2 - 62^\circ)} \not> 0.875\ B'$, the limiting anchorage length in the tests. Arranging as a subgrade restraint term, and for $\theta_1 = 94^\circ$ and $\theta_2 = 107^\circ$, then

$$q'_r = \frac{F_r}{B'} = 0.4\ c_u \quad (6.23)$$

Since the grid was not stationary in the soil but was tending to pull through it, the expression will give a conservative value of the work done because the increment of displacement δw_f does not include a contribution for the appropriate movement of the grid which is unknown.

6.2.4.1 Pull-out tests

To confirm the validity of the approach and allow a proper selection of parameters N_c and α in equation 6.20 some very simple pull-out tests were made using the model grid reinforcement. The test arrangement is illustrated in Figure 6.25 : remoulded Speswhite Kaolin at a moisture content between 56.3 and 57.3% was compacted in a series of layers in a small metal box; during this process the grid specimen was placed so that one end protruded through a slot located at a mid-height in one end wall of the box. In preparation of the grid for testing a hollow metal tube had been previously cast on to the free end using a low melting point Ostalloy metal and a thin wire threaded through this tube to pass over a pulley. The base of the Ostalloy casting, which had been finished to a smooth flat surface, was greased and supported on a lubricated flat sheet that was fixed horizontal and in line with the slot on the box.

Four samples were prepared for testing : the first was used as a check on the vane strengths of the compacted clay without any grid; the remaining tests included a grid specimen and were described by a single vane measurement made after preparation of the sample and before the pull-out test itself. In each test a pull-out force was applied quickly by pouring lead shot into a container suspended over the pulley, and the mass of shot to cause the grid to begin to pull out of the box measured. The results are summarised in Table 6.2.

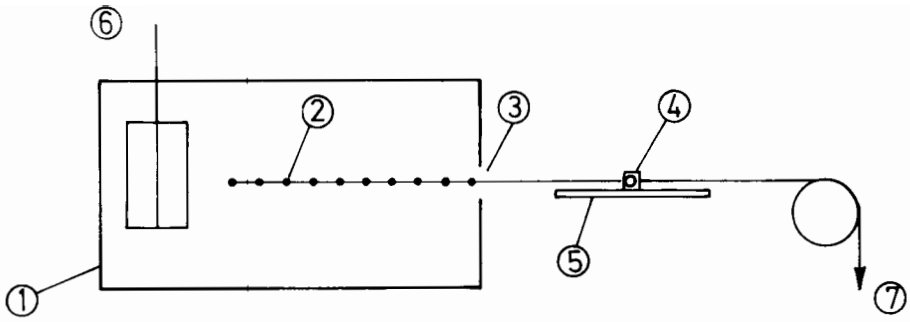

1. Box dimensions 200mm long x 120mm wide x 110mm deep
2. Buried grid specimen 13 apertures wide x 9.5 apertures long
3. Slot 15mm x 120mm
4. Greased end-cast
5. Lubricated sheet
6. Vane strength measurement
7. Pull-out force applied via pulley

Figure 6.25 Pull-out test arrangement

Table 6.2 Pull-out test results

Test No.	c_u (kN/m^2)	Pull-out force per unit width (kN/m)
1	4.4, 4.6, 4.4	-
2	4.4	0.190
3	4.7 (4.4)	0.179 (0.185)
4	4.2	0.187

Notes

(1) Mean value within parentheses

An expression of the required pull-out force per unit width is given by equation 6.20, and by substitution for the dimensions of the gird specimen then

$$T = \frac{(N_c \times 4.4(2.4 \times 13 \times 10)\times 10^{-6} + \alpha \times 4.4(2 \times 5.9 \times 13 \times 9.5)\times 10^{-6}}{0.109}$$

$$= (1.373N_c \times 10^{-3} + 6.412\alpha \times 10^{-3}) / 0.109 \qquad (6.24)$$

The theoretical variation of T with α and N_c is given in Table 6.3, and is seen to be in agreement with the mean of the experimental observations for a value of α=0.7 and corresponding load factor 11.34. Given the small amount of scatter in the results, a value of α=0.6 reported for a similar plastic grid by Ingold (1984) compares very reasonably.

Table 6.3 Theoretical variation of T with α and N_c

α	0.5	0.6	0.7	0.8	0.9	1.0
N_c	10.82	11.09	11.34	11.56	11.77	11.94
T	0.166	0.175	0.184	0.193	0.201	0.209

Notes

(1) Load factor N_c after Randolph and Houlsby (1984)

(2) T(kN/m) from equation 6.24

6.2.5 Membrane action

Membrane action is a well accepted consequence of large deformations which cause a vertical component of the reinforcement tension to contribute to the bearing capacity of the system. As such it is a function both of grid orientation, and tension T per unit width given by

$$T = s.\varepsilon \tag{6.25}$$

where s is the stiffness of the grid defined by a modulus value and ε is the strain in the material.

Burd (1986) has shown maximum tension to occur beneath the footing and an approximate variation of tension along the reinforcement as illustrated in Figure 6.26. The upward acting component of the membrane action between M and O is therefore seen to be $2T\sin\psi$, where T is the tension per unit width between these points and ψ is the inclination of the grid at the points. Additionally the downward acting components outside this region must be considered and for a virtual work approach as before, Figure 6.27, then a membrane contribution to the footing load per unit width is given by

$$F_m \delta w_f = 2T\sin\psi\ \delta w_f + T\sin\psi\ 0.75\delta w_f \sin 45^\circ + T\sin\psi\ 0.88\delta w_f \sin 45^\circ \tag{6.26}$$

and arranging as a membrane term

$$q'_m = \frac{F_m}{B'} = \frac{3.2\ T \sin\psi}{B'} \tag{6.27}$$

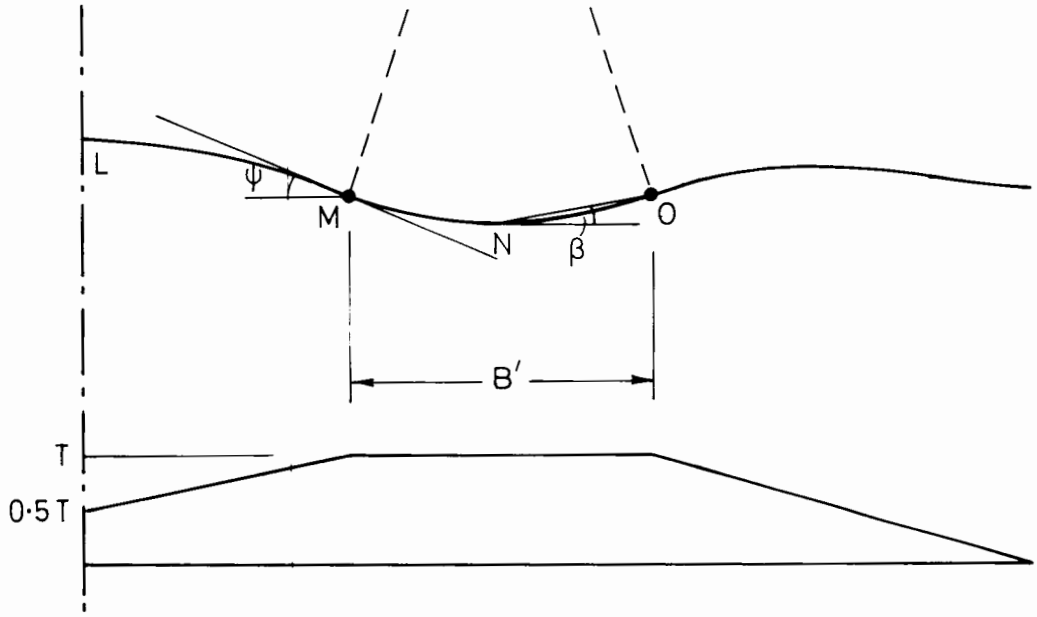

Figure 6.26 Simplified variation in tension/unit width in a grid reinforcement (from Burd, 1986)

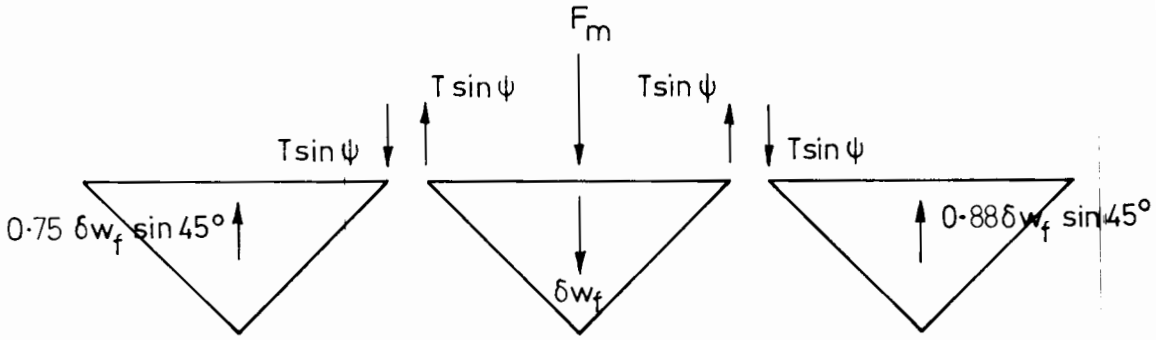

Figure 6.27 Membrane action: deforming block analysis

Now, ψ can be easily obtained from examination of the displacement profiles. However it was not feasible to measure reinforcement strains in the laboratory tests, and so an estimation of the strain magnitude must be made from the geometry of the deformations; tension per unit width in the grid may then be established using the appropriate modulus value. Several approaches are possible: for a simple straight line representation to the curves MN and NO, strain between M and O is constant and given by,

$$\varepsilon = \frac{1}{\cos \beta} - 1 \qquad (6.28)$$

This will obviously be a smaller value of strain than one calculated for the curved surface, yet from a practical viewpoint an underestimation of the theoretical value is an acceptable simplification considering the effect of slip on tensioning of the grid.

Ultimately, and at large displacements, some limiting value of tension per unit width will be reached which is necessarily a function of the anchorage to the reinforcement. Indeed depending on the relative strengths of the materials in bearing and sliding, it would not be unreasonable to expect that the limiting value T_{limit} in these very soft clays might be less than a previous maximum value T_{max}, particularly if interlock with the granular material was lost in the course of testing. Considering this point, observations and post-test examination of the position of the grid clearly indicated that the limiting tension was mobilised by an anchorage in the subgrade rather than a bond with the

granular layer, and for these particular conditions and from equation 6.21,

$$T_{limit} = \left[11.34c_u\left(\frac{a_b}{a}\right) + 0.7c_u\left(\frac{2a_s}{a}\right) \right] L_a$$

$$= 0.3c_u L_a \qquad (6.29)$$

where L_a is the available anchorage length, given by 0.875B′.

6.2.6 Summary

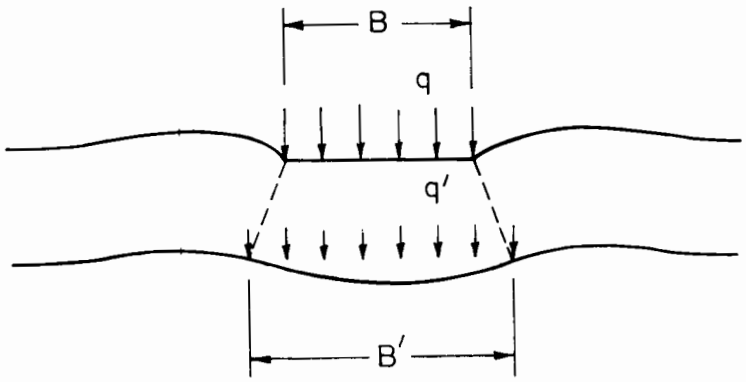

Figure 6.28 Load distribution

Assuming that the footing load per unit area q is uniformly distributed over an effective footing width B′,

$$\int_{-B/2}^{+B/2} q \, dB = \int_{-B'/2}^{+B'/2} q' \, dB' \qquad (6.30)$$

and so

$$q = q' \left(\frac{B'}{B} \right) \qquad (6.31)$$

For an unreinforced system, and from equation 6.16

$$q_u = q'_b \left(\frac{B'}{B} \right)$$

$$= q_b \qquad (6.32)$$

For a reinforced system, and from equations 6.16, 6.27 and either 6.19 or at large displacements ($\delta \simeq 50mm$) equation 6.23

$$q_R = (q'_b + q'_r + q'_m) \frac{B'}{B}$$

$$= q_b + q_r + q_m \qquad (6.33)$$

CHAPTER 7

FULL SCALE TEST RESULTS

7.1 Test programme

This chapter describes a series of large scale tests made to investigate the effectiveness of a Tensar SS2 geogrid in improving the bearing capacity of a granular layer over a weak clay subgrade. The study was carried out using test bay facilities of the Ground Engineering Division of the Transport and Road Research Laboratory, and involved monotonic loading of rigid footings bearing on to the surface of a compacted granular material. During loading, measurements were made of footing load and penetration, together with general deformations of the clay and granular layer.

The test arrangement was constructed in a covered bay, and is illustrated in Figure 7.1(a). In each test the performance of unreinforced sections was compared with that for sections reinforced with a geogrid located at the base of the granular layer. Two types of tests were made: axi-symmetric conditions were observed for circular footings of diameter 300mm, while predominantly two-dimensional conditions of deformation were observed for a rectangular footing 300mm wide and 1500mm long.

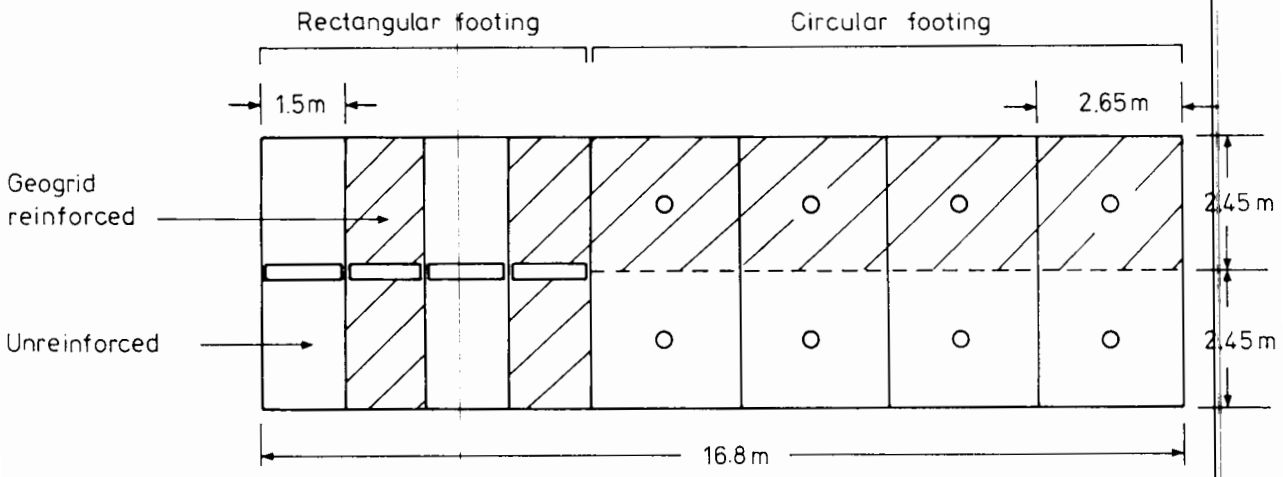

Figure 7.1(a) Test bay arrangement

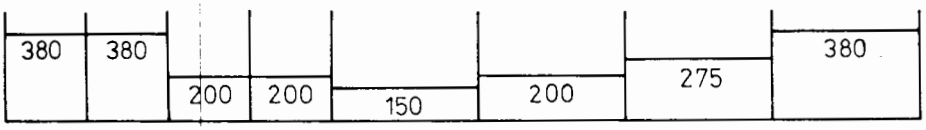

Figure 7.1(b) Nominal thickness of the granular layer in each test section

Plate 7.1 Test bay: general view during placement of the subgrade

Parameters varied in the test programme were thickness of the granular layer and shear strength of the subgrade clay. A schematic section along the length of the test bay Figure 7.1(b) illustrates the four layer thicknesses 150, 200, 275 and 380mm considered in the study. A first series of footing load tests was made for a subgrade of nominal undrained shear strength 35kN/m^2; the tests were later repeated in a second series for a reconstituted and weaker subgrade of nominal undrained strength 10kN/m^2.

7.2 Test bay preparation

The test bay measured 16.8m long and 4.9m wide, with vertical concrete side walls, and a base to the 0.96m deep bay simply formed by the naturally occurring soil, the Bagshot beds.

Preparation of the test arrangement involved filling the lower part of the test bay with a clay. Granular material was then placed and compacted over this subgrade in sections of different layer thickness, each with and without geogrid reinforcement. The materials and construction stages are described separately below.

7.2.1 Clay

The subgrade was a London clay taken from a local borrow pit: the soil had a liquid limit of 72%, a plastic limit of 24% and a maximum dry density of 1.61Mg/m^3 at an optimum moisture content of 22%. Inspection on delivery showed it to be free of large stones, and well suited for

immediate mixing and wetting to the strength requirements of the first test series. This process, which was completed in a series of batches, involved spreading the clay on a prepared apron to a depth of 250-350mm and making repeated passes with a tracked rotovator, using the cutting action of the blades to mix the clay. Following each series of passes with the rotovator, the clay was wetted up and sheeted over with polythene to promote an ingress of the water. In the course of mixing, strength was recorded using a Pilcon hand vane by taking measurements in the well-compacted material of the rotovator track path, together with a comparison of these values against some unconfined compression tests. The mixing and wetting process was repeated until a reasonably uniform consistency was achieved throughout the batch, at which point the prepared clay was taken from the mixing apron and stockpiled next to the test bay, where it was again sheeted over. The procedure was continued until sufficient material had been prepared and in total four batches, nearly 90 tonnes, were mixed and wetted.

The remoulded clay was placed in the test bay in four lifts, each one spread to a level datum using a bucket excavator and compacted with a vibrating pedestrian tandem roller. Shear strength of the successive layers was measured with the Pilcon hand vane at 24 locations according to a grid coverage of the bay, while occasional local hard spots were reinstated by excavation and replacement of the poorly rotovated material. Moisture contents were also determined for these positions at a depth 75mm from the finished subgrade surface, and a number of quick-undrained triaxial tests made on samples taken from this same surface layer.

Table 7.1 Subgrade strength and moisture content measurements

Test series	Depth below surface (mm)	Pilcon vane shear strength mean	Pilcon vane shear strength SD (kN/m^2)	U-U triaxial tests (mean values) c_u (kN/m^2)	U-U triaxial tests (mean values) mc (%)	Moisture content from test bay samples (mean) (%)
1	75	28	3	(31)	(36.8)	38.0
	240	35	3			
	350	36	6			
	480	49	15			
2	75	10	2	(6)	(48.0)	48.0
	240	(11)	(3)			
	350	(11)	(2)			
	480	(13)	(4)			

Notes

(1) Figures within parentheses are post-test measurements
(2) Triaxial tests corrected for rubber membrane strength

Table 7.2 Some C-U triaxial test results

Cell press σ_r (kN/m^2)	B	c_v (cm^2/s)	q_f (kN/m^2)	u_f (kN/m^2)	Ø′
398	0.92	5.94×10^{-5}	233	155	18.3
603	0.94	10.27×10^{-5}	289	255	17.2

Note

(1) $B = (\Delta u / \Delta \sigma_r)$

For the first test series the clay was placed to a mean thickness of 530mm. For the second test series it was necessary to wet and mix the clay in situ with the excavator bucket because it was found to be too soft to allow the passage of plant. A summary of the subgrade strength measurements is given in Table 7.1. Generally a more uniform shear strength was observed throughout the second test series; the measured values indicate a variation in strength with depth, yet a reasonable uniformity across each layer except that of the base layer of the first test series. This was the first batch to be rotovated and probably suffered from a poor initial preparation technique.

A few consolidated-undrained triaxial tests were made on samples taken from this second test series, but unfortunately some of the samples were inadvertently damaged, and results for only two tests are presented in Table 7.2. The ratio between confining pressure and pore pressure response (pore pressure parameter B) indicates the clay was not fully saturated, while values measured for the coefficient of consolidation are similar to those which would be expected for a London clay.

7.2.2 Geogrid reinforcement

The type of reinforcement used throughout the test series was a Tensar SS2 geogrid manufactured by Netlon Ltd, for which strength properties and general specifications have already been described in section 5.2. In all tests the geogrid was placed directly onto the surface of the prepared clay formation, without restraint or artificial

tensioning of any kind. Test areas 2.65m x 2.45m prepared for the circular footing were reinforced with a grid of the same plan dimension (longitudinal x transverse); test areas 1.5m x 4.9m prepared for the rectangular footing were reinforced with a 1.5m length of grid cut from the full 4.02m width of the manufactured roll.

7.2.3 Granular material

The granular material was a well graded crushed limestone. Particle size distribution curves, Figure 7.2, indicate it lay within the grading limits for a Type 1 granular sub-base material according to the D.Tp. Specification for Road and Bridge Works (1976). Shearbox tests carried out on particles passing the BS 14mm sieve are summarised in Figure 7.3 (after Kirk, 1985). Samples were prepared to a density of 2.4Mg/m^3 at a moisture content of 4.0%, and tested in a box of plan area 300mm x 300mm.

The material was placed in loose layers approximately 100mm thick, and compacted to the required finished thickness in each section using a vibrating plate compactor (700kg/m^2). Circular footing tests were made on granular layers of 150, 200, 275 and 380mm nominal thickness; rectangular footing tests were made on granular layers of nominal thickness 200mm and 380mm. Partition boards were used to preserve the integrity of the granular layer in each section, and to isolate each section from the next during loading. In order to reduce any restraint to movement of the granular material during load testing, these separators and the vertical side walls to the test bay were sheeted with a double layer of polythene before placement of the granular material.

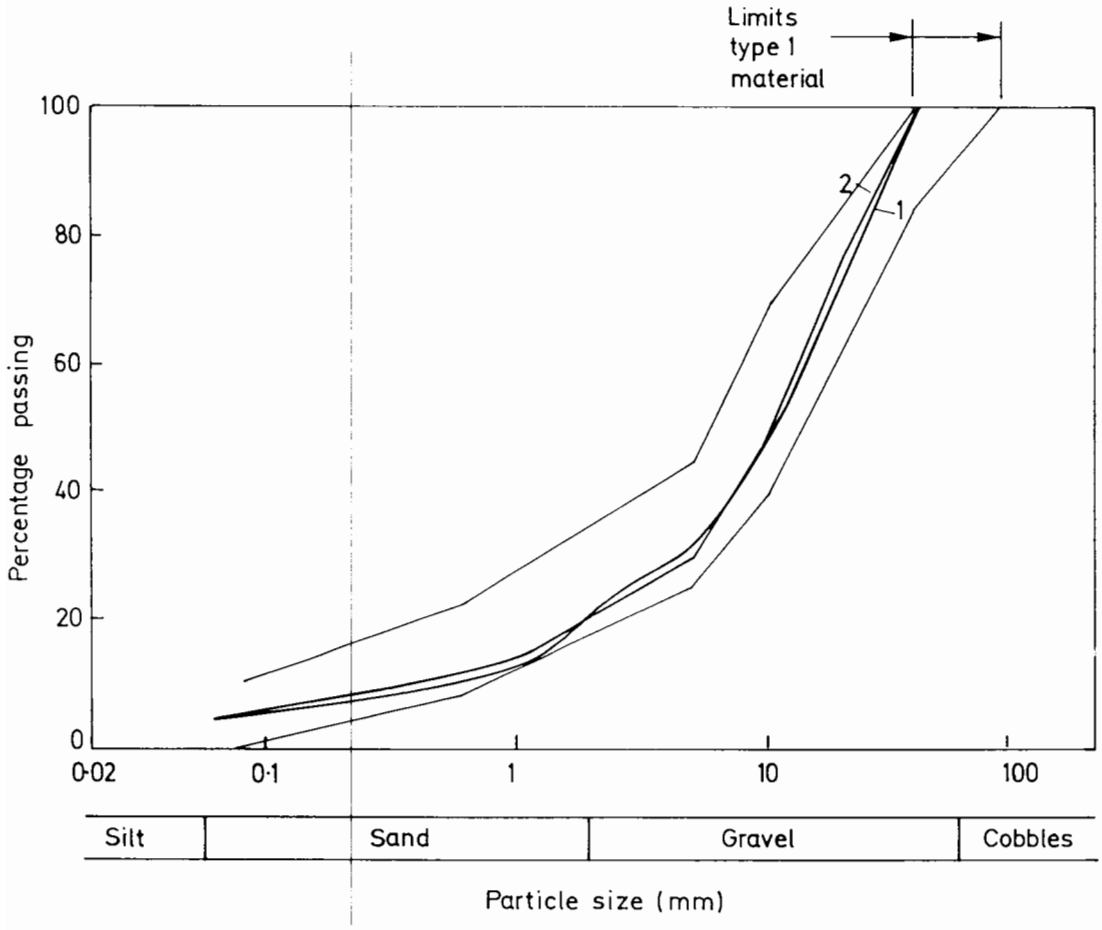

Figure 7.2 Particle size distribution curves for the Type 1 crushed limestone

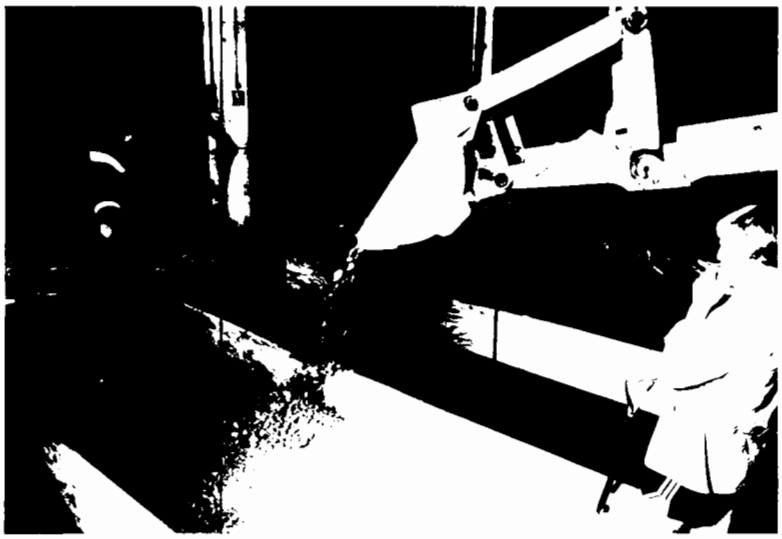

Plate 7.2 Placement of the granular material

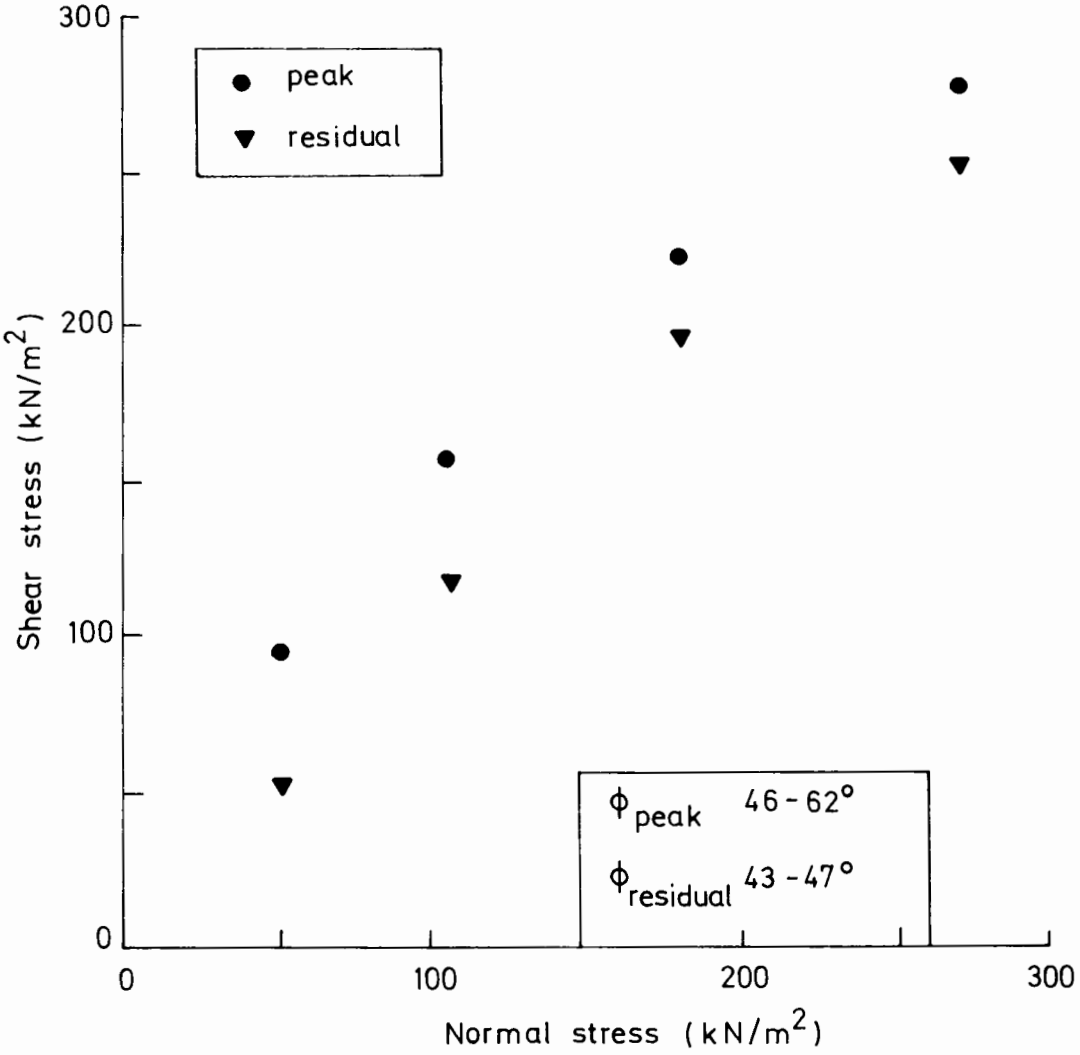

Figure 7.3 Shearbox test results (after Kirk, 1985)

It was considered that full compaction might not be possible on the very weak subgrade of the second test series, and consequently the compactive effort applied to the layers did not completely meet that recommended by D.Tp. Specification for Road and Bridge Works. A

determination of the dry density of the granular material was made using the sand replacement method/large pouring cylinder method, BS1377: 1975 Test 15(C), and the results are summarised in Table 7.3. For both reinforced and unreinforced sections a mean dry density in the range 2.33 to 2.36Mg/m^3 was achieved, indicating a very well compacted material.

Table 7.3 Summary of compaction densities for the granular layer

Test series	Layer	Mean value ρ_{dry} (Mg/m^3)	Mean value mc (%)
1	Reinforced	2.360	3.61
	Unreinforced	-	-
2	Reinforced	2.330	3.61
	Unreinforced	2.330	2.28

7.3 Instrumentation

Measurements were made of footing load and penetration, displacements along the surface of the granular layer, and in the rectangular footing tests only, vertical movements of the geogrid and strain in the subgrade. The instrumentation scheme for the rectangular footing is illustrated in Figure 7.4.

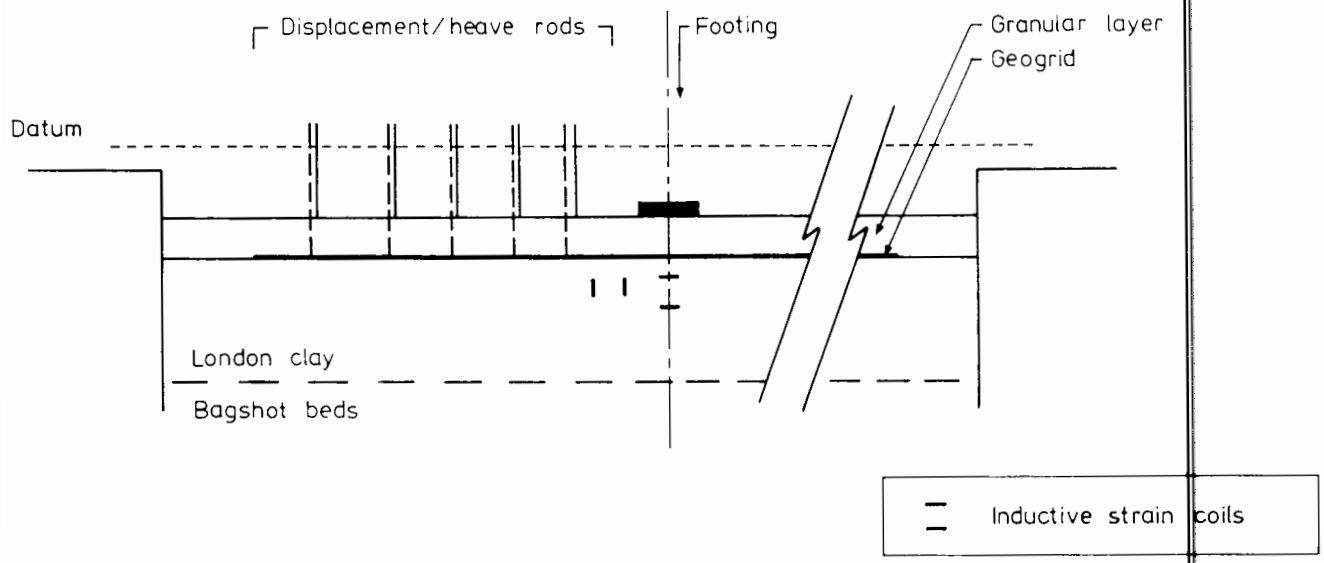

Figure 7.4 Instrumentation scheme for the rectangular footing

Footing load was measured by a strain gauged load cell located between the footing plate and a hydraulic loading ram. Manufactured by Elliott Brothers Ltd, the load cell had a 40 ton maximum capacity and was powered by a 10V DC supply. During testing, the rate of penetration and absolute displacement of the footing plates were recorded using dial gauges (accurate to 0.01mm) and graduated rules (accurate to 0.5mm).

In all tests, surface displacements of the granular layer were measured from the vertical movement of guided rods against a datum, with each rod seating on to a small base plate. In the rectangular footing tests a profile of the grid position at five locations was also recorded from the movement of sleeved guided rods passing through the granular material. Installation of the sleeves for the rods was made in stages,

and is illustrated in Figure 7.5. After placement of the first loose granular layer, a metal base plate and extension was positioned directly on to the geogrid with a cushioned plug (1) to the extension tube; compaction of the first layer was then made. Subsequent local excavation of the compacted material allowed a longer replacement plug (2) to be inserted before compaction of the next layer. The procedure was repeated to the finished layer thickness, at which stage excavation then allowed the plug to be removed and a rod sleeve of smaller inside diameter to be inserted; backfilling around the sleeve with coarse grit and tamping of the finished surface with a hand tamper fixed the assembly in position.

In all reinforced and unreinforced rectangular footing tests, permanent soil strain in the subgrade close to the footing was calculated from the relative displacements of 'Bison' inductive coils located in the clay, Figure 7.6. Powered by a commercially supplied unit, they operate on a principle of electromagnetic coupling between the coils inducing an output voltage. Successive signal nulling for each movement of the coils permits measurement of the signal amplitude component which is directly related to the sensor spacing. Calibration and accuracy of the coil arrangements are discussed in Appendix B. They were installed after placement and compaction of the clay, with care taken to ensure sufficient slack in the cable to avoid any restraint of movement. Vertical strain was determined from a pair of coils in parallel and co-axial alignment along the axis of loading; a second pair aligned along an axis perpendicular to that of the footing determined lateral subgrade strain. Unfortunately partial success only was obtained with this

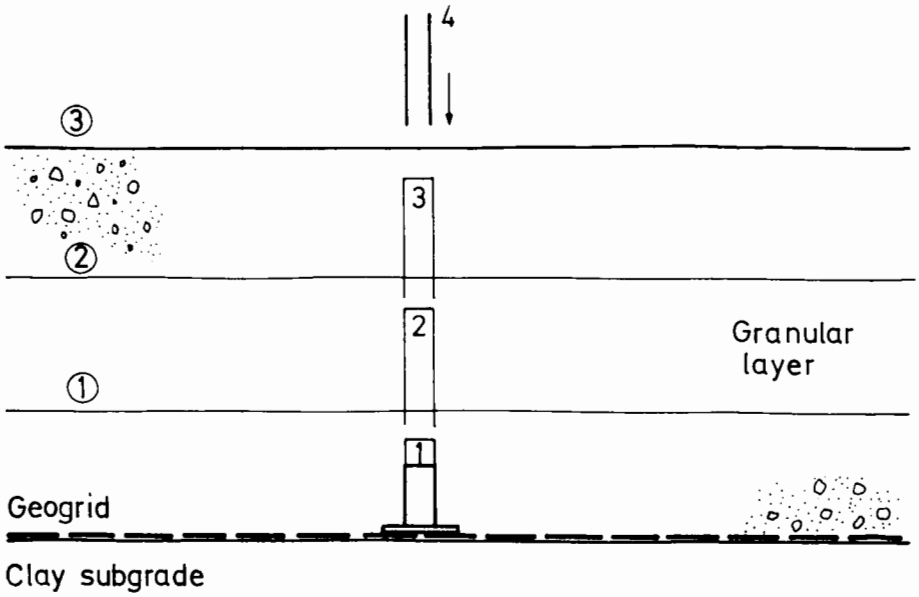

Figure 7.5 Schematic view of rod sleeve installation

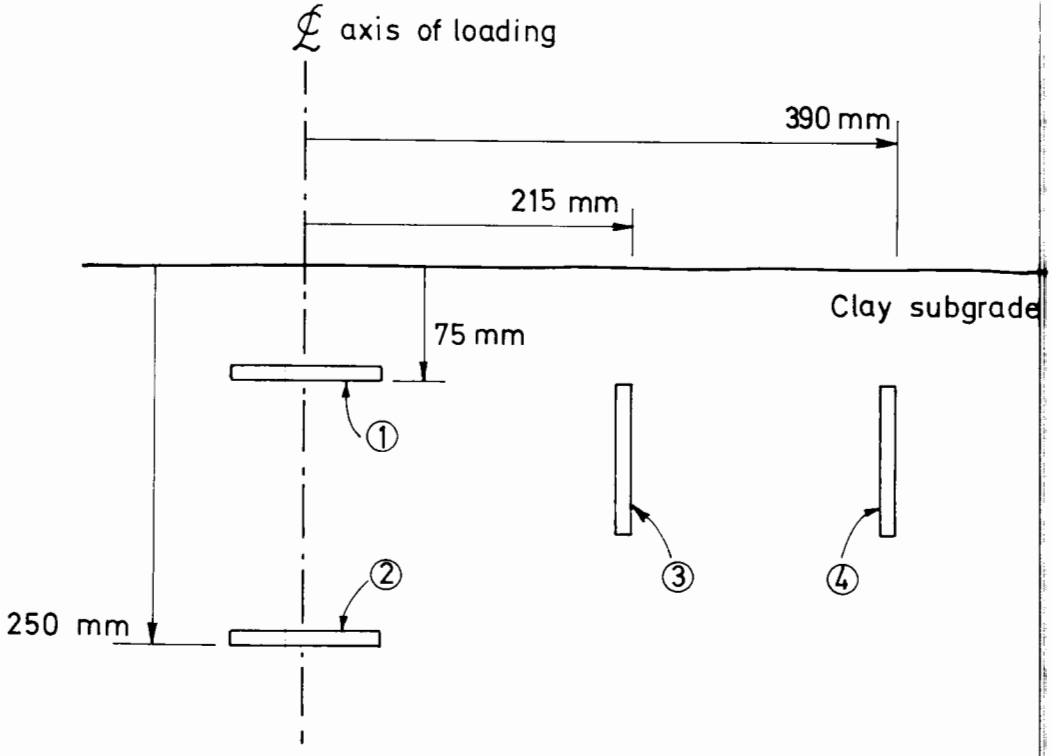

Figure 7.6 Strain coil arrangement

arrangement because of a non-axial movement between coils 3 and 4 which could not be defined uniquely in the calibration procedure.

7.4 Load test procedure

Load was applied to the footings by a hydraulic cylinder acting against a reaction point on a kentledge frame. Before each test the footing plate was seated level on a thin layer of blinding material and the frame manoeuvred on wheel rollers into position. The datum beam against which all movements were recorded was then placed across the test bay beneath the frame and displacement rods located as required. At this stage an initial profile of the granular layer surface was measured from the datum and a series of readings taken.

In all tests discrete increments of load were applied to a footing, and instrument readings taken for each increment when there was no perceptible increase in footing penetration, considered to be a rate of displacement less than 0.01mm/min. For the circular footing tests, load was increased to failure or a limiting value 6.5 tonnes. Footing load and mean penetration were recorded together with surface displacments of the granular layer. Typically each test took between 3 and 5 hours.

For the rectangular footing tests, load and mean penetration were recorded together with surface deflections as before. Inductive coil readings were also taken and vertical displacements of the geogrid measured. Footing load was increased incrementally to impending failure or a limiting value of 22.5 tonnes. The footing was then unloaded and

reloaded to the previous maximum for five cycles of application. Following this the footing was again unloaded, and load finally applied incrementally to failure or the limiting value. Typically each test took between 8 and 10 hours. At the end of all tests a profile of the granular layer surface was measured for the footing unloaded.

7.5 Results of tests on circular footings

A summary of the load-penetration results for the circular footings on the firm subgrade ($c_u \simeq 35 kN/m^2$) is illustrated in Figure 7.7. From the general relationship of the curves for the unreinforced tests, an increase in granular layer thickness is clearly associated with a corresponding increase in the bearing capacity of the system. For all sections except the thickest layer where little surface displacement occurred, inclusion of grid reinforcement caused an additional bearing capacity to be mobilised. The improvement due to reinforcement was such that load-penetration curves representing the reinforced and unreinforced condition for any similar granular layer tended to separate with increasing footing penetration, a separation which was apparent even at small displacements of 5-10mm. This suggests a reinforcing action that increased with increasing penetration, but one which was not wholly dependent on mobilising large displacements. Importantly, the substantial failure of the thinnest reinforced layer, with an associated small increase in bearing capacity, indicates a potential upper limit to any improvement from the grid.

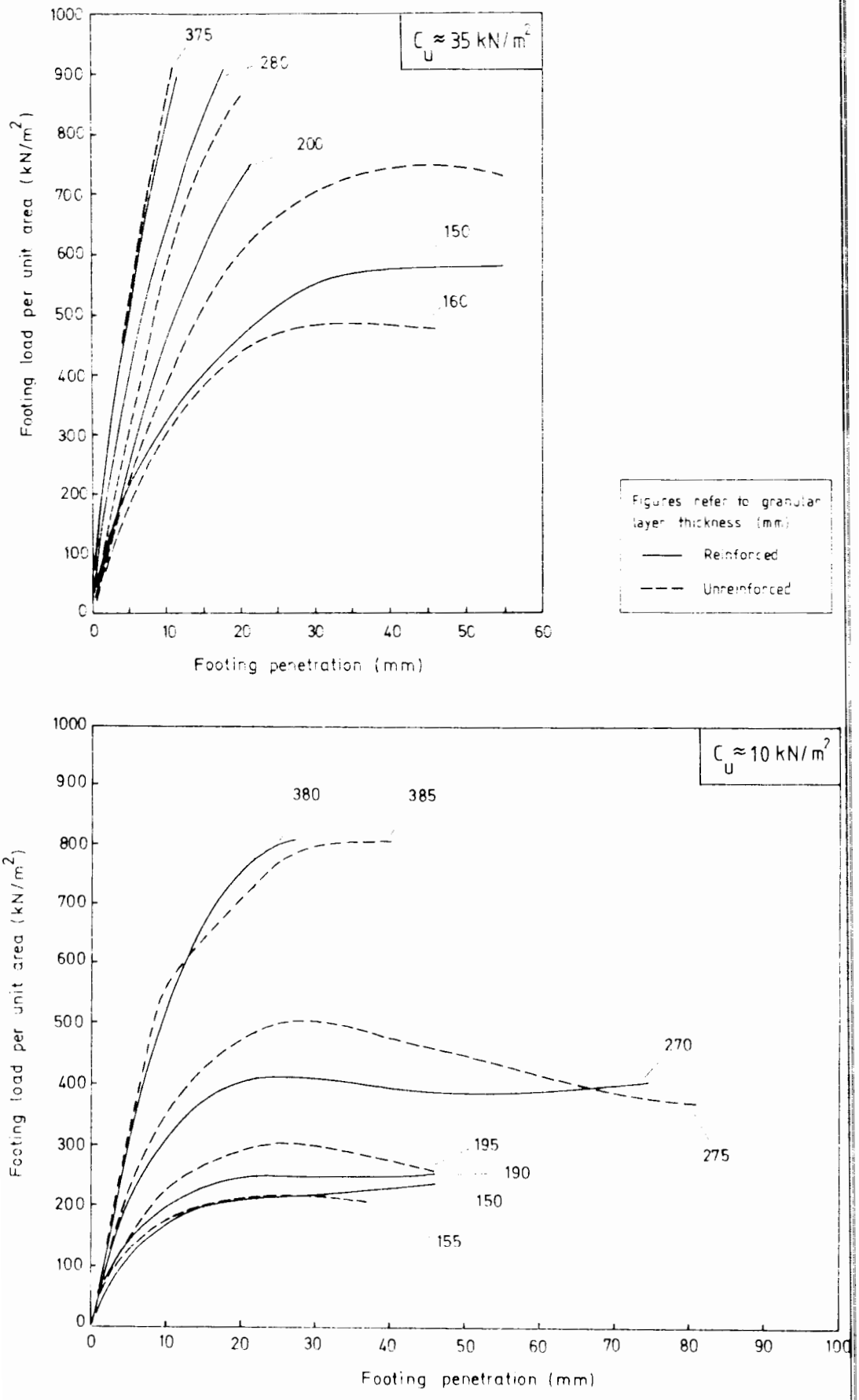

Figure 7.7 Effect of incremental loading on the circular footing

On the very soft clay subgrade ($c_u \simeq 10kN/m^2$), all of the test sections were loaded to failure, and further load increments were applied to investigate behaviour subsequent to failure and at large footing penetrations, Figure 7.7. In two tests the performance of the reinforced and unreinforced sections was almost identical; in the other two tests the peak load of the unreinforced section was greater than that of the reinforced section. However, while there was a marked tendency for the bearing capacity of the unreinforced tests to decrease with further footing penetration, the capacity of the reinforced tests tended to increase, so that at large displacements the reinforced sections began to outperform the unreinforced sections.

Generally these results illustrate a common response to loading of the circular footings: failure of an unreinforced section, irrespective of granular layer thickness or subgrade strength, was catastrophic and associated with a reduction in bearing capacity; reinforced sections however demonstrated a tendency to maintain or improve the bearing capacity at failure. These characteristic failure mechanisms suggest a reinforcing effect mobilised at large displacements which was dependent on generating substantial deformations of the reinforcing grid, one that was essentially non-brittle in its nature. Additionally there is evidence to suggest a reinforcing effect on the firmer subgrade which was not wholly dependent on large surface displacements, an early improvement that was noticeably absent from the results of the tests made on the very soft subgrade.

7.6 Results of tests on rectangular footings

A summary of the load penetration curves for the rectangular footings is presented in Figures 7.8 and 7.9. Consider firstly the results for the thinner 200mm granular layer: on the firm subgrade the unreinforced system failed completely and cycling of the load contributed to a further reduction in bearing capacity, Figure 7.8. In contrast the reinforced section exhibited an additional 15-20% increase in bearing capacity over the unreinforced section during the initial loading stage, an improvement which increased substantially after cycling of the load. Although the response of the reinforced system was noticeably stiffer, this may be partly a consequence of it not having reached the same state of impending failure before unloading. On the very soft subgrade complete failure of the reinforced section was again avoided and a 15-20% improvement during the initial loading stage observed, Figure 7.8. However a similar response to load cycling in both of these tests was followed by a smaller, yet increasing improvement in the bearing capacity of the reinforced section over the unreinforced section with continued footing penetration.

The results for the thicker 380mm granular layer show a striking similarity in behaviour of the reinforced and unreinforced sections. On the firm subgrade the load-penetration curves are virtually identical and no indication of an impending failure was observed, Figure 7.9. This response, which was also characteristic of the circular footing tests, suggests that the applied magnitude of load was not sufficient to cause distress even in the granular layer, and that at these relatively small

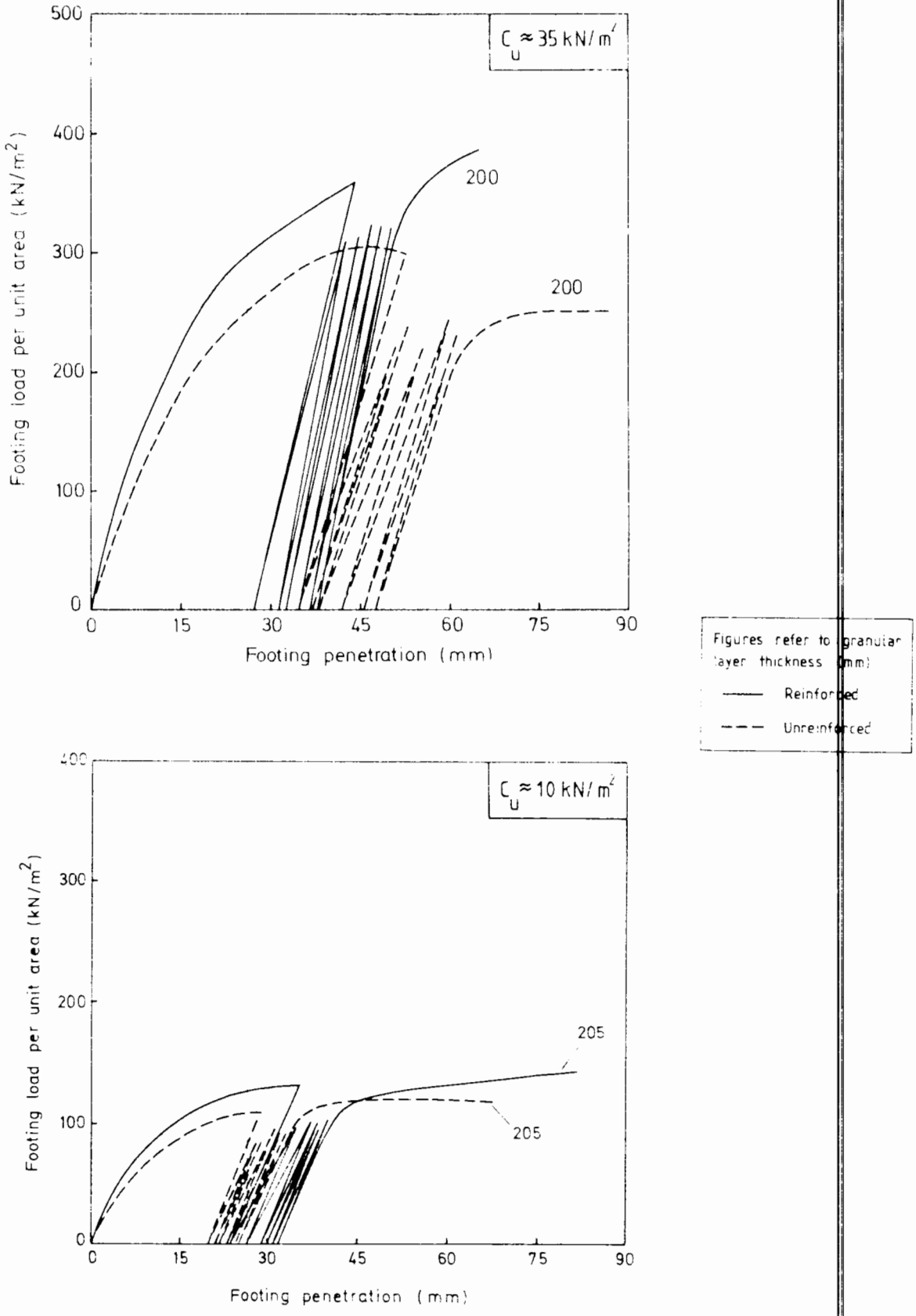

Figure 7.8 Effect of incremental repeated load on the rectangular footing (200mm granular layer)

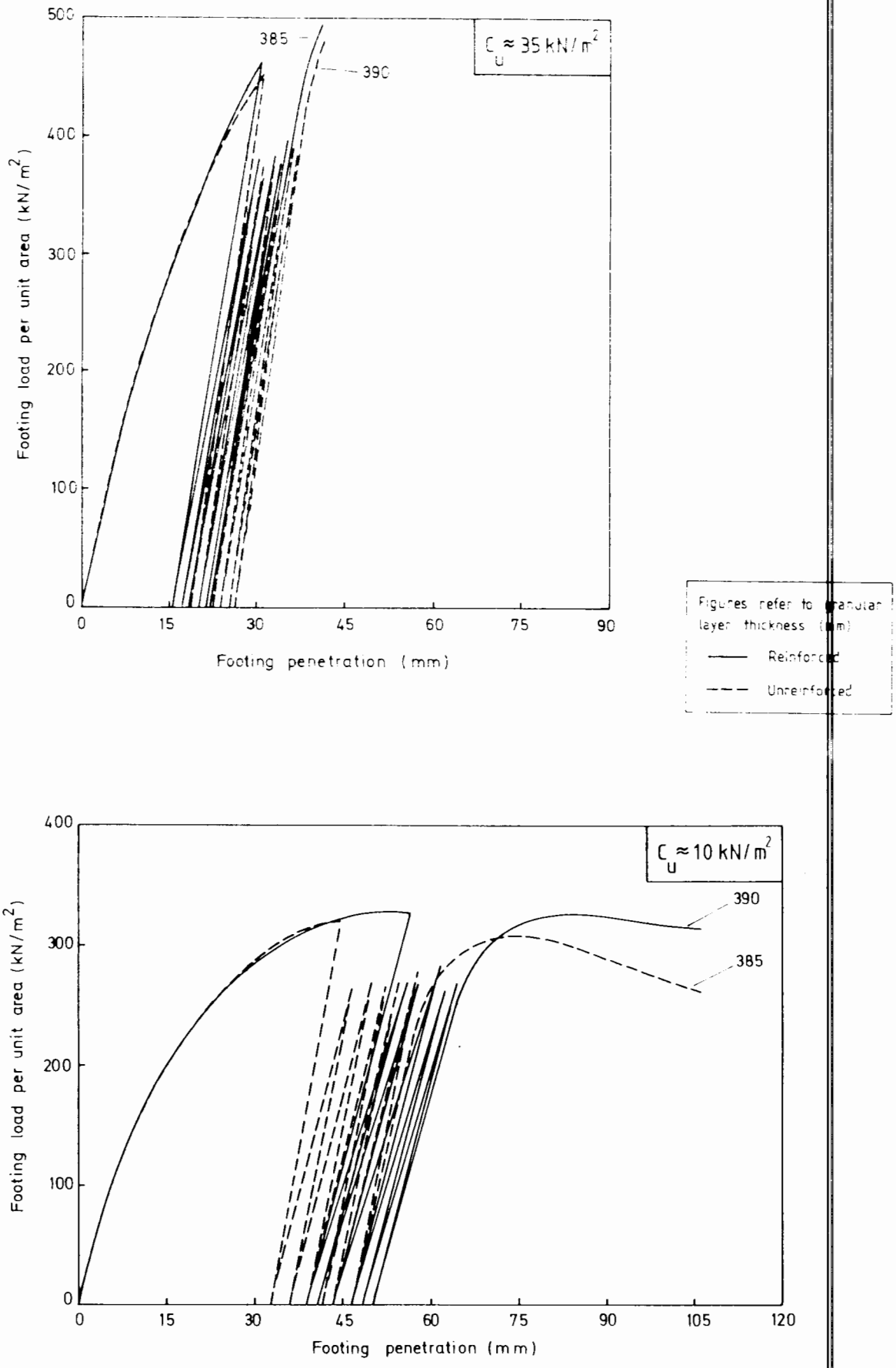

Figure 7.9 Effect of incremental repeated load on the rectangular footing (380mm granular layer)

displacements on such a strong system, any reinforcing action in the grid had yet to be mobilised. On the soft subgrade it was only after cycling of the footing load that any clear improvement in the reinforced section was observed, Figure 7.9.

Generally the results indicate a benefit from reinforcement in the early stages of loading which was only mobilised on the thinner granular layers. Thereafter it was through application of cycles of load to the footing and a breakdown in the integrity of the granular layer that substantial improvements in the bearing capacity of the grid reinforced sections were realised in comparison with the unreinforced sections.

Vertical compressive strain in the subgrade was computed from the buried inductive coils, and results are illustrated in Figure 7.10 for initial loading of the footing designated by 'I' and reloading of the footing after cycling of the load designated by 'R'. While the development of strain during initial loading for tests made on the 380mm granular layers was observed to be very similar in both the reinforced and unreinforced sections, substantially smaller strains were measured in reinforced tests on the 200mm layer, with up to a 30-35% reduction during initial loading of the firm subgrade and a 15-20% reduction for the soft subgrade. Without exception, strain measurements before and after unloading of the footings showed a slightly greater recovery in the reinforced sections. Thereafter, strain during reloading was in general agreement with the observed load-penetration results.

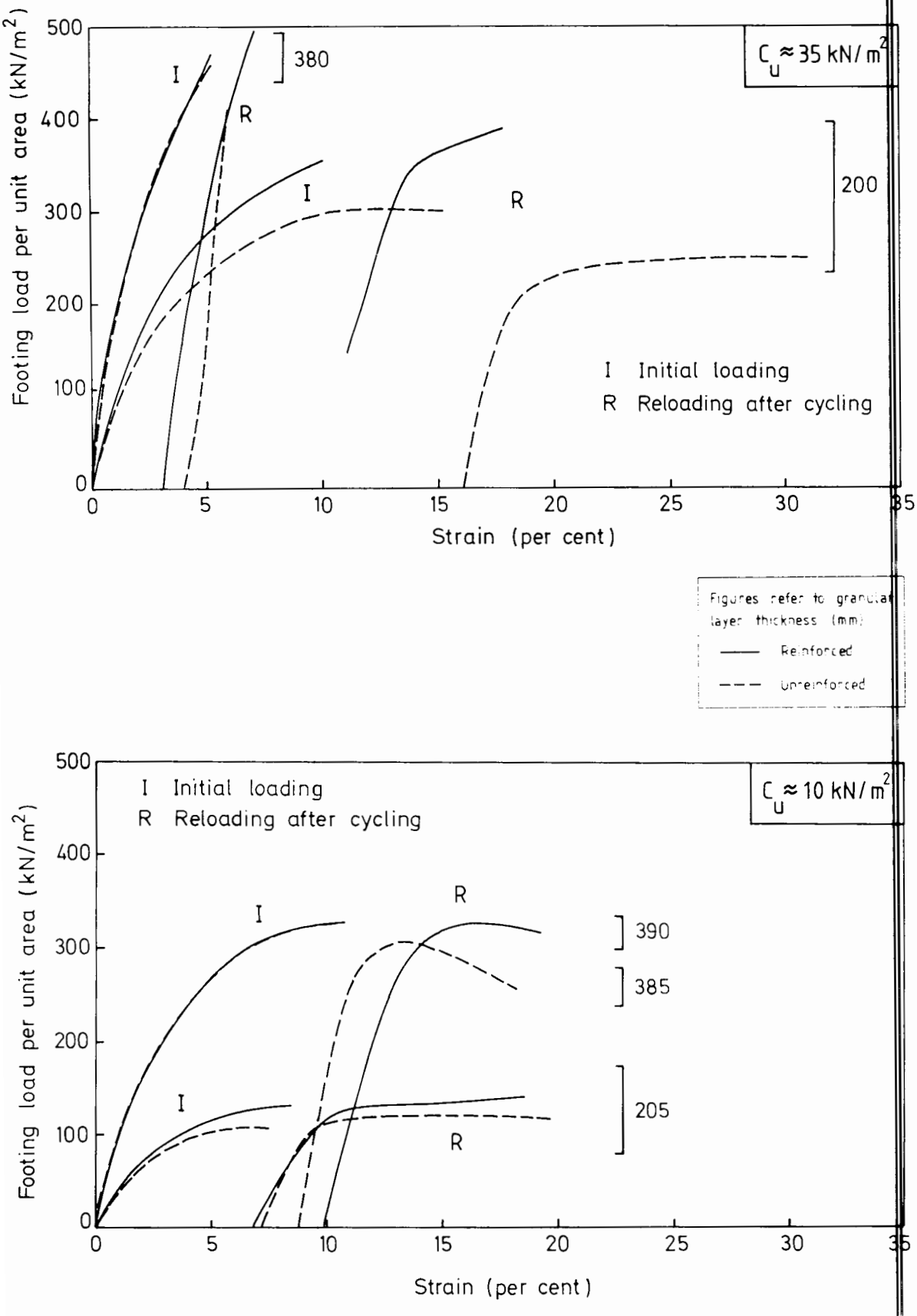

Figure 7.10 Vertical strain in the clay subgrade 155m below formation

The development of surface and grid displacements during loading is illustrated in a sequence of profiles for two tests in Figure 7.11. In making comparisons between the tests it should be noted that the vertical scale is twice that of the horizontal scale. Clearly overall displacements in the reinforced section were smaller than those in the unreinforced section where rupture of the compacted material contributed to the serverity of the profile. From a series of such profiles recorded for each granular layer after unloading of the footing at the end of a test, Figures 7.12 and 7.13, the general influence of the grid in reducing the magnitude of heave was apparent: notwithstanding a greater footing penetration in some unreinforced tests, those sections with reinforcement invariably took a greater load while at the same time experiencing smaller and less localised displacements.

7.7 Post-test observations

The nature of the interface between the granular layer and the clay subgrade was established either by local excavation after the circular footing tests, or by digging a trench through a section of the granular layer after the rectangular footing tests. Typically in the process of removing granular material, the upper surface of a clear fracture could be identified which extended through the layer at rather shallow angles in the range 25-35^{o} to the horizontal.

In most tests the interface was well defined, always with a small zone of contaminated gravel and clay. In an unreinforced section this

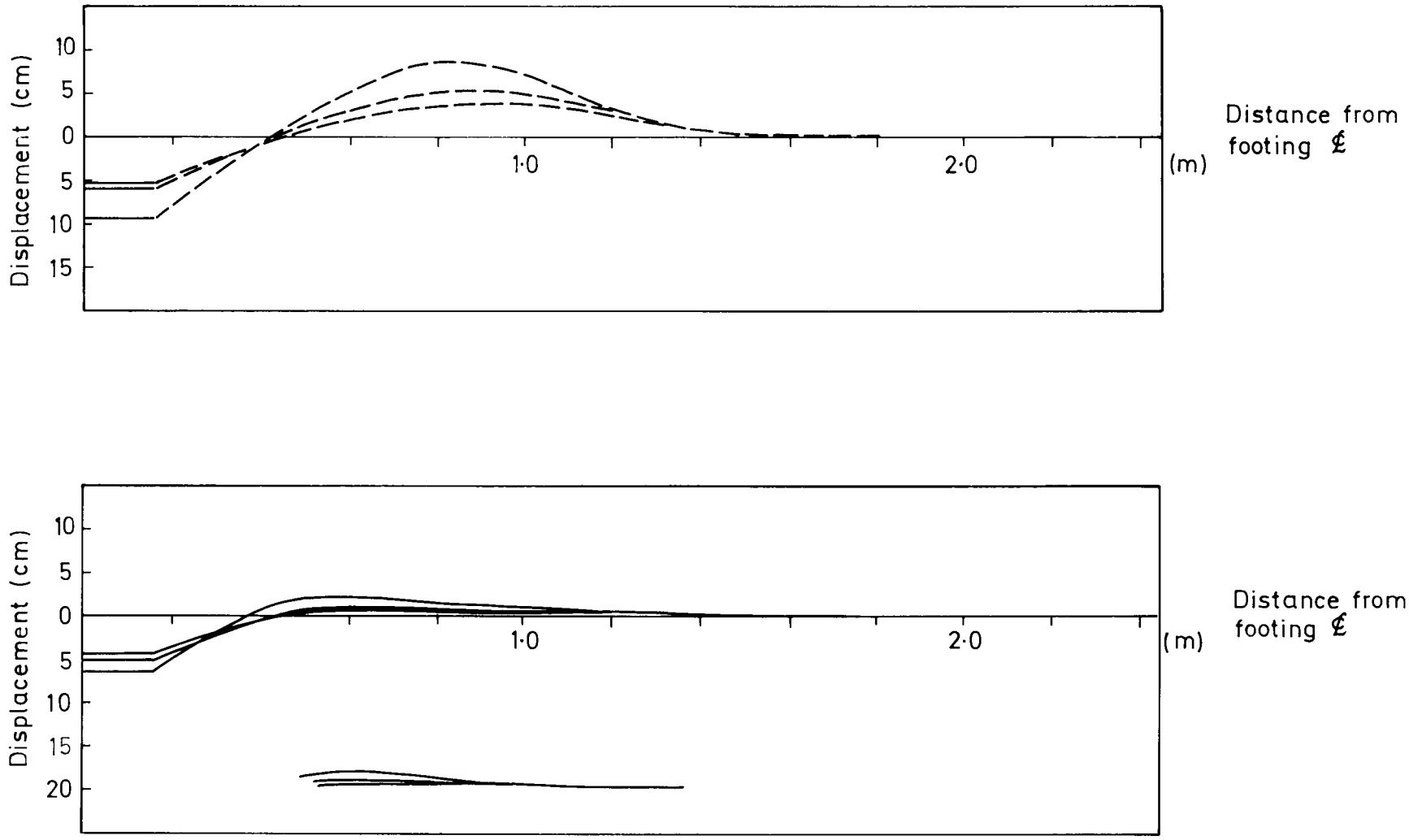

Figure 7.11 Measured displacements during two tests

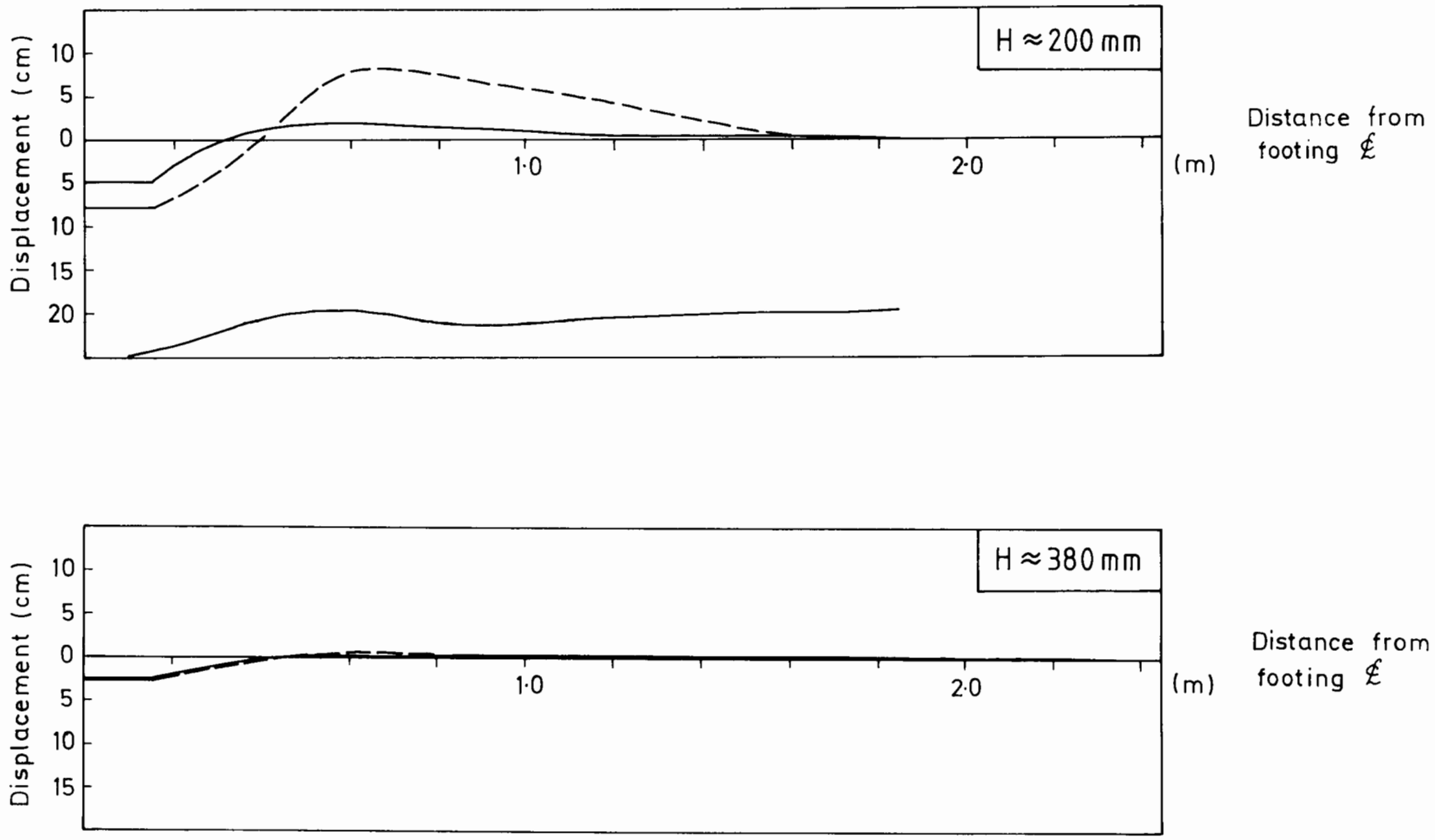

Figure 7.12 Unloaded profiles : first test series

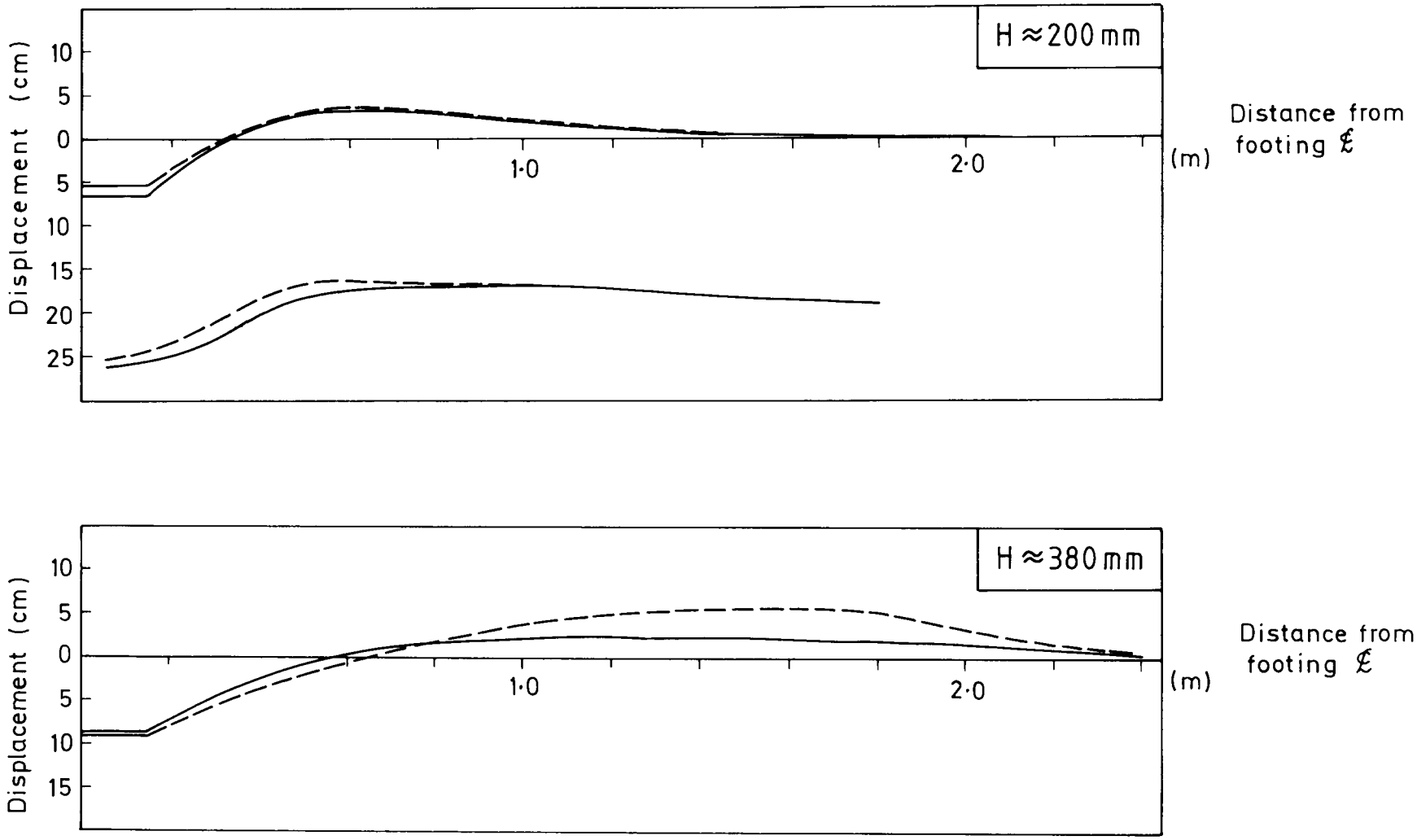

Figure 7.13 Unloaded profiles : second test series

zone was generally about 10mm thick on the firm subgrade and 25mm thick on the very soft subgrade, with occasional large particles partially buried in the clay. In the reinforced sections the grid was located at the base of this contaminated zone in the clay, and while the extent of the zone was nearly the same for all sections in the first test series, it appeared that the reinforced sections experienced a lesser degree of contamination on the very soft subgrade. Characteristically, large granular particles bore directly on to the surface of the grid, while medium to small size particles were driven about 5mm into the aperture. Again intermixing of the clay with the granular material was observed, to the extent that on the very soft subgrade any interlock with the particles of the granular layer was severely compromised.

CHAPTER 8

DISCUSSION

8.1 Monotonic loading

8.1.1 Model test results

The equations given for a dual footing in summary 6.2.6 were derived from an analysis of observed failure mechanisms in the monotonic tests. In Table 8.1 values for a separate bearing, restraint and membrane contribution calculated from these equations are compared with the footing load measured in the tests, with the results expressed as a calculated load per unit area on the footing q_U or q_R and a measured value q_M. The correlation is particularly strong for the simpler case of the unreinforced tests; yet there is good agreement for the reinforced tests as well, and while the match is less encouraging at $\delta \simeq 50$mm it was at this stage in the reinforced tests that the upper bound solution was likely to be somewhat conservative as a result of movement of the grid that occurred at large footing penetrations, see section 6.2.4.

Each test is described by the index value of undrained shear strength determined in section 5.1.3.2 and given in Table 5.3. Although undrained strength of the clay was observed to increase moderately with depth, any potential improvement this might have brought to the bearing capacity of the footing was almost entirely compromised by the strength anisotropy of the test samples, see section 5.1.3.3. The index value,

Table 8.1 Calculated and measured footing loads

Test code	c_u	B′	q_b	q_r	q_m	q_U	q_R	q_M
		δ≃25mm						
U9100M	11.0	193	86			86		75
U6125M	6.9	210	59			59		59
R9100M	11.2	187	81	12	16		109	102
R6125M	7.1	213	58	9	8		75	82
RR6125M	7.3	218	61	9	9		79	88
		δ≃50mm						
U9100M	11.0	178	79			79		77
U6125M	6.9	190	53			53		58
R9100M	11.2	196	86	7	7		100	106
R6125M	7.1	207	56	4	4		64	79
RR6125M	7.3	210	59	5	4		68	91

Notes

(1) B′ units (mm); all other units (kN/m^2)
(2) q_U and q_R defined by eqns. 6.32 and 6.33

Table 8.2 Grid tension/unit width

Test code	δ≃25mm				δ≃50mm				★
	ψ°_{av}	β°_{av}	ε	T	ψ°_{av}	β°_{av}	ε	T	
R9100M	16.4	13.0	2.6	2.4	27.0	19.5	6.1	0.4	
R6125M	14.0	10.0	1.5	1.3	27.5	21.0	7.1	0.4	
RR6125M	15.0	10.5	1.7	1.5	26.0	20.5	6.8	0.4	

Notes

(1) ε(%) from eqn. 6.28
(2) T(kN/m) from eqn. 6.25
(3) T(kN/m) from eqn. 6.29 ★

which was measured close to the mid-depth of the deforming zones, was therefore very acceptable for this bearing capacity analysis.

Measurements of the effective footing width B′ in the tests show that any nominally identical reinforced and unreinforced tests exhibited a similar value of B′ at $\delta \simeq 25$mm, confirming that the presence of reinforcement had little effect on the initial angle of load spread in the overlying granular material, which was about 20° to the vertical. As footing penetration continued however, there was a noticeable reduction in the value of B′ measured in the unreinforced tests which did not occur to the same extent in the reinforced tests. This observation suggests it is misleading to believe that the inclusion of reinforcement in an unpaved road will cause any angle of load spread mobilised in the granular layer to increase. Instead the reinforcement simply acts to maintain the initial load spread of the layer, which is otherwise reduced by a greater amount in an unreinforced section as deformations continue and a punching action develops with an associated loss of material from beneath the loaded area through lateral displacement or flow.

Tension per unit width, T, in the grid was calculated in the early stages of a test ($\delta \simeq 25$mm) from a consideration of strain in the reinforcement material: angles ψ_{av} and β_{av} were measured directly from profiles of the granular layers, strain calculated using equation 6.28, and T established from the appropriate force/extension curve for the model grid material, Figure 5.12. The results are presented in Table 8.2. In the final stages of a test ($\delta \simeq 50$mm) a limiting condition of tension was calculated using equation 6.29. Interestingly, for the

geometric profile of the grid immediately below the footing to approximate to a parabola then,

$$\psi_{av} = 2\beta_{av} \qquad (8.1)$$

Yet measured values of these angles clearly do not agree with such a relationship, and suggest that the actual shape of this interface is significantly less rounded.

Notwithstanding the limitation of anchorage on the contribution of a membrane action in the later stages of a test, the results show a substantial improvement in bearing capacity that is mobilised in the reinforced tests from a maintenance of the load spreading capacity of the granular layer together with lateral restraint of the subgrade. The potential therefore for a significant increase in the capacity of a geogrid reinforced system at relatively small footing penetrations is very dependent on an adequate interlock between the granular material and the grid. Indeed without a good interlock, which was the situation for some of the full scale tests where the grid was placed directly on to a very soft clay formation and compaction of granular material made with a vibrating plate, then this early reinforcing mechanism can be completely lost due to slip over the reinforcement itself, see Figure 7.7. At large displacements the importance of a firm anchorage was clearly demonstated in the models, wherein the limiting tension that was developed in the reinforcement was found to be largely a function of the subgrade strength rather than the material stiffness.

8.1.2 Full scale test results

The load-penetration curves of some of the full scale test described in Chapter 7 may be compared with four similar model test results reported by Love (1984). These quarter-scale tests were performed in conditions of plane strain for monotonic loading of a 75mm wide single footing on a compacted granular layer over a clay subgrade. The tests were made at a rate of footing penetration of 2.5mm/s, and reinforced tests included a scaled Tensar SS1 type geogrid at the base of the granular layer. A summary of the parameters in the four tests is given in Table 8.3.

Table 8.3 Test conditions (after Love, 1984)

Test code	c_u (kN/m^2)	H(mm)
H1M reinforced	8.8	100
H2M unreinforced	8.5	
B1M reinforced	8.9	50
B2M unreinforced	8.8	

The results presented in Figure 8.1 are for footing load and penetration in the model tests multiplied by the scaling factor of 4. While a discussion of the trends in the results is very reasonable, any direct comparison would have to consider the different tensile modulus of the Tensar SS1 and SS2 geogrid materials (see Figure 8.2), the different

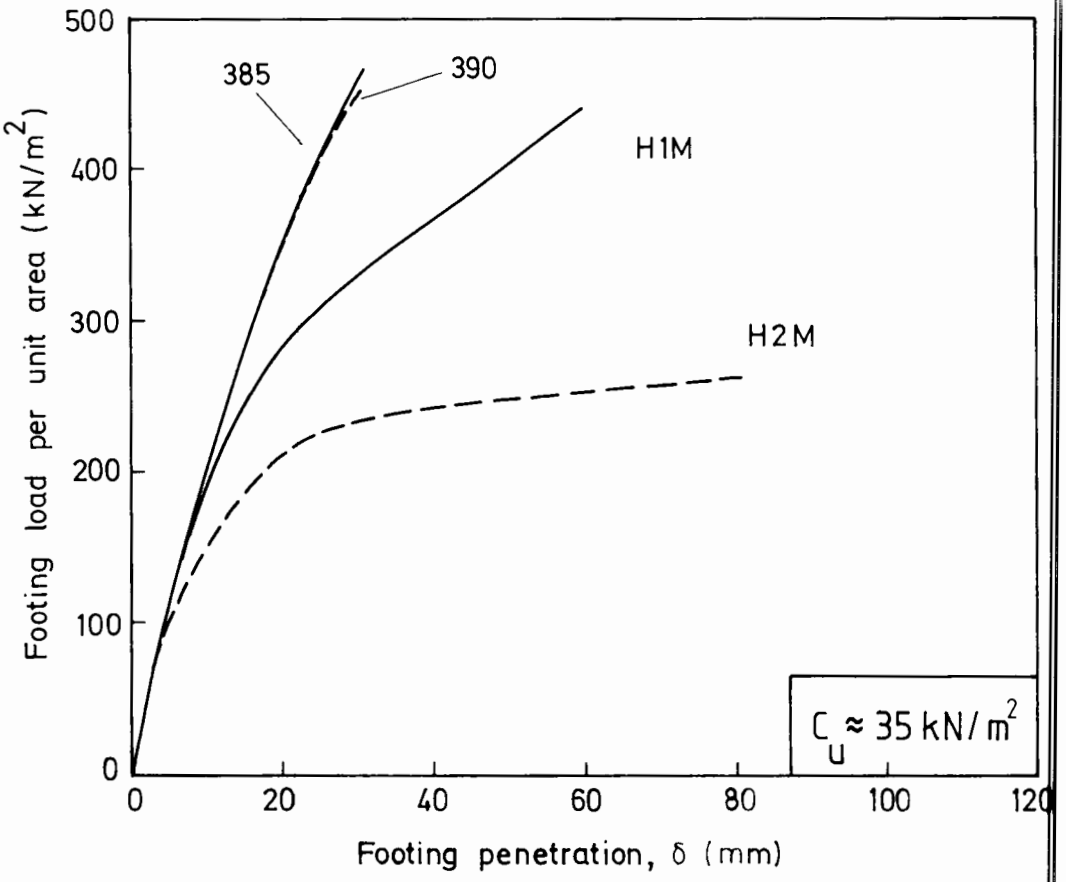

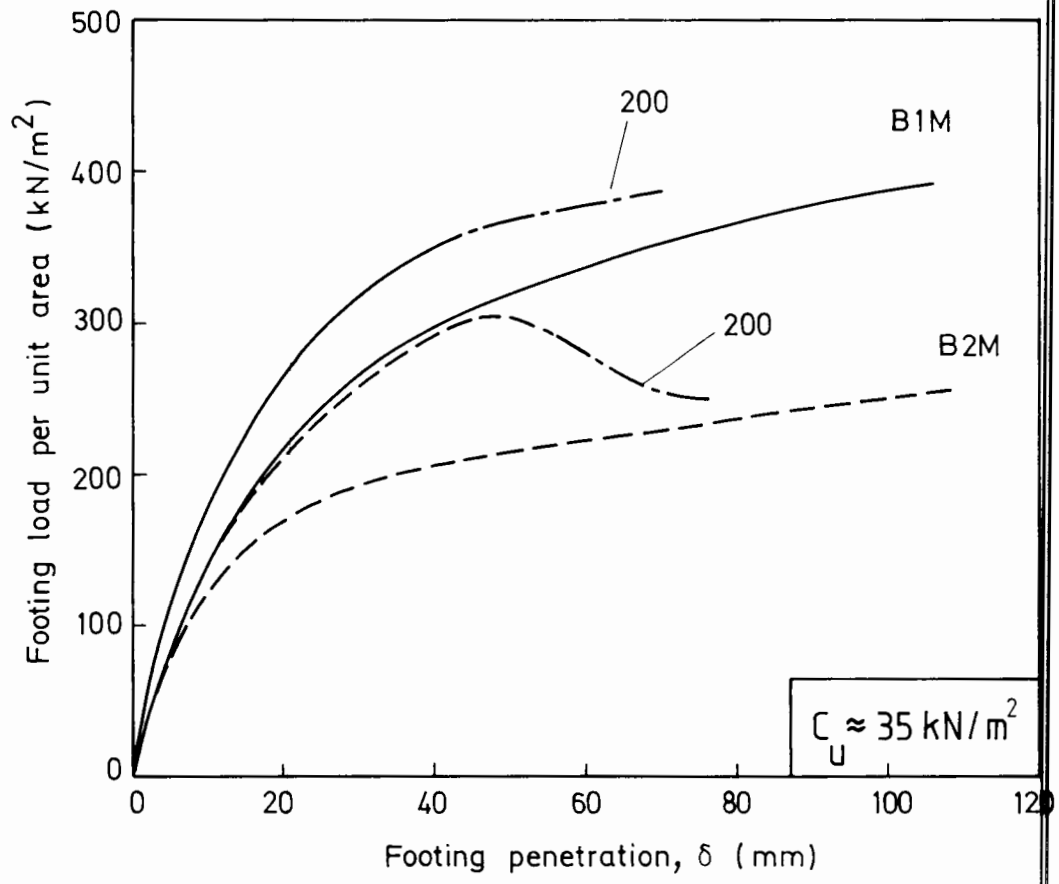

Figure 8.1 A comparison of the full scale and model test results

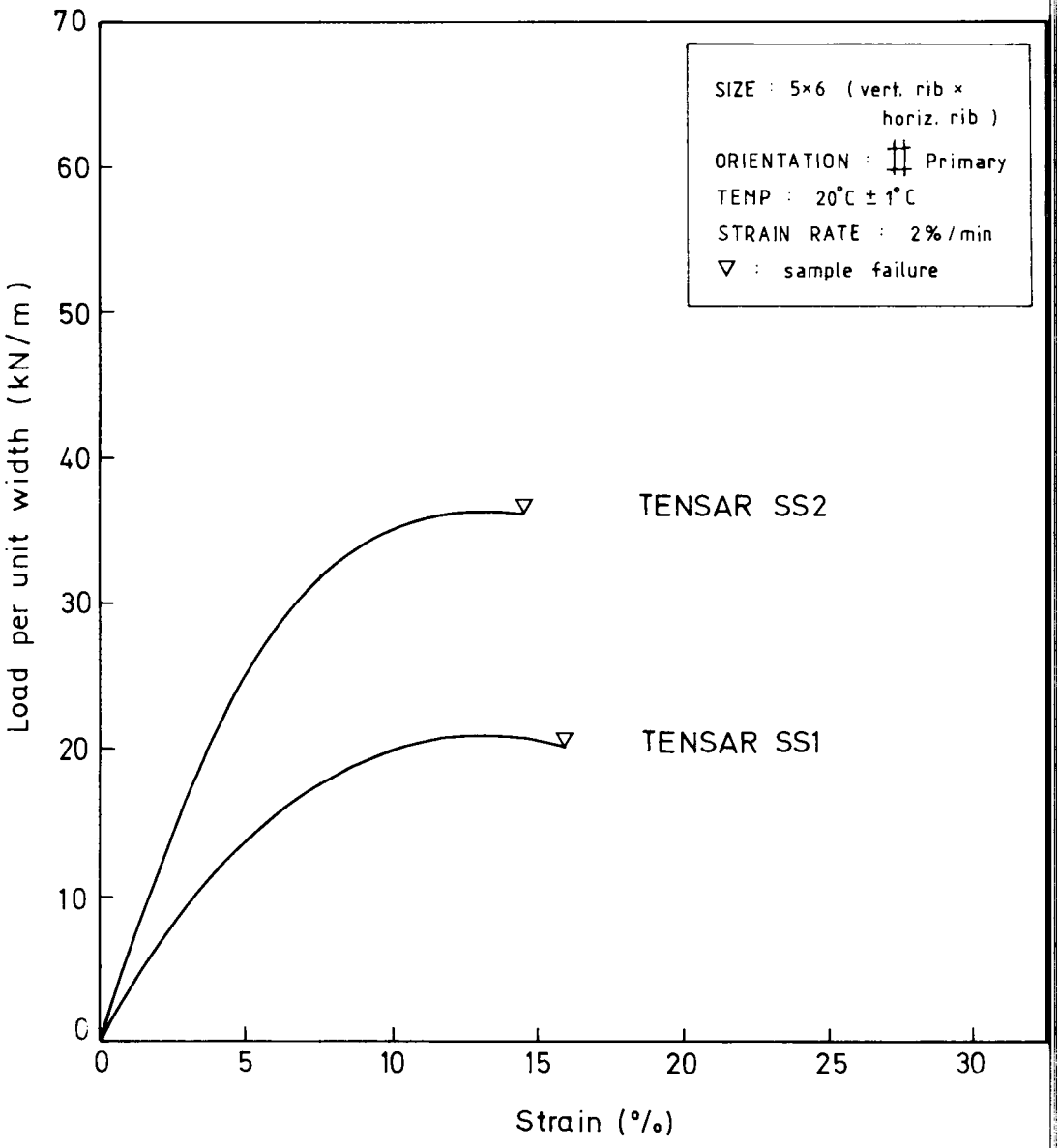

Figure 8.2 Tensar test data (after McGown, 1982)

rate of loading that was applied, the variations in experimental arrangement, and as such is not feasible.

On the thinner granular layer the reinforced tests exhibit a similar response throughout loading, while the unreinforced tests although radically different in initial response show an encouraging similarity with increased footing penetration. A possible reason for this behaviour is the very good quality of the compacted granular layer that was constructed in the full scale tests (dry density about 2.36Mg/m^3), which was greatly superior to the granular layers of the model test (dry density about 1.78Mg/m^3) and probably unrepresentative of conditions in low volume unpaved roads in general. It would explain the distinct brittle peak in the unreinforced test, as well as the typically greater strength of the full scale sections. This latter feature is clearly demonstrated in the results for the thicker layer where curves for the model tests show an apparently disappointing agreement, and the loading response in the full scale tests remained very much stiffer.

Such a general comparison of the test results for monotonic loading is very much an assessment of the extent to which the model test results are a reasonable prediction of full scale behaviour. Considering the incompatibility of compaction densities, it would appear for the thinner layer that after cycling of load to the footing in the full scale test and a resultant breakdown in the integrity of the granular layer there was an encouraging similarity. Since this breakdown did not occur after load cycling on the thicker layer, the lack of agreement between model and full scale test is understandable.

8.2 Cyclic loading

8.2.2 Model test results

The cyclic tests may be described in a similar manner to the monotonic test using separate bearing, restraint and membrane components. Each test is again characterised by the index value of undrained shear strength, and a summary of the results is presented in Table 8.4.

The trend in effective footing width B′ agrees well with the previous observations; nearly equal values of B′ were measured for reinforced and unreinforced tests at a penetration $\delta \simeq 25$mm, and at the end of a test they were very similar in absolute magnitude to those of the monotonic tests.

Tension per unit width T in the grid was calculated using the procedure of the monotonic tests, though of course the same force/extension curve and therefore tensile modulus was not applicable in the cyclic tests since the rate of strain in the grid reinforcement was much smaller. Estimates of the rate of strain $\dot{\varepsilon}$ indicate a variation between tests, with an approximate rate of strain $2\%\text{min}^{-1}$ for those tests in which any significant membrane tension was mobilised. Values of tension per unit width in the grid for $\delta \simeq 25$mm were therefore calculated for this relationship, while a limiting condition dependent on anchorage was used at $\delta \simeq 50$mm as in the monotonic tests, Table 8.5. Measured angles of ψ_{av} and β_{av} again suggest the profile of the grid below the footing was less curved than that of a parabola, which in practice would cause

Table 8.4 Calculated and measured footing loads

Test Code	c_u	B′	q_b	q_r	q_m	q_U	q_R	q_A	$\frac{q_A}{q_U, q_R}$	N
		δ≈25mm								
U6125	6.2	215	54			54		46	0.85	15
R6100	7.1	213	58	9	5		72	65	0.90	30
U9100	10.4	206	87			87		62	0.71	24
R9075	11.9	167	77	12	9		98	71	0.72	39
R9100	9.9	203	77	12	2		91	64	0.70	52
R6125	6.9	221	59	9	5		73	64	0.88	52
U9125	9.9	224	90			90		66	0.73	85
R9125	11.0	221	94	14	1		109	71	0.65	142
		δ≈50mm								
U6125	6.2	198	50			50		46	0.92	30
R6100	7.1	195	53	4	4		61	65	1.07	45
U9100	10.4	179	75			75		62	0.83	53
R9100	9.9	196	75	6	4		85	64	0.75	100
R6125	6.9	207	55	4	4		63	64	1.02	100
U9125	9.9	203	81			81		66	0.81	185
R9125	11.0	209	89	7	4		100	71	0.71	470

Notes

(1) B′ units (mm); all other units (kN/m^2)
(2) q_U and q_R defined by eqns. 6.32 and 6.33

Table 8.5 Grid tension/unit width

Test code	δ≈25mm					δ≈50mm				
	ψ°_{av}	β°_{av}	ε	T	$\dot{\varepsilon}$	ψ°_{av}	β°_{av}	ε	T	★
R6100	12.0	9.0	1.2	1.1	2.4	25.5	19.0	5.8	0.4	
R9075	16.0	10.0	1.5	1.3	2.3	35.0	21.5	7.5	0.6	
R9100	10.0	6.0	0.6	0.5	0.7	22.0	14.0	3.1	0.5	
R6125	13.5	8.0	1.0	0.9	1.2	35.0	22.0	7.9	0.3	
R9125	8.0	5.0	0.4	0.4	0.2	15.0	9.5	1.4	0.6	

Notes

(1) ε(%) from eqn. 6.28
(2) T(kN/m) from eqn. 6.25
(3) T(kN/m) from eqn. 6.29 ★

any vertical component of reinforcement tension or membrane action to be less than a theoretical prediction.

A useful insight into the behaviour of each test is given by the ratio $\frac{q_A}{q_U}$ or $\frac{q_A}{q_R}$ against N illustrated in Figure 8.3, where,

q_A is the mean applied footing load

q_U or q_R is the calculated bearing capacity of the test arrangement

N is the number of applied cycles of load

In any test arrangement the initial value of the ratio is largely dependent on the strength of the clay, the granular layer thickness and tension per unit width in the reinforcement. If the ratio $\frac{q_A}{q_U}$ or $\frac{q_A}{q_R} > 1$ then a bearing failure will ensue since the applied load will be in

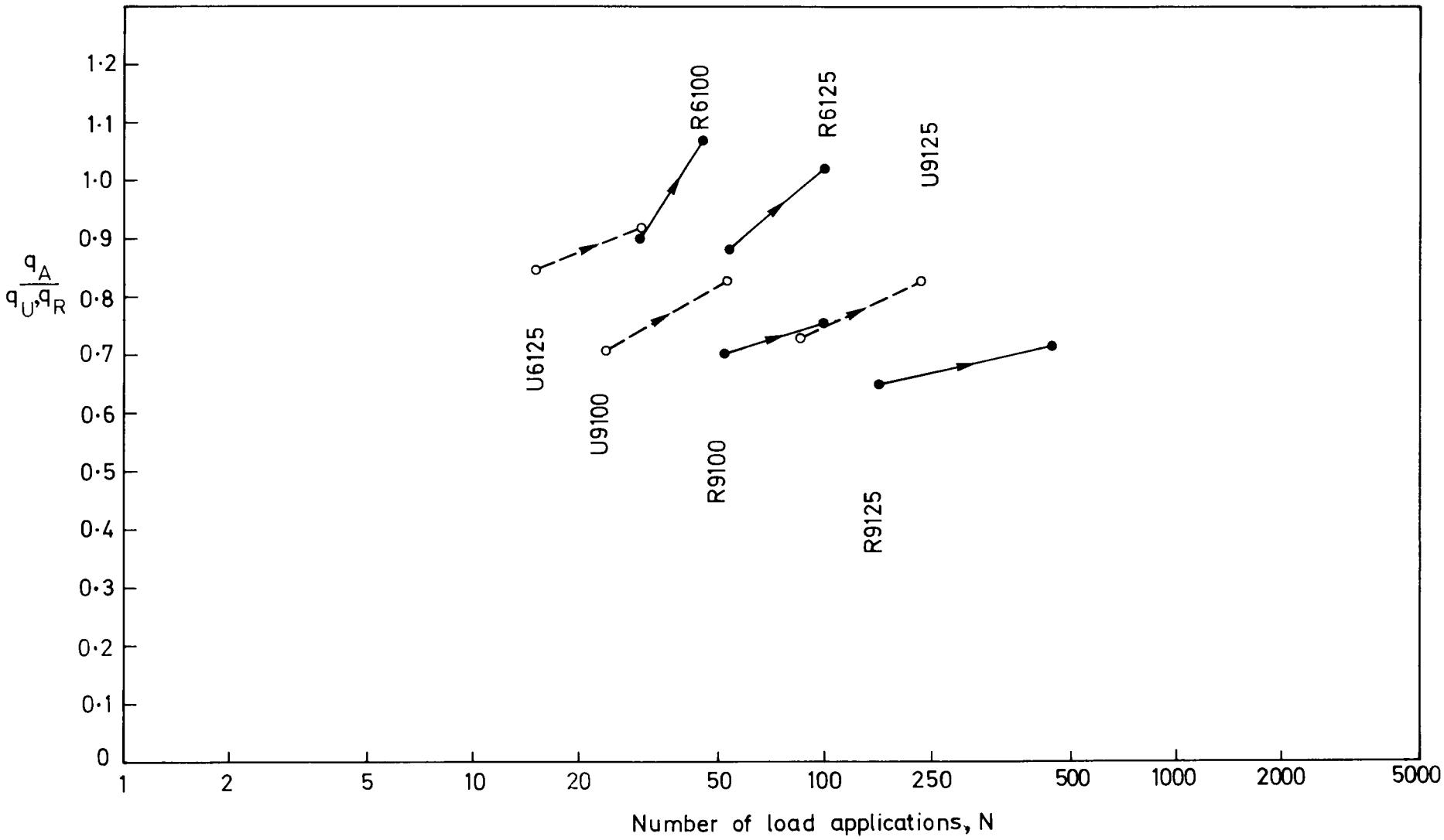

Figure 8.3 Model test performance during cyclic loading

excess of the bearing capacity, which explains why a nominal footing contact pressure 68kN/m^2 was unacceptable on the very weak U6125 test arrangement.

During testing the value of the ratio tended to unity in most unreinfoced and reinforced systems since B′ decreased with increasing N, while in the reinforced tests the contribution from the reinforcing mechanisms was insufficient to compensate. Yet the advance of a general failure condition was least rapid for those tests in which the ratio was initially smaller, illustrated by tests R9100 and R9125. Examining the separate contributions to the bearing capacity of the footing set out in Table 8.4, these are seen to be the only tests in which the magnitude of the contribution from a membrane and inward-acting lateral restraint term increased between $\delta \simeq 25$mm and $\delta \simeq 50$mm, so almost maintaining the bearing capacity.

8.2.2 Full scale traffic studies

In a similar approach to that of the monotonic tests, the cyclic tests may be compared with other traffic studies, and while the results cannot be considered in any manner a validation of the model similitude they nevertheless serve as a useful, qualitative assessment of the model performance. In making such comparisons two aspects of the model test results are considered below, firstly the shape of the curves for footing penetration (δ) against number of load applications (N) and secondly the nature of the improvement observed in the geogrid reinforced layers.

Delmas et al. (1986) report a full scale trial for a heavily loaded vehicle (axle load 180kN) trafficking a 0.4m thick unpaved road over a soft-to-firm clay subgrade of undrained strength varying between 30 and 50kN/m^2. Two different types of geotextile were used to reinforce the base of the granular layer (see Table 8.6) and a summary of the results is presented in Figure 8.4. Also included in the figure is a curve for a model test R9100, which given the scaling factor of 4 approximates to a c_u of 40kN/m^2 and H=400mm. While the physical conditions were rather similar in the model and full scale study, the reinforcement type and vehicle loading were different, and any direct comparison between number of vehicle passes at full scale and number of load applications in the model would also have to account for the simplifying assumptions made in the model study that were reported in section 3.2.3.2 and consider the somewhat low compaction densities of the granular layer in the model tests. Yet a significant difference in behaviour was recorded in the traffic study which was dependent on reinforcement length, and comparing the model test with the results for the shorter 4.5m lengths of reinforcement then a very reasonable similarity is observed in the shape of the curves. They all exhibit an obvious change in gradient leading to unacceptable deformations that would constitute a serviceability failure.

In another study, Chaddock (1985) describes the performance of a granular layer trafficked by a vehicle with a standard axle load and a Tensar SS1 geogrid included at the base under one wheel path only. The clay subgrade had a CBR around 4.5% (100 kN/m^2) and the Type 1 granular material was compacted to D.Tp. (1976) specifications. The relationship between deformation and number of vehicle passes presented in Figure 2.7

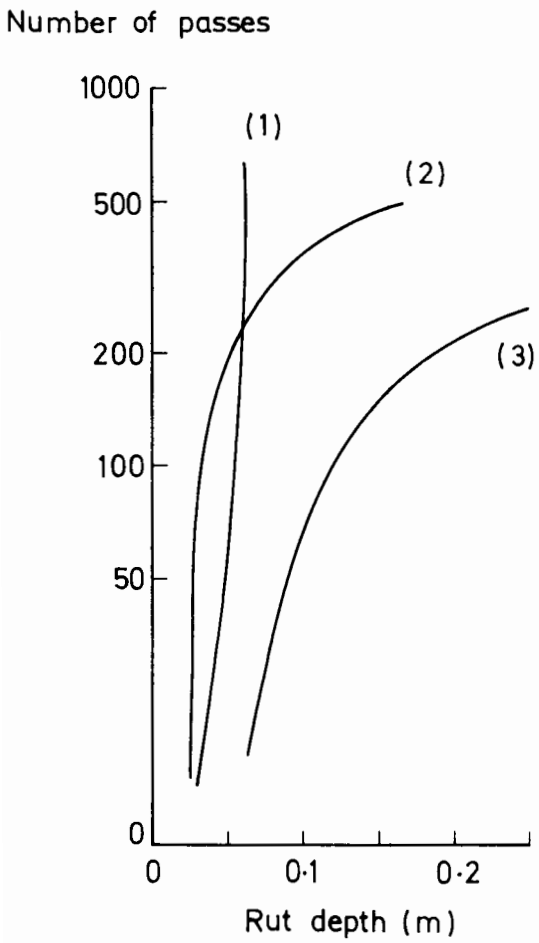

Figure 8.4 (a) Full scale trial results (after Delmas et al., 1986)

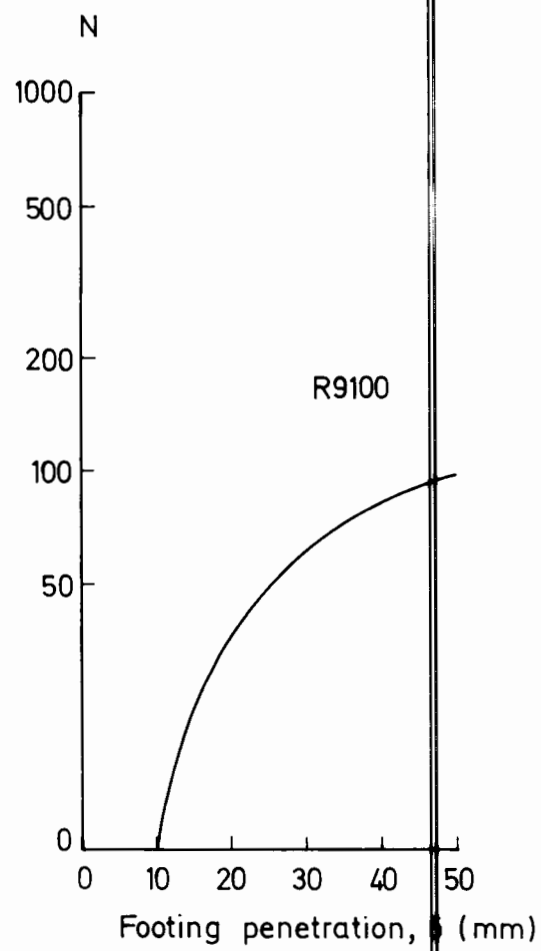

Figure 8.4 (b) Model test result

Table 8.6 Geotextile data (after Delmas et al.,1986)

Reinforcement	Length (m)	Force/unit width at failure (kN/m)	Tensile stiffness (kN/m)
(1) Woven	7·0	27·5	200
(2) Woven	4·5		
(3) Needle punched	4·5	16·0	40

demonstrates an early improvement in the reinforced section that was common to the model test results, and which analysis would suggest is a consequence of lateral restraint. Considering the analytical approach that was used for the model tests, by extrapolation from Figure 2.7 the unreinforced section might be expected to take nearly 1000 passes to a deformation of 100mm, equivalent to $\delta \simeq 25$mm in the model study. For a standard axle loading q_A of 270kN/m^2 (from Appendix 3), and given $H \simeq 225$mm, a dual tyre width of 540mm (from Appendix 3) and an angle of load spread approximately $\tan^{-1}0.5$, then from equation 6.16

$$q_b \simeq 5.47 c_u \frac{B'}{B}$$
$$\simeq 775 \text{kN/m}^2$$

and
$$\frac{q_A}{q_U} \simeq 0.35 \qquad (8.2)$$

To plot this data point with the information given in Table 8.4 would require the 1000 vehicle passes to be considered as 2000 wheel-axle load applications in the context of the model test, and although the two types of test may only be generally compared because of the simplifying assumptions referred to above, it would imply a fair correlation with an extrapolation of the model data illustrated in Figure 8.3. The reinforced sections in this traffic study gave a much better improvement than that of the model study, yet considering the different anchorage configuration to the grid and the likelihood of a maintained greater compaction density in the granular layer such a behaviour might not be unexpected.

CHAPTER 9

CONCLUDING REMARKS

Any attempt to observe the behaviour of a full scale structure by model testing in the laboratory must involve compliance with the laws of dimensional similitude and account for deviations from them. By selecting conditions of plane strain loading the behaviour of a transverse section across an unpaved road was examined in the model study, yet considering the direction of vehicle loading and the nature of the reinforcement action this is a very reasonable approach. In preparation for testing, a granular layer was compacted over a saturated clay subgrade. The requirements of the model grid used in the tests, namely that the geometry and tensile stiffness of the material appropriately scaled a Tensar SS2 geogrid, proved to be difficult to combine and while it was a remarkably good Tensar equivalent, both the size of the grid apertures and secant tensile modulus were slightly larger than the ideal.

An electro-hydraulic control system was developed to apply either monotonic or cyclic footing loads, operating on a principle of position or load feedback. Loading of the arrangement was made by the dual footing to a serviceability failure criterion. It was necessarily a simplification of wheel loading, and while the variation of contact pressure with time was typical of that observed in the field, the repeated cycles to failure comprised a loading routine that was more

severe than might be expected on even a heavily trafficked road and none of the cyclic tests tended to a stable limit.

Since it was not possible to examine the response of the test arrangement in any quantitative manner at small footing penetrations, the analytical procedure involved an interpretation of values of footing load which were measured after moderate displacements had occurred in the granular layer and clay subgrade. As such, analysis of the results infers that the reinforcement mechanisms which were acting at these stages in the test also governed the early response. Of course the relative contribution of each mechanism varied throughout a test, and this is not to suggest for instance that membrane action was important at small footing penetrations.

In the analytical procedure, plots of marker movements on the front-face surface of the subgrade were used to identify the extent of deforming clay zones. An obvious similarity was observed in the pattern of the deformations for equivalent monotonic and cyclic load tests, indicating that any monotonic tests may be considered to be an adequate representation of the reinforcing mechanisms that occur during cyclic loading. The general nature of the deformations was in agreement with expectations of classical bearing capacity for adjacent surface footings and a virtual work approach like that described by Atkinson (1981) for isolated foundation footings was used to analyse the unreinforced test results, with further considerations made to account for the actions of the geogrid reinforcement.

While the shortcomings of the model tests are such as to preclude rigorous extrapolation to a prototype structure, the results indicate the nature of the reinforcement mechanisms and the relative importance of each contribution. They also correct some misconceptions that have existed regarding early reinforcement benefits. A bearing capacity factor appropriate to the dual footing was shown to be 5.47, which is slightly greater than a value of $(\pi+2)$ for a single footing because of interaction in the granular layer between the two footing plates. While there was no significant difference either in the compacted density of the granular material or the early load spreading ability of this layer due to the grid, it mobilised an improved performance in the reinforced sections by interlocking with the granular material and applying an inward acting lateral restraint to the subgrade which was being displaced away from the loaded area.

As surface deformations continued the deformed profile of the grid was observed to be less rounded than that of a parabola, and generally small strains were developed that were less than 3% at $\delta \simeq 25$mm and not greater than 8% at the end of a test. The vertical component of the grid tension per unit width contributes to a membrane action that is well accepted and acts to reduce the load transmitted to the subgrade directly below the footings, as well as limiting heave movements either side of the loaded area through a reverse curvature. At large footing penetrations the grid tended to lose its interlock with the granular layer in this region, so that lateral restraint offered to the subgrade was only by an inhibition of movement past the grid and the efficiency of the reinforcement action was consequently somewhat reduced.

Some significant features of the tests involve construction practicalities for geogrid reinforced unpaved roads. The full scale tests on the very soft subgrade demonstrated the importance of adequate interlock between granular material and grid members beneath the footing to the mobilisation of any early reinforcement action. Regarding general performance characteristics, a qualitative comparison of these test results with some model tests indicated that the reinforcement was of greater benefit in a less well compacted layer, and that on the very well compacted layers a major action of the grid was in promoting a more ductile response to loading in the reinforced layers while preventing the sudden and brittle failure that occurred in the unreinforced layers.

The efficiency of reinforcement in the model tests was also shown to be very dependent on the anchorage imparted to it by the surrounding soil. To develop fully the potential of a stiff reinforcement it would appear that emphasis should therefore be placed in achieving a best possible restraint to the material. In the case of a geogrid this would most likely involve laying it onto a thin 'keying' layer of granular material rather than directly onto the subgrade soil, site conditions permitting of course, to encourage a complete interlock with the base material of the granular layer. In contrast, for a typically smoother geotextile it might involve using a greater width of reinforcement so that allowance could be made to wrap it back into the granular material near the edges of the base layer.

The comparisons of maximum applied footing load in the cyclic tests with a back analysis value of the bearing capacity of these test

arrangements have obvious implications for the development of a design approach; selection of a granular layer thickness could be made for a design load, and then appropriate consideration made for the relationship between single and repeated loads to achieve a particular deformation that would also account for the quality of the granular material, maintenance of the trafficked surface and importantly the envisaged pattern of vehicle usage. However before such a method may be applied with confidence, further research should aim to examine more extensively the relationship between single and repeated loads. This might involve cyclic loading with incremental stages and the inclusion of rest periods as well as a correlation against a single monotonic load test. Future studies should not be limited to very soft soils either, since it would appear that the reinforcing mechanisms of a geogrid are equally significant on firm soils.

APPENDIX A

DUAL FOOTING DESIGN CONSIDERATIONS

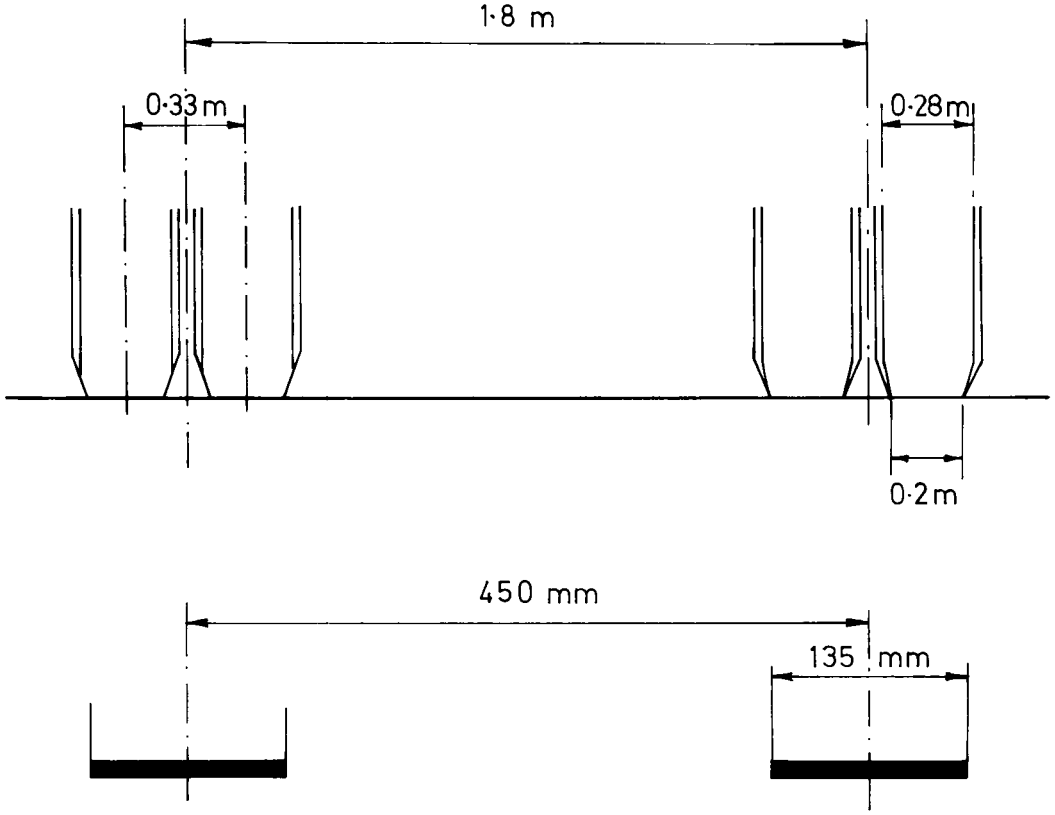

Figure A1 Dual footing dimensions

Typical dimensions of a vehicle are shown in Figure A1. The equivalent dual footing dimensions for this study at a quarter scale are as indicated, an approach which assumes that the two closely spaced wheels effectively act as a single loading to the granular layer.

Consider contact between wheel and ground. An initial approximation to this would be a circular shape, Figure A2.

For a standard axle load, $L = 80kN$

and typical inflation pressure, $p_c = 4.5bar$

Figure A2 Wheel contact areas

then the contact area of a single tyre A_T (shaded) is given by

$$A_T = \frac{L}{p_c} \div 4 = 0.044m^2$$

This may be better refined to an elliptical shape for which

$$A_T = \pi xy = 0.044m^2$$

From Figure A1, for $x = \frac{0.2}{2} = 0.1m$

then $y = 0.14m$

In terms of prototype soil loading, the encompassing rectangle A_P gives the loaded area for the granular layer where

$$A_P = 2y(0.33 + 2x) = 0.1484m^2$$

and so,

$$\text{prototype contact pressure, } P_P = \frac{L}{2A_P} = 270kN/m^2$$

$$\text{model contact pressure, } p_m = \frac{P_P}{4} = 68kN/m^2$$

The selection of loading frequency is less well defined. For a worst case of no rest periods between load repetitions, and from Figure 3.8.,

$$\text{freq} = \frac{\text{vehicle speed}}{\text{axle separation}}$$

From a combination of typical vehicle speeds and axle separations, Table A1, a representative loading frequency of one cycle per second was chosen.

Table A1 Variation of loading frequency

Speed	Axle separation (m)			
(kph)	5.0	4.5	4.0	3.5
10	0.5	0.6	0.7	0.8
15	0.8	0.9	1.0	1.1
20	1.1	1.2	1.3	1.4

APPENDIX B

CALIBRATIONS OF INSTRUMENTATION

Sangamo Transducers: D95/15000 load cell

The load cell was calibrated, mounted on the dual footing, in an Instron model TT-C. Applied load was measured with a proving ring.

Supply voltage : 14.93V DC

Sensitivity : 5.49N/mV/V

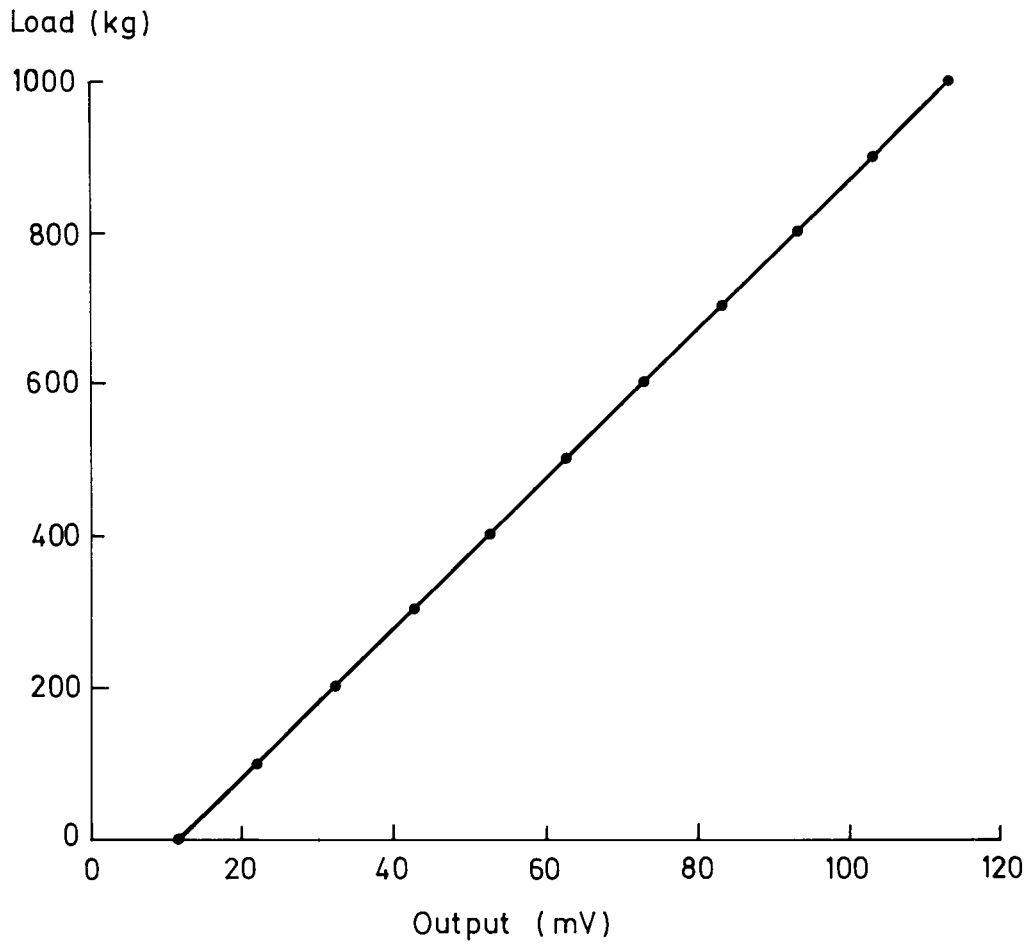

Figure B1 Load cell calibration

RDP Electronics Ltd.: D5/2000 (No.1130) LVDT

Supply voltage : 4.93V DC

Sensitivity : 0.06mm/mV/V

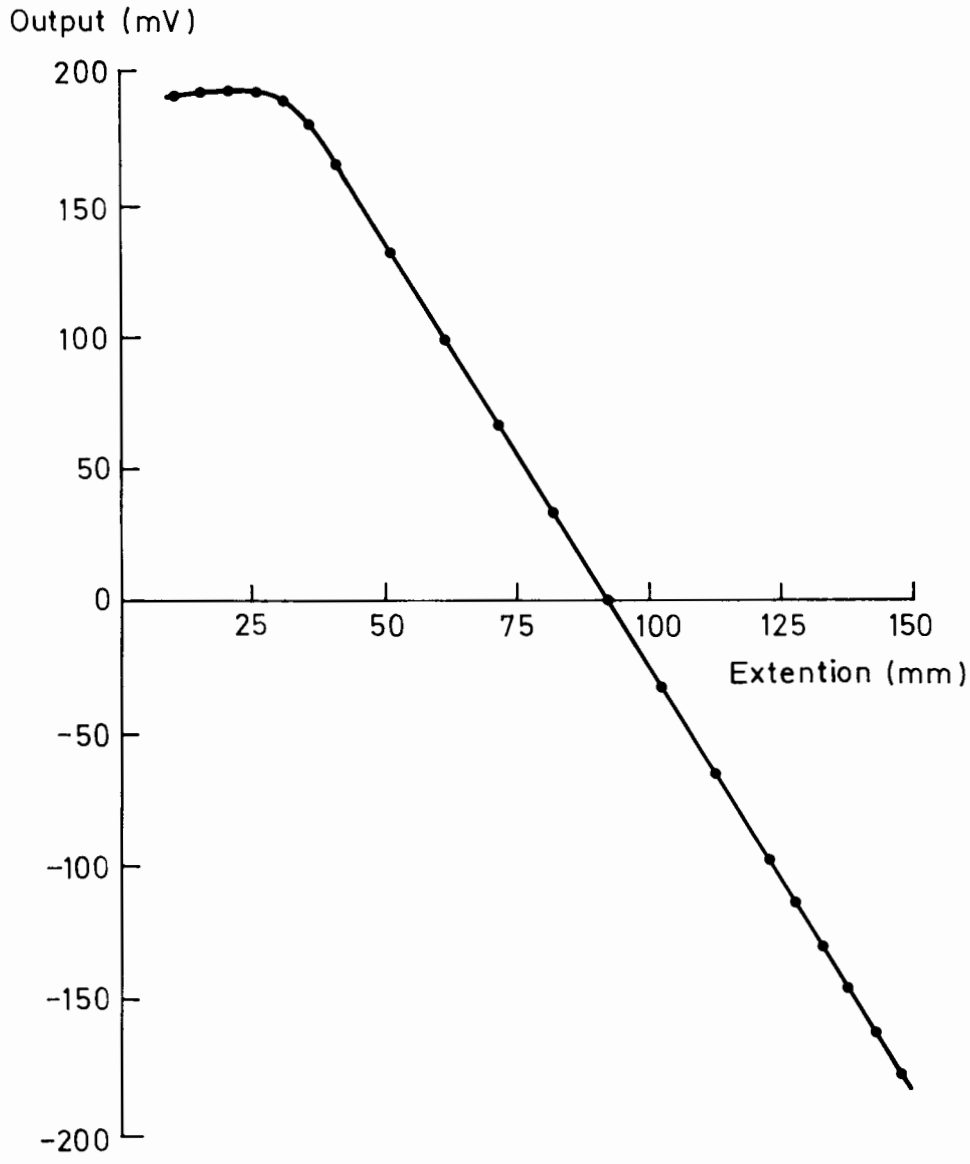

Figure B2 LVDT calibration

Druck Ltd.: PDCR81/SN2514 pore pressure transducer

Supply voltage : 4.98V DC

Sensitivity : 0.456kN/m^2/mV/V

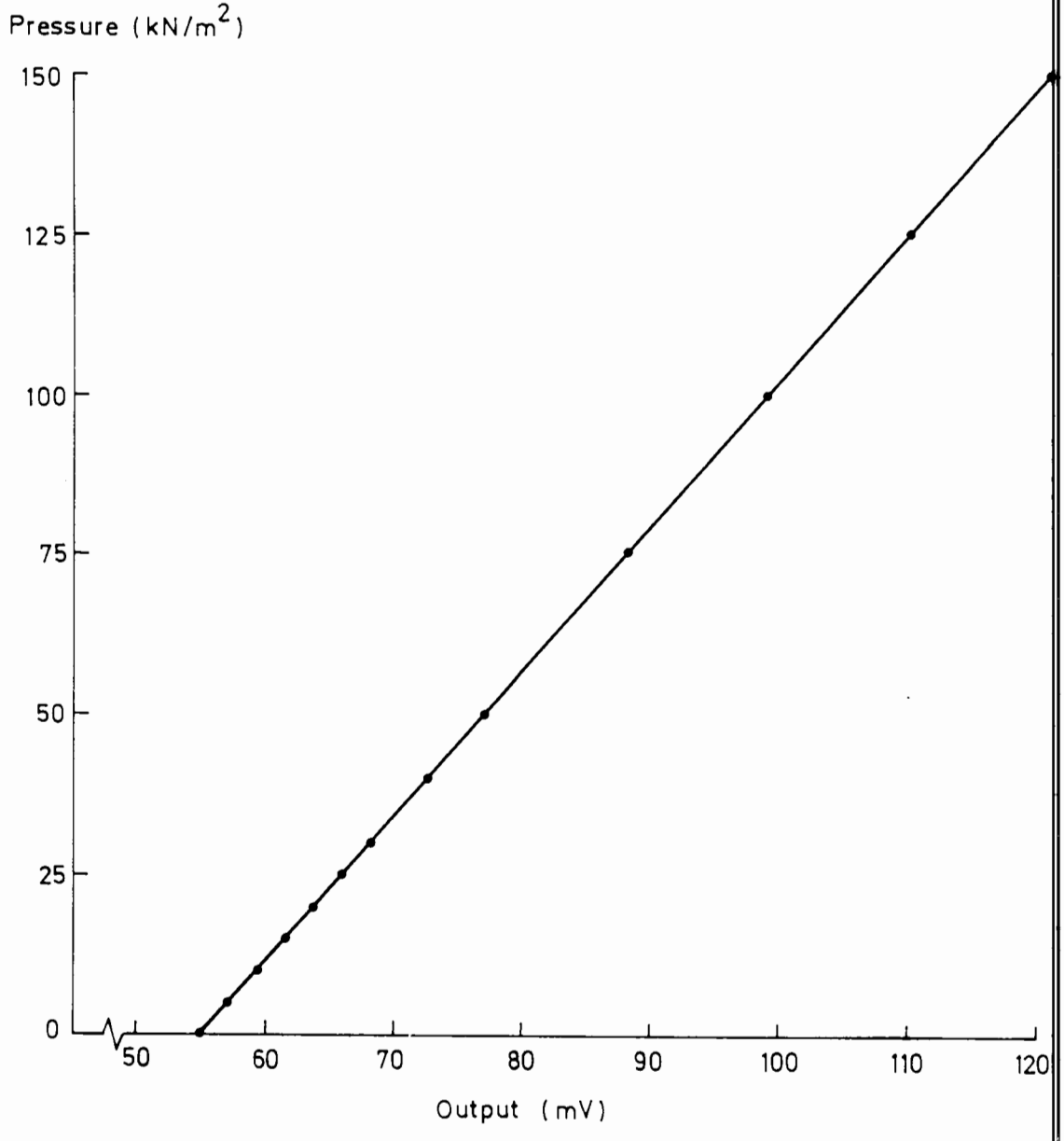

Figure B3 Pore pressure transducer calibration

Pilcon Hand Vane (DR 358)

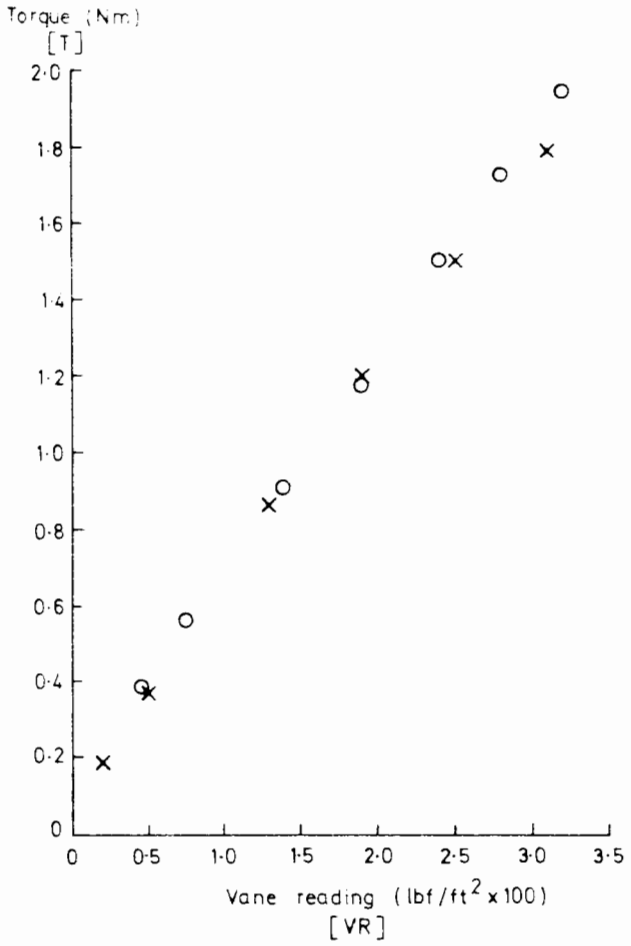

Figure B4
Vane calibration

$$\frac{T}{c_u} = \pi D^2 \left(\frac{H}{2} + \frac{D}{6} \right) \quad \text{.... BS1377:1975}$$

and for the large vane, where H=50mm and D=33mm

$$\frac{T}{c_u} = 0.014m^3$$

Calibration gives,

$$T = 0.61[VR] + 0.06$$

and combining,

$$c_u = 5.87(V.R.) + 0.58$$

'Bison' inductive coils

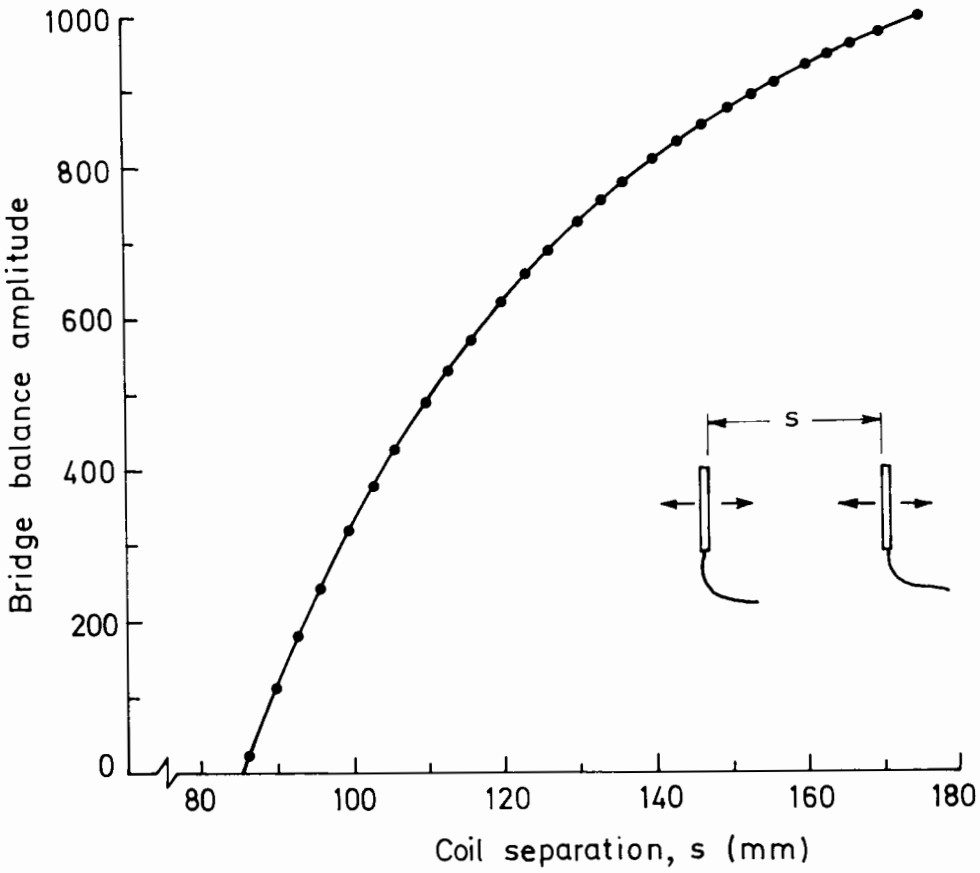

Figure B5 Variation in output reading with coil separation

The inductive coils were calibrated in a mounting frame arranged in parallel and co-axial alignment: the calibration procedure was necessarily made 'in-air', and during installation in the soil the recorded outputs were compared against the nominal coil spacings to check for gross effects of embedment. For operation on Range 1 (corresponding to a coil separation between 1 and 2 diameters), the variation of bridge balance amplitude with face-to-face separation was recorded, as shown above. While the relationship is non-linear, a straight line

interpolation between each point is a very reasonable simplification, and approximating the gradient of the curve to 0.1mm/unit of amplitude, an initial gauge length in the soil about 165mm (see Figure 7.6) corresponds to a strain resolution that was conservatively taken to be ± 0.1%.

The manufacturers recommend that for coil pairs powered from the same instrument and with similar cable lengths, then calibration of one pair of coils will be sufficient. Since identical cable lengths were used for all coils in the study, this relationship was checked and was found to be applicable. Medium-term performance characteristics of the coils were monitored from a comparison of readings taken immediately after installation of the coil pairs with other readings for the footing in position on the compacted granular layer before testing. The results indicated an insignificant change in output with time.

APPENDIX C

CORRECTION FOR STRENGTH OF TRIAXIAL MEMBRANE

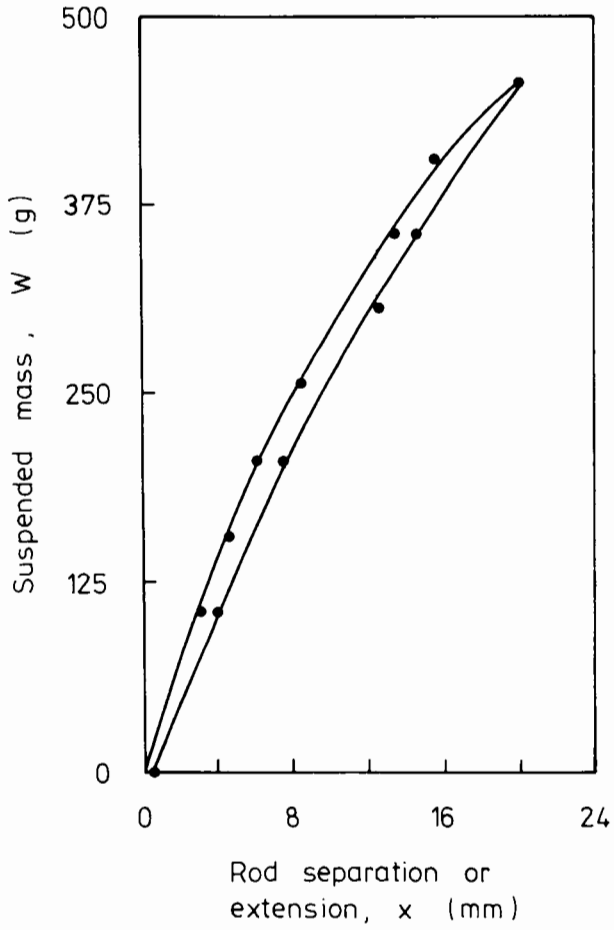

Figure C1 Data from extension modulus test on the membrane

membrane diameter = 36.6mm

width = 25mm

thickness = 0.25mm

rod diameter = 3mm

Nominal initial length = π x 37 = 115

For a strain of 15%,

$$x = 0.5 \times 0.15 \times 115 = 8.6\text{mm}$$

From graph, corresponding mass W $\simeq$ 255g

$$\text{Modulus} = \frac{\text{tension per mm width}}{\text{strain}} = \frac{0.5 \times 255 \times 9.81}{1000 \times 0.15 \times 25} = 0.33\text{N/mm}$$

Note: the test was repeated and gave a value 0.31N/mm, an average value for the extension modulus 0.32N/mm was assumed.

REFERENCES

Atkinson, J.H. (1981) 'Foundations and Slopes', McGraw-Hill (U.K.).

Atkinson, J.H. and Evans, J.S. (1985) Discussion, Geotechnique 35 No.3 pp 378-380.

Atkinson, J.H., Evans, J.S. and Ho, E.W.L. (1984) 'Non-uniformity of triaxial samples due to consolidation with radial drainage', Geotechnique 34 No.3 pp 353-355.

Bakker, J.G. (1977) 'Mechanical behaviour of membranes in road foundations', Proc. Int. Conf. on the use of fabrics in Geotechnics, Paris, Vol.1 pp 3-8.

Bassett, R.H. (1979) 'Discussion: The use of physical models in design', Proc. 7th ECSMFE, Brighton, Vol.5 pp 253-270.

Bauer, A. and Preissner, H. (1986) 'Studies on the stability of a geotextile reinforced two-layer system', Proc. 3rd Int. Conf. on Geotextiles, Vienna, Vol.4 pp 1079-1084.

Bishop, A.W. and Henkel, D.J. (1962) 'The measurement of soil properties in the triaxial test', Edward Arnold (Publishers) Ltd.

Brown, S.F., Lashine, A.K.F. and Hyde, A.F.L. (1975) 'Repeated load triaxial testing of a silty clay', Geotechnique 25 No.1 pp 95-114.

BS1377: 1975 (1975) 'Methods of test for soils for civil engineering purposes' British Standards Institution, London.

Burd, H.J. (1986) 'Large displacement finite element analysis of a reinforced unpaved road', D.Phil. Thesis, University of Oxford.

Chaddock, B.C.J. (1985) 'Deformation of a haul road reinforced with a geomesh', Proc. 2nd Symp. on unbound aggregates in roads, University of Nottingham.

Chestnut, H. and Mayer, R.W. (1961) 'Servomechanisms and regulating system design, Vol.1', Wiley and Sons.

Christopher, B.R., Holtz, R.D. and Bell, W.D. (1986) 'New tests for determining the in-soil stress-strain properties of geotextiles', Proc. 3rd Int. Conf. on Geotextiles, Vienna, Vol.3 pp 683-688.

Cullingford, G., Lashine, A.K.F. and Parr, G.B. (1942) 'Servo-controlled equipment for dynamic triaxial testing of soils', Geotechnique 22 No.3 pp 526-529.

Davidson, C.S. (1980) 'The shear modulus of clays', Part II project, University of Cambridge.

Delmas, P., Matichard, Y., Gourc, J.P. and Riondy, G. (1986) 'Unsurfaced roads reinforced by geotextiles - a seven years experiment', Proc. 3rd Int. Conf. on Geotextiles, Vienna, Vol.4 pp 1015-1020.

Francescon, M. (1983) 'Model pile test in clay - stresses and displacements due to installation and axial loading', Ph.D. Thesis, University of Cambridge.

Giroud, J.P. and Noiray, L. (1981) 'Geotextile reinforced unpaved road design', J. Geotech. Div. ASCE, Vol.107(GT9) pp 1233-1254.

Giroud, J.P., Ah-line, C. and Bonaparte, R. (1984) 'Design of unpaved roads and trafficked areas with geogrids', Proc. Symp. on polymer grid reinforcement in civil engineering, ICE London.

Gourc, J.P., Perrier, H. Riondy, G., Rigo, J.M. and Perfetti, J. (1982a) 'Chargement cylic d'un bicouche renforce par geotextile', Proc. 2nd Int. Conf. on Geotextiles, Las Vegas, Vol.2 pp 399-404.

Gourc, J.P., Matichard, Y., Perrier, H. and Delmas, P. et al (1982b) 'Capacite portante d'un bicouche, sable sur sol mou, renforce par geotextile', Proc. 2nd Int. Conf. on Geotextiles, Las Vegas, Vol.2 pp 411-416.

Gourc, J.P., Perrier, H. and Riondy, G. (1983) 'Unsurfaced roads on soft subgrade: mechanism of geotextile reinforcement', Proc. 8th ECSMFE, Helsinki, Vol.2 pp 495-498.

Gourc, J.P., and Riondy, G. (1985) 'Modelisation du comportement a la fatigue des chaussees provisoires renforcees par geotextile', Proc. 2nd Canandian Symp. on Geotextiles and Geomembranes, Edmondon, pp 1-8.

Gue, S.S. (1984), 'Ground Heave around driven piles in clay', D.Phil. Thesis, University of Oxford.

Ingold, T.S. (1982) Discussion J. Geotech. Div., ASCE, Vol.108(GT2) pp 1654-1657.

Ingold, T.S. (1983) 'A laboratory investigation of grid reinforcement in clay', ASTM Geotechnical Testing Journal, Vol.6, No.3 pp 112-119.

Jarrett, P.M. (1984) 'Evaluation of geogrids for construction of roadways over muskeg', Proc. Symp. on polymer grid reinforcement in civil engineering, ICE London.

Jarrett, P.M. (1986) 'Load tests on geogrid reinforced gravel fills constructed on peat subgrades', Proc. 3rd Int. Conf. on Geotextiles, Vienna, Vol.1 pp 87-92.

Jarrett, P.M., Lee, R.A. and Ridell, D.V.B. (1977), 'The use of fabrics in road pavements constructed on peat', Proc. Int. Conf. on the use of Fabrics in Geotechnics, Paris, Vol.1 pp 19-22.

Jessberger, H.L., (1977) 'Load bearing behaviour of a gravel subbase - non woven fabric - soft subgrade system', Proc. Int. Conf. on the use of Fabrics in Geotechnics, Paris, Vol.1 pp 9-13.

Kenter, C.J. and Sellmeijer, J.B. (1983) 'Increase in bearing capacity due to the application of Geolon fabric below a granular base of a road', Delft Soil Mech. Lab. report CO - 254920/20.

Kinney, T.C. (1979) 'Fabric induced changes in high deformation soil-fabric-aggregate systems', Ph.D. Thesis, University of Illinois.

Kinney, T.C. and Barenberg, E. (1982) 'The strengthening effect of geotextiles on soil-geotextile aggregate systems', Proc. 2nd Int. Conf. on Geotextiles, Las Vegas, Vol.2 pp 347-352.

Kirk, G. (1985) 'Results of shear box tests on limestone aggregate on behalf of Transport and Road Research Laboratory', CSO/1802/TRRL332/363/01, Middlesex Polytechnic.

Love, J.P. (1984) 'Model testing of geogrids in unpaved roads', D.Phil. Thesis, University of Oxford.

McGown, A. (1982) Progress report to Tensar Steering Committee, December

McGown, A., Andrawes, K.Z. and Kabir, M.H. (1982) 'Load extension testing of geotextiles confined in-soil', Proc. 2nd Int. Conf. on geotextiles, Las Vegas, Vol.3, pp 793-798.

Mair, R.J. (1979) 'Centrifugal modelling of tunnel construction in soft clay', Ph.D. Thesis, University of Cambridge.

Nadarajah, V. (1973) 'Stress-strain properties of lightly overconsolidated clays', Ph.D. Thesis, University of Cambridge.

Nageswaran, S. and Houlsby G.T. (1982) 'A study of consolidation with radial drainage', Paper presented at a workshop on the implementation of critical state soil mechanics in finite element computations, Cambridge, June 29 - July 1.

Nieuwenhuis, J.D. (1977) 'Membranes and the bearing capacity of roadbases', Proc. Int. Conf. on the use of Fabrics in Geotechnics, Paris, Vol.1 pp 3-8.

Ovesen, N.K. (1979) 'Discussion: the use of physical models in design', Proc. 7th ECSMFE, Brighton, Vol.5 pp 253-270.

Palmeira, E.M. (1981) 'Utilizaco de geotexteis como reforco de aterros sobre solos moles', M.Sc. Thesis, Federal University of Rio de Janeiro.

Potter, J.F. and Currer, E.W.H. (1981) 'The effet of a fabric membrane on the structural behaviour of a grannular road pavement', Transport and Road Research Laboratory, Lab. Report 996, Crowthorne, England.

Ramalho-Ortiago, J.A. and Palmeira, E.M. (1982) 'Geotextile performance at an access road on soft ground near Rio de Janeiro', Proc. 2nd Int. Conf. on Geotextiles, Las Vegas, Vol.2 pp 353-358.

Randolph, M.F. and Houlsby, G.T. (1984) 'The limiting pressure on a circular pile loaded laterally in cohesive soil', Geotechnique 34, No.4 pp 613-623

Robnett, Q.L., Lai, J.S., Lavin, J.G., Murch, L.E. and Murray, C.D. (1980) 'Use of geotextiles in road construction: laboratory study', Preprint to 1st Canadian Symposium on Geotextiles, Calgary, pp 113-124.

Robnett, Q.L., Lai, J.S. and Murch, L.E. (1982) 'Effect of fabric properties on the performance and design of aggregate-fabric-soil systems', Proc, 2nd Int. Conf. on Geotextiles, Las Vegas, Vol.2, pp 381-386.

Rocha, M. (1957) 'The possibility of solving soil problems by the use of models', Proc. 4th Int. Conf. on Soil Mechanics, London, Vol.1 pp 183-188.

Ruddock, E.C., Potter, J.F. and McAvoy, A.R. (1982a) 'Report on the construction and performance of a full-scale experimental road at Sandleheath, Hants', Project record 245, CIRIA.

Ruddock, E.C., Potter, J.F. and McAvoy, A.R. (1982b) 'A full-scale experiment on granular and bituminous road pavements laid on fabrics', Proc. 2nd Int. Conf. on Geotextiles, Las Vegas, Vol.2 pp 365-370.

Sarsby, R.W. and Marshall, C. (1983) 'A method for determining the interactive behaviour of polymer grids and granular soils', Report No. BCS.G1/2A Bolton Ints. of Higher Ed.

Seed, H.B. and Fead, J.W.N. (1959) 'Apparatus for repeated load tests on soils', ASTM STP254 pp 78-87.

Sellmeijer, J.B., Kenter, C.J. and v.den Berg, C. (1982) 'Calculation method for a fabric reinforced road', Proc. 2nd Int. Conf. on Geotextiles, Las Vegas, Vol.2 pp 393-398.

Serota, S. and Jangle, A. (1972) 'A direct-reading pocket shear vane', Civ. Eng. ASCE (Jan), pp 73-74.

Sorlie, A. (1977) 'The effect of fabrics on pavement strength - plate bearing tests in the laboratory', Proc. Int. Conf. on the use of Fabrics in Geotechnics, Paris, Vol.1 pp 15-18.

Sowers, G.F., Collins, S.A. and Miller, D.G. (1982) 'Mechanism of geotextile-aggregate support in low-cost roads', Proc. 2nd Int. Conf. on Geotextiles, Las Vegas, Vol.2 pp 341-346.

Snaith, M.S. and Brown, S.F. (1972) 'Electro-hydraulic servo-controlled equipment for the dynamic testing of bituminous materials', Proc. Int. Symp, on deformation and rupture of solids subjected to multiaxial stresses, Cannes, Vol.3 pp 139-154.

Steenfelt, J.S., Randolph, M.F. and Wroth, C.P. (1981) 'Instrumental model piles jacked into clay', Proc. 10th ICSMFE Stockholm, Vol.2, pp 857-864.

Stuart, J.G. (1962) 'Interference between foundations, with special reference to surface footings in sand', Geotechnique 12 No.1 pp 15-22.

Thom, N.H. and Brown, S.F. (1985) 'Design of road foundations', Dept, of Civ. Engineering Report No. NHT/1, University of Nottingham.

Webster, S.L. and Watkins, J.E. (1977) 'Investigation of construction techniques for tactical bridge approach roads across soft ground', U.S. Army Engineer W.E.S., Vicksberg, Tech. Report S-77-1.

Webster, S.L. and Alford, S.J. (1978) 'Investigation of construction concepts for pavements across soft ground', U.S. Army Engineer W.E.S., Vicksberg, Tech. Report S-78-6.

Wroth, C.P. (1984) 'The interpretation of in situ soil tests', Geotechnique 34, No.4 pp 449-489.

Wroth, C.P. (1975) 'In situ measurement of initial stresses and deformation characteristics', Proc. Speciality Conf. on in situ measurement of soil properties, ASCE/Releigh, NC., pp 181-230.

Wroth, C.P., Randolph, M.F., Houlsby, G.T. and Fahey, M. (1984) 'A review of the engineering properties of soils with particular reference to the shear modulus', OUEL Report No. 1523/84, University of Oxford.